Experimental study of the hydrodynamics of pool scrubbing for different flow regimes : applications on the retention of iodine in FCVS and SGTR situations

Mohamad Farhat

NNT/NL : 2022AIXM0485/043ED353

THÈSE DE DOCTORAT

Soutenue à Aix-Marseille Université
Le 13 Décembre 2022 par

Mohamad Farhat

Etude expérimentale de l'hydrodynamique du barbotage pour différents régimes : applications au piégeage des iodes en situations de FCVS et RTGV

Discipline
Sciences pour l'ingénieur

Spécialité
Mécanique et Physique des fluides

École doctorale
ED 353 – Sciences pour l'ingénieur : Mécanique, Physique, Micro-nanoélectronique

Laboratoires
IUSTI (Université d'Aix-Marseille) / Institut Universitaires des Systèmes Thermiques et Industriels

L2EC (IRSN) / Laboratoire Expérimentation Environnement et Chimie

Composition du jury

Sabine RODE Rapportrice
Professeure, Université de Lorraine (ENSIC)

Nicolas RIMBERT Rapporteur
Professeur, Université de Lorraine (LEMTA)

Véronique ROIG Examinatrice / Présidente du jury
Professeure, Université de Toulouse (IMFT)

Olivier VAUQUELIN Directeur de thèse
Professeur, Université d'Aix-Marseille (IUSTI)

Maxime CHINAUD Co-directeur de thèse
Maître de conférences, Université d'Aix-Marseille (IUSTI)

Philippe NERISSON Invité
Ingénieur de recherche, IRSN Cadarache

Table of contents

Affidavit

Je soussigné, Mohamad Farhat, déclare par la présente que le travail présenté dans ce manuscrit est mon propre travail, réalisé sous la direction scientifique de Olivier Vauquelin, dans le respect des principes d'honnêteté, d'intégrité et de responsabilité inhérents à la mission de recherche. Les travaux de recherche et la rédaction de ce manuscrit ont été réalisés dans le respect à la fois de la charte nationale de déontologie des métiers de la recherche et de la charte d'Aix-Marseille Université relative à la lutte contre le plagiat.

Ce travail n'a pas été précédemment soumis en France ou à l'étranger dans une version identique ou similaire à un organisme examinateur.

Fait à Marseille, le 22 septembre 2022

Affidavit

I, undersigned, Mohamad Farhat, hereby declare that the work presented in this manuscript is my own work, carried out under the scientific direction of Olivier Vauquelin, in accordance with the principles of honesty, integrity and responsibility inherent to the research mission. The research work and the writing of this manuscript have been carried out in compliance with both the French national charter for Research Integrity and the Aix-Marseille University charter on the fight against plagiarism.

This work has not been submitted previously either in this country or in another country in the same or in a similar version to any other examination body.

Place Marseille, date 22 septembre 2022

Liste de publications et participation aux conférences

1) Liste des publications[1] réalisées dans le cadre du projet de thèse :

1. Farhat, M., Chinaud, M., Nerisson, P., & Vauquelin, O. (2021). Characterization of bubbles dynamics in aperiodic formation. *International Journal of Heat and Mass Transfer*, *180*, 121646.
2. Farhat, M., Chinaud, M., Nerisson, P., Vauquelin, O., & Cantrel, L. (2022). Bubbles dynamics under pool scrubbing conditions for iodine compounds trapping applications. *The 10th European Review Meeting on Severe Accident Research, Karlsruhe, Germany - May 2022.*
3. Farhat, M., Chinaud, M., Nerisson, P., & Vauquelin, O. (2022). *Piégeage de composés iodés par barbotage : aspects hydrodynamiques*. *25^{éme} Congrès Français de Mécanique, Nantes, France – Septembre 2022*
4. Farhat, M., Nerisson, P., Cantrel, L., Chinaud, M., & Vauquelin, O. (submitted to Chemical Engineering Research and Design). Hydrodynamics aspects of aerosols pool scrubbing.
5. Farhat, M., Nerisson, P., Cantrel, L., Chinaud, M., & Vauquelin, O. (en cours). Hydrodynamics aspects of volatile iodine pool scrubbing

2) Participation aux conférences[2] et écoles d'été au cours de la période de thèse :
   1. Journées des thèses IRSN, *Conférence interne en ligne, Mars 2021. (Présentation orale)*
   2. Journées des thèses IRSN, *Conférence interne à La Colle sur Loup, Mars 2022. (Présentation orale)*
   3. The 10th European Review Meeting on Severe Accident Research*, Karlsruhe, Germany - May 2022 (Présentation orale)*
   4. 25^{éme} Congrès Français de Mécanique*, Nantes, France – Septembre 2022 (Présentation orale)*

[1] Cette liste comprend les articles publiés, les articles soumis à publication et les articles en préparation ainsi que les livres, chapitres de livre et/ou toutes formes de valorisation des résultats des travaux propres à la discipline du projet de thèse. La référence aux publications doit suivre les règles standards de bibliographie et doit être conforme à la charte des publications d'AMU.

[2] Le terme « conférence » est générique. Il désigne à la fois « conférence », « congrès », « workshop », « colloques », « rencontres nationales et/ou internationales » … etc.
Indiquer si vous avez fait une présentation orale ou sous forme de poster.

Résumé

Le barbotage (pool scrubbing) est un mécanisme de filtration qui vise à réduire le rejet de produits de fission tels que l'iode dans différents scénarios d'accidents nucléaires sur un réacteur à eau pressurisée, notamment pour la gestion des accidents (FCVS : Filtered Containment Venting System), ou dans les cas de rupture de tube de générateur de vapeur (RTGV). L'injection du gaz à travers un bain liquide conduit au piégeage des produits de fission par des mécanismes de rétention, à savoir un ensemble de processus physiques et chimiques. Cette thèse vise à caractériser l'hydrodynamique du barbotage pour différentes conditions d'écoulement (caractérisées par le nombre de Weber), ainsi qu'à quantifier le piégeage de plusieurs composés iodés.

Deux campagnes expérimentales ont été réalisées, l'une à l'IUSTI-Marseille principalement pour développer les méthodes hydrodynamiques, et l'autre à l'IRSN-Cadarache (TYFON). Des essais couplant les mesures hydrodynamiques et celles du facteur de décontamination ont été effectuées, permettant ainsi d'étudier le piégeage de différents composés iodés (CH_3I gazeux, I_2 gazeux, et CsI aérosols).

L'hydrodynamique dans la zone d'injection a été caractérisée et les régimes d'écoulement ont été décrits. Une approche phénoménologique a été développée pour déterminer la taille des bulles, montrant davantage de cohérence que les approches usuellement mises en œuvre dans les modèles de la littérature. D'autre part, les piégeages de CsI et I_2 apparaissent dépendants de l'hydrodynamique et du régime de l'écoulement ainsi que, pour CsI, des contributions des différents mécanismes de rétention d'aérosols. Par ailleurs, le piégeage de CH_3I n'est pas affecté par l'hydrodynamique mais dépend de la chimie de la solution, tout en restant relativement faible.

Mots clés : Barbotage, hydrodynamique des bulles, facteur de décontamination, régimes des écoulements.

Abstract

Pool scrubbing is a filtration mechanism that aims to reduce the release of fission products (e.g., iodine) in different nuclear accident scenarios on a pressurized water reactor, notably as an accident management system in in Filtered Containment Venting Systems (FCVS), or in cases of Steam Generator Tube Rupture (SGTR). The injection of the carrier gas through the liquid pool leads to the trapping of fission products by retention mechanisms, namely a set of physical and chemical processes. This thesis aims to characterize the hydrodynamics of pool scrubbing for different flow conditions (characterized by Weber number), and to quantify the trapping efficiency of several iodine compounds.

Two experimental campaigns were carried out, one at IUSTI-Marseille mainly for developing the hydrodynamic methods, and other at IRSN-Cadarache. The facility at Cadarache, TYFON, is designed to afford the coupling of hydrodynamic and Decontamination Factor measurements, permitting to investigate the retention mechanisms of different iodine compounds (gaseous methyl iodide CH_3I, gaseous molecular iodine I_2, and caesium iodide aerosols CsI).

Bubble hydrodynamics in the injection zone were characterized and flow regimes were classified. A phenomenological approach for determining bubbles sizes has been provided, showing more consistency than usual approaches implemented in models described in the literature. On the other hand, CsI and I_2 trapping appear dependent on hydrodynamics and flow regime. Besides, CsI trapping also depends on various contributions of aerosol retention mechanisms. Otherwise, CH_3I trapping is not affected by the hydrodynamics but depends on pool chemistry, while remaining relatively weak.

Keywords : Pool scrubbing, hydrodynamics, decontamination factor, flow regimes.

Acknowledgement

This thesis was performed in the French Institut de Radioprotection et de Sûreté Nucléaire (IRSN), cofounded by the Région Sud (PACA) and with the financial support of Electricité de France (EDF) and the VERREX company.

No matter what one writes or how he writes, the words will be always unable to describe the feelings or even deliver the thanks to people who deserve.

I wish to express my sincere gratitude to my tutor Philippe Nerisson for his invaluable guidance, keen interest, motivation, continuous support during these years. His patience, support, and kindness helped me a lot. Even that I lack the words but I would like to thank you for your continuous, very well appreciated support. I would like to thank thesis directors Olivier Vauquelin and Maxime Chinaud for giving me the opportunity to carry out my PhD – but not only for that. I would also like to thank them for always believing in the project (and also in me being capable of pulling it off), being themselves passionate about and involved in the work. Your sharp criticism knocked down the work many times and, although it was hard sometimes, it eventually let me to rebuild the work with better foundations.

I express my sincere gratitude to all the members of the jury for having accepted to examine it: to Sabine Rode and Nicolas Rimbert for having reported my work and for their pertinent questions and remarks, to Veronique Roig for having chaired and animated the discussions.

Many thanks go to Laurent Cantrel for welcoming me in the lab L2EC, his critical opinion and direct style of communication were always appreciated. I would also like to thank Catherine Marchetto who always shared her suggestions and support towards the contents of the work.

For all the members of L2EC, the contribution of each one was indispensable. First, I would like to deeply thank Laurent Martinet and Charlie for their availability, their interest, their sense of humor, and their answers to my numerous questions. I would like to thank them in particular for making the experimental work possible in my thesis. As well as them, I would like to thank Guillaume for his kindness and availability. Elouan, Julie, Coralie, Fouzia, Claire, Martial, I want to thank you for your help and the time you have spent with me. I wish you all the best in your life.

I would like to bring thanks to all the members of the SEREX, notably Christophe, Christian, Emmanuel, Nathalie, Raphael, Alain, and Severine.

Last but definitely not least, I would like to express gratitude to my family. To my mom and dad, my sisters and brothers, and especially towards the one person that is only mentioned in this section of the thesis but is nonetheless the most important person regarding emotional support. This is my wife Shaimaa. Thank you for believing in me and offering support, even when it was difficult and I was not the most even-tempered person.

Thank you all.

List of Figures

List of Tables

Nomenclature

In the nomenclature below, the symbols and their corresponding definitions are presented. In general, the subscript g denotes the gas phase, and the subscript l denotes the liquid phase.

In what follows:

- When other notations are used, for the sake of literature representation, they are clearly defined.

- If the units of the symbols are not indicated, then they follow this nomenclature. Otherwise, the units will be clearly defined and precised.

Symbol	***Definition***	***Unit***
a	Bubble interfacial area	$[m^{-1}]$
Bo	Bond number $Bo = \frac{g\,(\rho_l - \rho_g)\,D_0{}^2}{\sigma}$	[-]
d_b	Bubble diameter	[m]
d_G	Globule equivalent diameter in the injection zone	[m]
d_p	Particle aerodynamic diameter	[m]
d_r	Bubbles diameter in the bubble rise zone	[m]
D_0	Nozzle diameter	[m]
D_p	Particle diffusion coefficient	$[m^2.s^{-1}]$
DF	Decontamination Factor	[-]
DF_{ci}	Decontamination Factor by centrifugal impaction	[-]
DF_{di}	Decontamination Factor by diffusion	[-]
DF_{gs}	Decontamination Factor by gravitational settling	[-]
DF_{imp}	Decontamination Factor by inertial impaction	[-]
DF_{inj}	Decontamination Factor in the injection zone	[-]
DF_m	Modelled Decontamination Factor	[-]
DF_{rise}	Decontamination Factor in the rise zone	[-]
DF_{sc}	Decontamination Factor by steam condensation	[-]
DF_{trans}	Decontamination Factor in the transition zone	[-]
Eff_{imp}	Efficiency of deposition by inertial impaction	[-]
f_b	Frequency of bubble departures	[Hz]
f_G	Frequency of globule formation	[Hz]
f_{max}	Maximum frequency of bubbles formation	[Hz]

Fr	Froude number: $\mathrm{Fr} = \frac{U_b}{\sqrt{g\, d_b}}$	[-]
G	Gravitational acceleration	[m.s^{-2}]
H_{pool}	Submergence of nozzle / Level of water in the pool	[m]
k_m	Mass transfer coefficient	[m.s^{-1}]
l	Length of bubble's curve	[m]
L_{inj}	Length of the injection zone	[m]
L_{rise}	Length of the rise zone	[m]
L_{trans}	Length of the transition zone	[m]
$\dot{m}_{in}$	Inlet aerosol mass flowrate	[kg.s^{-1}]
$\dot{m}_{out}$	Outlet aerosol mass flowrate	[kg.s^{-1}]
p	Binarized pixel value	[-]
Q_{inj}	Injected air volume flowrate	[m^3.s^{-1}]
Q_{exp}	Experimental flowrate ($Q_{exp} = V_G \times f_G$)	[m^3.s^{-1}]
r	radial distance in the injection zone	[m]
r_b	Bubble radius	[m]
Re_b	Bubble Reynolds number: $Re = \frac{U_b\, d_b}{\nu_l}$	[-]
Re_O	Nozzle Reynolds number: $Re = \frac{D_0\, U_{inj}}{\nu_g}$	[-]
S_G	Surface area of globule volume in the injection zone	[m^2]
$S_{g,\ rise\ zone}$	Surface area of gas in the bubble rise zone	[m^2]
S_r	Surface area of bubble volume in the rise zone	[m^2]
St	Stokes number $St = \frac{\rho_p\ {d_p}^2\ U_{inj}}{18\ \mu_g\ D_0}$	[-]
Str	Strouhal number $Str = \frac{f_G\, D_0}{U_{inj}}$	[-]
t	Time	[s]
t_b	Time for bubble growth and departure	[s]
t_{res}	Total residence time of gas bubbles in the pool	[s]
Δt_{inj}	Residence time of gas bubbles in the injection zone	[s]
Δt_{rise}	Residence time of gas bubbles in the rise zone	[s]
T_{gas}	Gas temperature	[°C]
T_{pool}	Pool temperature	[°C]
U_b	Bubble velocity	[m.s^{-1}]
U_d	Drift velocity	[m.s^{-1}]
U_G	Globule rising velocity	[m.s^{-1}]
U_{inj}	Gas injection superficial velocity	[m.s^{-1}]
U_{rel}	Bubble relative velocity	[m.s^{-1}]

U_r	Bubbles terminal velocity in the rise zone	[m.s^{-1}]
U_{Trans}	Bubbles rising velocity in the transition zone	[m.s^{-1}]
V_b	Bubble characteristic volume	[m^3]
V_G	Globule volume	[m^3]
$V_{g,\ rise\ zone}$	Gas volume in the bubble rise zone	[m^3]
V_r	Bubble volume in the rise zone	[m^3]
We	Nozzle Weber number: $We = \frac{\rho_g {U_{inj}}^2 D_0}{\sigma}$	[-]
We_s	Weber number for single bubbling regime	[-]
$We_{critical}$	Critical Weber number	[-]
x_{gc}	Distance travelled by geometric center of bubble	[m]
Y	Altitude above the nozzle	[m]

Greek symbols

α	Void fraction in the injection zone	[-]
ε_g	Void fraction in the rise zone	[-]
ρ_g	Gas density	[kg.m^{-3}]
ρ_l	Liquid density	[kg.m^{-3}]
ρ_p	Particle density	[kg.m^{-3}]
σ	Surface tension	[N.m^{-1}]
σ_g	Standard deviation	[-]
τ	Average residence time	[s]
ν_l	Liquid Kinematic viscosity	[m^2.s^{-1}]
ν_g	Gas Kinematic viscosity	[m^2.s^{-1}]
μ_g	Gas dynamic viscosity	[Pa.s]
μ_l	Liquid dynamic viscosity	[Pa.s]

General Introduction

The nuclear power plants continue to be an essential resource of the electrical energy production. Its contribution in world's energy is expected to increase in parallel with its environmental impact. However, one of the major concerns of nuclear reactors is the deployment of nuclear safety principles and measures. Indeed, there are many postulated severe accident sequences that can lead to a release of hazardous materials, which actually has already happened in Three Mile Island 1979, Chernobyl 1986, and Fukushima 2011. The nuclear facilities are therefore designed, constructed, and operate in such a way as to prevent potential abnormal and emergency situations and limit their hazardous consequences.

Many expert organizations have expressed their interest on increasing the knowledge on accident management and filtration systems, to lower the uncertainties on the interpretation of severe nuclear accidents and optimize the efficiency of deployed safety measures in nuclear power plants. One of the leading organizations is Institut de Radioprotection et de Sureté Nucléaire (IRSN) which is French public expert in the assessment and prevention of nuclear and radiological risks. IRSN has launched projects within the international framework in order to enhance the efficiency of filtration systems and has participated to different international projects [1-3]. Moreover, IRSN has been also pioneering in European projects such as PASSAM project [3] and the IPRESCA project [4]. This intensive French collaboration is due to the fact that nuclear power is a major source in France as it delivers about 75% of its electricity from nuclear energy derived from 58 Nuclear power plants (NPP), which have employed Filtered Containment Venting system (FCVS), based on sand bed filters, by 1990s [5]. However, there are ongoing efforts in France to upgrade progressively the French safety features in order to face the risks of any nuclear severe accident, and this comprises the feasibility study of other filtration systems

The featuring of nuclear power plants with accident management systems aims mainly at mitigation and reducing the release of fission products into the environment. Mitigation, hence, refers for all processes that may lead to the trapping and retention of containment atmosphere, thus, reducing the potential risks of radioactive material release into the environment. Efficient engineering systems for fission products retention are containment sprays, suppression pools in boiling water reactors, and filtered containment venting systems FCVS in pressurized water reactors.

FCVS installed in some NPPs containment are effective in condensing steam or removing heat from the containment atmosphere, reducing containment pressure, and reducing the amount of fission products released to the environment. The efficiency of these systems is expressed in terms of Decontamination Factor DF, which is defined as the ratio of the quantity of fission products at the inlet to the outlet of the filtration system. The retention process of radioactive substance is a serious concern in the evaluations of the source term and the post-management of the accident. This concerns notably the pool scrubbing, which is a filtration mechanism occurring in wet filtered containment venting systems FCVS, and also encountered following the steam generator tube rupture SGTR, where fission products could be directly released from the primary circuit to the secondary circuit.

Pool scrubbing refers to the mechanisms which lead to the retention of radioactive fission products, in the aerosol form and in the gaseous form, from being carried into the containment atmosphere or to the environment. The injection of the carrier gas through the pool leads to the formation of bubbles and, during their rise along the pool, fission products can reach the bubble surface due to aerosol deposition mechanisms and mass transfers for gaseous species and then, are trapped in water. Among the removal mechanisms and mass transfer from, the hydrodynamics' aspects of the flow possess a significant contribution to the filtration and scrubbing efficiency.

The investigation of pool scrubbing began in the late 1960s and early 1970s. It was extensively investigated in the 1980s' and 1990s' in several large research programs [6]. These investigations provided valuable insights into the effects of variables like particle type and size, gas flow rate, submergence, and carrier gas composition, on the decontamination factor. Most of these investigations were integral in nature and were carried under bubbly regime and jetting regimes. Upon these experimental programs, the most common pool scrubbing codes (SPARC, BUSCA, SUPRA) were developed on the established databases (Owczarski et al., 1985 [7]; Ramsdale et al., 1995 [8]; Wassel et al., 1991 [9]). As a result, calculations by both stand-alone and integral code models indicated good agreement with simple experiments for integral retention, however, the models didn't estimate the retention with more complicated geometries in the water pools. This is due to the fact that the models have been developed upon different assumptions for the simplification of the problem.

A general conclusion from these documents is that there still exist a number of items for which additional work is required. Therefore, a comprehensive characterization of the two-phase flow hydrodynamics during pool scrubbing sequences would be a necessary prerequisite for improved modelling of pool scrubbing phenomenon.

In this context, IRSN initiated experimental research within the current thesis on the experimental study of the hydrodynamics of pool scrubbing for different regimes. Two experimental campaigns were carried out, one at IUSTI-Marseille mainly for developing the hydrodynamic methods, and other at IRSN-Cadarache. The facility at Cadarache, named TYFON, was built during the thesis and it is dedicated to the examination of the pool scrubbing phenomenon. TYFON is designed to afford coupling of hydrodynamic and Decontamination Factor measurements, therefore, permitting the investigation of hydrodynamic aspects on the trapping and retention of different forms of iodine compounds (gaseous methyl iodide CH_3I, gaseous molecular iodine I_2, and caesium iodide aerosols CsI). The realized work throughout this thesis is reported in this manuscript, which is structured as follows:

Chapter I: State of art presents the context of accident managements systems in nuclear industry and highlights the pool scrubbing mechanism. The experimental programs carried out on pool scrubbing are discussed and the main conclusions of these programs are reported as well as their recommendations. After that, this chapter shows the reliance of pool scrubbing on hydrodynamics in determining its efficiency. Finally, the developed pool scrubbing codes as well as the ASTEC code developed by IRSN are presented.

Chapter II: Materials and Methods is dedicated to the description of experimental setups in IUSTI-Marseille and IRSN-Cadarache. The hydrodynamic measurements, data treatment, and experimental configurations for the decontamination factor measurements are described.

Chapter III: Hydrodynamics of pool scrubbing presents the experimental results of hydrodynamics in the injection zone. The different bubbling regimes depending on are classified and the morphologies are described. The aperiodic formation of bubbles encountered in our experiments due to the injection of gas at high flowrates, in relevance to pool scrubbing, was characterized. The hydrodynamics such as bubbles volumes, bubbling frequency, surface area, void fraction, and rising velocity are reported. This chapter also reports different investigations on the impact of pool scrubbing conditions such nozzle size, contamination of carrier gas, pool submergence on the bubble dynamics. Finally, a dimensionless analysis study is provided to characterize the bubbles formation.

Chapter IV: Decontamination factor measurements is devoted for the pool scrubbing experiments performed on TYFON facility to investigate the hydrodynamic aspects on the trapping of different iodine species. The examined iodine species were CsI in form of aerosols, molecular I_2 in gaseous form, and organic CH3I in gaseous form. The influence of pH, pool temperature, submergence, and temperature of inlet gas, gas flowrate, nozzle size on DF of the latter iodine compounds was investigated

Chapter V: Modeling Aspects reports our attempts of modeling applications on pool scrubbing using the experimental database established throughout this thesis with some supporting models from literature.

References

1- T. Albiol, L. Herranz, E. Riera, A. D. C. RSE, N. Losch, B. Azambre, C. Mun, and L. Cantrel, “Passive and active systems on severe accident source term mitigation (PASSAM project),”2017.

2- D. Jacquemain, S. Guentay, S. Basu, M. Sonnenkalb, L. Lebel, J. Ball, H. Allelein, M. Liebana, B. Eckardt, N. Losch, et al., “Oecd/nea/csni status report on filtered containment venting,” tech. rep., Organization for Economic Co-Operation, and Development, 2014.

3- B. Clément and B. Simondi-Teisseire, “Stem: An IRSN project on source term evaluation and mitigation, “Transactions, vol.103, no.1, pp.475–476, 2010

4- S. Gupta, L. Herranz, and J. Van Dorsselaere, “Integration of pool scrubbing research to enhance source-term calculations (IPRESCA),” in The 8th European Review Meeting on Severe Accident Research, Warsaw, Poland, 2017.

5- M. Bal, R. C. Jose, and B. Meikap, “Control of accidental discharge of radioactive materials by filtered containment venting system: A review,” Nuclear Engineering and Technology, vol.51, no.4, pp.931–942, 2019

6- Swiderska-kowalczyk, M., et al., *State-of-the-art review on fission product aerosol pool scrubbing under severe accident conditions*, 1996, Institute of Nuclear Chemistry and Technology: Poland. p. 48.

7- Owczarski, P. C., R. I. Schreck, and A. K. Postma. *Technical bases and user's manual for the prototype of a Suppression Pool Aerosol Removal Code (SPARC)*. No. NUREG/CR-3317; PNL-4742. Pacific Northwest Labs., Richland, WA (USA), 1985.

8- S. A. Ramsdale, S. Güntay, and H.-G. Friederichs, “Busca-jun91 reference manual,” tech. rep., Paul Scherrer Inst. (PSI), 1995.

9- Wassel, A. T., et al. "SUPRA: Suppression Pool Retention Analysis Computer Code." *Report EPRI NP-7518-CCML* (1991).

Chapter I: State of art

I.1. Safety measures in nuclear power plant

I.1.1. Introduction

Nuclear power is based on nuclear fission reactions that involve risks of emitting high levels of radioactivity, which its exposure results in health and environmental hazards. Along the continuous role of nuclear power in producing electricity, the public concern in the safety of nuclear plants continues especially after the occurrence of several accidents. This assures the importance of sophisticated safety measures implied and implemented in nuclear facilities.

I.1.2. Safety measures and concept of defense in depth

Nuclear power plants are designed with multiple back-up safety measures and diverse accident management systems as part of an approach of safety, called "defense-in-depth"[1-3]. This approach comprises the set of procedures and protocols, technical regulations, and management systems taken to protect the health and safety of workers, public, and the environment. These safety measures are considered in the whole life of nuclear facility from its design and construction, during its operation, and until the decommissioning and dismantling. Thus, three main axes are involved in the implemented safety measures during the different life phases [1]:

- First, ensuring normal operation of nuclear facility without excessive exposure for workers and excessive releases of radioactivity to the environment.
- Second, applying technical regulations to prevent possible incidents and accidents.
- Third, implementing of accident managements systems to mitigate the consequences of incidents and accidents, such as the release of radioactivity.

I.1.3. Barriers against release of radioactivity

Beside the accident management systems aforementioned in the third axis of this approach, multiple successive physical barriers exist to avoid the release of radioactive products in case of accident prevention failures [3]:

- The primary barrier is the fuel rod cladding, where radioactive fission products are generated, that is designed to contain radioactive material under the extreme conditions inside the reactor core.
- The secondary barrier is the reactor coolant system (RCS) that contains all the fuel elements and coolant (water) used to carry away heat for generating electricity.
- The final barrier is the primary containment building, a concrete and steel dome, which is designed to mitigate the release of radioactive material if both the primary and secondary barriers are compromised. The primary containment is supposed to withstand stresses resulted by most severe event.

Assuring the integrity of each of these physical barriers in any accident scenario constitutes the defense in-depth approach against the release of radioactivity to the public and environment [4].

I.1.4. Nuclear accidents and release of radioactive products

Since the 1955 Geneva conference to assess safety of nuclear facilities, which was the first gathering of nuclear reactor scientists from all around the world, several accidents have occurred [1]. These accidents are measured in severity according to the International Nuclear and Radiological Event Scale (INES) established in 1990 by the International Atomic Energy Agency (IAEA). According to the IAEA, “Events are classified on the scale at seven levels: Levels 1-3 are called 'incidents' and Levels 4-7 'accidents'” [5]. The scale is designed so that the severity of an event is about ten times greater for each increase in level on the scale. Two major accidents have occurred until now (level 7):

- The first accident is Chernobyl nuclear accident (26 April 1986), which is considered the worst nuclear accident ever in terms of death toll and cost. One of the reasons leading to the severity of this accident is the non-existence of containment building (third barrier) enclosing the RBMK reactors, used in Chernobyl NPP (see Figure I.1).

Figure I.1- The destroyed building of Chernobyl NPP, which design did not implement a containment building to enclose its reactor.

- The second accident is the Fukushima nuclear accident (11 March 2011), which is the most recent severe accident. All the Fukushima accidents were initially classified as Accident Level 4 on the IAEA scale; but it was later raised Level 7 after the release of iodine and cesium was measured [1, 6] (see Figure I.2).

Figure I.2- Release of fission products from Fukushima NPP.

Other accidents are the Kyshtym (29 September 1957, level 6), Windscale fire (10 October 1957, level 5), Three Mile Island TMI-2 (28 March 1979, level 5). The significant parameter in the classifying of the severity of these accidents was the radioactivate emissions and release of radioactive products.

I.2. Source term and release of fission products

I.2.1. Source term

The amount of radioactive materials released from the core into the containment and the environment following an accident is referred as source term. It is widely used term in industrial safety studies related to risk and environmental impact assessment analyses [2, 3]. Due to the significant consequences of such releases into the environment, and in accordance with the defence-in-depth approach, the evaluation of the source term is essential for the assessment of accident risks.

I.2.2. Fission products

The radioactive materials include fission products (FPs), activation products from core structural materials, and heavy nuclei such as uranium elements [1]. FPs, which are generated during the operation of fission reactor, are responsible for the most of core decay heat and the radioactivity that could be released into the environment.

I.2.3. Transport of fission products from the core into the environment

If an accident occurred leading to the failure of the first barrier (cladding), FPs are firstly released from the degrading core into the reactor coolant system. Then, if the second barrier fails, FPs are transported to the containment with physical and chemical characteristics and forms acquired during their presence in the reactor coolant system. The containment building is the final barrier before the release of the fission products into the environment. Finally, if the containment is subjected to loads that exceed the temperature and pressure conditions adopted for its design, it fails and loses its integrity and fission products are then likely to be released into environment.

I.2.4. Forms of fission products

Fission products can present in various chemical forms of gases and suspended aerosols [4, 7]. The form in which they are released depends on the equilibrium with their condensed phase in the fuel. This equilibrium varies during the accident, mainly due to variations in temperature, pressure, and oxidizing-reducing conditions. Some fission products may shift from one chemical state to another depending on the temperature of fuel, the oxygen content in the fuel, and the burnup rate. For example, fission products in form of aerosols are notably generated due to core-concrete interactions, pool boiling, or vapor condensation [7]. Notable exception are iodine and ruthenium, which can in certain circumstances remain in the gas form [4].

The impact of radioactive fission products, under accident conditions, is dependent on their degree of volatility. According to the analytical experiments of the VERCORS program and the integral tests of the PHEBUS program [8], fission products are classified into categories of volatility. There are the volatile, semi-volatile, low-volatile, and non-volatile fission products,

regardless of their scope of activity. It is reported that the main fission products that are believed to be released into the environment in case of nuclear accident are iodine (volatile), caesium (volatile), tellurium (volatile), xenon (volatile), and ruthenium (low volatile) [1-4, 7, 8].

I.2.5. Release of iodine compounds

In the composition of released radioactive elements, iodine (isotopes 133 and 131) is considered as one of the most worrying fission products, mainly due to its highly volatile nature from the degraded core and large radiological consequences to the environment and human health [6, 7]. Presence of relatively high concentrations of iodine (^{131}I) leads to over absorbed doses in thyroid gland, which causes cancer disease.

Studies of iodine behaviour in containment under accident conditions have identified a variety of chemical and physical interactions, which determine the forms of iodine and environments where radiochemical reactions may occur. It exists in volatile forms, especially I_2 and organic iodine such as CH_3I which is the most volatile. Moreover, based on severe accident measurements used to assess the chemical forms of iodine in containment, caesium iodide (CsI) is considered to be one of the dominant iodine aerosols form to be released as experimentally shown in the CHIP/CHIP+ programs [9-12].

For that, the transport of volatile FPs such as short-lived isotopes of iodine (^{133}I, ^{134}I, and ^{131}I) and caesium (^{134}Cs and ^{137}Cs) have been the issue of many international programs [13-16] to study and evaluate their retention and releases into the environment following a nuclear accident.

I.2.6. Mitigation of releases to the environment

Despite the emergency operation procedures, there may be certain cases where severe core damage or large fission product releases can still occur. In these cases, the third principle of defense in depth concept is addressed. The featuring of NPPs with accident management systems aim mainly at reducing the release of fission products into the environment. Safety-engineered systems can also lower the concentration of radioactive materials in the containment atmosphere before their release [2]. Mitigation, hence, refers for all processes that may lead to the trapping and retention of containment atmosphere and reduce the potential risks of radioactive material release into the environment. Efficient engineered systems for FPs removal are containment sprays, suppression pools in boiling water reactors, and filtered containment venting systems FCVS in pressurized water reactor.

I.2.7. Filtered containment venting systems FCVS

In managing the consequences of a nuclear accident, the overarching goal is always to protect people, both on-site and off-site, while bringing the reactor (and associated systems) back to a safe state. Actually, in case of severe accident, two antagonistic objectives must be completed:

- Limit the increase of pressure in the containment to maintain its integrity,
- Avoid the propagation of FPs outside the containment (to the environment).

Thus, the objectives of a FCVS installation are first to maintain the containment integrity by reducing its over pressurization by venting its atmosphere through a depressurization line, this also enhance the capability to maintain core cooling; second, to reduce the activity emission out of the containment to the environment and avoid large contamination and negative health effects, by possessing a filtration capacity.

After the Chernobyl nuclear accident, different European countries mandated the implementation of FCVSs by formulating regulations [17]. Then, after the Fukushima Daiichi nuclear accident, safety evaluations were performed, where severe accident mitigation systems received additional and major attentions. Since the latter accident, many states considered the implementation of filtered containment venting systems (FCVSs) at nuclear power plants where they were not yet applied, and on the other hand, their upgrading and enhancement at countries where they were already installed. At present, several new types of FCVSs have been developed, and most of them can be classified into three types: dry type, sand bed, and wet type [2, 3].

Some critical aspects for the dry solid filters were addressed such as the filter clogging and the reduced filter efficiency in wet conditions. On the other hand, sand bed filters (plus metallic pre-filters) showed-out inefficient for gaseous molecular and/or organic iodides; moreover, it was demonstrated that caesium iodide aerosols trapped in the sand filter during a severe accident are unstable allowing a potential delayed source term [18, 19]. Whereas critical aspects for the liquid scrubber filters were the filter efficiency and its maintenance for a prolonged use close to saturation conditions in severe accident situations [2].

Wet FCVSs are generally sort of integral large vessels, filled up to certain height by water or alkaline solution (pH ≈ 12), and in its upper level contain sections of sorbents and metallic fibers for the retention of fission products [17]. The system is located outside the containment and inserted in the depressurization line before the stack (see Figure I.3) [3]. In this figure, the FCVS and containment doesn’t respect the scale, as the containment is much larger than the FCVS vessel.

The venting of the atmosphere and contaminated gas (coming from the containment), through scrubbers or nozzles into the pool of the water in the FCVS, leads to the formation of bubbles or jet of air. During the residence of air bubbles inside the pool and before outflowing, fission products in different forms can be transferred and trapped into the water pool. This phenomenon of fission products retention in the pool is known as pool scrubbing [2, 16, 18].

I.2.8. Case of Steam Generator Tube Rupture (SGTR) in PWR

Pressurized water reactors PWRs use steam generators, large heat exchangers, that convert water into steam using heat produced in the reactor core. Inside the steam generators, hot radioactive water of the primary loop (RCS) is pumped through tubes (each steam generator can contain from 3,000 to 16,000 tubes, each about three-quarters of an inch in diameter) under high pressure to prevent it from boiling [20]. The water flowing through the inside of the tubes then heats non-radioactive liquid water on the outside of the tubes. This produces steam that turns the blades of turbines to make electricity in the secondary loop.

The steam is subsequently condensed into water and returned to the steam generator to be heated once again. These tubes have an important safety role because they constitute one of the primary barriers between the primary and secondary loops (i.e., radioactive and non-radioactive sides) of the plant. There is the potential risk that if a tube bursts while a plant is operating, radioactivity from the primary coolant system could escape directly to the atmosphere in the form of steam via the opening of the atmospheric valves of the steam generator (see Figure I.3) [20-22]. This accident scenario is referred as steam generator tube rupture (SGTR), where fission products leak from the primary circuit to the secondary side then bypassing the containment. These accident scenarios are very unlikely, but, given the potential consequences of a direct path for FPs from the primary coolant system to the environment, they are estimated to be important risk contributors. For this reason, the integrity of the tubing is essential in minimizing the leakage of water between the two "sides" of the plant. Moreover, many research programs were launched to assess and evaluate the accident scenarios of SGTR, more specifically, the release of fission products into the environment following this accident [22-25]. In case of discharging pressurized water, in the form of steam, into the non-radioactive water surrounding the tubes, the phenomenon of pool scrubbing is presented but within different conditions than that encountered in FCVS [24, 25] (will be detailed in the following paragraph).

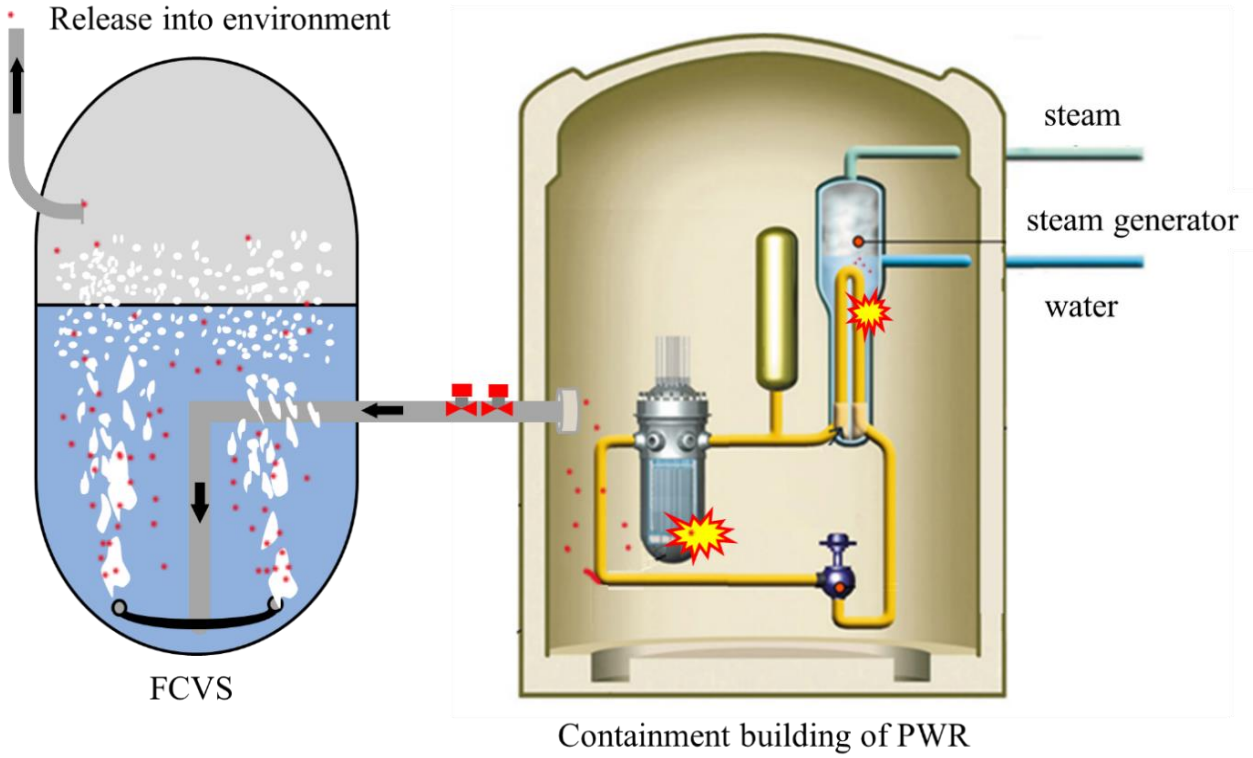

Figure I.3- Schematic presentation of pool scrubbing situations in case of FCVS and SGTR.

I.3. Concept of pool scrubbing

As it has been discussed, pool scrubbing occurs in FCVS as a filtration phase, introduced in this accident management system. Moreover, it may intervene in accident scenario in case of SGTR, as shown in Figure I.3. In nuclear industry, pool scrubbing refers to the removal of radioactive materials, present in the gas, by trapping them in liquid pool.

Several severe accident scenarios involve transport paths of fission product which include passages through stagnant pools of liquids, where pool scrubbing can occur (cases of BWR or PWR reactors). This phenomenon has been considered to be a potential reduction of the source term and plays a very important role in the mitigation of severe nuclear accidents involving the release of radioactive species to environment.

The concept of pool scrubbing as filtration mechanism was widely spread after the accident of the Three Mile Island TMI-2 [4, 7], where many NPPs aimed at installing FCVSs to mitigate the radiological consequences of core meltdown accidents. The Chernobyl accident (26 April 1986) brought additional attention to the issue of source term mitigation [4, 7, 14, 26].

Hence, pool scrubbing was extensively investigated in the 1980s and 1990s in several large research programs [27-34]. During this period, many status reports and proceedings considering the characterization of pool scrubbing were published. In this period, research institutes and organizations realized experimental programs and developed, upon the established experimental databases, pool scrubbing codes (will be discussed in the following graphs). Despite that most of developed codes in the 1990s haven't shown good predictions [15], the pool scrubbing mechanism showed a high efficiency of trapping fission products especially aerosols. The efficiency of pool scrubbing is expressed in terms Decontamination Factor DF, which is defined as the ratio of fission products mass flowrate between the inlet and the outlet of the liquid pool.

$$DF = \frac{\dot{m}_{in}}{\dot{m}_{out}} \quad (1)$$

Uncertainties on the characterization of pool scrubbing led to many organizational recommendations, aiming at setting better research approaches [3, 15]. However, the period from the beginning of 2000s until the accident of Fukushima (11 March 2011) witnessed a sharp decrease in the rate of research on pool scrubbing. This can be obviously noticed at the number of articles and technical/organizational reports published on this issue and can be justified by the tolerance of basic pool scrubbing codes at that time.

Post the accident of Fukushima (11 March 2011), many follow-up actions were taken notably considering the implementing and enhancing of FCVSs [2, 3, 6, 13, 26, 35]. Therefore, organizational interests reinitiated research programs on improving safety measures and programs within an international framework were launched, in order to better characterize the mechanism of pool scrubbing. Beside the international programs, many experimental benches were built, at many public and private institutes for particular research interests.

It is worth saying that there is difference between the experimental objectives adopted before 2000s and after Fukushima. Regardless of the experimental setup and enhanced techniques, the aim of experimental programs and approaches changed significantly. In the following paragraph, where experimental programs on pool scrubbing are considered, this remark is ought to be clarified.

I.4. Experimental programs on pool scrubbing

Experimental programs were performed mainly between 1980s and late 1990s, and post Fukushima. Due to the difference of research approach between these two periods, the experimental programs will be discussed as the following:

I.4.1. Experimental programs before 2000s

First, pool scrubbing was like a topic to discover, and which efficiency had to be examined. Experimental programs were performed to investigate the importance of parameters and their influence on the efficiency of pool scrubbing. In Table I.1, the pool scrubbing programs before 2000s are presented with their corresponding ranges of test parameters and decontamination factor measurements.

Table I.1- Ranges of decontamination factor measurements and tests parameters of the realized experimental programs before 2000s.

Exp. program	Species used	Aerosol size d_{ammd} (µm)	Gas	Steam mass fraction %	Pool temp. (°C)	Pool pressure (bar)	Injector type	DF
GE [27]	CsI	< 0.3	Air	0	20.	Atm.	Single nozzle	7 - 10
EPRI [28]	CsI TeO_2 Sn	0.2 – 3.0 0.4 – 2.7 2.7	Air, N_2 + steam	0 – 95	20 - 100	Atm.	Single nozzle	1.4 - 1600 110 - 6800
ACE [29]	CsI CsOH MnO	1.7 – 2.7 1.6 – 2.8 1.7 – 2.3	N_2	0.8 - 31	25 - 83	Atm.	Sparger	145 - 3000 11 - 260 47 - 1500
LACE-Espana [30]	CsI	1.7 – 7.2	N_2 + steam	7 – 85	110	3 bars	Single nozzle Multi-nozzle	16 - 3000
EPSI [31]	CsI	4.5	steam	1	273	11 bars	Single nozzle	2100 - 3300
JAERI [32]	DOP	0.3 – 10	Air	0	20	Atm.	Single nozzle	10 – 150
UKAEA [33]	I_2 vapour	-	Air + steam	0 - 100	20	Atm.	4 nozzles	14 - 240
POSEIDON [34, 36]	I_2 vapour	-	N_2	0	20 - 60	Atm.	Single nozzle Multi-nozzle	20 - 3×10^5

Owing to the importance of efficiency evaluation, and its dependence on many conditions and parameters, different pool scrubbing benches were designed and built. An experimental bench on pool scrubbing comprises three main systems:

- The generation system of gaseous/aerosols species which are supposed to imitate the FP.
- The pool (or bath, containing the injection system) where FPs are injected.
- The sampling system that is located after the pool to analyze/measure the outflow of FPs.

Despite the large experimental programs and due to the wide range of conditions that might occur during an accident event, a lack of systematic analysis of pool scrubbing was reported in the status reports and articles in late 1990s/beginning of 2000s.
Different chemical species were examined, this includes different iodine compounds (Caesium iodide, methyl iodide, elemental iodine) and oxide compounds (Caesium hydroxide, Tellurium dioxide, Manganese oxide, Tin oxide). Throughout the following review, we mainly concentrate on iodine compounds.

GE experiments (1981 – 1984)
General Electric is a private company that invested its own funds to develop the BWR as a commercial NPP (the NPPs in Fukushima Daiichi accident were BWRs manufactured by General Electric). For that, it was implied in the safety research of nuclear accident management systems. The aim of the GE experimental program [27] was to evaluate the effect of bubble size on the decontamination factor in BWR context, as a result of which the tests were performed in the isolated bubbly regime. Moreover, they realized hydrodynamics measurements in pool scrubbing conditions.

EPRI experiments (1982 - 1986)
The Electric Power Research Institute aimed at experimentally quantifying the effectiveness of BWR suppression pools in scrubbing aerosols from mixtures of steam and non-condensable gases (such as nitrogen).

The experimental program [28] was distinguished by comprising both hydrodynamic and aerosol scrubbing tests. Researchers performed hydrodynamic tests to determine parameters required for mathematical modelling of aerosol trapping. In the scrubbing experiments, measurements of aerosol characteristics such as size distributions and concentration at the inlet and outlet permitted quantification of the pool decontamination factors for several injection geometries and a wide range of test conditions. The parameters that were varied systematically included particle size, injector submergence, injection velocity, steam fraction, and water temperature. The results give some trends in decontamination factor as a function of the varied parameters. These data provide a valuable basis for assessing the adequacy of the SUPRA pool scrubbing code (detailed later).

ACE: Advanced Containment Experiments (1985 - 1989)
This was an international experimental program, managed by EPRI [29]. The experimental campaigns addressed different areas of nuclear accident managements systems, such as vented containment concepts, of which pool scrubbing was a main part. The temperature of the water

pool was set between 24 °C and 84 °C, whereas the pool pH was modified by buffering with boric acid and NaOH. The latter ranged between 8.9 and 10.

The results showed high efficiency of pool scrubbing, although it differed from species to species (CsI, CsOH, MnO), relying on the physical and chemical behaviours of the aerosol. Moreover, and opposite to expectations, DFs that were obtained with experiments with hot pools were higher than cold ones. This was recommended to investigated in later tests. Moreover, they observed an increase of DF with increasing steam fractions and deeper sparger submergence.
However, Berzal et al.[15] considered that these tests encountered uncertainties regarding the composition of aerosol carrier gas when it was injected into the pool. These uncertainties randomly varied between a test and another.

LACE-Espana experiments (1990 - 1992)
Light water reactor Aerosol Containment Experiments LACE-Espana is a Spanish experimental program consisting of eleven experiments performed to investigate the influence of different variables on aerosols pool scrubbing [30]. The main objective of these experiments was to determine the experimental decontamination factor of BWR suppression pools under accident conditions and to validate the pool scrubbing codes (BUSCA and SPARC). Hydrodynamic measurements were also performed for bubbly regime tests (defined in section I.5). The experiments were performed with an initial pool water temperature of 110°C, a temperature of the gas above the pool also of 110°C, and pool pressure around 3 bars. They reported a potential retention of large particles (1.7 - 7.2 µm). Moreover, an increase in DF by a factor of 10 with higher steam fractions was observed, which agrees with other experiments.

The comparison of their obtained experimental results with calculations obtained using the available pool scrubbing codes (mainly SPARC) showed discrepancies and deviations in the trend of decontamination factor.

EPSI experiments (1992)
These experiments were managed by the Japan Atomic Energy Research Institute JAERI [31]. EPSI stands for Experimental facility for Pool Scrubbing Investigation, that mainly aimed at studying the dependence of the decontamination factor on pool pressure and temperature. More specifically, the goal was to obtain experimental data on the effect of high pressure and high temperature on pool scrubbing behavior.

JAERI experiments (1988 – 1996)
The Japan Atomic Energy Research Institute (JAERI) carried out pool scrubbing experiments to quantify the efficiency of pool scrubbing in different cases of BWRs or PWRs [32]. Experiments were performed at ambient temperature and pressure. They investigated the injector submergence, gas flow rate, and aerosol concentration. The dependence of the increase of the DF with rising submergence was more significant for low aerosol concentrations. The DF was reported to increase with the inlet gas flow rate.

UKAEA experiments (1986 – 1996)
A series of tests were performed to investigate the retention of fission products at the United Kingdom Atomic Energy Authority UKAEA, to study the steam suppression system [33]. All the tests were carried out in the jet regime (defined in section I.5). Nevertheless, it was not

possible to correlate the tests and provide systematic analysis, in order to draw hydrodynamic conclusions. This is due to the fact that the studied parameters influenced other phenomena affecting the decontamination factor.

The objective of this experimental program was to investigate the elimination of iodine species by varying its fraction in inlet carrier gas, the effect of injector size, steam flowrate, the nature of gas in the flow, and submergence of injection system. The pool temperature during the experiments was cold (i.e., 0-l0°C), and its pH of the water was 6.8.

The conclusions drawn from these experiments were not similar and opposing the results found in the previous experiments, regarding the influence of parameters on the decontamination factor (no dependence on steam fraction).

For example, they reported that steam fraction had no influence, whereas this parameter was reported to increase the DF in ACE, EPRI, and Lace-Espana experiments. They justified that it was due to growth of particles by condensation when saturated steam was mixed with cold air. However, without specifying the inlet gas temperature, this is difficult to confirm. Moreover, they reported a decrease in DF with the increase of injection flowrate, which was not the case in EPRI and JAERI experimental programs.

POSEIDON experiments (1998 - 1999)
An experimental program was carried out at PSI in the POSEIDON facility (Pool Scrubbing Effect on Iodine DecontaminatiON), to assess aerosol and iodine retention models in integral computer codes mainly BUSCA, but also SPARC and SUPRA [34]. Code computations were compared with data from POSEIDON tests and the aforementioned experimental programs.

The objective was to enhance the knowledge on the iodine removal phenomena by characterizing the hydrodynamics phenomena involved. Around 100 tests were performed and the mainly investigated parameters were the pool submergence, size of nozzle (injection system), and pool temperature. Their observations consolidated the findings of previous experiments, especially regarding the impact of pool submergence.

Results of computer simulations with the BUSCA code show a fair agreement with the data at low pool heights (with low DFs) but are non-conservative for larger heights. Post-analysis of these experiments led to recommendations to better characterize the hydrodynamics of the flow especially in the churn-turbulent flow regimes.

Comments
These experimental programs have provided large experimental databases for pool scrubbing, comprising both hydrodynamics and decontamination factor measurements. Berzal et al. 1995 [15] discussed some common influences of the experimental parameters on the pool scrubbing experiments, however these conclusions were controversial in a way or another. In chapters 3 and 4 of this report, some of these relevant experimental databases obtained through these programs are compared and discussed with those obtained throughout this PhD program.

In fact, the main firm conclusion that can be drawn from these experiments is the global efficiency of filtration by pool scrubbing, mainly for aerosols and elemental iodine I_2, even if the range of results is wide ($\sim 10 \leq DF \leq \sim 10^5$). This latter point can be explained by the

diversity of parameters and variables studied in these campaigns: i.e., the chemical species and concentration, particles size (aerosols), gas flow rate, steam mass fraction, water submergence above the sparger or nozzle, injector diameter, injector type, pool temperature, pool pH, and pool pressure. These parameters induced differences in the type of study, explaining that the decontamination factor measurements were dependent on test conditions.

For that, the experimental databases were not sufficient to draw other firm conclusions than mentioned above. In other words, systematic analysis of pool scrubbing phenomenon had to be improved at this time.

On the other hand, the experimental campaigns have not characterized the overall phenomena, especially what is implied in hydrodynamics of bubbles. Despite the satisfactory comparison of pool scrubbing codes and experimental measurements in some cases, the code's validity extended only over the conditions encompassed by the data they were based on. Considering the different aspects imposed by the accident conditions on the pool's capacity of retention, it was recommended to better characterize the variation of physical and chemical aspect with flow conditions through additional experimental programs.

I.4.2. Experimental campaigns programs after Fukushima (2011)

The Fukushima accident has shown the vulnerability of nuclear facilities in the event of extreme and multiple natural aggressions. The integrity of nuclear facilities was back to light, this includes the design basis (earthquakes, floods) and safety measures. For example, the design basis of Fukushima plant considered safety analysis up to an earthquake of 8.2 intensity on Richter scale and a tsunami of 5 meters wave, whereas the occurred earthquake measured 9.0 and the tsunami induced by the earthquake elevated around 14 meters [1]. To avoid the reoccurrence of such accidents, additional improvements and enhancement of defence-in-depth concept are required.

On international level, the accident led to stricter safety measures and to the launching of new research programs. Two international programs were launched during the past 10 years that focused on source term mitigation, where pool scrubbing was mainly addressed. The PASSAM European project (2013-2016) [16] that aimed at broadening the knowledge through experimental research, establishing experimental database, and then enhancing existing pool scrubbing codes. The other project was IPRESCA (2018-2020) [37] which aimed at achieving new/improved models which could be implemented in codes such as ASTEC (see section I.7.3).

Moreover, one of the most important lessons learned from the accident is that wet FCVS can be crucial for effective accident management during severe accidents [2, 3]. Experimental campaigns on pool scrubbing were back again, in different countries where NPPs are installed.

These experimental campaigns were oriented towards the sensitivity analysis of pool scrubbing parameters and improving developed codes, rather than testing the efficiency of global pool scrubbing. Therefore, test matrices were planned in a way to determine the decontamination factor as function of one/several variable/s, with the other variables as parameters. Thanks to

many benches built at many sites, experimental databases are now increasing significantly. Some of these experimental benches are presented in Table I.2.

Table I.2- Realized experimental programs after the accident of Fukushima.

Institute/University	Name of facility	Main investigations	Situation of pool scrubbing
RSE [16, 38]	SCRUPOS	DF measurements + Hydrodynamics	FCVS
CIEMAT [24, 39]	PECA-SGTR	DF measurements + Hydrodynamics	SGTR
CIEMAT [40]	PECA-PS	DF measurements	FCVS
PSI[25, 41]	TRISTAN	Hydrodynamics	SGTR
PSI [42]	Mini-VEFITA	DF measurements	FCVS
KAIST [43, 44]	Two Pool scrubbing experimental facilities	DF measurements	FCVS
KAIST [45]	/	Hydrodynamics	FCVS
KAERI [46]	ARIEL	DF measurements	FCVS
KAERI [47]	/	DF measurements	FCVS
Juelich research center [48]	SAAB	DF measurements	FCVS
Shanghai Jia Tong university [49]	SAPOS	DF measurements	FCVS
Becker technologies [50]	THAI	DF measurements	FCVS
University of Tsukuba [51]	/	Hydrodynamics	FCVS
Harbin Engineering University [52]	/	DF measurements + Hydrodynamics	FCVS
Tokyo institute of technology [53]	/	Hydrodynamics	FCVS
Nuclear power institute of China [54]	/	DF measurements	FCVS

In Table I.3, some investigated parameters in different experimental works are listed with their impact on scrubbing efficiency, as described by the authors. Analyzing Table I.3, one can observe that dependence of pool scrubbing on test parameters is not simple issue, where comparison between experimental outcomes should be done carefully. For example, the investigation of injection flow rate has shown opposite senses regarding the retention

mechanisms between a facility and another, which is due to the scope of test conditions and facility scale parameters. Moreover, and for the same aforementioned reason, other parameters have shown different sensitivities/trends to retention mechanism, even if they showed a unique sense (favoring or hindering) in most experimental programs (pool submergence, steam mass fraction…). For example, DF was reported to increase with submergence in different trends (linearly or exponentially) in Dehbi et al. [36] and Li et al. [49], Xu et al. [54] and Li et al. [52].

The main outcome of Table I.3 is that the accurate study of pool scrubbing necessitates the characterization of physical and chemical aspects induced by each of the test parameters.

Regarding the physical aspects of pool scrubbing, these are all the phenomena implied in the hydrodynamics of flow. In fact, the current lack of systematic analysis of pool scrubbing is a result of a poor characterization of hydrodynamics in pool scrubbing conditions. This will be described/detailed in the next paragraph.

Table I.3- Impact of test parameters on the pool scrubbing efficiency observed in the literature.

Parameter	Impact	References	Remarks/Justifications
Injection Flowrate	Favorable	Herranz et al. 2018 [40] Yoon et al. 2022 [44]	Inertial impaction
	Competitive	Li et al. 2019 [52] Woo et al. 2022 [47]	Depending on submergence Aerosol removal mechanisms
	Unfavorable	Xu et al. 2021 [54] Beghi et al. 2018 [42]	Impact of flow regime
Nozzle size	Unfavorable	Kim et al. 2021 [43]	Increase of inertial impaction and interfacial area
Submergence	Favorable	Li et al. 2021 [49] Xu et al. 2021 [54] Li et al. 2019 [52] Woo et al. 2022 [47] Lee et al. 2018 [55] Sun et al. 2019 [56]	Residence time
Aerosol size	Favorable	Li et al. 2021 [49] Xu et al. 2021 [54] Li et al. 2019 [52] Kim et al. 2021 [43] Venne et al. 2022 [48] Becker et al. 2019 [50]	$d_{ammd} > 0.1\mu m$ Aerodynamic Mass Median Diameter
	Unfavorable	Li et al. 2019 [52] Venne et al. 2022 [48] Becker et al. 2019 [50]	$d_{ammd} < 0.1\mu m$
Concentration of species	Favorable	Beghi et al. 2018 [42] Lee et al. 2018 [55]	Diffusion
	Unfavorable	Sun et al. 2019 [56]	Lower centrifugal deposition
Steam fraction	Favorable	Li et al. 2021 [49] Lee et al. 2018 [55] Woo et al. 2022 [47]	Condensation
Inlet gas pressure	Favorable	Lee et al. 2018 [55] Dia et al. 2020 [57]	Enhance entrainment

I.5. Hydrodynamics of pool scrubbing

Bubble dynamics are highly regarded in the design of modern engineering systems and present within numerous industrial applications (filtration and scrubbing systems, food industry, sewage treatment, oil/gas separators...). The study of multiphase flows continues to occupy an important place in scientific innovation. For that, attempts of describing the experimental aspects of fluid behaviour, under different flow conditions, are increasing. In nuclear industry, the knowledge of flow dynamics is essential for determining the efficiency of severe accident management systems, such as the Filtered Containment Venting Systems (FCVS).

In this concept, as pool scrubbing efficiency is largely influenced by the hydrodynamics and considering that some crucial hydrodynamic phenomena have not been properly modelled or even ignored in the codes, it is necessary to recall the different aspects of bubble behaviour in liquid pool. Throughout our work, the hydrodynamics of pool scrubbing were characterized, and they are reported in chapter III.

I.5.1. Phenomenology

A bubble plume is a core of gas bubbles, surrounded by liquid pool, induced by the injection of carrier gas through a nozzle or multi-nozzles. Regardless of nozzle type or orientation, the rising stream of bubbles expands as it entrains a vertical flow towards the pool surface.

I.5.2. Hydrodynamic zones and bubble dynamics

Different behaviors of the bubble plume could be observed as it rises and expands in the pool:

- First there is an injection zone, near the nozzle, where there is either a globule bubble formation, or a formation of jet. The flow regimes (bubbly, jet) depend on test parameters, notably the controlling parameters of flow's inertia or gas momentum. The characterization of this zone, the classification of flow regimes, and different morphologies of bubbles are discussed in III.2.

- At a certain height, where the globule or jet breaks, the flow passes in a non-steady transition zone referred as a breakup zone. This zone is characterized by large instable bubbles, which may be subjected to series of coalescences and agglomeration. The bubbles then break up and split to form a swarm of smaller bubbles.

- Finally, the presented bubble swarm introduces the bubble rise zone, which is identified as a horizontally expanding bubble plume that consists of small bubbles having a relevant size distribution and a rising terminal velocity. Based on the different phenomenology encountered in each zone, we are able to distinguish qualitatively the beginning and end of each zone.

The main physical quantities associated to the plume (comprising the three zones) are bubbles shape, velocity, and void fractions in the pool. These physical quantities, referred as bubbles dynamics, exhibit different behaviour in the zones of the pool (detailed in next paragraph), as shown in Figure I.4:

- Bubbles shape (volume, surface area, equivalent diameter): it differs depending on its size, fluid properties, and subjected momentums (velocity, buoyancy). Clift et al. [58] considered that the shape of a bubble is one of the most important factors affecting bubble motion and heat and mass transfer from the bubble into the surrounding fluid. More specifically, it is common that the key parameter for the mass transfer is the interfacial area *a*, which is dependent of the volume, surface area, and size distributions of the bubbles. Generally, bubbles shape in pool scrubbing approaches are mainly determined in the injection zone as globules' volumes and surface area (V_G, S_G). In the bubble rise zone, we referred to bubble volumes as V_r and surface area as S_r. More detailed description of globule volume can be seen in II.2.2.2, and the characterization of these parameters is discussed (see III.3.3.2 for globule volumes V_G and III.3.3.4 for surface area of globules S_G).

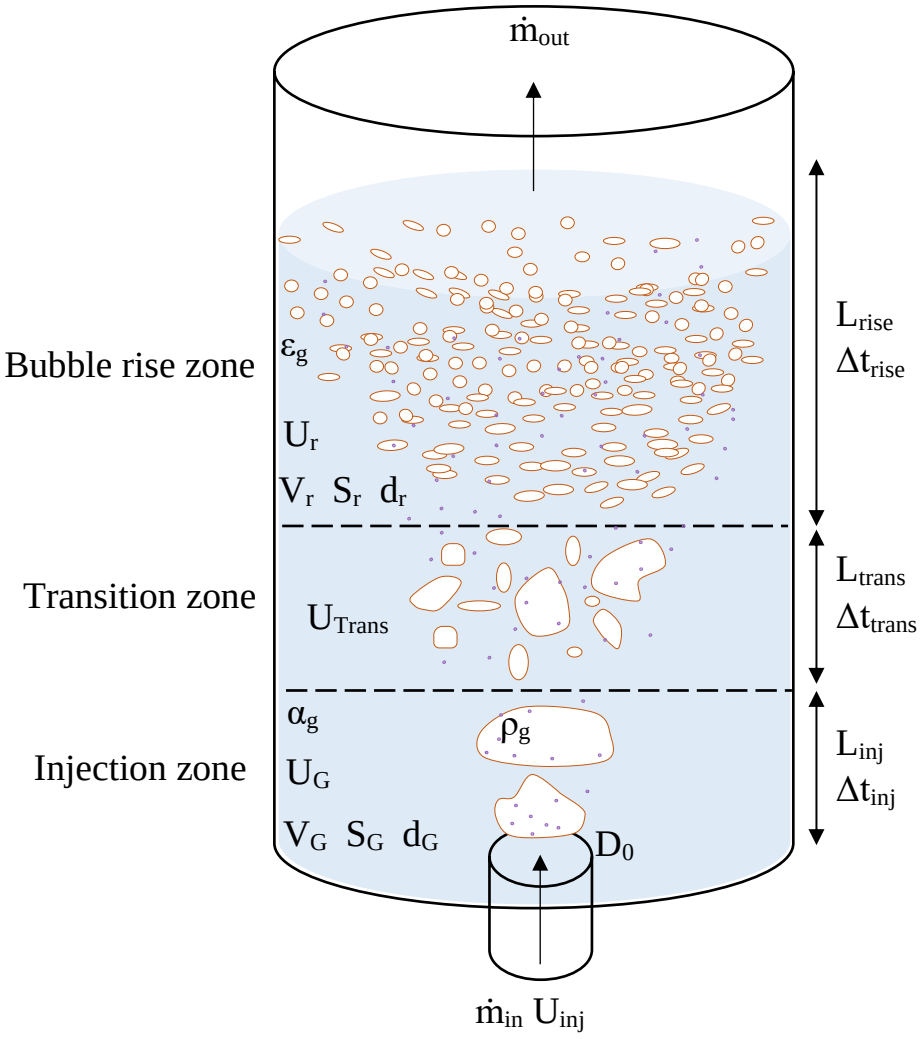

Figure I.4- Hydrodynamic zones and bubble dynamics in pool scrubbing.

- Bubbles velocity (residence time): It is the rising velocity of bubbles in the different zones, U_G in the injection zone, the transitional velocity (U_T) in the transition zone, and bubbles terminal velocity (U_r) in the bubble rise zone. Clift et al. [58] also correlated the terminal velocity in function of the equivalent diameter and the Bond number

(defined in I.5.4). Bubbles velocities in the different zones are regarded in the determining of bubbles residence time, which is an important parameter for decontamination factor measurements. In this manuscript, the rising velocity in the injection zone is characterized experimentally (see III.3.3.6).

- Void fraction: The void fraction (ε_g) is the ratio of the volume occupied by the gas to the total volume of the system. It can be considered and defined in each zone, for instance and as shown in Figure I.4, we define it as α_g in the injection zone (characterized experimentally in III.3.3.5) and as ε_g in the bubble rise zone. It is highly regarded in determining the average interfacial area in the bubble rise zone.

$$a_{average\ (bubble\ rise\ zone)} = {S_r\ \varepsilon_g}/{V_r} \quad (2)$$

These quantities exhibit different behaviours in three different zones, in which the determining of the physical quantities in each zone could be done through different approaches. These zones are known in pool scrubbing experimental campaigns by the hydrodynamic zones [27].

I.5.3. Flow regimes and patterns

In the injection zone, two types of regimes can present: the bubbly regime with the formation of a globule, and the jet regime. At first, stable or single bubbles may be formed at low velocities. With the increasing of gas velocity, the interface between gas bubbles and the surrounding liquid becomes instable due to the relative velocities between the phases. These instabilities induce bubble-bubble interactions which modify the flow patterns. The interactions comprise different phenomena such as coalescence, wake effects, and interference of bubbles.

Generally, the flow regimes in pool scrubbing are characterized as bubbly-dynamic (churn turbulent patterns) or jetting regime, rather than stable or single bubbling pattern [15]. The dynamic bubbly pattern or jet regime occur when inertial mechanisms dominate over other forces. Churn turbulent pattern is agitated and unsteady regime with different bubble-bubble interactions. This result in different morphologies and non-linear behaviour of bubbles formation or rising in the pool.

On the other side, with further increase of the gas velocity, the interface between the two phases varies from smooth into instable rippling behavior, then coalescence events of bubbles increase such that the gas phase dominates over the liquid phase. The latter events lead to a jet formation. Gaddis et al. [59] refer to the jet regime when the force due to the gas momentum exceeds the surface tension force, which is responsible for the reservation of bubble shape. In this case, the collapse of the surface tension force induces gas jet instead of bubbling.

We have investigated in literature the different criteria to classify each regime and determine the transition from bubbly regime to jetting, but also from a pattern to another. This will be discussed in III.2.2.

I.5.4. Dimensionless numbers

Before classifying the transition between regimes, it is important to introduce some dimensionless numbers based on the description of flow regimes encountered in pool scrubbing mechanism. In bubble dynamics, dimensionless numbers are generally used to facilitate the comparison of bubbles behaviour between experimental works of different scales. The use of dimensionless numbers reduces the number of parameters describing test matrix, which is relevant and necessary in the case of pool scrubbing experiments (taking in consideration the large number of pools scrubbing experimental campaigns). The importance of dimensionless numbers is the capability of characterizing different physical phenomena (inertial forces, gravitational forces, viscous forces) and compares them to each other. According to the hydrodynamic phenomenology of pool scrubbing, these numbers can represent the experimental flow conditions and prospect the hydrodynamic aspect of the flow. For example, Clift et al. [58] introduced a generalized graphical chart correlating the bubble shape in bubbly flows with dimensionless numbers, considering the bubbles parameters, as shown in Figure I.5.

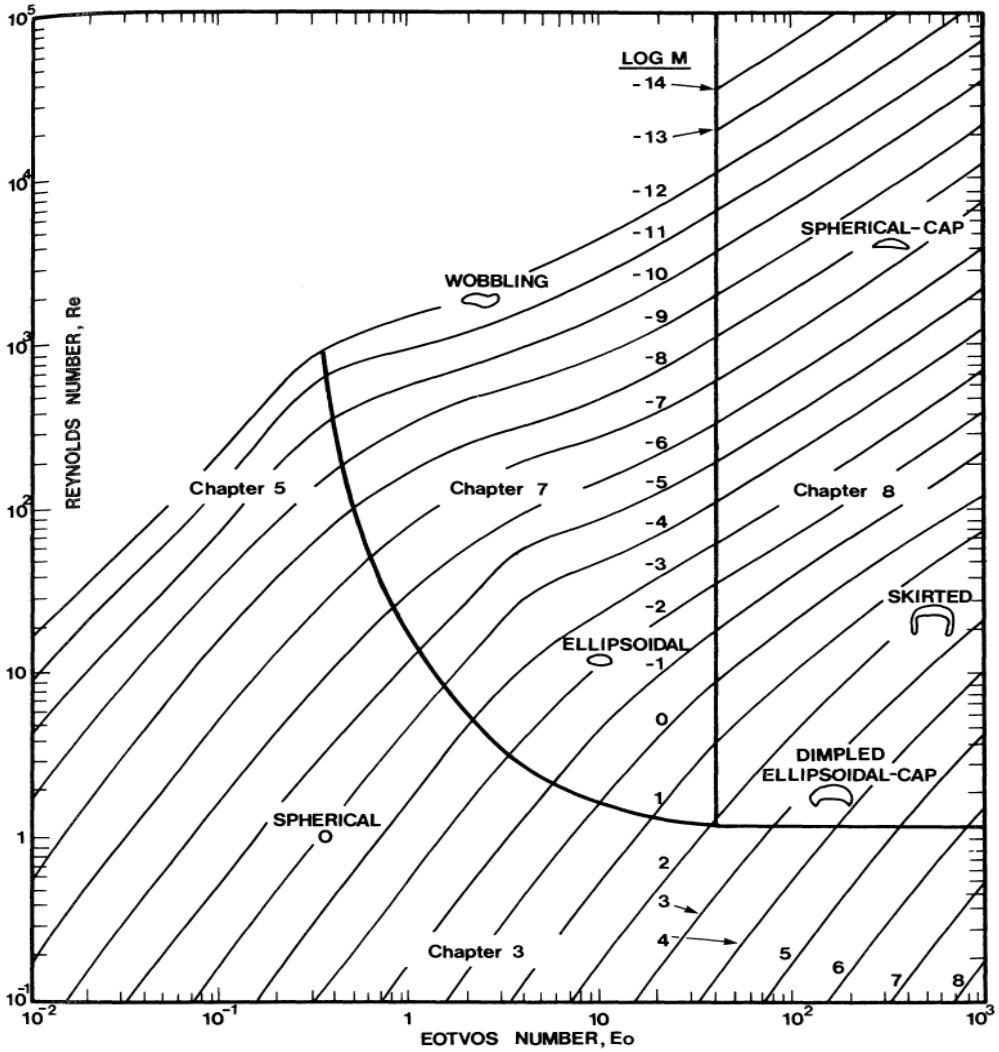

Figure I.5- Bubble shapes in function of dimensionless numbers developed by Clift et al. [58].

In this manuscript, these dimensionless numbers are expressed in terms of experimental conditions, in other words, instead of considering the bubble diameter d_b and velocity U_b as

Clift et al. [58], we considered the diameter of the nozzle D_0 and injection velocity U_{inj}. These numbers are detailed and presented below.

- Weber number (We): The ratio of inertial forces to surface tension.

$$We = \frac{D_0 \, {U_{inj}}^2 \, \rho_g}{\sigma}$$

- Reynolds number (Re): The ratio of inertial forces to viscous forces.

$$Re = \frac{D_0 \, U_{inj}}{\nu_g}$$

- Froude number (Fr): The ratio of inertial to gravitational forces.

$$Fr = \frac{U_{inj}}{\sqrt{g \, D_0}}$$

- Bond number (Bo): The ratio of buoyancy forces to the surface tension.

$$Bo = \frac{g \, (\rho_l - \rho_g) \, {D_0}^2}{\sigma}$$

I.5.5. Transition from bubbly to jetting regime

The characterization of flow pattern to another, or from bubbling regime to jetting regime was classified by different dimensionless number (Weber, Reynolds, Froude, Bond) in each experimental work. Zhao et al. [60] applied combined Kelvin–Helmholtz and Rayleigh-Taylor instability analysis, in order to obtain the critical Weber number for transition from bubbling to jetting regime. This critical Weber number $We = 10.5 \, (\rho_l / \rho_g)^{0.5}$, whereas $We_{critical} = 326$ for water/air and $We_{critical} = 420$ for water/steam. However, this critical number is found to be controversial between the experimental works, as shown in the Table I.4:

Table I.4- Transition between bubbly and jet regime according to dimensionless numbers.

References	Water/Air
Leibson et al. 1956 [61]	$Re_{critical} = 10000$
Hoefle et al. 1979 [62]	$Fr_{modified} = 250$
Gaddis et al. 1986 [59]	$We_{critical} = 4$
Zhao et al. 1990 [60]	$We_{critical} = 326$
Kyriakides et al. 1997 [63]	$Re_{critical} = 20000$
Cai et al. 2010 [64]	$Re_{critical} = 11000$

The disparities on the criteria to identify the bubbling–jetting transition in literature is possibly due to the different experimental and theoretical approaches, notably the definition of jetting. In fact, even the classification of flow patterns differs from an author to another due to the different descriptions and the nomenclature of observed morphologies and patterns. For example, Kyriakides et al. [63] classified the bubbling phenomena to various stages in a dimensionless form of Froude number as function of Bond number, as shown in Figure I.6. This approach is consistent with a simple observation of bubble-liquid flows: for example, behaviour appears very different between single bubbling and chaining, even if classified as bubbly in both cases. However, different approaches were adopted in Badam et al. [65] and Hur et al. [66]. Therefore, there is still no universal criterion for the transition between bubbling to jetting regime.

Characterization of bubble dynamics and classification of flow regimes and their transitions are essential for understanding the trapping of fission products in the pool. This is due to their strong implication in the retention mechanisms of fission products, whether these latter present in gaseous or aerosol forms. In the following paragraph, we present the reliance of decontamination factor on bubble hydrodynamics.

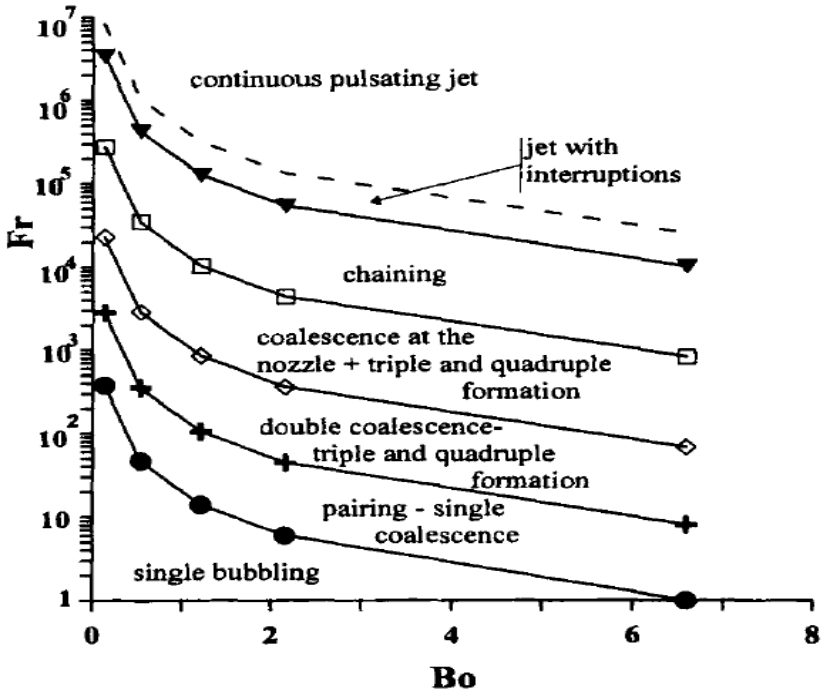

Figure I.6- Transition between the various bubbling stages in a dimensionless representation for the air/water system according to Kyriakides et al. [63].

I.6. Decontamination factor measurements

The decontamination factor (DF) is ratio of FPs mass flow rate at the inlet to that at the outlet of the pool, as shown in eq.(1).

Another term, which represent the decontamination factor but in other way, is considered in the literature which is the scrubbing efficiency:

$$\eta_e = 100 \times {}^{MF_{retained}}/_{MF_{in}} \quad (3)$$

Here $MF_{retained}$ represents the mass of fission products retained in the pool and MF_{in} is the mass of fission products injected in the pool. Both terms are correlated such that:

$$\eta_e = (1 - \frac{1}{DF}) \times 100 \quad (4)$$

Through literature, the use of scrubbing efficiency η_e shows the retention in percentage form, as shown in Table I.5.

Herranz et al. [40] used this term, and they concluded that scrubbing efficiency η_e is not apparently affected. If a comparison is made with DF term, a variation will be observed as shown in Table I.5, and that's why some authors prefer the DF term more than the scrubbing efficiency.

Table I.5- Correspondence between using scrubbing efficiency η_e and decontamination factor DF in Herranz et al. tests (ref).

Test	PSP0	PSP1	PSP2	PSP3	PSP4	PSP5	PSP6
η_e	92.86	97.78	99.51	99.66	99.66	98.93	99.68
DF	14	45	204	294	294	93	312

Moreover, the decontamination factor in a certain pool can be the product of the decontamination factor in each hydrodynamic zone, such that:

$$DF_{tot} = DF_{inj} \times DF_{trans} \times DF_{rise} \quad (5)$$

The retention and decontamination of iodine compounds can be classified mainly into two main approaches:

- For gaseous iodine, mass transfer and chemical reactions.
- For aerosols, aerosol removal mechanisms (in addition to mass transfer and chemistry if non-inert).

I.6.1. Aerosol removal mechanisms

As the gas rise the in the pool water, FPs in aerosol form suspended in gas can be transferred due to several retention mechanisms, as shown in Figure I.7: gravitational settling, centrifugal impaction, Brownian diffusion, inertial impaction, and the steam condensation:

- Gravitational sedimentation DF_{gs}: gravitational settling of aerosol particles in the bubble to the gas-liquid interface. The terminal settling velocity that characterizes the sedimentation phenomenon is reached when achieving the equilibrium between the drag force and the gravitational force

- Inertial impaction DF_{imp}: particles affected by this mechanism tend to collide with the bubble surface during the formation and detachment of the bubble from the nozzle due to their inertia. This phenomenon is more relevant for particles of equivalent diameter d_{ammd} larger than 0.5 μm.

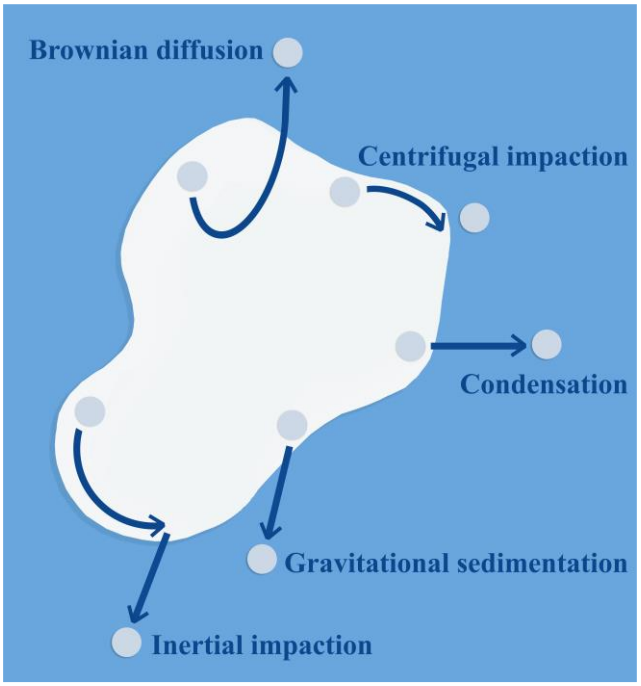

Figure I.7- Aerosols' removal mechanisms in rising gas bubble

- Brownian diffusion DF_{dif}: This process is caused by a particle concentration gradient in the gas phase, which leads to a net transport of particles from a region of higher concentration to a region of lower concentration.

- Centrifugal impaction DF_{ci}: This process is caused by the friction between the gas and liquid phases, generated by the bubble motion through the liquid, which leads to re-circulation of the particles located near the bubble surface. This mechanism is considered to be the dominant removal process, followed by sedimentation, for particle sizes d_{ammd} approximately larger than 1 μm.

- Steam condensation DF_{sc}: The net transfer of vapor across the gas-liquid interface can either favor (in the case of condensing steam) or hinder (in case of evaporating liquid) the deposition of particles on the bubble surface. A temperature gradient in the gas phase (thermophoresis) can also generate a net motion of particles in the direction of the decreasing temperature, this is due to the greater momentum transfer from the gas molecules to the aerosol particles in the region of the gas at higher temperature.

When bubbles hydrodynamics exhibit different behaviours, the aerosol removal mechanisms differ from a zone to another. Hence, each of these removal mechanisms have expression for their contribution in the decontamination factor, or a deposition velocity (Zablackaite et al. [53]), in each hydrodynamic zone. All these considerations highlight the strong influence of hydrodynamics on decontamination factor.

The total decontamination factor for each zone is determined by multiplying the above contributions of individual removal mechanisms from this zone [78, 79], such that:

$$DFtot = \prod_i DF_i = DF_{gs} \times DF_{imp} \times DF_{di} \times DF_{ci} \times DF_{sc} \quad (6)$$

I.6.2. Mass transfer and chemical reactions

For gaseous iodine, only the diffusion removal mechanism is significant from the aforementioned mechanisms. It is an important mechanism, as well as the mass transfer through the gas phase. For determining DF in gaseous iodine, mass balance equations for each volatile iodine species (CH_3I, I_2) should be formulated in both phases, based on mass transfer, solubility of these species in liquid and chemical reactions at the bubble interface with the liquid in the pool. Here, an important number is dedicated to characterizes how a soluble gas partitions itself between a gas and liquid phase at equilibrium, which is the Henry number. A small Henry number implies a very soluble gas and probable gas side-controlled mass transfer; conversely a large Henry number implies a sparingly soluble gas and probable liquid side-controlled mass transfer. According to Henry's law of solubility, the solubility of gas at constant temperature is directly proportional to the pressure of the gas, and this will be developed in chapter V.
Moreover, the mass transfer coefficients depend on several parameters and some of them are function of the bubble size and the bubble terminal velocity. Several models have been developed to predict and describe the mass transfer, such as two-film model, penetration theory, Higbie model, etc. The volumetric mass transfer coefficient $k_l a$ is considered widely when realizing the mass balance equation in the liquid phase:

$$V_{\mathrm{TYFON}(m^3)} \cdot \frac{dC}{dt}_{(g.m^{-3}.s^{-1})} = Q = k_{l_{(m.s^{-1})}} \times S_{\mathrm{g}(m^2)} \times (C^* - C)_{(g.m^{-3})} \quad (7)$$

After developing this equation, it becomes:

$$\int_{C_0}^{C} \frac{dC}{(C^* - C)} = k_l \times a \times \int_{t0=0}^{t} dt \quad (8)$$

$$\frac{C^* - C}{(C^* - C_0)} = e^{-k_l.a.t} \quad (9)$$

where C is the concentration of species in the pool, C_0 is the initial concentration, C^* is the saturated concentration, and V_g and S_g are the volume of gas and surface of interface respectively. Despite that, different chemical factors affect the transport of species from a phase into another. Consequently, the hydrodynamics of bubbles should be determined to perform the mass balance equation for gaseous phases transfer. The latter comprises the bubbles velocity, interfacial area, size of bubbles in the swarm, its terminal velocity, and the void fraction.

On the other side, it is worth saying that the retention efficiency of gaseous iodine is strongly dependent of pool temperature, chemical additives, pH control of the pool. The latter conditions provoke several chemical kinetics in decomposition and hydrolysis, that enhances the retention of these species.

One can note that chemical effects can also be taken into consideration for reactive aerosols, notably CsI which is moreover soluble.

I.7. Pool scrubbing codes – ASTEC code

Most of the common pool scrubbing codes are based on the databased realized in the experimental programs [24-31], even though there has been further development of these codes recently [67, 68]. A set of parametric studies was performed with the codes to measure the decontamination factor and its reliance on variables such as particles diameter and shape, swarm rise velocity, gas residence time and void fraction. The ranges covered of these variables were based on the analysis of the implemented hydrodynamic models. Within the codes, several phenomena and particle capture mechanisms are recognized to affect the scrubbing process. These phenomena are globule formation, bubble swarm dynamics, interfacial water vapor and heat and mass transfer, particle growth, and vent exit behavior.

However, several experimental and theoretical data show that some pool scrubbing related phenomena are still not included in the codes. Below, we summarize the overview of the different existing codes.

I.7.1. SUPRA, BUSCA, and SPARC

SUPRA (Suppression Pool Retention Analysis) was developed by EPRI (Electric Power Research Institute) to calculate the retention of aerosol particles and gaseous fission products passing through the water in the pool [69]. On the other hand, a mechanistic code, which incorporates full coupling of thermal-hydraulics and decontamination of a bubble rising through a water pool, is considered in BUSCA (Bubble Scrubbing Algorithm) [70]. The bubble may consist of a mixture of steam and non-condensable gases combined with aerosols and I_2 vapor contaminants. BUSCA was originally developed at SRD (part of the UK Atomic Energy Authority in the mid 1980's) [71]. It models the removal of aerosol from a bubble as it rises through water. BUSCA estimated that the entrance impaction of aerosols is the most efficient mechanism in removing the fission products, from the gaseous stream to the pool [72]. Furthermore, SPARC (Suppression Pool Aerosol Removal Code) considered the removal mechanism is dominant during the bubble rise through the pool, as the bubbles undergo inertial mechanism and sedimentation [73]. It is a computer code initially developed by U.S. Nuclear Regulatory Commission (NRC), to serve as a tool for calculating aerosol particle retention in boiling water reactor (BWR). The hydrodynamic models implemented in SPARC and BUSCA differ in their basis and their results, although they show several weaknesses, due to the missing of hydrodynamic phenomenology (spherical shape of bubbles) [72].

I.7.2. MELCOR

MELCOR is fully integrated code which models the progression of severe accidents and it was developed by Sandia National Laboratories for the U.S. Nuclear Regulatory Commission [74]. However, the implemented models to estimate the decontamination factor during pool scrubbing are not sufficiently verified, yet. It underestimates the experimental data in the injection zone where the gas rise velocity is high in pool scrubbing phenomena. As a consequence, further studies on the modelling of pool scrubbing are required to enhance the reliability of the computed results using this code.

I.7.3. ASTEC code

ASTEC is a software system developed by IRSN that aims to simulate all the phenomena occurring during a core meltdown accident in a nuclear reactor, from the initiating event to the release of radioactive products outside the reactor containment [75]. On the other side, it is used to determine the amount of radionuclides released into the environment during a severe accident. For this purpose, ASTEC consists of 11 coupled modules (CESAR, ICARE, CPA, MEDICIS, RUPUICUV, COVI, SYSINT, ELSA, SOPHAEROS, ISODOP, and DOSE), as shown in Figure I.8.

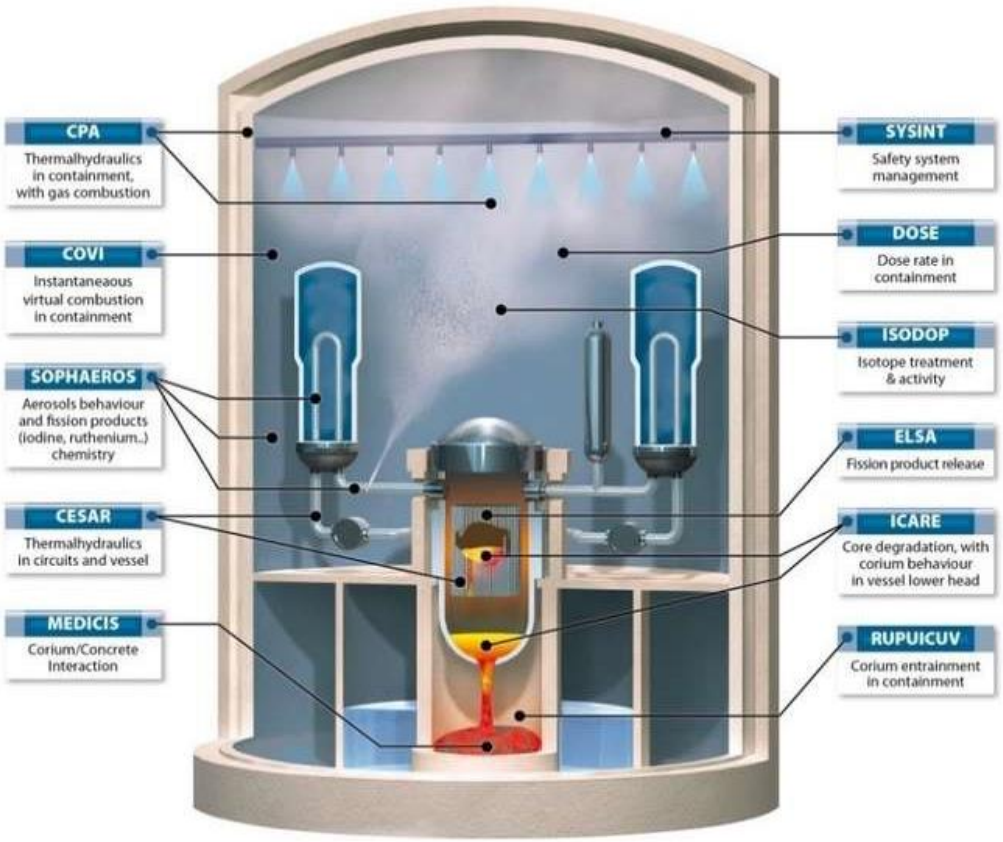

Figure I.8- ASTEC structure with its modules.

Pool scrubbing is addressed in the improvements dedicated for lumped parameter modelling in the ASTEC code. The ASTEC/SOPHAEROS module aims at predicting the DF for evaluating the transport and the chemistry of FP in severe accidents that may occur in light water reactors. Currently, the models of SPARC code are integrated in ASTEC for determining the DF linked to pool scrubbing.

A special pool version of ASTEC, containing forthcoming results of experimental investigations is expected to be developed [76, 77]. When the pools are emptied during the crisis, the current version of ASTEC should be used to quickly calculate the time periods prior to significant releases. Fortunately, that scenario apparently did not occur. Still, it sent a strong message that work on the issue of accidents involving irradiated fuel in pools must be continued. Moreover, a literature review dedicated to the modelling work on pool scrubbing within the ASTEC code is presented in the two reports of C. Marchetto [78, 79].

I.8. Objective of the current work

The retention process of radioactive substance is a serious concern in the evaluations of the source term and the post-management of the accident. This concerns notably pool scrubbing, occurring in wet filtered containment venting systems, and also encountered following the steam generator tube rupture, where fission products could be directly released outside. Many experimental campaigns in the last 40 years are attempting to characterize the pool scrubbing phenomena and its dependence on various parameters and test conditions. Those experiments permitted to establish a huge amount of experimental data, which contributed to the understanding of mitigation system's performance. However, the experimental databases have not yet characterized scientifically the overall phenomena encountered in pool scrubbing. This could stem from conventional theoretical models and assumptions on flow regimes for the sake of simplification, which are implemented within the codes. Moreover, these codes' validity extends only over the range of conditions encompassed by the data they were based on. Therefore, a systematic analysis between bubble hydrodynamics in the pool, the aerosol removal mechanisms, and the mass transfer should be maintained scientifically. This requires many experiments that follow a well-organized matrix. Coupling tests are recommended, where characterization comprises all the encountering phenomena. In these latter, the dependence and sensitivity of hydrodynamics and retention mechanisms on each other, but also on the test conditions, are investigated.

Throughout this thesis, an extensive bibliographic and experimental work [80-83] are performed in order to converge the experimental database, comprising both hydrodynamics and decontamination factor measurements. The experimental facilities developed permitted conducting experiments for different flow conditions and enabled the injection of different iodine compounds (CsI aerosols, I_2 elemental iodine, CH_3I gaseous methyl iodide).
Later on, this experimental database will be used for comparison/validation of existing models within the ASTEC code developed at IRSN.

Chapter II: Materials and Methods

II.1. Introduction

In this chapter, we present the experimental means of characterizing the pool scrubbing phenomena throughout the PhD work. As clarified in chapter 0, experimental programs on pool scrubbing phenomenon started around 40 years ago, and enormous research is ongoing since the accident of Fukushima. It is also illustrated in the chapter 0 that the established experimental database for the development of codes is not sufficient yet, so these codes still need improvements. From experimental point of view, the latter fact stems from some poor methodologies of describing the bubbles hydrodynamics and retention mechanisms. Below are some observations that justify the continuous need of better characterization of pool scrubbing.

- Limitations of adopted techniques for bubbles hydrodynamics. Different techniques have been used in the literature for investigation of bubbling at submerged nozzle: electrical capacitance tomography ECT [64, 84], phase Doppler [85], high speed framing [65, 86, 87], particle image velocimetry PIV [88], Laser-photodiode [89]. However, different bubbles behaviour limits the capability of techniques that provide local measurements, due to the bubble-bubble interactions. For that, Cieslinski et al. [89] have reported that laser photodiode system cannot be applied at high flowrates.

- Other point is that bubble hydrodynamics in pool scrubbing situations examine non-linear behaviour, where the corresponding experimental variables (bubble size, velocity, size distribution, etc.) are still not well experimentally characterized due to underestimation of the impact of bubble-bubble interaction [90-92]. These interactions are shown to have significant impact on the flow morphology in the different hydrodynamic zones [92, 93]. Otherwise, classical approaches for these variables were adopted, such assuming spherical or elliptical shape of bubbles in the different hydrodynamic zones [51, 53, 94].

- For the decontamination factor measurements, the adopted experimental methods are generally sufficient to accurately measure the DF. However, these experiments lacked consistent approaches to well characterize the mechanisms responsible of trapping (aerosol removal mechanisms, mass transfer, and chemical reactions) [15]. These mechanisms are function of experimental variables such as the bubbles hydrodynamics, which are eventually influenced by test conditions. For that, careful selections of the test parameters are required to study and evaluate the decontamination factor measurements. This would reduce the spectrum of uncertainty and lead to better understanding of the pool scrubbing phenomenon.

In this experimental work, two experimental campaigns were carried out:

- At IUSTI-Marseille mainly for developing the hydrodynamic methods.

- At IRSN-Cadarache, where the facility at Cadarache was built during the thesis and it is dedicated to the examination of the hydrodynamics pool scrubbing phenomenon.

II.2. Experimental work at IUST-Marseille

The experimental work realized at IUSTI-Marseille was dedicated for hydrodynamic characterization of the bubbling in the injection zone. It is a zone where there is formation of one large bubble (globule) or several bubbles that coalesce.

II.2.1. Experimental setup

The experimental setup used to study the bubble formation process is shown in Figure II.1. Compressed air is injected at single submerged nozzle in a cubic tank. The tank is made of plexiglass plates, allowing the implementation of optical metrological methods, forming a 0.34 m^3 cube (0.7 m × 0.7 m × 0.7 m). Water is fed into the tank to achieve a fixed height of 50 cm. The diameter (D_0) of the nozzle is 12 mm, and the air is supplied to the tank under constant flow conditions, by a compressor through a manometer and at ambient temperature.

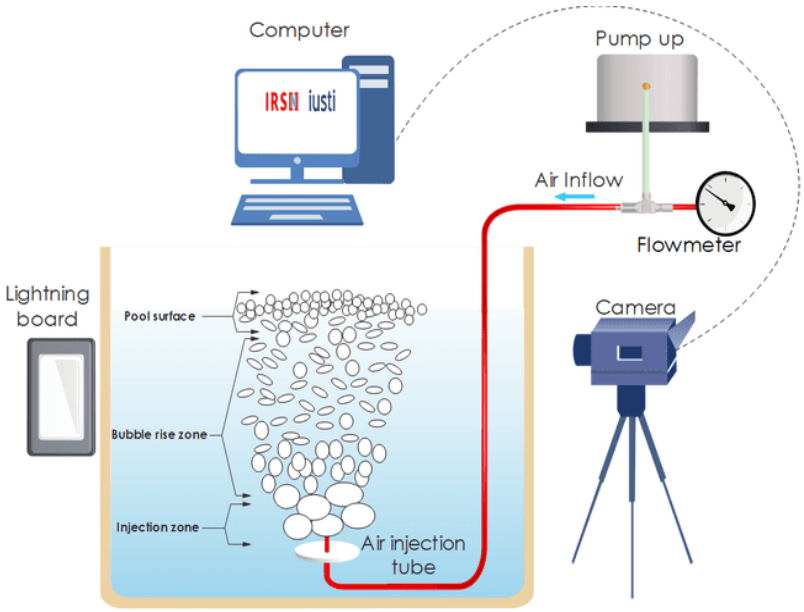

Figure II.1- Schema of experimental setup at IUSTI-Marseille

The measurement system for bubble hydrodynamics is composed of a high-speed camera, a LED light source with a diffuser, and computer to control the acquisitions by a CAM-WARE software. The position of the high-speed video camera is fixed at 40 cm from the tank, and it records the bubble formation process with a frame grabbing of 500 frames/s for an exposure time of 0.1 ms. Each acquisition of images (1280 × 1024 pixels) lasts for 10 seconds, corresponding to 5000 images. On the other side, the LED light is installed behind the transparent tank in order to compensate the illumination while setting low aperture values of the camera. The latter serves in decreasing the obscurity of images due to the rapid motion of bubbles.

II.2.2. Data treatment

Bubble hydrodynamic measurements were carried out thank to an optical technique developed by Farhat et al. [82], based on image processing.

II.2.2.1. Image processing

After the acquisitions of raw images, these images are subjected to treatment in order to describe the flow and extract information such as bubbles size, shape, spatial distribution and velocity using MatLab codes. The treatment is based on shadowgraph technique [86], where the dispersed phase (gas) is captured and detected.

The light filters and contrast of the raw images are applied and adjusted to reduce background noise. This is followed by removing noise from images and filtering the grey-scale images using a pixel-wise adapting filter. Thanks to grey-scale gradient, the gas phase is isolated from the continuous phase, this is followed by returning a binarized image. The latter image contains two values of pixel, where 0 (black color) corresponds to the liquid phase and 1 (white color) corresponds to the gas phase. Holes that could appear inside the bubbles due to light refraction or the alignment of the light source are filled in order to have homogeneous binarized images. The contour of gas bubbles is then detected using the edge detection algorithm (see Figure II.2).

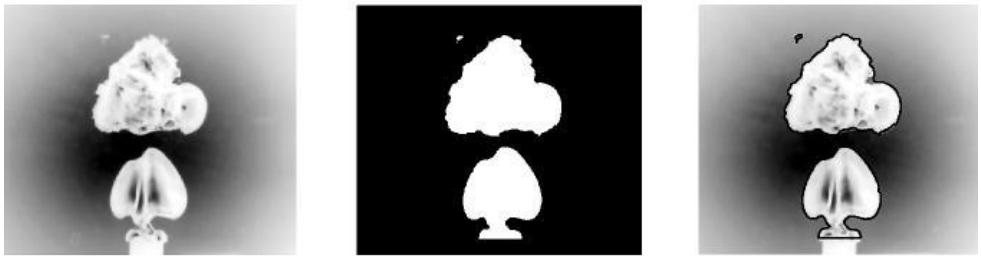

(a) (b) (c)

Figure II.2- Image processing; (a): Filters applied to raw image, (b): Binarization, (c): Detection of bubbles contours

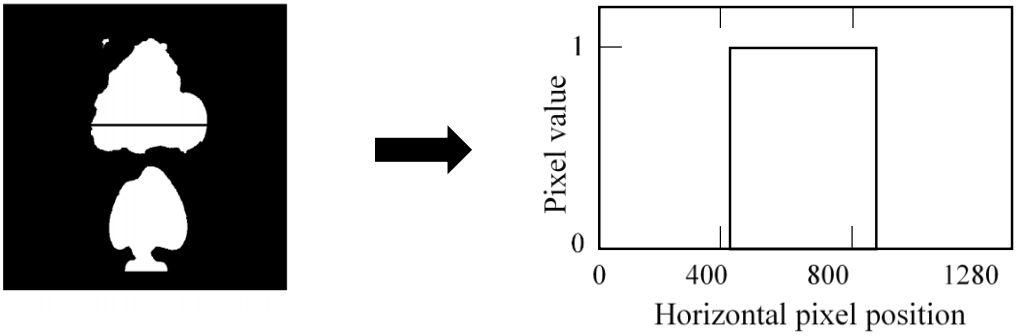

Figure II.3- Imposing line sensors for the detection of phase at height above the nozzle.

After image treatment and detection of binarized structures, a series of horizontal lines are imposed in the images, which could be considered as phase sensor, and are situated at different altitudes above the nozzle. Each of these lines phase will record 1 or 0 when crossing respectively dispersed phase (gas) or the continuous phase (liquid), as shown in Figure II.3.

Applying this technique to the acquisition of large number of images will reproduce the so-called XT diagram, shown in the Figure II.4. XT diagram represents the evolution of the bubbles at a certain altitude for the whole time of the acquisition. This XT diagram is discussed in III.3.1.1 with emphasizing its advantages in the temporal description of bubbling. Moreover, after the binarization of the images in the optical field, the binarized structures can be analyzed

in detail, to extract information about bubble size and shape, besides tracking their motion, departure from the nozzle, coalescences, and breakup.

Figure II.4- XT diagram

II.2.2.2. Globule characterization

The multiphase flows that occurred in these experiments could be characterized as bubbly regimes, however comprising different morphologies depending on the flow rates that are regulated by the flowmeter (6 L/min < Q_{inj} < 60 L/min) corresponding to (0.16 < We < 16). Generally, within these flow conditions, the formation process taking place that led us to introduce the globule bubble (see Figure II.5). It is the largest bubble formed after an event or several events of coalescence.

Gas bubble starts to form at the level of the nozzle. The bubble growth continues as it rises, however it is still connected to the nozzle through a neck. Prior to the bubble detachment, the width of the neck increases due to the formation of trailing bubble, which penetrates the leading bubble. Eventually, the two bubbles coalesce into large bubble (globule), which is detached finally from the nozzle. This morphology is described by Prince et al. [95] in dynamic regimes, where dynamic and inertial forces are important. That's why we considered the Weber number to analyze this bubbling process, as it is the ratio of inertial forces to the surface tension. The coalescence of bubbles and formation of large globule is also observed as by Badam et al. [65], Mosdorf et al. [92], Hur et al. [66], and Kyriakides et al. [63] in dynamic regime formation, in the range 0.1 < We < 200, where a non periodic formation is reported.

Figure II.5- Experimental observation of bubble formation process

The number of bubbles that coalesce and the position of coalescence vary with the variation of the injection flowrate or Weber number. For that, a sort of tracking the formation of globule, number of coalescences, and the position of coalescences is required to study the formation process.

II.2.2.3. Tracking of structures

In order to characterize the bubble hydrodynamics within this non-periodic behaviour of bubbles formation, it is essential to track the formation, departure and the coalescence of bubbles. Thanks to image processing and binarization of images, structures are distinguished from the continuous phase. Beyond this treatment, these structures are algorithmically labelled.

In Figure II.6, the procedure of tracking is depicted. It consists of splitting the record of bubbles into 3 different displays recording at same instant t. The first display tracks the structures as long as they are attached and connected to the nozzle. A departure event is recorded whenever there is a detachment from the nozzle, and since then, the second display tracks the departed structure. In case where a bubble connected to the nozzle interferes with a bubble in the second display, the merged structure is reshown in the first display. A coalescence is considered whenever there is a merging of two or more structures resulting in one labelled structure. Whenever, in case there is more than one structure that is detached from the nozzle, the second display tracks the new structure and therefore, the preceding structures tracked in this display 2 will be shifted to the third display. Throughout this tracking, it is possible to investigate the formation of bubbling frequency and globules formation, mainly by analyzing the evolution of bubbles in the first display.

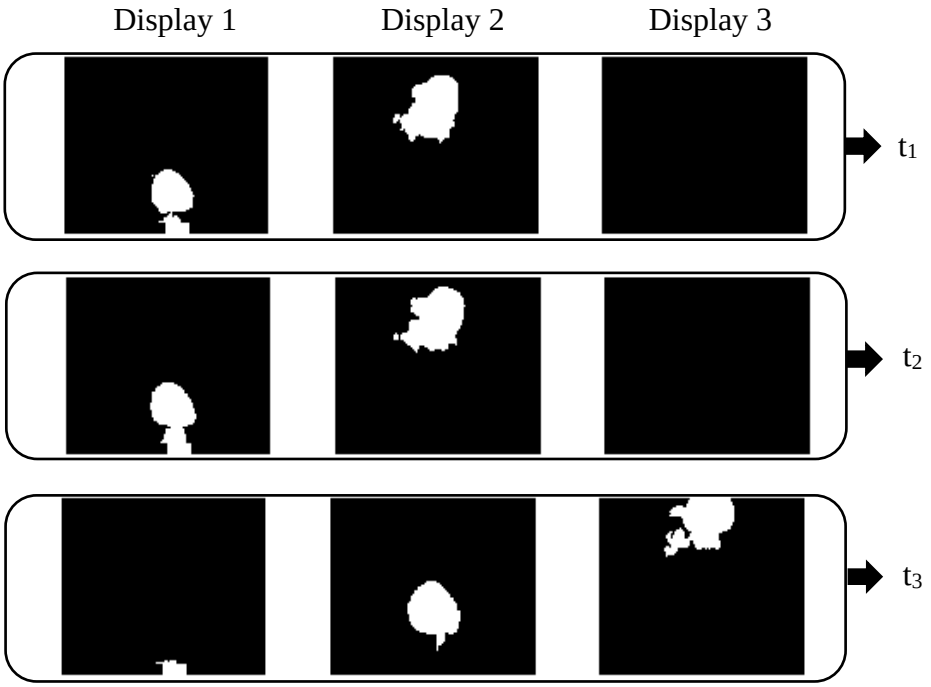

Figure II.6- Tracking the bubble departure and formation of globules

II.3. TYFON and experimental work at IRSN Cadarache

An experimental facility dedicated to characterization of pool scrubbing was built in IRSN Cadarache at our laboratory "L2EC". TYFON, which stands for Trapping and hYdrodynamics of FissiON products behavior in pool scrubbing, allows to perform experiments coupling the hydrodynamics and chemical parameters. Different flow conditions are modifiable:

- gas flowrate,
- gas temperature,
- gas mixture (add of steam or other species…),
- size of injector nozzle,
- water submergence in the pool (level of water in the pool),
- temperature of water in the pool.

On the other hand, the decontamination factor measurements were performed for various FP compounds diluted in airflow (iodine compounds such as elemental gaseous iodine I_2, gaseous methyl iodide CH_3I, Caesium iodide aerosols CsI). Eventually, this allows to investigate the dependence of the bubble hydrodynamics and decontamination factor on the different experimental aspects.

Before carrying out experiments on this facility, a series of tests and procedures were performed to qualify the hydrodynamic and decontamination factor measurements.

II.3.1. TYFON

TYFON facility, shown in Figure II.7, comprises different complementary parts:

- **Bubble column DN500**: The bubble column is of 500 mm internal diameter and a maximum pool submergence of 1.3 m of corresponding to a volume of 250 L. The interior walls of the column are made up of stainless steel ‘‘mirror polished’’, which effectively prevents the adsorption of fission products on its surface. Moreover, it is equipped with six transparent windows permitting visualization of flow using different optical measures at two different altitudes.

- **Injection system**: The injection line comprises different junctions enabling the injection of other gases. This system ends inside the DN500 column with a vertical injector tray, where

five different sizes of injectors (2 mm, 5 mm, 10 mm, 20 mm, and 50 mm) can be mounted. The temperature of injected gas can be monitored by Vulcanic fluid circulation heater up to 150 °C, where gas circulates afterwards within an insulated flexible to maintain its temperature.

- **Heating system**: The column is thermally insulated, and liquid can be heated up to 90 °C by the wrapping around its surface. The five thermocouples are distributed between the injection and the height of the free surface of the pool, to maintain the temperature's measurement of the pool.

Figure II.7- TYFON facility.

- **Thermal hydraulics:** Five pressure sensors are equipped for the measurement in the pool (3 sensors axially position and apart by 30 cm), at the injection (1 sensor), and at the top of the column (one sensor). All/one of these pressure sensors can be replaced by a sampling valve depending on the pool submergence, in order to measure the retention of aerosols inside the pool. Five temperature sensors (thermocouples) permit to control pool temperature, also the gas temperature in the upper part of the column (just above the pool surface). This latter is connected to an extraction line for evacuating the gas flow. Both pressure and temperature sensors are shown in Figure II.8. Sampling is possible at this level, by means of a simple tap for sampling the gas phase, as well as an isokinetic cane for aerosol sampling (will be detailed hereafter).

Figure II.8- Pressure and temperature sensors plugged to TYFON column.

- **Software:** The injected gas is provided by an air compressor installed outside the experimental hall. The flowrate of injected gas into the column is regulated by computer software “Labview”, shown in Figure II.9, as well as the heating of liquid in the column. The latter has an interface showing the instantaneous pressure and temperature readings as well as their evolution as function of time. Thanks to the pressure sensor at the bottom of the column, the level of water “submergence” can be adjusted while feeding water into the column.

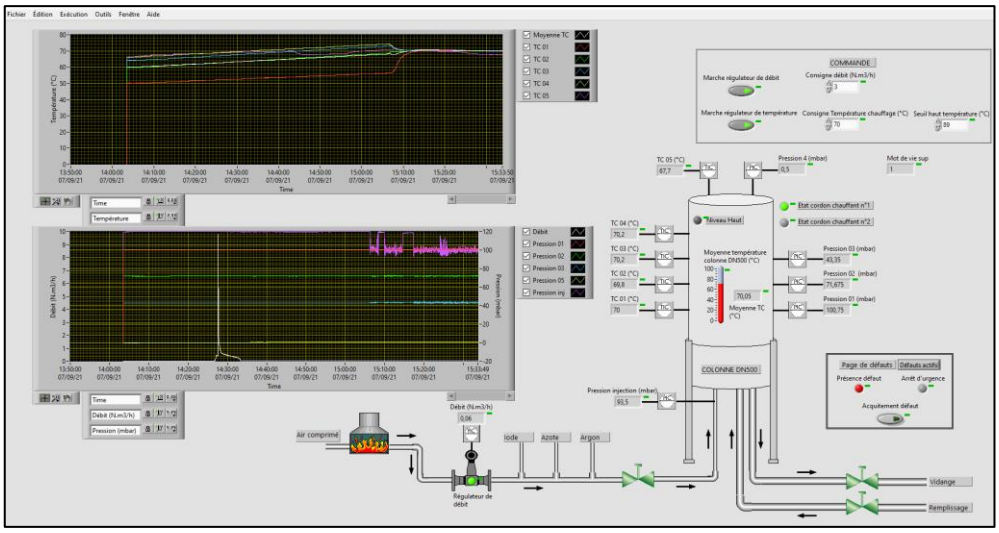

Figure II.9- The interface of the monitored software “Labview”.

II.3.2. Hydrodynamic measurements in the injection zone

Acquisition of images have been taken using an advance high-speed camera ‘’Phantom Speed sense VEO-E’’ (see Figure II.10), which can take 3500 image per second at 1280 × 800 pixels. A background light is used on the opposite window to the camera, in order to compensate the illumination while setting low aperture values of the camera. In fact, the latter serves in decreasing the obscurity of images due to the rapid motion of bubbles. The MatLab codes developed at IUSTI-Marseille for data and image processing (see section II.2.2.1) were adapted to the difference in the optical effects of the facility at IRSN-Cadarache.

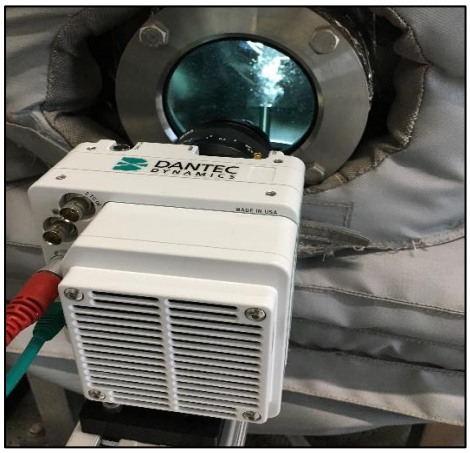

Figure II.10- Phantom Speed sense VEO-E high speed camera.

Air is injected from single nozzle submerged in the stagnant liquid column. The injection system permits the modification of the nozzle tray, where five sizes of nozzle can be mounted (2 mm, 5 mm, 10 mm, 20 mm, and 50 mm), as shown in the Figure II.11.

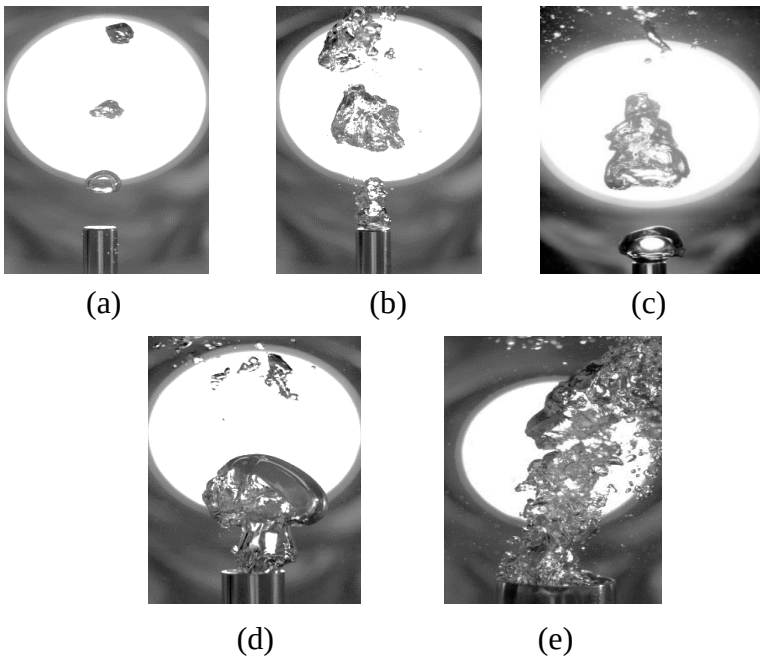

Figure II.11- The nozzle injectors where gas was injected to the column. (a) D_0 = 2 mm, (b): D_0 = 5 mm, (c) D_0 = 10 mm, (d) D_0 = 20 mm, (e) D_0 = 50 mm.

The variation of nozzle size, within the range of flowrates (0 – 17 m^3/h), permits to cover wide range of Reynolds and Weber number (0.07 < We < 10000), in other words, to induce wide range of flow regimes.

Experiments were carried out to characterize the injection zone, comprising the different flow regimes from single bubbling regime to jetting regime. As flow conditions were modifiable, which is the case for pool scrubbing phenomenon, their effects on the globule formation and jetting were examined. Throughout this work, we discuss the following investigations detailed below, with corresponding results developed in chapter :

- Impact of nozzle size (see III.4.1).
- Impact of gas contamination (see III.4.2).
- Impact of pool submergence (see III.4.3).

II.3.2.1. Effect of gas contamination with iodine compounds

Experiments were performed with carrier gas mixed with CH_3I, or with CsI aerosols suspended in the injected air.

II.3.2.2. Effect of nozzle size

For the nozzles D_0= 2 mm, D_0= 5 mm, D_0= 10 mm, D_0=20mm (shown in Figure II.12), globule volumes and frequencies were determined and compared for different injection flowrates. For the 50 mm nozzle, no globule formation was observed. Instead, a swarm of smaller bubbles was formed within the tips of the nozzles. This can be due to the weak effect of surface tension (nozzle – air – water) in front of the inertial and gravitational forces.

Figure II.12- Injectors of different nozzle sizes.

II.3.2.3. Effect of submergence

The level of water in the pool H_{pool} was set to different altitudes, such that $H_{pool} = L_{inj}$ (≈ 10 cm), 30 cm, 60 cm, 100 cm, and 120 cm. Moreover, for each flow conditions the length of injection zone L_{inj} was determined. This length corresponds to the position on which the globule starts to break after its formation. At each of these altitudes, the globules volume was determined and compared to examine the influence of pool altitude.

II.3.2.4. Effect of gas and pool temperature

In addition to previous parameters, ranges of pool temperatures and gas temperatures were examined thanks to the TYFON facility and Vulcanic fluid circulation heater respectively. The pool temperature was varied between 25 and 70 °C. On the other side, the gas temperature ranged between 20 °C and 90 °C, without inducing steam mixture at the inlet.

The range of experimental parameters on the TYFON facility for hydrodynamic measurements are presented in Table II.1.

Table II.1- Range of experimental parameters examined in the TYFON facility.

Tests parameters	Carrier Gas	Species used	Injector size D_0 (mm)	Submergence H_{pool} (cm)	Pool temperature T_{pool} (°C)	Gas temperature T_{gas} (°C)
TYFON	Air	CH_3I CsI	$2 < D_0 < 20$	$L_{inj} \leq H_{pool} \leq 100$	$25 < T_{pool} < 70$	$20 \; T_{gas} < 90$

II.3.3. Decontamination factor measurements

Depending on the different form of the iodine compound, the systems of their generation or injecting into the TYFON facility varies, as well as the sampling process, and the analysis technique for their measurements.
Before the test campaign, the duration of tests has been estimated according to the characteristic time τ, corresponding to the time required for 1 renewal of the volume of empty TYFON (250 L without water) by the injected gas:

$$\tau = {V_{TYFON}}/{\dot{Q}_{injection}} \quad (10)$$

With the hypothesis of well-mixed gases in empty TYFON, the evolution of concentration C in TYFON of a compound diluted in gas flow, at initial concentration C_0, will increase according to:

$$C = C_0(1 - e^{(-t/\tau)}) \quad (11)$$

Thus, at $t = 3\tau$, $C = 0.95\ C_0$ and at $t = 5\tau$, $C = 0.99\ C_0$. These considerations permit to have a rapid estimation of time needed to reach a steady state for each We (flowrate) considered, in other words the duration of each experiment. Of course, this duration may be modified by the

liquid presence in pool scrubbing tests, so it has to be adapted, according to concentration amounts measured in the exhaust flow (steady state reached when this latter is stabilized). According to that, the duration of tests varied from 2 to 5 hours, mainly depending on flow regime: the lower the flow, the longer the test.

The three iodine compounds that were examined in pool scrubbing experiments are caesium iodide (CsI) in the form of aerosols, elemental iodine (I_2) in gaseous form, methyl iodide (CH_3I) in gaseous form. The range of experimental parameters for each iodine compound is presented in Table II.2.

Table II.2- Experimental parameters of the decontamination factor measurements for each iodine compound

Tests parameters	Weber	Injector size (mm)	Submergence (cm)	Pool temperature (°C)	Gas temperature (°C)
CH_3I	$10^{-2} < We < 10^{3}$	5, 20	$H_{pool} = 100$	$25 < T_{pool} < 70$	$25 < T_{gas} < 70$
CsI	$10^{-2} < We < 10^{4}$	2, 5, 20	$10 < H_{pool} < 100$	$25 < T_{pool} < 70$	$25 < T_{gas} < 70$
I_2	$10^{-2} < We < 5\times10^{2}$	5, 20	$H_{pool} = 100$	25	25

The carrier gas for all these experiments was injected from the air compressor. According to each configuration and test, we attempted to study the effect of the pool matrix (pH). The latter was adjusted by adding corresponding volumes of 1M sodium hydroxide (NaOH), such that the pH range in our experiments was $7 < pH < 13$.

II.3.3.1. Verifications prior to the tests

For each experiment, the conditions are adjusted carefully. That is to say the setting of pool submergence, its temperature, and gas conditions. The preparation of the test starts by filling the column with the demineralized water and then heating the pool, which takes several hours to reach the requested temperature. In case of alkaline pool such that pH =12, the pH is adjusted by adding approximately two liters of 1 molar sodium hydroxide to the demineralized water. The pool pH is then verified by a pH meter. For the injection of carrier gas, the air flowrate is regulated in volumetric value at normal conditions (1 atmosphere, 0 °C), and adjusted considering the injection pressure at the bottom of the column and the gas temperature. . Thanks to the pump and flowmeter in the sampling system, the sampling flowrate is also adjusted.

Before injection of the iodine compound, a verification of possible leaks is performed in the injection line until the end of the sampling line. Moreover, sampling is done in the two lines (pool and bubblers) to make sure that there is no prior contamination or pollution.

II.3.3.2. Configuration of tests on methyl iodide (CH_3I) retention

The schema of the experimental configuration for the gaseous methyl iodide injection is shown in Figure II.13. This compound is injected from commercial bottle of compressed air with [CH_3I] = 1000 ppmv. The flowrate of dilution air, which carries CH_3I into TYFON, is regulated such that the inlet concentration of the carrier gas is 5 ppmv for the different series of tests. In order to determine the decontamination factor DF, gas phase samples are collected from the injection line before being injected into TYFON, in order to verify the desired inlet concentration. After traversing the column, gas phase samples are sampled from the downstream flow in the outlet duct, in order to measure the outlet concentration. Therefore, the decontamination factor of the pool can be determined.

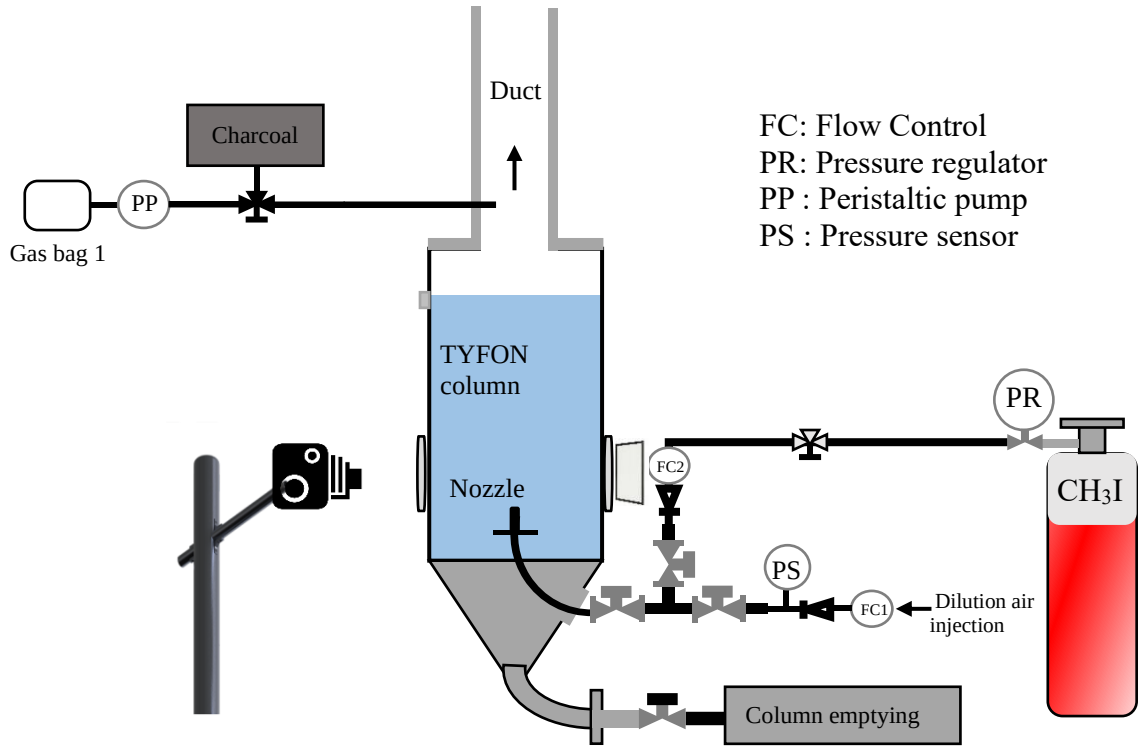

Figure II.13- CH_3I tests configuration on TYFON facility.

II.3.3.3. Configuration of tests on caesium iodide aerosols (CsI) retention

Caesium iodide aerosols are generated using Palas AGK 2000 generator [96, 97] as shown in Figure II.14.

The compressed air injected into the AGK, containing the aqueous solution of caesium iodide, nebulizes the solution so that dehydrated aerosols are fed into the gas flow at the downstream of the AGK. The median mass aerodynamic diameter (MMAD) for CsI aerosols is 1 µm (dispersion σ_g = 1.8), and the average aerosols flow rate is 10 mg/h. The generation method of AGK is reported in Appendix 1.

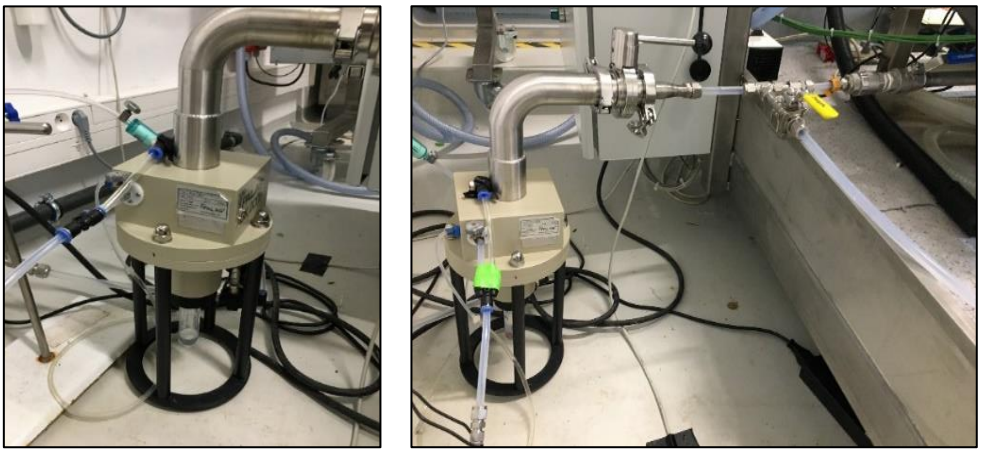

Figure II.14- Palas AGK 2000 aerosols generator.

The regulation of injection flowrate into TYFON is subjected to a range of flowrates, due to the generator's operational pressure. Thus, another injection line (compressed air) is considered. Actually, regarding the gas/aerosol flow rate imposed by AGK 2000, some configurations cannot be reached in this configuration (very low We for example). The schema of the experimental configuration of CsI aerosols is shown in Figure II.15.

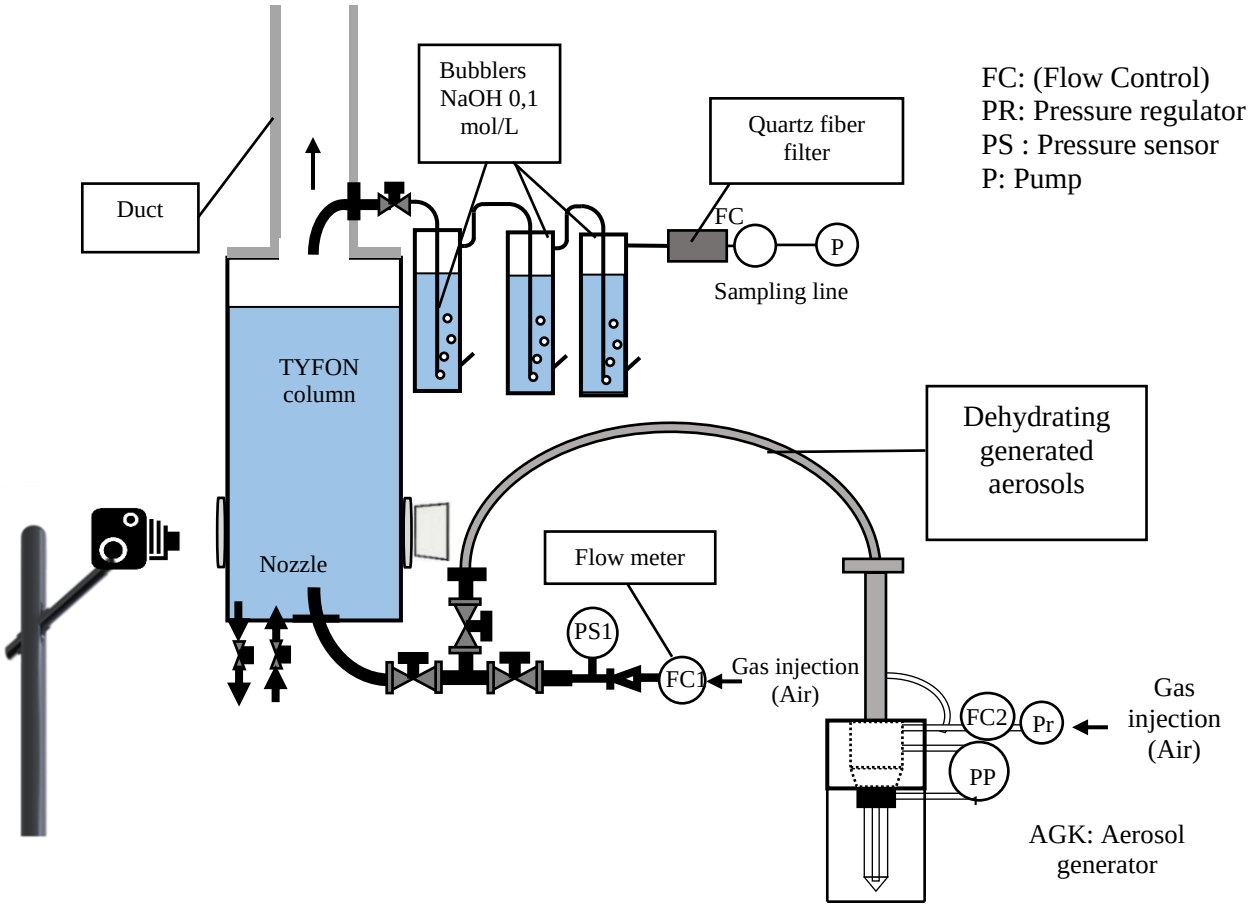

Figure II.15- CsI tests configuration on TYFON facility.

Contrary to the manipulations with CH_3I configuration, the determination of decontamination factor is considered in a different way due to the deposition of aerosols on the different parts of the sampling line (isokinetic cane, tubes, and filters). The amount of CsI aerosols injected into

TYFON corresponds to the sum of amount of CsI trapped in the pool added to the amount of CsI that has flown out the column through the duct. Therefore, DF is calculated such that:

$$DF = \frac{m_{in_{(t)}}}{m_{out_{(t)}}} = \frac{m_{trapped_{(t)}} + m_{out_{(t)}}}{m_{out_{(t)}}} \quad (12)$$

For the quantity of CsI aerosols trapped in the column, a valve permits to collect liquid sample from the pool inside the column.

For the quantity of CsI in the downstream, air is vented from the main exhaust through the cane at a flowrate in order to maintain the same velocity of carrier gas in the exhaust and the sampling line. This isokinetic sampling method [98] aims at better representing the actual outflow in the exhaust in terms of aerosol concentration . To compensate, a dilution factor (ratio of sampling flow on total flow) permits to represent the actual CsI amount in the downstream. The sampling system composed of 3 bubblers, quartz fiber filter, flowmeter, and a pump as shown in Figure II.16. The three bubblers of known masses are filled with 0.1 molar sodium hydroxide to have same submergence, and then weighed. Actually, CsI is known to have good solubility by bubbling in alkaline solution traps [99]. The quartz fiber filter, whose filter integrity permits to trap all the outgoing aerosols from the bubblers, is the end of the sampling line.

16

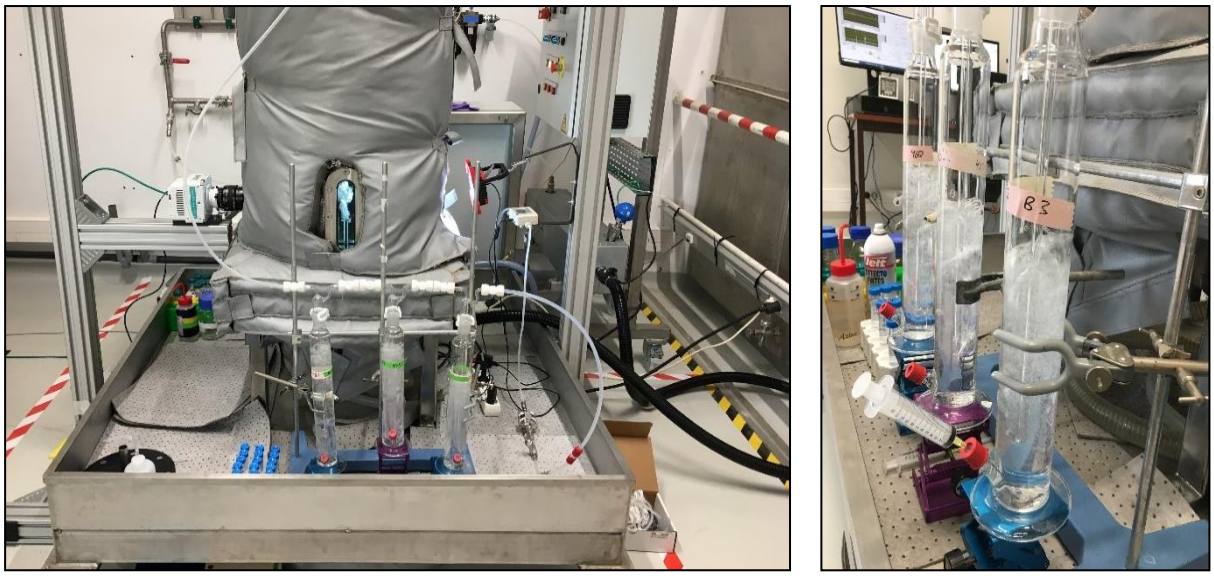

Figure II.16- The sampling system

Taking in consideration the aerosol deposition on the surfaces, notably in the sampling system (isokinetic cane, pipes), a sample washing is performed with NaOH at the end of the experiment in order to collect all the deposited quantity of CsI aerosols.

II.3.3.4. Configuration of tests on elemental iodine (I_2) retention

Concerning the elemental iodine I_2, diatomic iodine (I_2) is stored in solid state within the iodine generator of L2EC laboratory [100], as shown in Figure II.17, and then it is sublimated.

Figure II.17- Diatomic iodine generator.

The generator is composed of a carrier gas dryer and two reactors containing around 500 g of solid iodine flakes. These reactors are placed in a thermostatic pool at 25°C to sublimate the iodine. the configuration of experimental setup is similar to that of caesium iodide, except for the generation side. Nevertheless, the configuration of experimental setup, as shown in Figure II.18, is similar to that of caesium iodide, except as mentioned above for the generation side.

As for CsI experiments, parameters linked to I_2 generator prohibit to easily explore some configurations (very high flowrates for example, due to fixed exhaust pressure of I_2 generator). Besides, I_2 is also known to have a good solubility in alkaline traps [19].

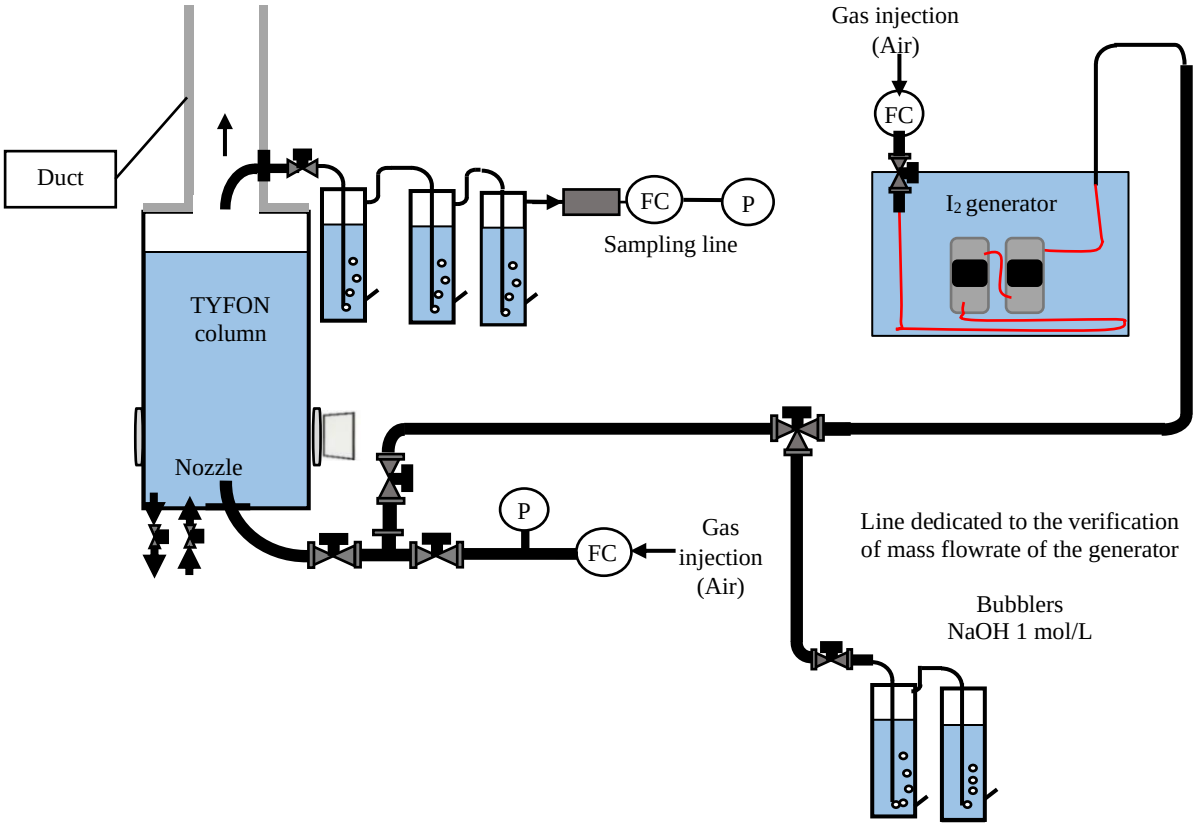

Figure II.18- I_2 tests configuration on TYFON facility.

II.3.3.5. Chemical analysis measurements

For the measurements of iodine compound, two analytical machines are used, the Inductively Coupled Plasma – Mass Spectrometry (ICP-MS) and the Gas Chromatography (GC).

ICP-MS (see Figure II.19), is a measurement technique that allows the determination of low concentrations of ranges ppm (parts per million) and until ppb (parts per billion) in aqueous solutions. This technique is shown to be effective in the analysis of iodine composites in the different research programs within the laboratory (L2EC) [101]. The concentration of liquid samples taken from the CsI and I_2 experiments were measured on this machine. The principle of ICP-MS is detailed in Appendix 2.

Figure II.19- Inductively Coupled Plasma – Mass Spectrometry (ICPMS).

On the other hand, the sampling of methyl iodide was performed in gaseous state [102], therefore a Gas Chromatography (GC) was used for the measurements of its concentration. Gas chromatography (GC), shown in Figure II.20, is a widely used analytical machine, that possess separation techniques applicable to gaseous compounds or compounds that can be volatilized by raising temperature without their decomposition. The principle of the GC is detailed in Appendix 3.

Figure II.20- Gas Chromatography (GC).

Chapter III: Hydrodynamics of pool scrubbing

III.1. Preface

The study of multiphase flows continues to occupy an important place in scientific innovation. More specifically, bubble dynamics are highly regarded in the design of modern engineering systems and present within numerous industrial applications (Filtration and scrubbing systems, food industry, oil/gas separators…). Recently, the fields studying the bubble dynamics have been highly developed and attempts of describing the experimental aspects of fluid behavior, under different flow conditions, are increasing. The knowledge of bubble dynamics is essential for determining the efficiency of filtration systems that depends on injecting contaminated gas, from a submerged nozzle, through liquid column or facility. However, bubbles' size and shape, their velocities, residence time, frequency, and gas holdup differ dramatically between microscopic and macroscopic problems, as we could address different aspects of flow phenomena, due to variation of the impact of inertial, viscous, and gravitational forces. These forces could induce surface tension instabilities, which lead to deformation of the bubble shape. Dimensionless numbers, according to the experimental conditions, are introduced to analyze the corresponding phenomena upon the balance between the inertial forces, viscous forces, surface tension, and gravitational forces. These dimensionless numbers are the Weber number, Reynolds, Froude number, and Bond number as shown respectively in eq.(13), eq.(14), eq.(15), and eq.(16).

- Weber number (We): The ratio of inertial forces to surface tension.

$$We = \frac{D_0 \, {U_{inj}}^2 \, \rho_g}{\sigma} \tag{13}$$

- Reynolds number (Re): The ratio of inertial forces to viscous forces.

$$Re = \frac{D_0 \, U_{inj}}{\nu_g} \tag{14}$$

- Froude number (Fr): The ratio of inertial to gravitational forces.

$$Fr = \frac{U_{inj}}{\sqrt{g \, D_0}} \tag{15}$$

- Bond number (Bo): The ratio of buoyancy forces to the surface tension.

$$Bo = \frac{g \, (\rho_l - \rho_g) \, {D_0}^2}{\sigma} \tag{16}$$

In this chapter we present the work that aimed to characterize the hydrodynamics of the pool scrubbing and investigate its aspects on the flow. Three hydrodynamic zones present in pool scrubbing (injection zone, transition zone, and bubble rise zone) as discussed in chapter 0 and II, as each of these zones are characterized by different morphology and contribution to pool scrubbing. The realized work of hydrodynamics in the current thesis was dedicated mainly to investigate the injection zone, thanks to the device at IUSTI-Marseille (see II.2.1) and TYFON at IRSN-Cadarache (see II.3.1).

III.2. The injection zone and flow regimes

The injection zone is the onset of pool scrubbing that occurs at the very beginning of the injection point of carrier gas, whether through safety piping (case of FCVS) or ruptured tube (case of SGTR). Analysis of pool scrubbing codes and experimental campaigns showed a significant contribution to the trapping of fission products (especially for aerosol particles) in this zone [103].

From experimental point of view in our work, this zone is near the submerged nozzle. The boundaries or length of this zone are dependent of the flow regime, where depending on different parameters, two main types of flow regime can present.

- There is the bubbly regime with formation of bubbles despite the periodic or aperiodic manner of bubbling (static, dynamic, or churn-turbulent) [95]. In pool scrubbing where the gas momentum is expected to be high [15, 36, 104] and inducing dynamic of formation of bubbles as McCann et al. and Davidson et al. [95, 105, 106] reported, bubble-bubble interactions are induced leading to the formation of the so-called “globule”. The latter is formed following the bubbles interaction and coalescences above the nozzle. Therefore, the length of injection zone L_{inj} is the position on which the globule starts to break.

- On the other side in jetting regime, with the increase of inertia, a continuous stream of gas is formed from the nozzle. In this case, the length of injection zone L_{inj} is the altitude from the nozzle until the position where jet starts to break.

III.2.1. Flow regimes and morphologies of bubbling regimes

Thanks to phenomenological description of the flow regimes that were observed throughout the experiments, we divided the regimes into bubbly regimes, transition regimes, and jetting regimes. The hydrodynamics (volume and frequency of bubbles, surface area, void fraction, and rising velocity) carried out through the thesis were performed for the globule in bubbly regimes, as it is not possible to determine the aforementioned hydrodynamics for transition and jetting regime. However, and within the bubbly regimes, the variation of experimental conditions induced different morphologies, which are discussed in the following paragraphs.

III.2.1.1. Single bubbling

An appropriate starting point is to define static stable bubbling. Through literature analysis, we have determined that this single bubbling regime was described by Reynolds Re by some authors and by Weber number by other authors, as shown in Table III.1.

Author	D0 (mm)	Bo	Single bubbling regime	
Kyriakides et al. [63]	1 - 2	0.13	We < 0.04	Re < 100
Badam et al. [65]	2	0.55	We < 0.1	Re < 230

Cieslinski et al. [89]	1.6	0.36	We < 0.1	Re < 205
Zhang et al. [93]	2	0.55	We < 0.08	Re < 205
Mosdorf et al. [92]	2	0.168	We < 0.06	Re < 130
This work	2	0.55	We < 0.08	Re < 200
This work	10	13.89	No single bubbling regime observed at We = 0.1 corresponding to Re = 510	
This work	20	55.55	No single bubbling regime observed at We = 0.08 corresponding to Re = 650	

In this table, we calculated these two dimensionless numbers in order to compare the reliance of classifying the single bubbling regime on these numbers.

The transition from single bubble regime effectively relies on the increase of the flowrate, corresponding to the onset of bubble-bubble interactions. This is consistent with the approach of Weber number in characterizing the regimes, where Weber number is the ratio of inertia effects (i.e., linked to injection flowrate) to the surface tension. This latter tends to reserve the spherical shape of bubbles.

Table III.1- Upper limit of the single bubbling regime according to nozzle Weber number.

Author	D_0 (mm)	Bo	Single bubbling regime	
Kyriakides et al. [63]	1 - 2	0.13	We < 0.04	Re < 100
Badam et al. [65]	2	0.55	We < 0.1	Re < 230
Cieslinski et al. [89]	1.6	0.36	We < 0.1	Re < 205
Zhang et al. [93]	2	0.55	We < 0.08	Re < 205
Mosdorf et al. [92]	2	0.168	We < 0.06	Re < 130
This work	2	0.55	We < 0.08	Re < 200
This work	10	13.89	No single bubbling regime observed at We = 0.1 corresponding to Re = 510	
This work	20	55.55	No single bubbling regime observed at We = 0.08 corresponding to Re = 650	

However, the different experimental works reporting single bubbling regimes in the literature used small nozzles ($D_0 \leq 2$ mm). At large nozzle sizes, single bubbling regime did not occur for our experimental work when using $D_0 = 20$ mm, even at low Weber number. In fact, through the investigation of Kyriakides et al. [63], the flow regimes are classified to various stages in a

dimensionless form of Froude number as function of Bond number (see Figure I.6). In this figure, it is shown that whatever is the magnitude of inertial forces represented by the Froude number, as $B_o > 7$ no single bubbling can occur. It is worth mentioning that this classification was also found to be consistent by Badam et al. [65].

According to the bubbling stages of Kyriakides et al. [63] and experimental dimensionless numbers (Bo, Fr) shown in Table III.2, the single bubbling can only be obtained in our experiments for the smallest nozzle D_0 = 2 mm. This is consolidated throughout our observations, where this regime was observed only at low flow rates for the smallest nozzle D_0 = 2 mm that was mounted to TYFON facility as shown in Figure III.1.

Table III.2- Bond number *Bo* and minimum Froude *Fr* of different nozzle sizes.

Nozzle diameter D_0 (mm)	2	5	10	20
Bond number	0.5	3.5	13.9	55.5
Froude number	Fr > 40	Fr > 7.1	Fr > 1.7	Fr > 0.4

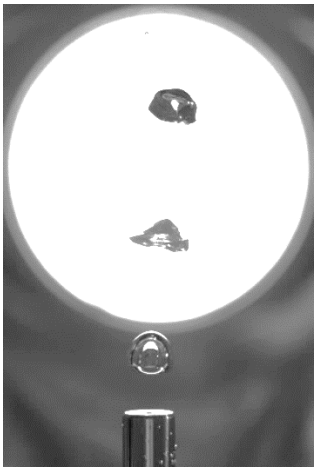

Figure III.1- Single bubbling regime in TYFON facility.

III.2.1.2. Classification of bubbly morphologies

Beyond the single bubbling regime, the classification of different morphologies differs between authors, depending on the description and the nomenclature of the morphology. Some authors have used the Reynolds number [63, 64] and others used modified Froude number [62] or Weber number [59]. Throughout our thesis, we referred to these regimes by an aperiodic bubbling, where departures of bubbles are not controlled solely by flow conditions, but also according to the interactions of bubbles (coalescence and interference). In terms of dimensionless numbers, the boundaries of these regimes were described by critical Reynolds number and a critical Weber number, as shown in Table III.3.

Table III.3- Critical dimensionless numbers for the bubbly regimes

Nozzle diameter D_0 (mm)	2	5	10	12
Critical Re	8250	8800	8850	8000
Critical Weber	130	60	30	20

The different bubbles' morphologies are classified based on the position of the possible coalescences of the bubbles. Indeed, as we found that with the further increase of the flow rate, the coalescences position becomes closer to the nozzle.

III.2.1.3. Pairing and doublet bubbles (0.1 < We < 1)

The stage where formation of two successive bubbles that mostly coalesce far above the nozzle, referred as pairing regime, is dominant in this range of Weber number, as shown in Figure III.2. The leading bubble which is not affected by wake of other bubbles takes foremost a spherical shape, however and after the formation of the trailing bubble, which is entrained by the wake of leading bubble and accelerated, it elongates vertically and distorts the shape of the leading bubble. As we increase the flow rate within this regime, the frequency of bubble formation is observed to be increasing as well as the size of bubbles.

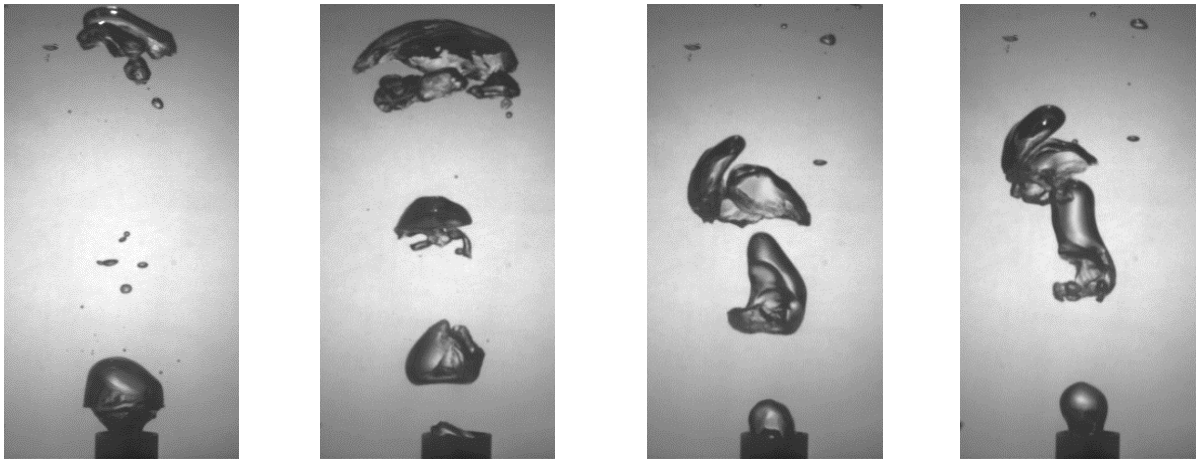

Figure III.2- Pairing and double coalescence of bubbles (D_0 = 12 mm - IUSTI Marseille setup).

III.2.1.4. Coalescence above the nozzle (1 < We < 5)

As the flowrate increases, the position of the coalescence takes place closer to the nozzle. This regime is characterized by the increased rate of the coalescence where we can observe a globule formed by the coalescence of two or three bubbles (see Figure III.3). In case of triple bubble coalescence, the first two bubbles are coalesced and form an irregular bubble shape, after that, another bubble is entrained and accelerated by the wake of the double bubbles thus penetrating them. The wake of the bubbles leads to the penetration of trailing bubble into the leading one, thus inducing the irregularity of shape of the large single bubble.

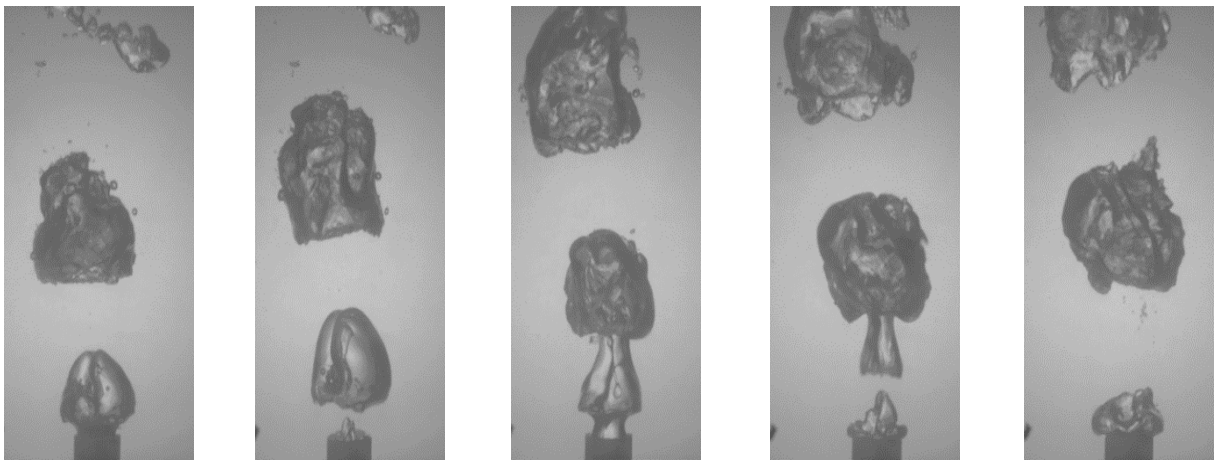

Figure III.3- Formation of globule by the coalescence above the nozzle (D_0 = 12 mm - IUSTI Marseille setup).

III.2.1.5. Coalescence at the edge of the nozzle (5 < We < 15)

The position of the coalescence continues to descend until it reaches the edge of the nozzle as we increase the injection flowrate, as shown in Figure III.4. Successive formation of bubbles with coalescence that forms one large globule can be identified. Two or three successive bubbles are coalesced at the tip of nozzle, and after that it is followed by another coalescence with a fourth bubble.

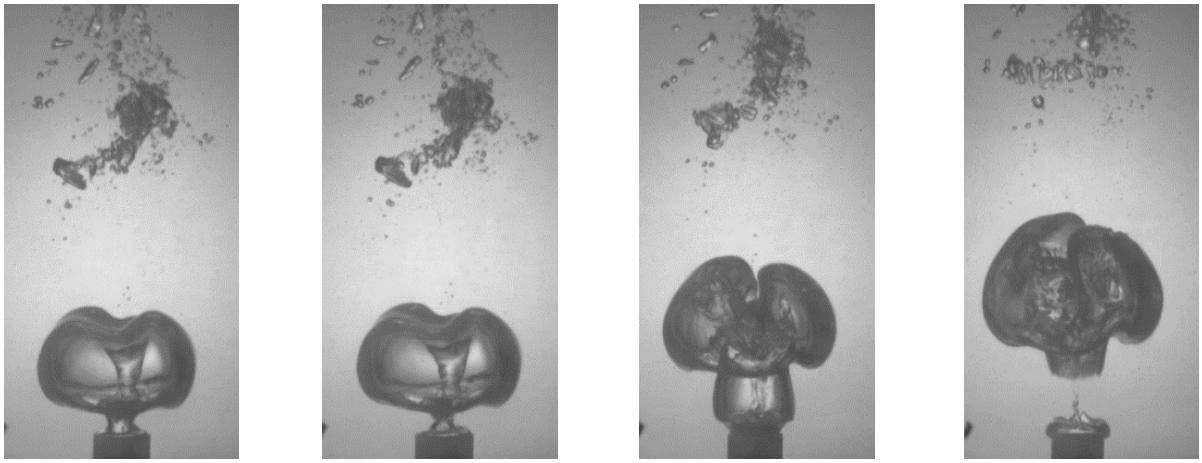

Figure III.4- Coalescence at the nozzle (D_0 = 12 mm - IUSTI Marseille setup).

III.2.1.6. Chaining (We > 15)

The rate of successive coalescence continues to increase, where the connectivity of the bubbles to the nozzle is demonstrated as shown in Figure III.5. As We > 20, the bubbles are vertically elongated after several formations and coalescences until they are finally detached from the nozzle. We refer to this phenomenon by chaining and it is more evident as we increase the Weber number for different nozzle sizes.

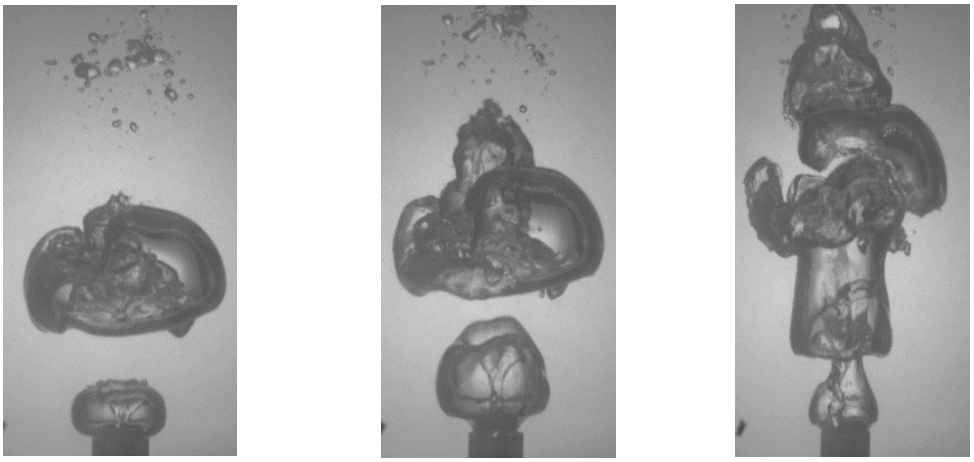

Figure III.5- Chaining and vertical elongation of bubbles (D_0 = 12 mm - IUSTI Marseille setup).

III.2.2. Transition from bubbly to jetting regimes

Beyond bubbling regimes, notably the chaining morphology, the regime would be described as churn turbulent or transition regime. In this range, the flow morphology could not be described as bubbly because the large rate of coalesced bubbles introduces vertically elongated gas structures, on the other hand, there is no continuous gas jet. The transition criterions reported by Cia et al. [64] with the Reynolds number, ($Re_{transition}$ = 11000) nor by Kyriakides et al. ($Re_{transition}$ = 20000) seem not to be consistent as shown in Figure III.6. However, the transition criterion of Zhao et al. [60] ($We_{transition}$ = 306) was more relevant. Therefore, we considered a transition regime corresponding to 150 < We < 300 (see Figure III.6 and Figure III.7).

(a) (b) (c)

Figure III.6- Transition regime for 150 < We < 300; (a): D_0 = 2 mm, We = 205, and Re = 10350, (b): D_0 = 5 mm, We = 250, and Re = 18070, (c): D_0 = 10 mm, We = 260, and Re = 26060 (TYFON facility).

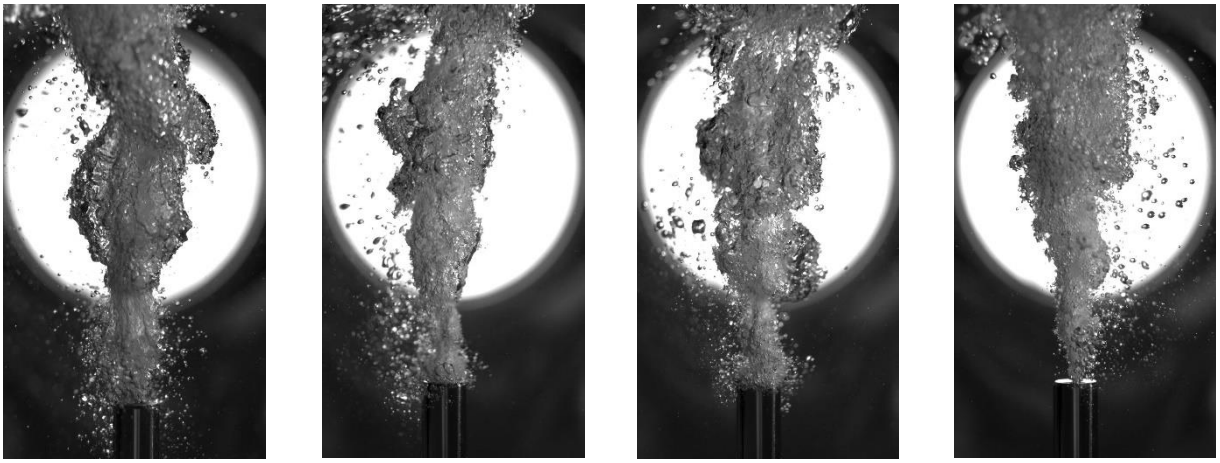

(a) (b) (c) (d)

Figure III.7- Jetting regime;(a): D_0 = 2 mm, We = 330, and Re = 13000, (b): D_0 = 5 mm, We = 330, and Re = 20760, (c): D_0 = 5 mm, We = 370, and Re = 31100, (d): D_0 = 2 mm, We = 2000, and Re = 32300 (TYFON facility).

The relevance of Weber number is highlighted in Figure III.7. Beyond the criterion of Zhao et al. [60], using the Weber number, the jet is observed for the different nozzle sizes. Regardless of the interruptions of the jet, a continuous gas stream is observed. On the other hand, in Figure III.7-(c) and Figure III.7-(d) nearly same Reynolds number is obtained but the morphology is not the same, as there are no interruptions interfering the jet at We = 2000.

III.3. Aperiodic formation of bubbles

The previous description of the bubble morphologies emphasizes that conventional phenomena, which are investigated in the majority of revised experimental works in the literature, are not common with our experiments. It stems from the fact the pool scrubbing mechanism links between uncommon flow conditions, compared to conventional approaches of understanding the hydrodynamics and mass transfer of bubbles.

The experimental results in the present section (published in Farhat et al. [82]) are presented as following temporal description of bubbling, the approach of globule volume and shape characteristics, the void fraction, and the rising velocity. The latter parameters were characterized on the IUSTI-Marseille device (see II.2) using the nozzle of size D_0 = 12 mm.

III.3.1. Temporal description

Taking in consideration the non-periodic behavior of the bubbling, it is important to investigate the dependence of bubbling within the time on the flow conditions, which could be correlated afterwards with the variation of bubbles size. This is shown in the given formula $V_b = \frac{Q_{inj}}{t_b}$, which holds the relation between the formation of a characteristic bubble volume V_b, formed by the injection flowrate of gas Q_{inj}, and the time corresponding its growth then its departure t_b. The frequency of bubbling due to the bubble-bubble interactions, affects respectively the bubbles volume released from the submerged nozzle.

III.3.1.1. XT diagrams

XT diagram, in other words space-time diagram introduced in II.2.2.1 and Figure II.4, represents the evolution of the bubbles at a certain altitude above the nozzle for the axial position during a period of time.

For that, it consolidates visually the bubbling frequency. At low flow rates, the flow exhibits pairing bubbles at higher altitudes, which are departed singularly, each one being considered as a globule, as shown in Figure III.8-(a), (d).

For higher flowrates and at low altitudes, the coalescence phenomena of the trailing and leading bubbles are detected and exposed as shown in Figure III.8-(b), (c). At higher altitudes, XT diagrams show the conception of globule formation beyond the coalescences of trailing and leading bubbles as shown in Figure III.8-(d), (e), and (f). Hur et al. [66] have shown the leading and trailing bubbles in the form of two peaks in their detachment period distributions, while these peaks could be visualized clearly through our XT diagrams.

It is important to note that the XT diagrams have no relevance with the real morphological description of bubbles.

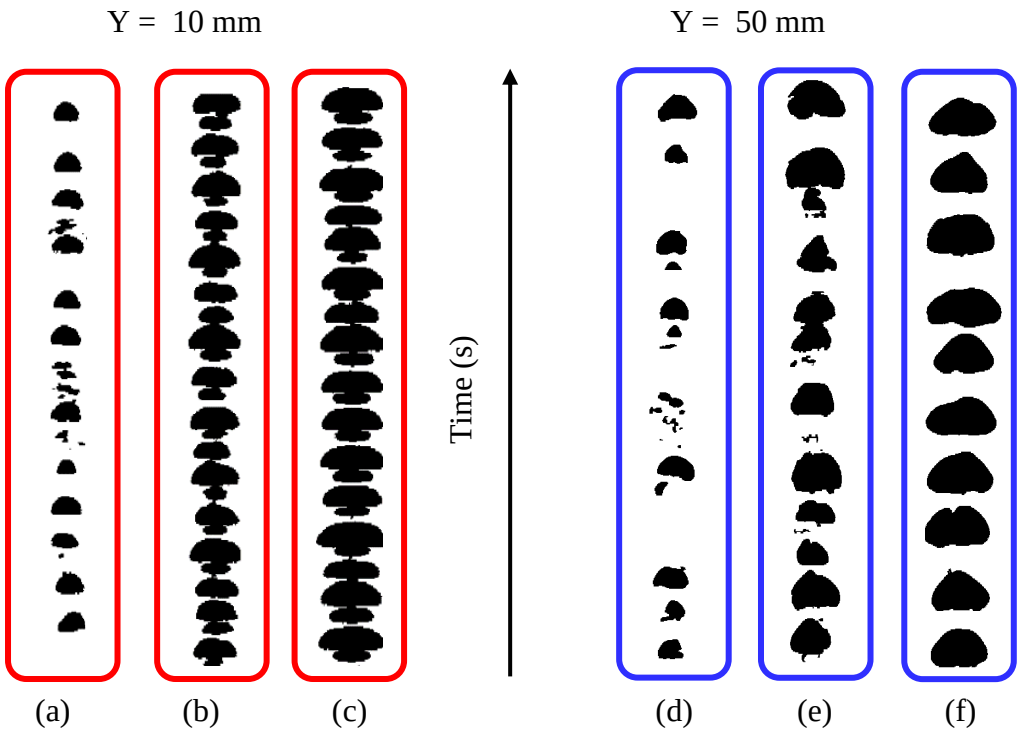

Figure III.8- XT diagrams at different altitudes and for different flowrates; at Y = 10 mm, (a): Q_{inj} = 6 L/min, (b): Q_{inj} = 24 L/min, (c): Q_{inj} = 54 L/min and at Y = 50 mm, (d): Q_{inj} = 6L/min, (e): Q_{inj} = 24 L/min, (f): Q_{inj} = 54 L/min.

III.3.1.2. Frequency of bubbling

As bubbles are affected by the wake and entertainment (dragging) of each other, a non-periodic bubbles formation is induced. Therefore, the approach of bubbling frequency is considered by tracking the departure of the bubbles and also the formation of one large globule in order to take in account the impact of bubble coalescence. Therefore, two means of bubbling frequency area investigated, the frequency of departure of bubbles f_b and the frequency of globule f_G. An example for the difference between the two events is given in the
Figure III.9.

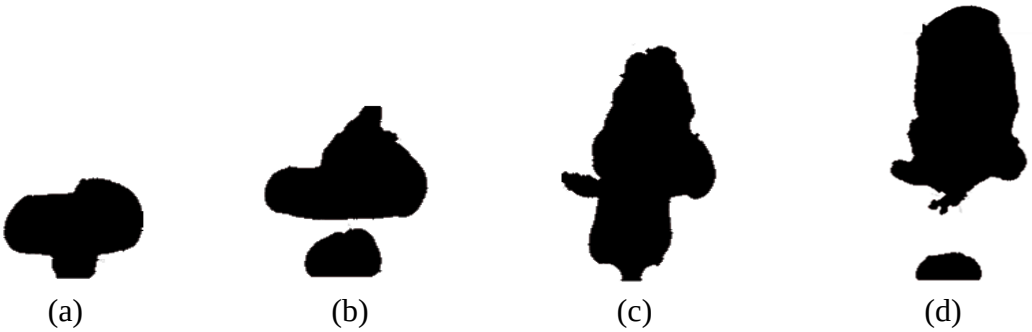

Figure III.9- Departure of bubbles resulting in globule formation.

A bubble is formed, and its neck is collapsing prior to its detachment, so that after detachment, we consider that one departure event has been achieved (

Figure III.9-(b)). Here, counting an event for globule formation is not yet ensured, and this depends on the following stages subjected to the bubble. Consequently, after the detachment, the entrainment of the latter bubble induces the accelerated formation of a trailing bubble, which is vertically elongated, and it is still connected to the nozzle (
Figure III.9-(c)). After the detachment of the resulting globule, consisting of the coalesced bubbles, another departure event is considered as well as an event of globule formation (
Figure III.9-(d)). Thus, in this case two departure events lead to one globule formation. More generally, $f_G \leq f_b$.

III.3.2. Classical approach of predicting bubble size

Through literature review, we have found that most of the developed models, within the single bubbling regime, established force balance approaches, which neglected bubbles interaction, and made assumptions of spherical shape of the bubble. In this paragraph, we computed the characteristic bubble size by mean of determining bubble formation time t_b in our experiments, such that $t_b = 1/f_b$.

III.3.2.1. Departure frequency f_b

For the departure frequency, an event is recorded at the instant where there is a structure detachment from the nozzle. In case this bubble is re-attached to the nozzle by mean of coalescence, the following departure of merged structure is considered as second event as shown in
Figure III.9. After recording bubbles departure, the frequency distribution is depicted in Figure III.10. At low flowrates "pairing morphology", the doublet bubble is formed after the acceleration induced by the leading bubble on the trailing one, due to the wake effect. However, this doublet will not affect the growth of the following bubble. This phenomenon affects departure frequency, and it is shown in the distribution of Figure III.10-(a). The position of coalescence descends as we increase the flowrate, thus the wake effect of bubbles intervenes continuously during the flow.

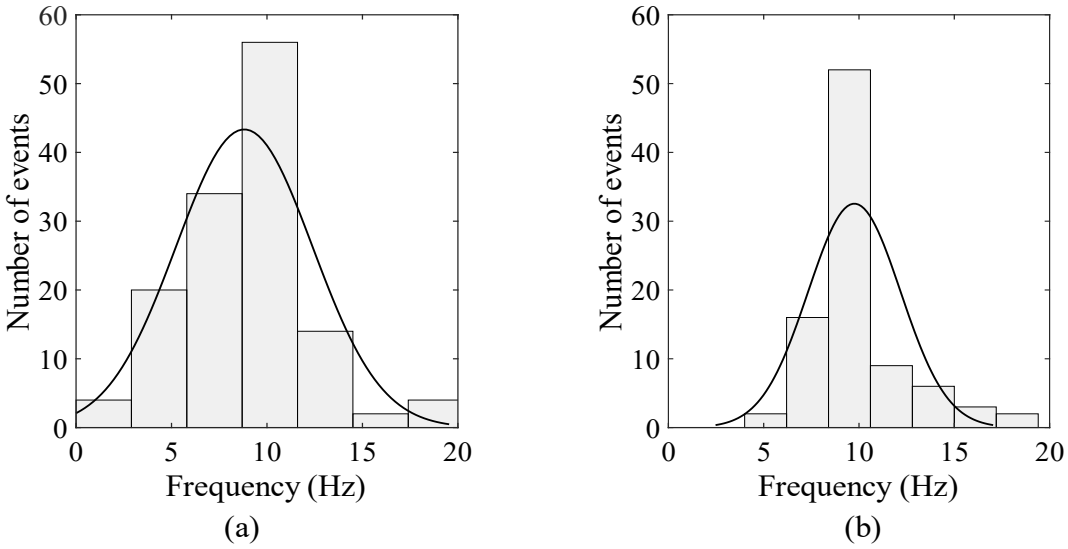

Figure III.10- Histograms of departure frequency f_b; (a): Q_{inj} = 6 L/min (We = 0.16), (b): Q_{inj} = 36 L/min (We = 5.7).

The variation of departure frequency for different flowrates is depicted in Figure III.11. There is a considerable increase from low to intermediate flowrates until reaching a maximum value at Re = 1790 (Q_{inj} = 18 L/min & We = 1.4). After that, with a further increase of the flowrate, the frequency decreases until it fluctuates around a constant value. Hur et al. [66] reported that frequency of departure increases as the nozzle diameter decreases, as they used three different sizes of nozzles. In our experiments, the used nozzle (12 mm diameter) is much larger than theirs, and therefore we obtained lower frequencies of bubbles departure (see Figure III.11). It is worth mentioning that, the profile of frequency evolution, upon the variation of the flowrate, is comparable to Hur et al. [66].

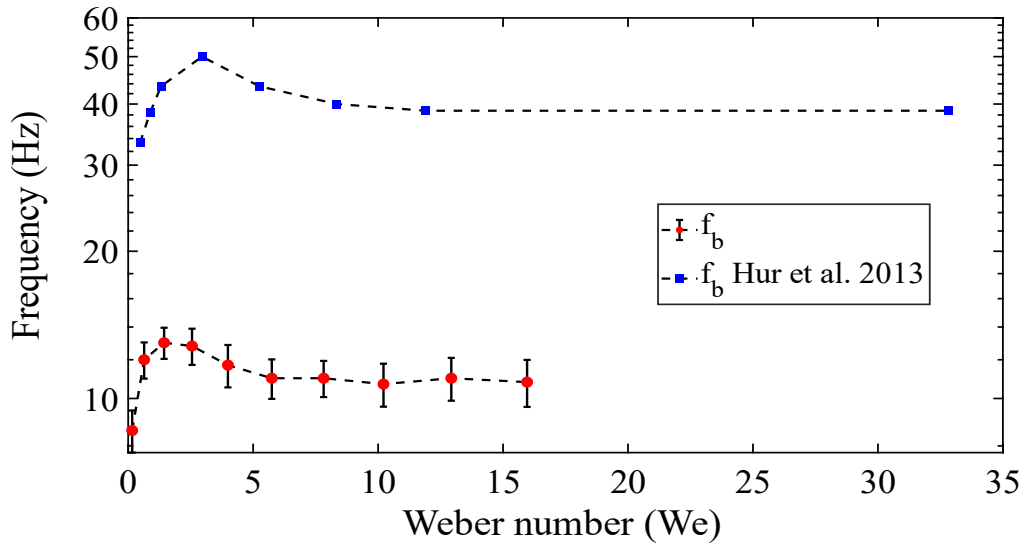

Figure III.11- Variation of departure frequency f_b as function of Weber number.

III.3.2.2. Bubble characteristic volume V_b

Based on the bubble formation time and under the constant gas inflow, we computed $V_b = Q_{inj} \times t_b = Q_{inj}/f_b$. This volume corresponds to the bubble formed withough exhibiting any coalescence, supposing a single bubbling regime. In literature, some of the different correlations for predicting the bubble volume V_b are shown in Table III.4.

Table III.4- Correlations developed to predict the bubble volume in single bubbling regime

Reference	Correlation	Range of validity
Gaddis et al. [59]	$V_b = \frac{\pi}{6}\left[\left(\frac{6\,D_o\sigma}{g\,\rho_l}\right)^{4/3} + \left(\frac{8\,\mu_l Q_{inj}}{g\,\rho_l\,\pi}\right) + \left(\frac{135\,Q_{inj}^{\,2}}{4\,\pi^2 g}\right)^{4/5}\right]^{3/4}$	0 < We < 4
Krevelen et al. [107]	$V_b = 1.722\left(\frac{Q_{inj}^{\,2}}{g}\right)^{3/5}$	-
Davidson et al. [105]	$V_b = 1.138\left(\frac{Q_{inj}^{\,2}}{g}\right)^{3/5}$	-

Gaddis et al. [59] precised the validity range of their model such that 0 < We < 4. They justified that by referring to a critical Weber number We = 4 (see Table III.4), where they consider a transition from single bubbling regime to jetting regime. These correlations were developed, within the single bubbling regime, by establishing a force balance approach. Bubble-bubble interactions were neglected, and assumption of spherical shape of the bubble has been made.

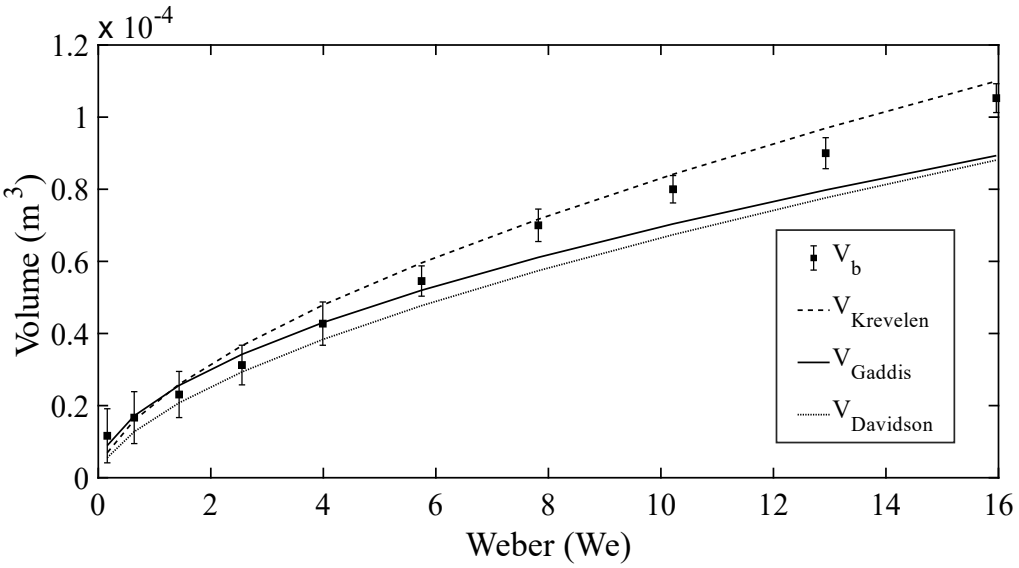

Figure III.12- Comparison between bubble characteristic volume V_b obtained in our study with models from literature: Gaddis et al. [59], Krevelen et al. [107], and Davidson et al. [105].

In Figure III.12 we show the good agreement of the characteristic bubble volume for the different correlations which are well common in literature. As mentioned before, these correlations have assumed of spherical shape of the bubbles. Hence, we determined the equivalent diameter d_b of sphere (see Figure III.13) such that $d_b = \sqrt[3]{\frac{6}{\pi} V_b}$. Without surprise regarding to the V_b results, d_b fits well the models.

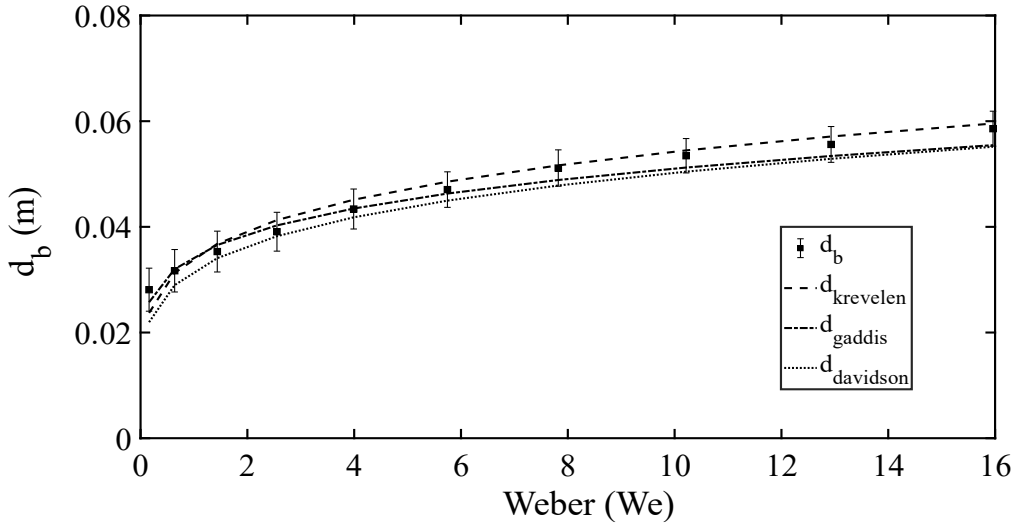

Figure III.13- Comparison between equivalent diameter d_b with models from literature

On the basis of the morphological description of bubbles presented in this report, the spherical assumption is not consistent with the bubbles shape observed experimentally. It is considered a critical limitation especially in aperiodic formation of bubbles (non-single bubbling), amid bubble-bubble interactions that deforms considerably the shape of bubble (non-spherical shape). This inaccurate characterization of bubbles has a negative impact on the modelling of bubble dynamics in industrial applications, where air is injected at high flowrates. The latter is relevant to pool scrubbing, where the precision is of key importance. Based on what stated, we tried to improve the determination of a characteristic bubble volume in the injection zone by a phenomenological approach. Thus, the determination of the volume of large bubbles called "globules" resulting from the bubbles coalescence in the injection zone, is investigated in the following paragraphs.

III.3.3. Phenomenological approach and globule volume

This phenomenological approach was the subject of a published paper in the international journal of heat and mass transfer by Farhat et al. [82], but the latter paper didn't included the characterization of surface area, which is discussed here in III.3.3.4.

In aperiodic behavior, bubble-bubble interactions affect the size of the detaching bubble, thus broaden the size distribution [66]. Wake effect of leading bubbles influences the size of trailing bubbles [93], and accelerates the departure of a certain bubble thus minimizing its size.

On the other hand, bubble-bubble coalescence at the edge of the nozzle increases the size of the departed bubble. In relevance for what is given above, we intend as a first step to avoid the controversial determination of departed bubbles, instead we opted to characterize the size of globules i.e., the largest structure that can be formed in this zone in bubbly regime (most suitable for mass transfer considerations later). Given that, the position of globule formation varies according to the number of bubbles forming this globule, the temporal and size characterizations depend on the tracking of globule formation, which could occur at different altitudes [63, 89, 93], as shown in Figure III.14.

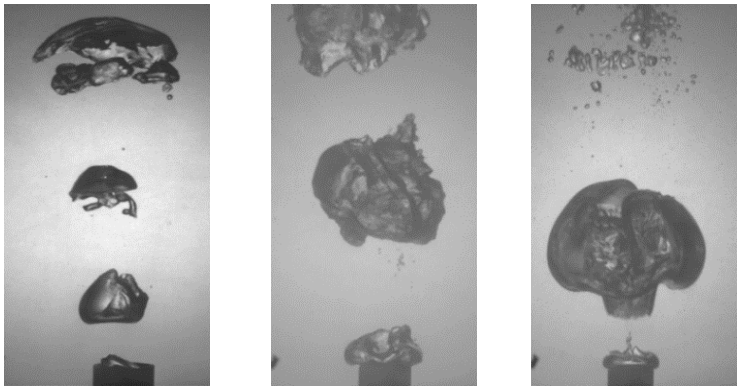

Figure III.14- Globule formation at different altitudes.

III.3.3.1. Frequency of globules f_G

For the frequency of globule, the detection of globule formation is recorded by tracking the growth and the rise of bubbles that have detached from the nozzle. In our experimental work, it is noted that for characterizing the formation of globules, an additional post-treatment of the bubble evolution presented is required. The numerical quantification of the globules' formation is done through analyzing a chronograph of bubbles evolution (see Figure III.15), on which we are capable of differentiating between the events of bubbles formation, detachment, and coalescences. To recall, an event is recorded when a complete formation of a globule is achieved, whether it is a single bubble or a result of coalescence of two or more bubbles, when it is detached completely and finally from the nozzle.

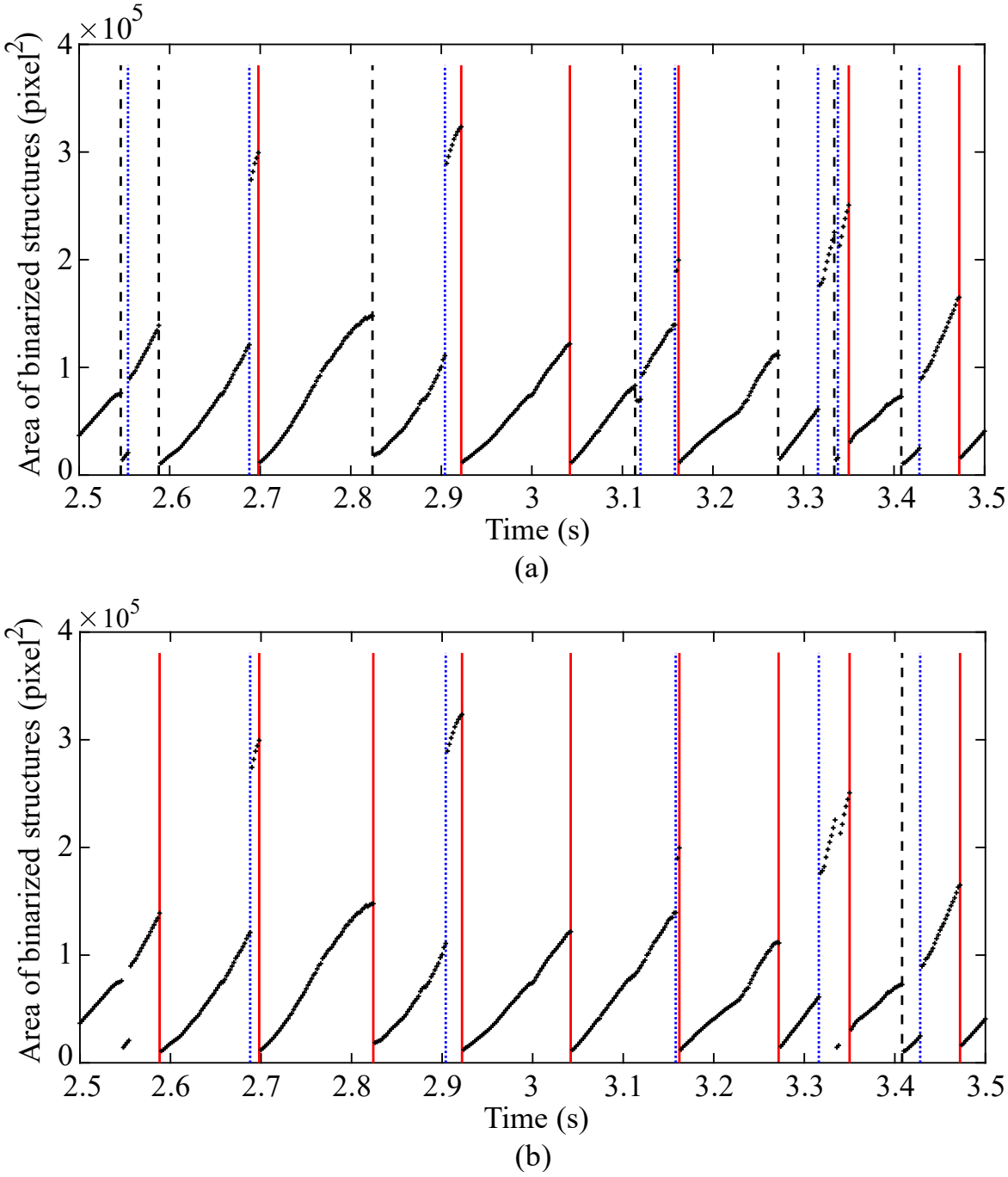

Figure III.15- Chronograph of bubbling events; Bubble birth (red solid lines), Breakup followed by coalescence and re-attachment to the nozzle (black dashed lines), and coalescence (blue dotted lines); (a): Raw chronograph, (b): Filtered chronograph

Therefore, and after the filtration of the chronograph (see Figure III.15-b), a globule event is depicted in each red solid line, whereas its lifetime and interferences and coalescence (black dashed line and blue dotted line) are depicted between two red lines.

Binarization errors (t = 2.55 s, t = 3.12 s) and channeling effects (t = 3.34 s) are filtered automatically. This is done by setting a threshold of minimum period time in order to consider a new event. Then the events of bubble formation and departure are manipulated manually (t = 2.83 s), upon the observation of the chronograph.

The distributions of globule frequencies are shown in Figure III.16. In comparison with Figure III.10, we can observe that the frequency of departure (Figure III.10-a) is the same as the frequency of the globule (Figure III.16-a) for low Q_{inj} = 6 L/min. This could be justified by the fact that there is no coalescence phenomena at low flowrate [51, 105, 106]. However, this occurs after considering each departure bubble as a globule, since this pairing occurs at high altitudes beyond the tracking. As the flowrate increases, bubble-bubble interactions are generated, and then coalescence of bubbles occur.

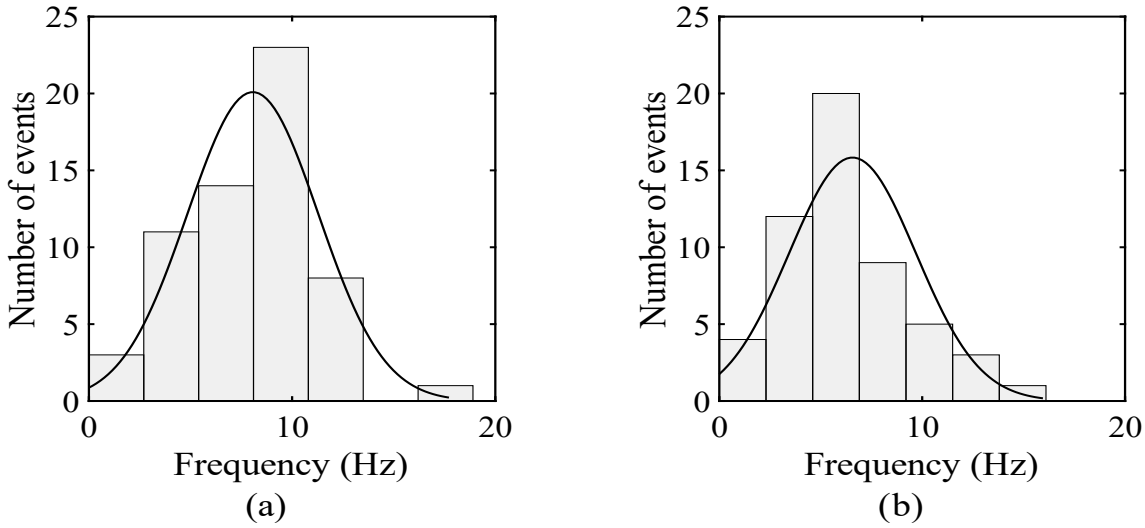

Figure III.16- Histograms of globule frequency f_G; (a): Q_{inj} = 6 L/min (We = 0.16) , (b): Q_{inj} = 36 L/min (We = 5.7).

A globule event occurs after several bubbles' coalescence. As mentioned before, this results in a difference between the events counting for bubbles departure (Figure III.10-b) and that of globule formations (Figure III.16-b): $f_G \leq f_b$. For the globule frequency evolution as shown in Figure III.17, it takes nearly the same profile of evolution of departure frequency (see Figure III.11) but at lower frequencies and with maximum frequency corresponding to Q_{inj} = 12 L/min.

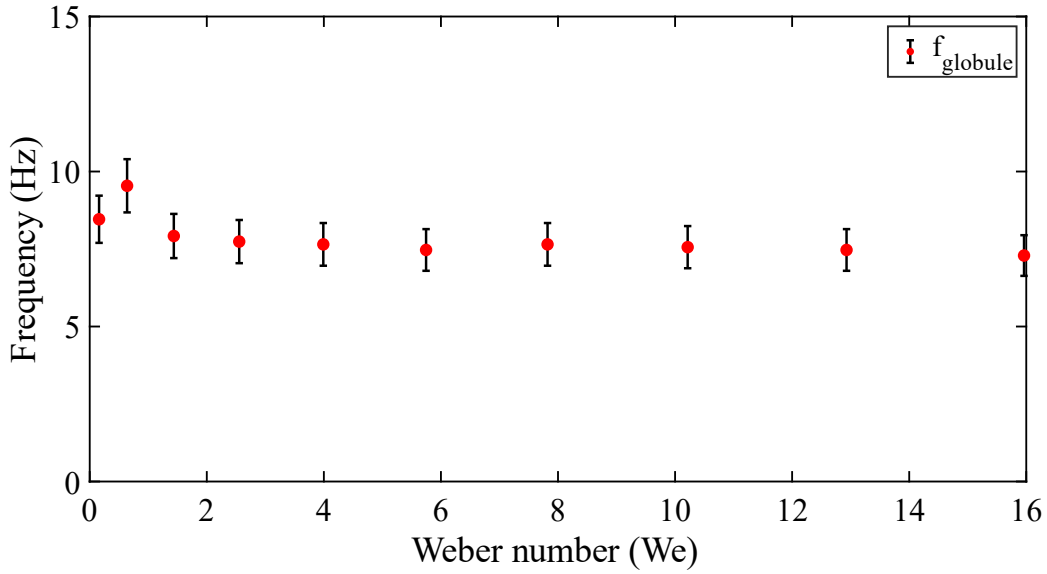

Figure III.17- Variation of globules formation's frequency as function of Weber number

III.3.3.2. Globule volumes

The globule volume is computed numerically once its definitive size is achieved (detected as mentioned in the methodology above). For that, a cylindrical revolution of the pixels is assumed around an equidistant line (Figure III.18-a), which bisects the structure radially into two equal parts at each vertical position of the structure. Actually, one part is rotated at 360° around the equidistant line with axisymmetric assumption (the two volumes induced by each part are equal in this case). Thus, the volume of revolution (1-pixel torus) is computed for each pixel (rotation, see Figure III.18-b). Therefore, the volume of each cylindrical slice of the structure is the sum of all 1-pixel torus volumes of the corresponding slice. Finally, the volume of the structure is the sum of all cylinder volumes calculated along the vertical equidistant line.

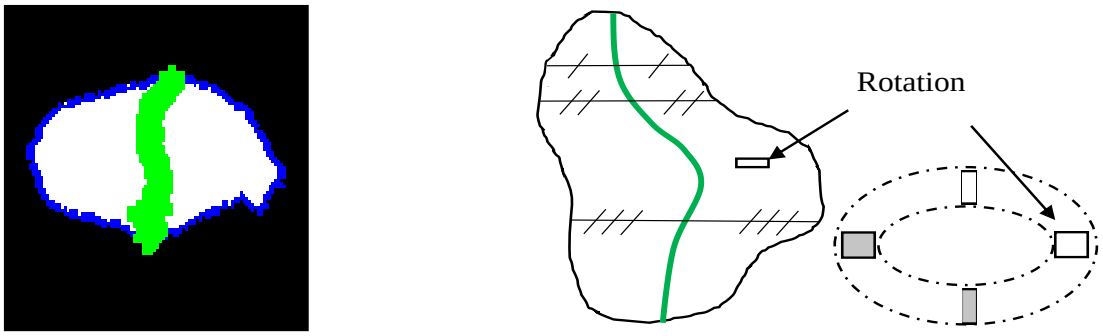

(a) (b)

Figure III.18- Tracking and numerical computation of globule volume $V_{G;}$ (a): Tracked globule, (b): Schema of unitary volume of a pixel.

Signals recording the evolution of bubbles volume, tracked until their final detachment from the nozzle, are constituted. Figure III.19 shows a raw signal for the volume evolution of bubbles, while they are attached to the nozzle, corresponding to Q_{inj} = 48 L/min.

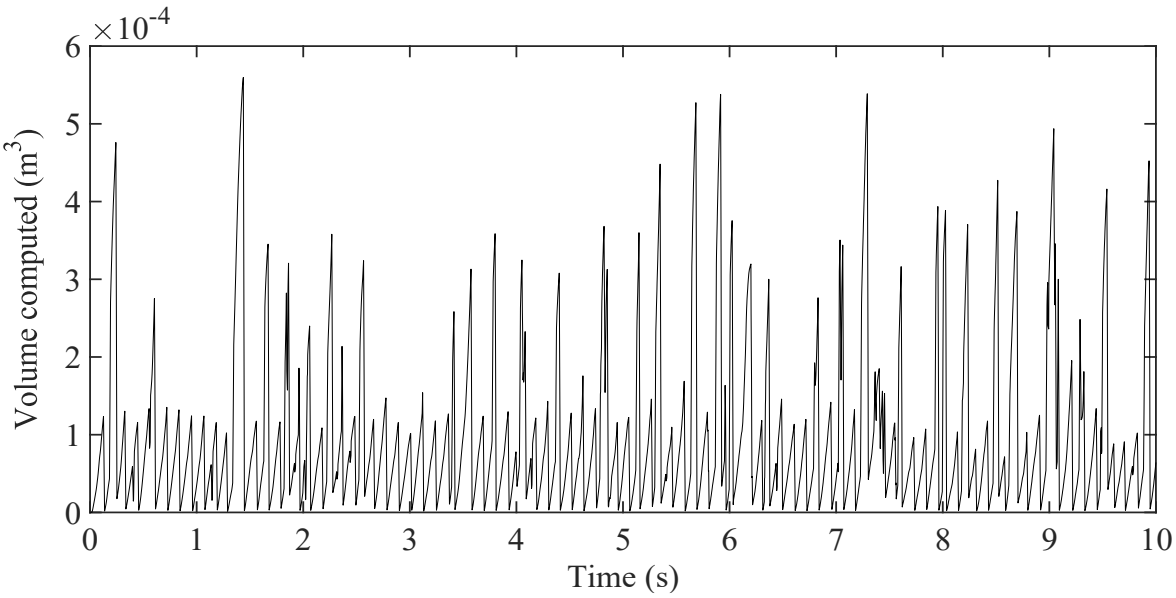

Figure III.19- Evolution of bubbles volume as function of time for Q_{inj} = 48 L/min and D_0 = 12 mm (We = 10.2).

Low amplitude peaks corresponding to one bubble or globule are observed. Moreover, high amplitude peaks corresponding to structures attached to the nozzle are observed, which are formed of several bubbles, due to coalescences, vertical elongation, and chaining. The post-treatment of these signal aims to reconstruct the filtered signals representing the formation of globules through two successive steps described below.

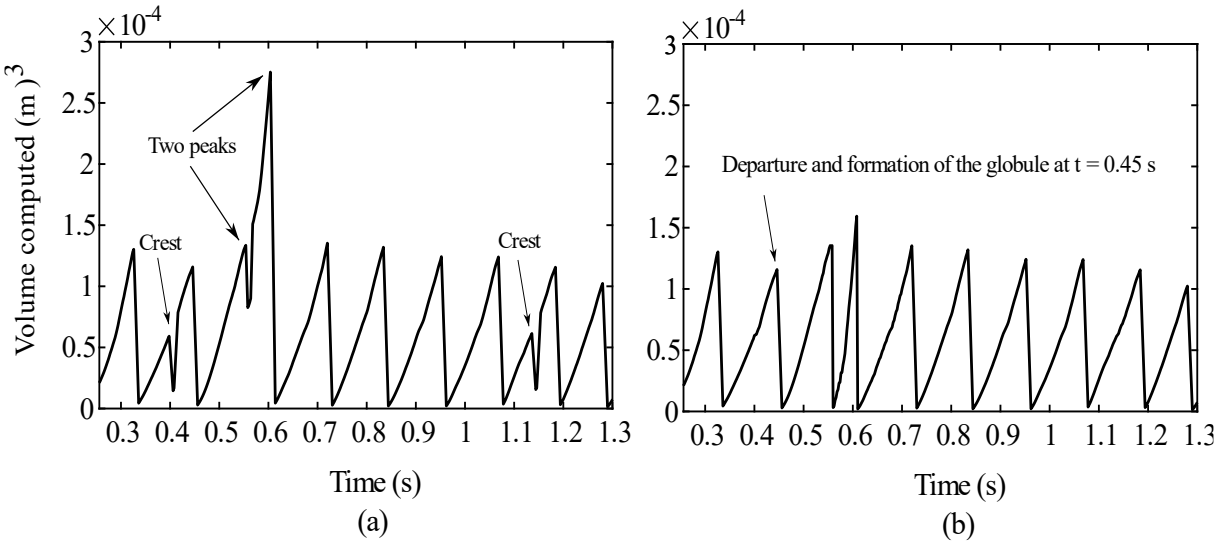

Figure III.20- Post-treatment of volume signal; (a): Raw signal, (b): Treated signal

- The first step considers the rectification and filling of the cracked crests appearing at t= 0.4 s and t= 1.15 s in Figure III.20-(a). As structures are tracked as long as they are attached to the nozzle, their volume is computed until their departure (Figure III.21-(a)), then the computation begins for another bubble that is undergoing formation that appears as a slip in the signal like at t = 0.4 s and t = 1.15 s in Figure III.20-(a). Consequently, as the trailing bubble penetrates into the previous bubble, a jump in the signal can be seen since the new

structure, formed by these two bubbles, is attached to the nozzle and so it is tracked (Figure III.21-b), therefore, the globule volume is computed until its final departure (Figure III.21-c). Hence, in order to avoid overestimation in the quantification of peaks representing the globules formation, the filling of the cracked crest is done as shown in Figure III.20-(b).

(a) (b) (c)

Figure III.21- Tracking of globules; (a): Bubble departure at t = 0.4 s, (b): Coalescence and reattachment to nozzle at t = 0.42 s, (c): Departure and formation of the globule at t= 0.45 s.

- The second step relies on the splitting and differentiation of crests, corresponding to chaining formed by more than 2 bubbles, into globules. This could be seen in Figure III.20-(a) at t = 0.55 s and 0.6s, where there were two peaks existing in one crest. However, in the filtered signal they are spitted into two crests with each has its own peak, representing a globule formation. It is justified by the fact the chaining of bubbles represents several coalescences of globules, which are vertically elongated.

Therefore, the post-treated signals are constructed where the maxima of their peaks represent the final volume of globules V_G at the instant of detachment. A histogram is constructed to inspect the distribution of globule volumes, for each flowrate, as shown in Figure III.22.

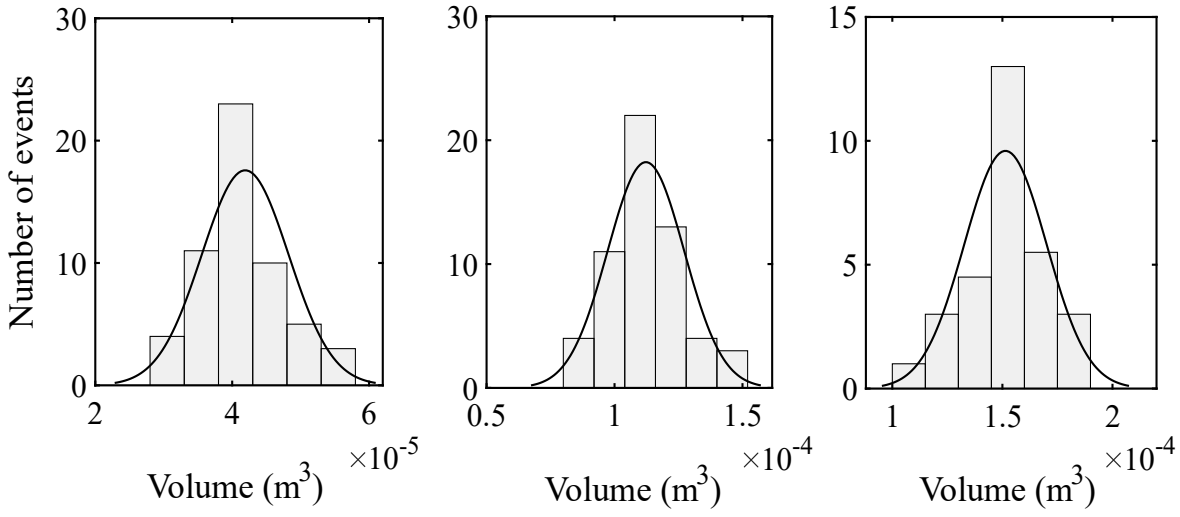

(a) (b) (c)

Figure III.22- Histograms of V_G distribution; (a): Q_{inj} = 18 L/min (We = 1.43), (b): Q_{inj} = 42 L/min (We = 7.8), (c): Q_{inj} = 60 L/min (We = 16).

Moreover, Gaussian curves fitting the histograms provide an average globule volume for each flow rate. These results have shown that increasing the flowrate influences the variation of bubbles volume while conserving static bubbling frequency [65].

At low flow rates, bubbles tend to exhibit spherical and elliptical shapes, however, the increase of flowrate induces more bubble-bubble interactions, so that the shapes become irregular depending on the position and number of coalescences.

Figure III.23 shows both the variation of bubble volume V_b and average globules volume V_G as function of Weber number, upon varying the flowrate. For each flowrate an acquisition of 10000 images was taken corresponding to 20 s, so the uncertainties presented in the globule volumes corresponds to the standard deviation of the Gaussian distributions determined for each flow rate (see Figure III.22).

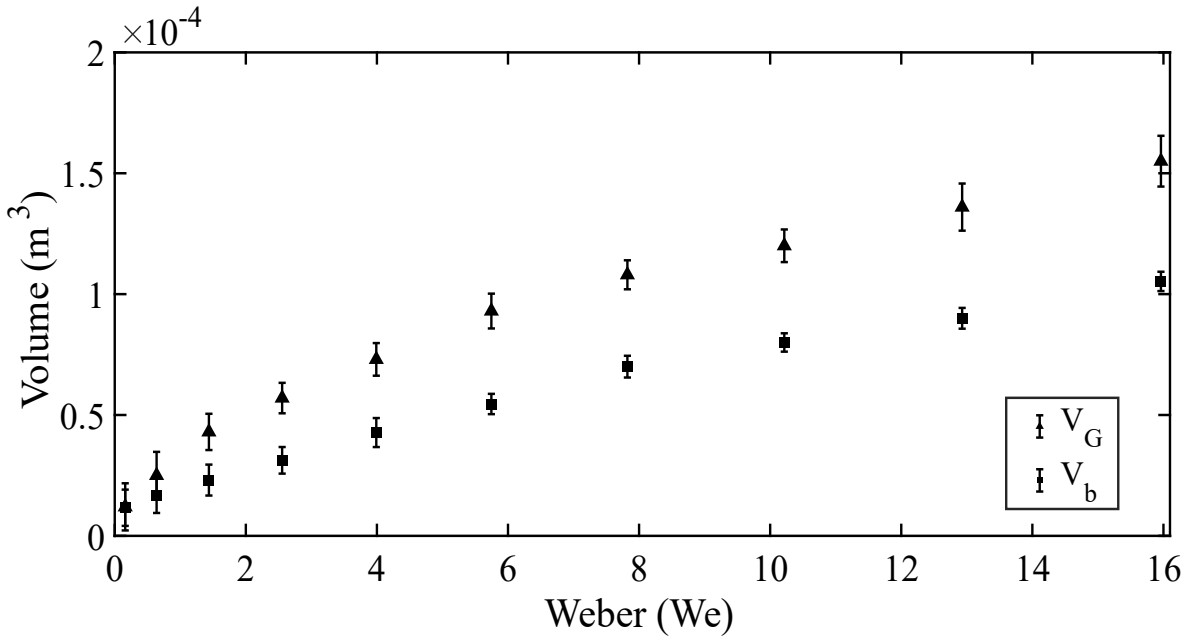

Figure III.23- Difference between classical (V_b) and phenomenological (V_G) determination of bubble volume.

At low flowrates, globule average volume is comparable to the characteristic bubble volume, thus fitting the literature models (see Figure III.12). This is due to the fact that at the corresponding regime, the conception of globule formation is not attained yet, although the acceleration of bubbles formation is induced. In other words, the volume of bubbles in this regime corresponds to single bubbles formed without prior coalescence.

However, with the increasing of flowrate and the onset of globules formation, the divergence of average bubble volume is apparent. Moreover, this difference increases with the increase of flowrates, which means that V_G is not fitted in models anymore.

III.3.3.3. Validation of the phenomenological approach

We postulated that the formation of globule is the relevant volume of formed bubble along the different flow morphologies in the injection zone, in bubbly regime. In order to show the consistence of V_G, Figure III.24 shows the computed flowrate experimentally ($Q_{exp} = V_G \times f_G$) as function of the real injected flowrate Q_{inj}, adjusted during experiments. The satisfactory agreement consolidates the phenomenological approach of globule characterization, as well as the axisymmetric assumption for V_G computation.

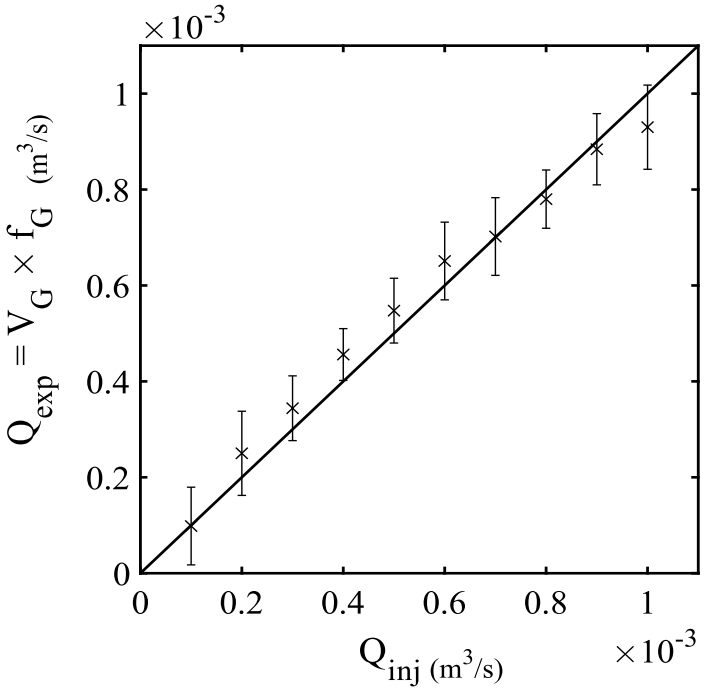

Figure III.24- Validation of the experimental flowrate with the real injected flowrate Q_{inj}.

This non-negligible difference between V_b and V_G confirms the impact of bubble-bubble interaction. The comparison between both approaches shows the weak applicability of literature models to predict bubbles size at high flowrates and suggests the phenomenological approach in characterization of bubbles dynamics.

This disparity between phenomenological investigation and conventional approach is relevant for pool scrubbing, where carrier gas is often injected at high flowrates. Therefore, awareness is raised in modelling of such applications regarding the precision of dynamics quantification, notably mass transfer mechanisms. As at high Weber number, the contrast of bubble volumes determined by the two approaches present the more significant difference between the relative exchange surfaces. For example, if we suppose a spherical shape of bubble at, We = 16, and then compute the surface areas determined by the different approaches, we will have an underestimation of 23%. Besides, this margin of error will probably increase with the non-spherical shape shown in morphological description. Hence and regardless of the bubble shape, a considerable difference in mass transfer would appear when comparing the conventional and the phenomenological approach, regarding the high dependence of these transfer on interfacial area as discussed in the paragraph below.

III.3.3.4. Surface area of globules

After determining the globule volume upon its formation, a method developed by Legendre et al. [108] was used to determine the surface area, as shown in Figure III.25.

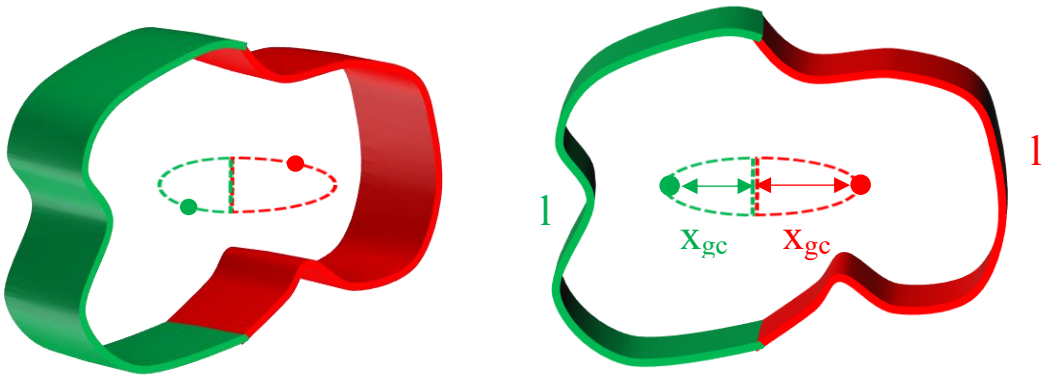

Figure III.25- The adopted method for determining the surface area of globules.

The method states that the surface of revolution generated by rotating a curve about an axis of rotation is equal to the product of the curve length, l, and the distance traveled by its geometric centroid x_{gc} such that:

$$S_G = 2\,\pi\, l\, x_{gc} \qquad (17)$$

Thanks to the edge detection algorithm showed in II.2.2.1, the contour of the bubble is determined and eventually the geometric center of the bubble and the position of the vertical axis. Then, the bubbles interface is cut into two parts (left and right), where it is relatively easy to determine x_{gc}, C, and l as shown in Figure III.26.

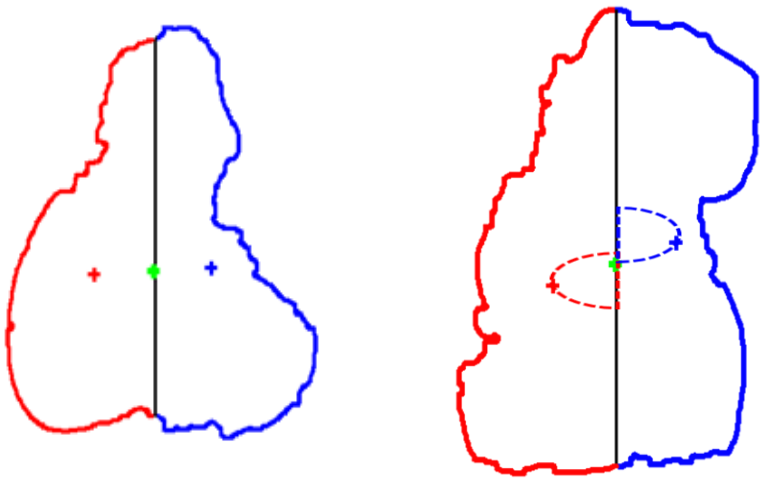

Figure III.26- The right and left side of the globule according to its geometric center.

Using this technique, the globule surfaces are estimated such that it is average of the surface of the left side and right side (eq. 18).

$$S_G = \frac{S_{G\,left} + S_{G\,right}}{2} \quad (18)$$

Figure III.27 shows the comparison between the surface area of globules and the surface of sphere with the equivalent diameter d_G such that $S_{sphere} = \pi\, d_G^2$ and $d_G = \sqrt[3]{\frac{6}{\pi}\, V_G}$.

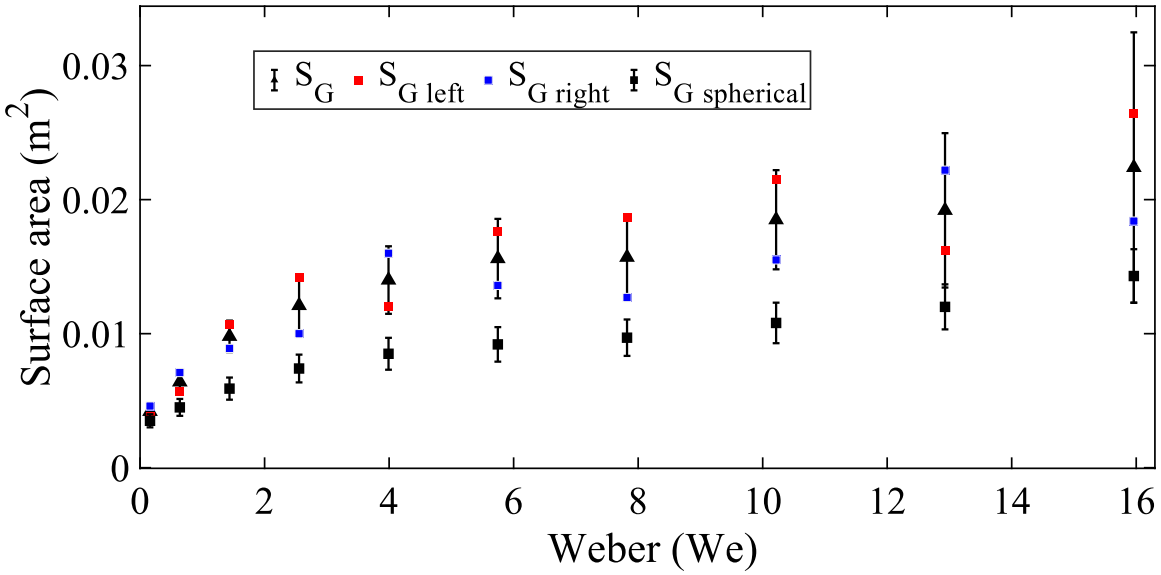

Figure III.27- Surface area of globules and the limitation of the technique for high flowrates.

It was expected that the phenomenological approach in determining the surface area of globules would yield in larger surface areas considering the spherical assumption ($S_G > S_{G\ spherical}$) because generally spherical shapes have the minimum surface area of any object of a certain volume.

A significant variation appears at We > 1, as the phenomenological aspect of the flow varies with the bubble-bubble interactions as shown in Figure III.26. The standard deviation, which is estimated by averaging the data determined for 20 s of bubbling, increase sharply when the injection flowrate is increasing, especially when the flow is close and beyond the chaining morphology. For that, we considered that the phenomenological aspect of the flow poses limitations to the adopted technique as We > 10. This precaution should be taken for surface area of bubbles, as this parameter is important in transfer phenomena between gas and liquid, especially that it permits the determining of the interfacial area of the globules, a_G, and the volumetric interfacial area in the pool (will be discussed in Chapter V).

III.3.3.5. Void fraction

The void fraction, ratio of the volume of the dispersed phase (air) to total volume of dispersed and continuous phase (air + water), is considered as an important parameter in the mass transfer between the dispersed and the continuous phase, and its knowledge contributes to determine the global interfacial area between the gas and liquid. Moreover, void fraction describes the

expansion of the bubble plume in the axial and radial direction, that is why it is also considered as a criterion for classifying the flow regimes [109]. Within the development of the ASTEC code, models determining the void fraction are requested, especially in the bubble rise zone. Optical sensors are often used to measure the local void faction, where the sensor provides an average void fraction over the sensor length and this spatial resolution. In literature, other techniques than optical probes are used, one of them is the image processing.

Through our experiments on the IUSTI facility, which are based on image processing and data treatment, we achieved to measure the local void fraction along the radial profile, and to provide the tomographic reconstruction in order to visualize the void fraction distributions. The local void fraction along the radial profile is defined as the ratio between cumulative gas time to the total test time measured, and in terms of image processing, it is computed such that

$$\alpha_{i,j} = \frac{1}{N}\sum_{k=1}^{N} p_{i,j,k} \quad for\ 1 < i < 1280\ and\ 1 < j < 1024 \tag{19}$$

Where $\alpha_{i,j}$ is the gas fraction at the radial coordinate i (horizontal axis) and at altitude j of the optical field (which size is 1280x1024, in which 1 cm corresponds to 64pixels). Thus, $p_{i,j}$ is the value of pixel at the coordinate (i,j), where $p_{i,j}$ = 0 corresponds for liquid and $p_{i,j}$ =1 for gas. N is the total number of images which corresponds to time. For each flow rate, the total number of images N is 10000 which is equivalent to 20 seconds. By recurrence to the XT diagram (III.3.1.1), the radial profile of void fraction could be determined by averaging the XT diagrams with respect to time.

Abe et al.[51] have depicted these diagrams in order to present void fraction at different height positions. Radial void fraction profiles in a bubble plume are commonly described by Gaussian curves [110]. In Figure III.28, we show the void fraction for Q_{inj}= 24 L/min at altitude Y = 20 mm (j is fixed), where the comparisons between experimental data and curve fits show that the radial void fraction profiles are very well represented by Gaussian curves, as they are seen to be symmetrical and exhibiting a bell shape. All the parameters such as the maximum and width of the profile could therefore be determined by a standard fitting procedure. The distribution of the void fraction varies upon the variation of the altitude above the nozzle, as well as we can also observe that the variation of the width of the Gaussian upon the variation of the gas flow rate, due to the horizontal expansion.

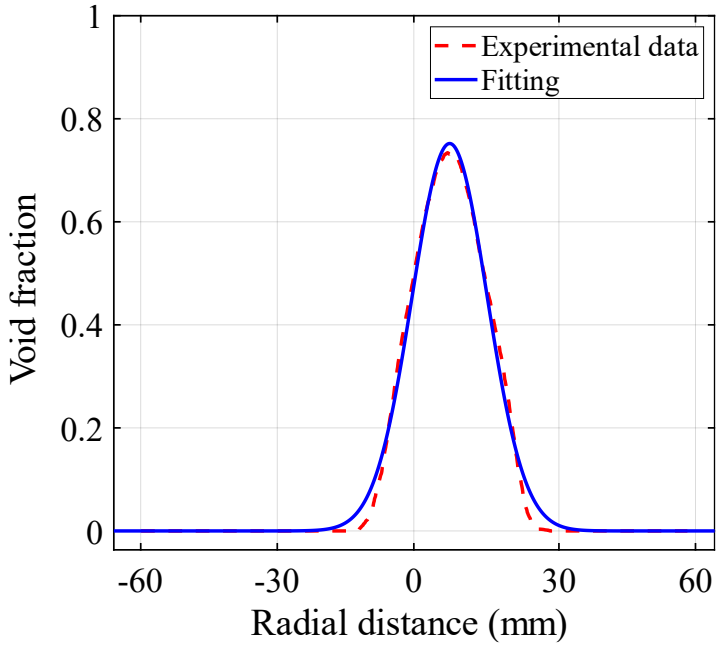

Figure III.28- Gaussian fitting of the void fraction curves for Q_{inj} = 24 L/min (We = 2.55) at Y = 20 mm.

Figure III.29 shows the impact of flow rate and the altitude on the profile of the void fraction represented by the Gaussian curve. The spatial distribution of the void fraction varies with altitude, as we also observe that the width of the Gaussian increases upon increasing the altitude, as shown for each Q_{inj} in Figure III.29. This is due to the fact that as bubbles rise, their diameter increases as they continue growing above the orifice. Besides at low altitudes, the flow is mainly composed of the formed globule which is located in the centerline of the plume, and that is why we obtain a smaller width.

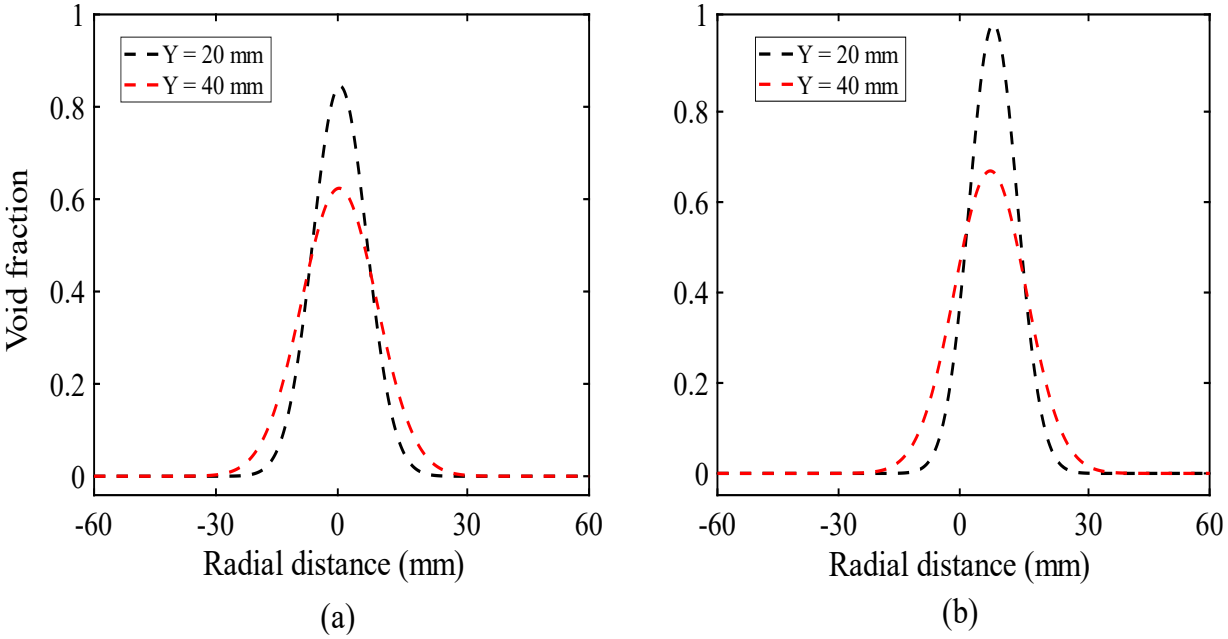

Figure III.29- Gaussian fitting profiles of void fraction variation as function of flowrate and altitude above the nozzle D_0 = 12 mm; (a): Q_{inj} = 30 L/min, (b) Q_{inj} = 60 L/min.

In the other hand, the void fraction and also the width of its profile increases with the increasing of the flowrates, which is expected due to the increase in the bubble volume and its spatial expansion. In other experiments, other authors assigned this relation to the bubbling frequency. However, in our experiments and after demonstrating through the temporal description that the frequency of bubbling does not undergo considerable variation, we assign the variation of void fraction as function of flowrate to the spatial evolution of bubbles.

The tomographic reconstruction which aims to visualize the void fraction distribution in the optical field is reported in Figure III.30. We recall that $\alpha_{i,j,k}$ depicts the void fraction at each point of coordinate (i, j) in the image k such that $0 < \alpha_{i,j} < 1$. In other words, regarding this tomographic reconstruction, it designates the probability of gas presence at any position in the field. For a certain flowrate, we are able to visualize the gradual decrease of void fraction as we increase in the altitude above the nozzle and at the same time, the increase in the width of the void fraction due to the plume expansion.

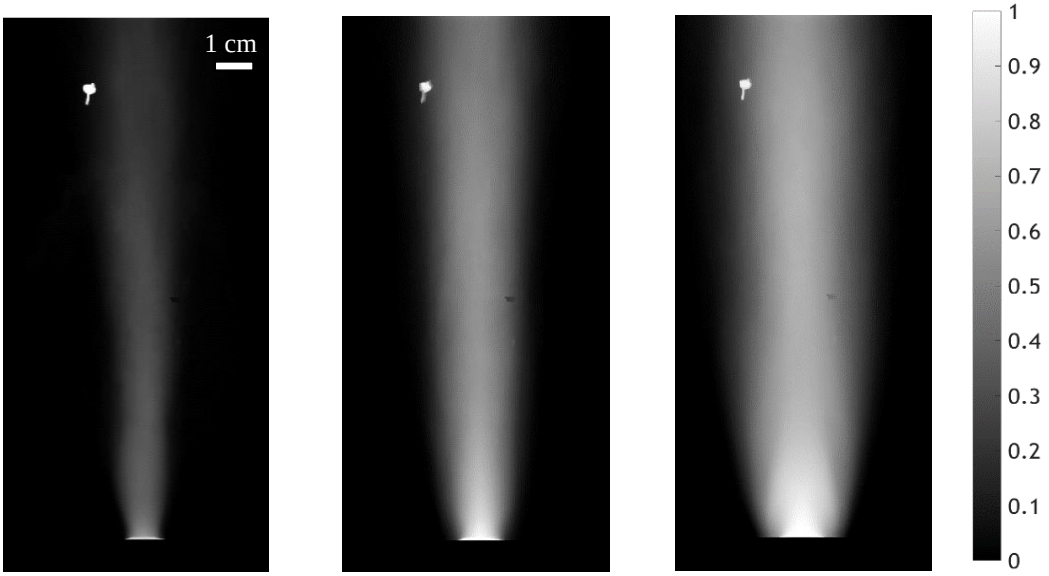

(a) (b) (c)

Figure III.30- Tomographic reconstruction of void fraction variation distribution for N = 10000 images ; (a): Q_{inj} = 6 L/min, (b) Q_{inj} = 24 L/min, (c): Q_{inj} = 54 L/min.

Castillejos et al. [111] have performed experiments on air-water bubble plumes injected from a submerged nozzle, and proposed a void fraction correlation on the basis of their experimental data that is independent of the different axial positions above the nozzle. They approximated it through the following normalized correlation in eq.(20), where:

$$\frac{\alpha_g(r)}{\alpha_{g_{max}}} = e^{(-0{,}7(\frac{r}{r_{\alpha_{max/2}}})^{2,4})} \quad (20)$$

- α_g is the radial gas fraction
- $\alpha_{g_{max}}$ is the maximum value along the radial profile

- r is the radial distance

- $r_{\alpha_{max/2}}$ is the radial distance from the axis of symmetry to the position where the gas fraction is half the maximum value.

Within this concept and through our experimental data, void fraction is normalized at different axial positions above the nozzle, and then compared with their correlation, as shown in Figure III.31. It is noted that this correlation is similar and comparable to that of Zhang et al. [93].

At low and intermediate flowrates, our experimental data fits with their correlation, see Figure III.31-(a). However, at the onset of the chaining regimes where bubbles exhibit a vertical elongation, the distribution of gas converges towards the centerline of the flow, and this justifies why experimental data deviates from the correlation at $r/r_{\alpha_{max/2}} > 1$, as shown in Figure III.31-(b).

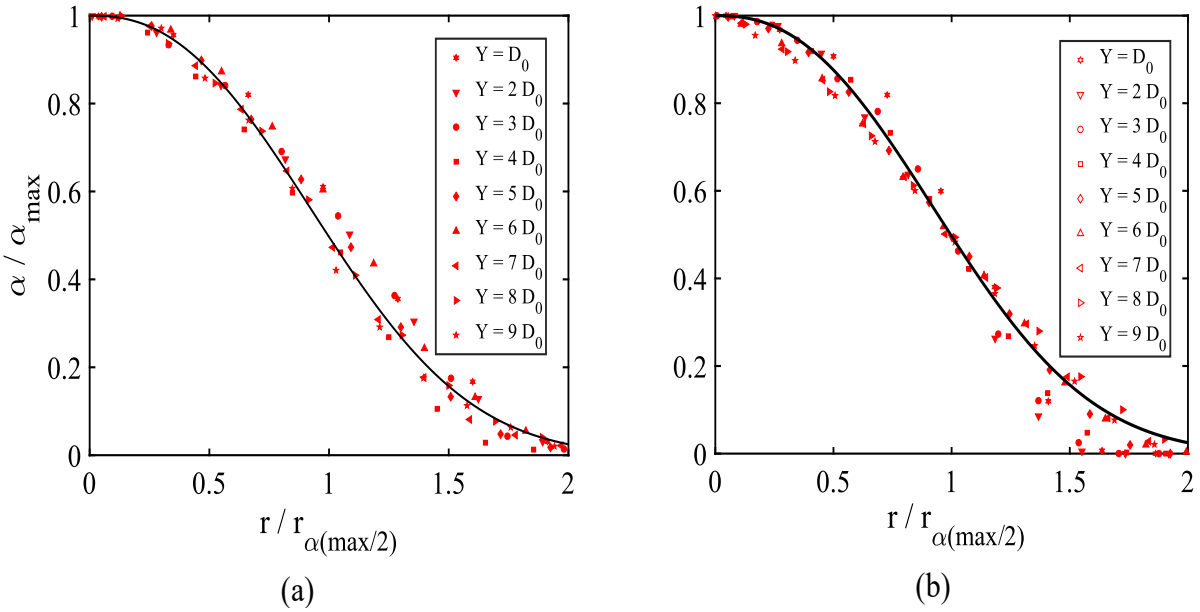

Figure III.31- Comparison between the experimental data obtained for void fraction variation and the normalized correlation of Castillejos et al. [111] for D_0 = 12 mm; (a): Q_{inj} = 18 L/min, (b): Q_{inj} = 48 L/min.

III.3.3.6. Rising velocity

Determining the bubbles velocity is a major point regarding the resident time and mass transfer between the bubbles and the liquid phase. Models and correlations developed to determine the rising velocities depend strongly on the size and the shape of the bubbles [94, 112, 113]. Thanks to the tracking of globules formation and image processing codes (MatLab) as explained in II.2.2.3 and III.3.3.2, the velocity of formation could be characterized by tracking its center of gravity until the detachment of the globule from the nozzle, as shown in Figure III.32. The latter variable is determined algorithmically from the binarized structures.

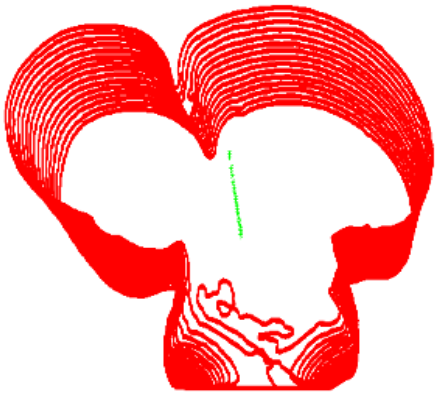

Figure III.32- Tracking the center of gravity of globule during its formation and rising.

A similar data treatment of globules formation is performed, except that here the globule's center of gravity is tracked. A post-treatment of signals aimed to reconstruct the filtered signals representing the axial position of globules center of gravity, as in III.3.3.2 (see Figure III.20). For each globule formation and detachment during a period, which is considered an event, a rising velocity could be determined, and this is shown in Figure III.33 that depicts 8 events.

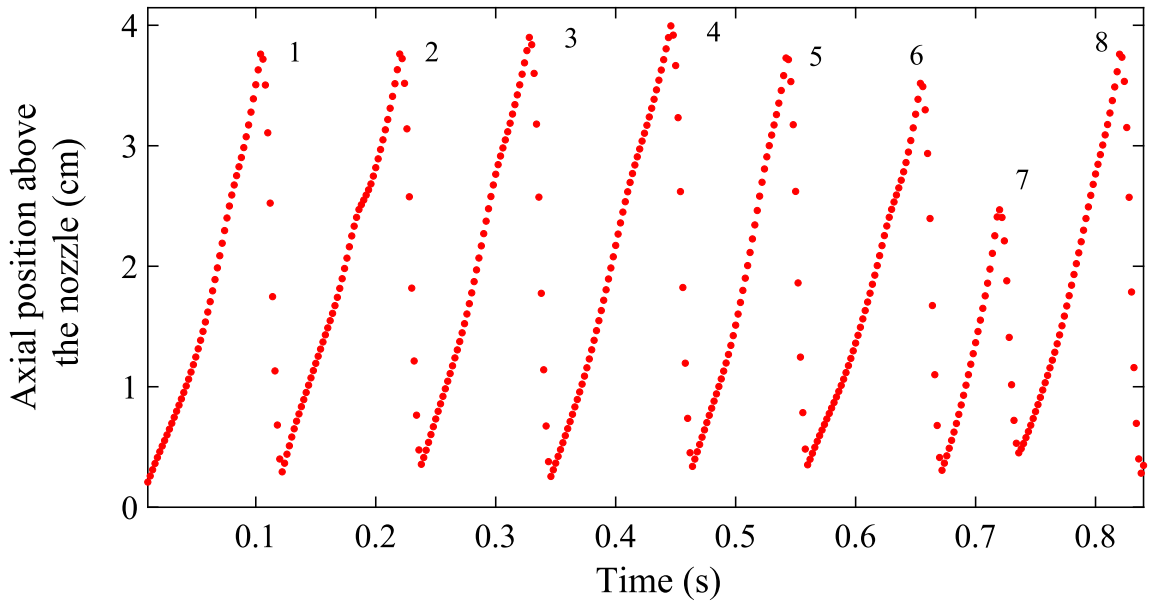

Figure III.33- Treated signal of the axial position of bubble's center of gravity during their formation and rising until their final detachment (eight events are shown).

For each test configuration, a minimum of 5 seconds acquisition was required so that the rising velocity of globules fluctuated around an average velocity represented by a horizontal line midst the events, as shown in Figure III.34.

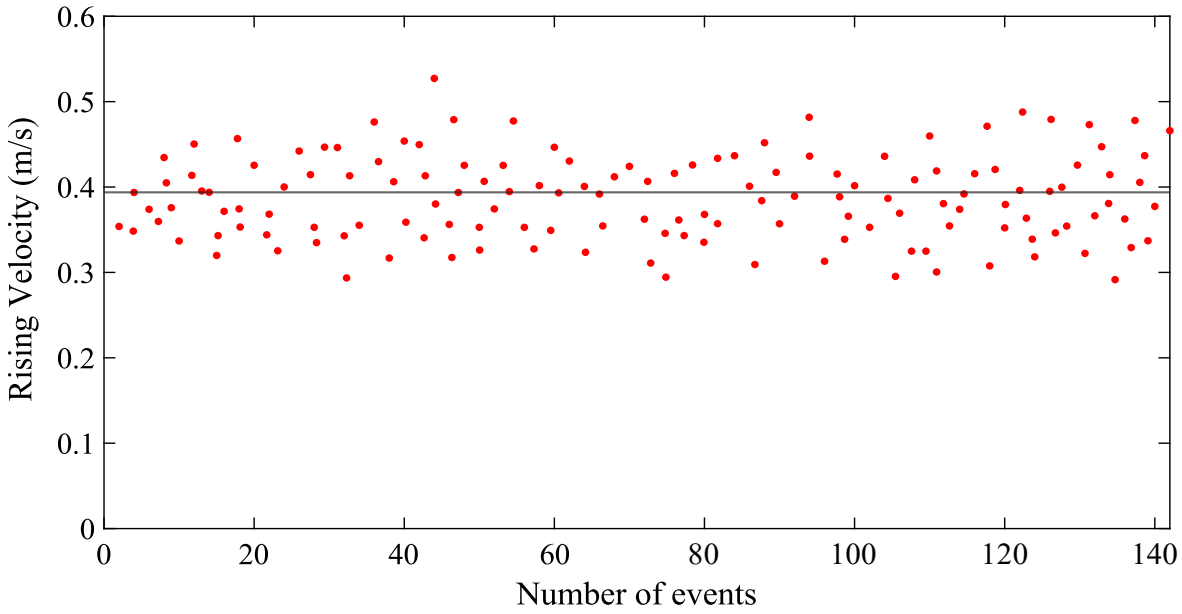

Figure III.34- Average and distribution of bubbles rising velocities for Q_{inj} = 30 L/min.

In Figure III.35, other way of representation is shown for the determination of the average rising velocity, which consolidates the convergence of the database into an average value.

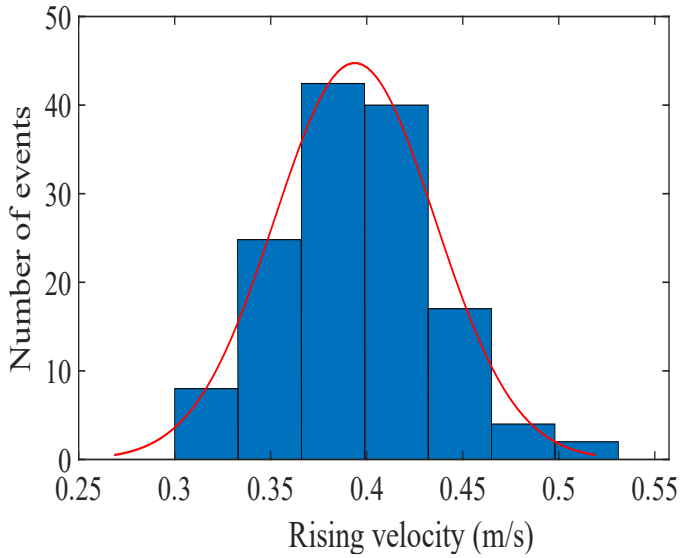

Figure III.35- Histogram of globule rising velocities U_G for Q_{inj} = 30 L/min.

Following this treatment, the rising velocity of globules for different test configurations are determined as shown in Figure III.36. When the flow is characterized by pairing and double bubble coalescence (see III.2.1.3), the increase of injection flowrate significantly affects the rising velocity of a formed bubble and its departure and rising.

At higher Weber, and when coalescence of bubbles is induced, the increase of flowrate will induce more coalescence events and an increase in globule volume, thus a longer time to constitute a globule formation [63]. Davidson et al. [105] reported that in these morphologies

(dynamic regime), the bubbles undergo comparable frequency of formation but with different sizes. Therefore, the formation and rising velocity of globules follow an asymptotic average velocity with the increase of injection flow rate Q_{inj}, as shown in Figure III.36.

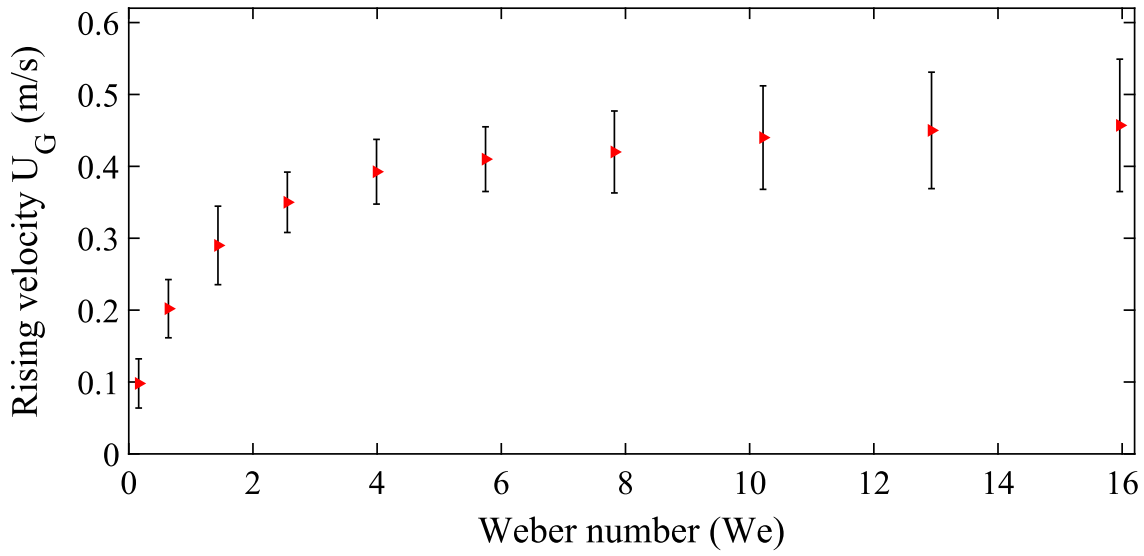

Figure III.36- Variation of averaged globule rising velocities as function of Weber number.

The comparison with the mean injection velocity U_{inj} shows a relatively sharp drop of globules rising velocity above the nozzle, as shown in Figure III.37.

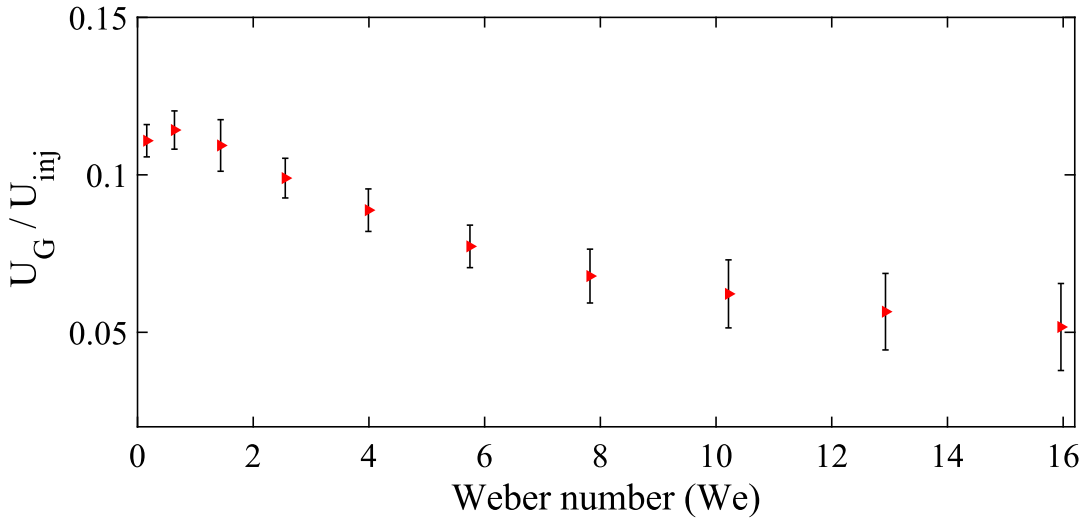

Figure III.37- The comparison between globule rising velocity U_G and the mean injection velocity U_{inj}.

This is due to resistive forces acting on the bubbles such as the drag forces or surface tension forces. We considered this problem, and we supposed an equilibrium of forces acting on the globules in order to introduce a terminal velocity of the globule in the injection zone $U_{G\ terminal}$.

Beyond the formation of globule, consisting of two or more bubbles, we considered in a first approach the equilibrium from drag force F_D and buoyancy F_B of the globule leading to uniform rising velocity $dU_G/dt = 0$, therefore it we can write:

$$\rho_g V_G \frac{d\overrightarrow{U_G}}{dt} = \overrightarrow{F_D} + \overrightarrow{F_B} = \vec{0} \tag{21}$$

$$\frac{1}{2}\rho_l \frac{\pi}{4} {d_G}^2 C_D {U_T}^2 = V_G(\rho_l - \rho_g)g \tag{22}$$

Where $C_D = 0.45$ when the bubble Reynolds number $Re_b > 1000$ [93, 114, 115] such that $Re_b = U_G d_G/\nu_g$. From eq. (22), the terminal velocity of the globule in the injection zone U_T can be determined as:

$$U_T = \sqrt{\frac{8\, g\, V_G}{\pi\, {d_G}^2 C_D}} = \sqrt{\frac{4\, g\, d_G}{3\, C_D}} \tag{23}$$

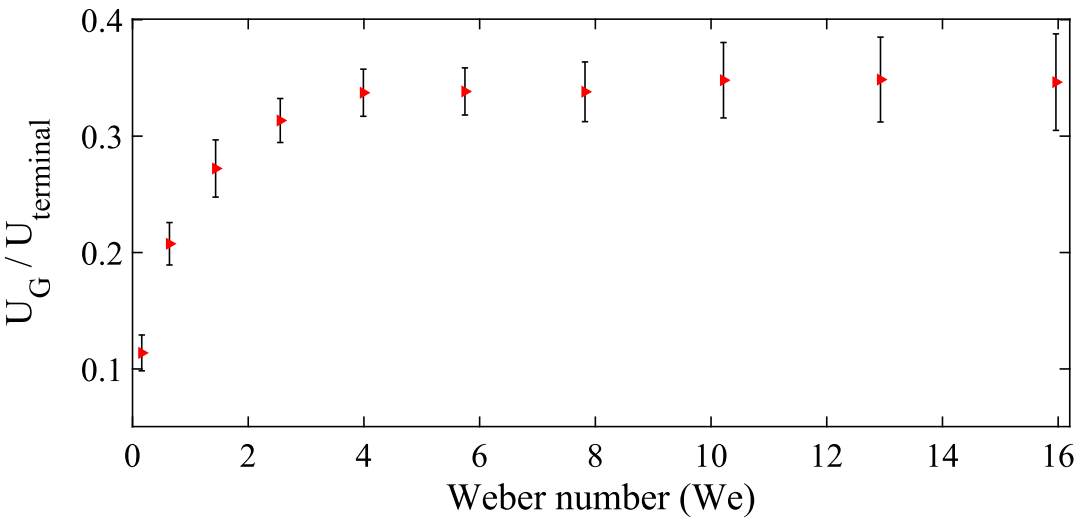

Figure III.38- The comparison between globule rising velocity U_G and its assumed terminal velocity U_T.

According to the above assumptions regarding the equilibrium between drag force F_D and buoyancy force F_B, the terminal velocity correlated to globule size d_G is shown to be greater than the globule rising velocity (see Figure III.38), which is determined experimentally. In fact, this result yields that the assumed equilibrium of forces underestimates the resistive forces that attenuated the rising velocity of globules. It is therefore suggested that other drag forces present, which are the due to the wake of trailing bubbles.

III.4. Globules' dynamics in pool scrubbing conditions

Pool scrubbing might be implemented in different situations, which imply different conditions. Thus, it is therefore important to investigate the influence of tests parameters on the bubble dynamics, as they may favor or hinder the retention of fission products. In this section, the impacts of contamination, nozzle size, and pool submergence, are characterized on the globule formation in the injection zone at $T_{pool} = T_{gas} = 25$ °C. These experimental campaigns were realized on the TYFON facility in IRSN-Cadarache (see II.3).

III.4.1. Impact of nozzle size D_0

Generally, bubble volumes have been reported to be a strong function of the nozzle diameter [105, 106, 116-119]. In Figure III.39, the globule volumes are presented as function of Weber number that varies due to both the nozzle size and injection flow rate. A significant increase in globule volume is shown with higher nozzle size for same Weber number.

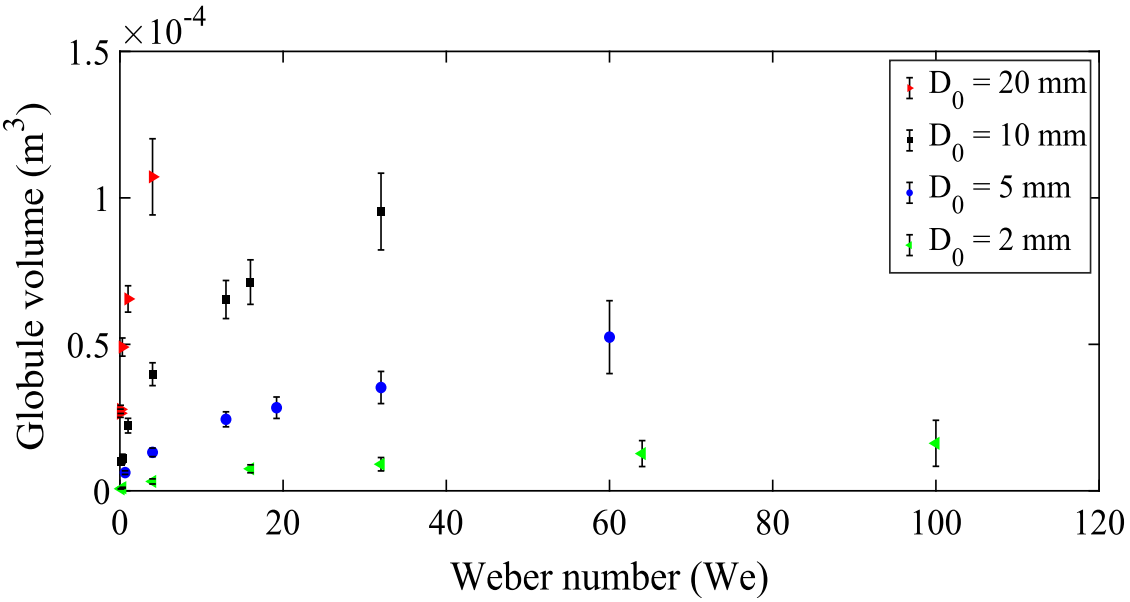

Figure III.39- Variation of globule volume for different nozzles as function of Weber number.

Owing to the strong dependence of Weber number on the nozzle size, and in order to differentiate between the contribution of nozzle size and injection flow rate, the impact of gas flow rate for different nozzles is presented in Figure III.40. Despite the size of nozzle, comparable values of globule volumes for same flow rate are maintained for the small nozzles ($D_0 = 2$ mm, $D_0 = 5$ mm, $D_0 = 10$ mm). For nozzle of $D_0 = 20$ mm, there is slight increase which is due to the higher formation time needed in order to form bubbles between the tips of the nozzle.

Figure III.41 illustrates and consolidates the latter statement, where the globules frequency for $D_0 =$ 20 mm nozzle is smaller than other globule frequencies of different nozzles sizes. Davidson et al. [106] suggested that a maximum frequency of air bubbles formation is reached beyond a certain flowrate for certain nozzle size. Moreover, Clift et al. [58] stated that frequency becomes weakly dependent on flowrate in dynamic regimes. In our experiments, as We > 1,

The further increase in injection flow rate, consequently Weber number, affect only the volume of globules, whereas the frequency is the same for the different sizes of nozzles.

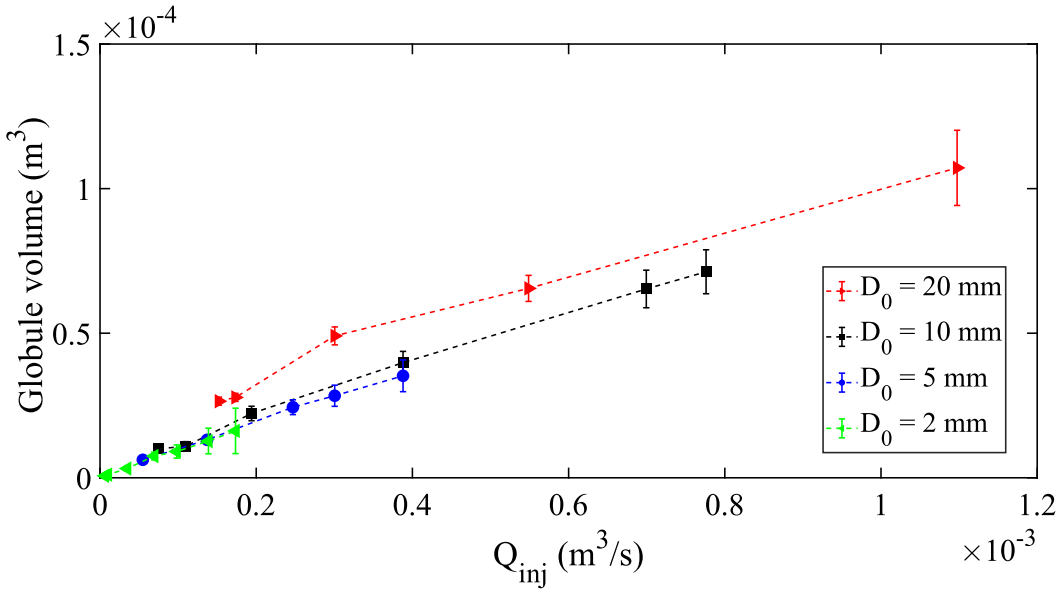

Figure III.40- Variation of globule volumes as function of injection flowrate Q_{inj}.

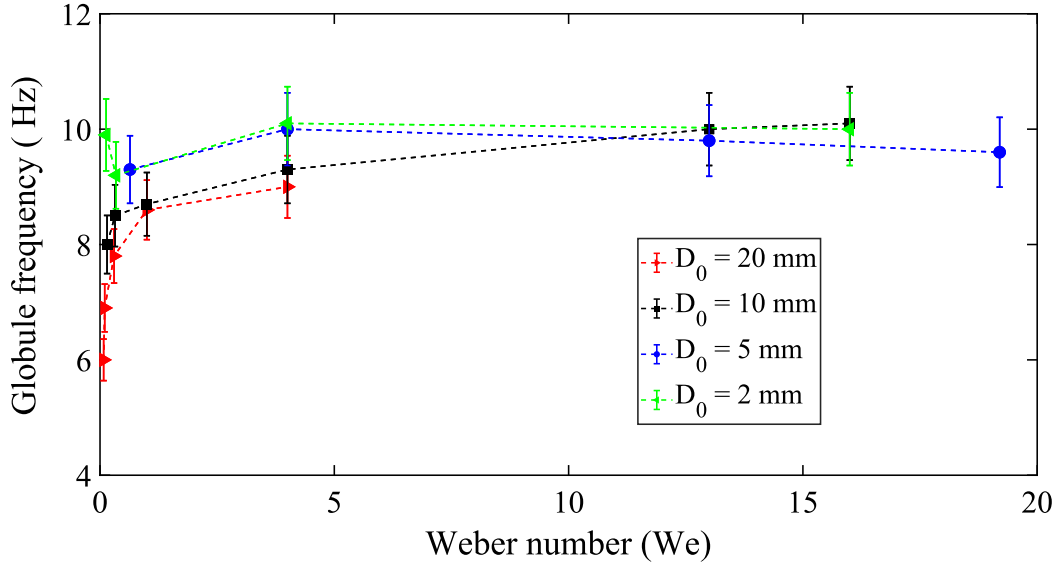

Figure III.41- Globule frequencies for different nozzles.

Moreover, we assume that $Q_{exp} = V_G \times f_G$, where V_G and f_G are respectively the volume and frequency of the globules. This assumption stems from the fact the formation of globule is common and relevant along the different flow morphologies. Therefore, and as explained in III.3.3.3 to validate the method, the injection flowrate (Q_{inj}) is correlated to the volume of globule V_G formed at frequency f_G. In Figure III.42, it is shown that the experimental data is fitting reasonably the actual injection flowrate for the different nozzles mounted on the TYFON facility.

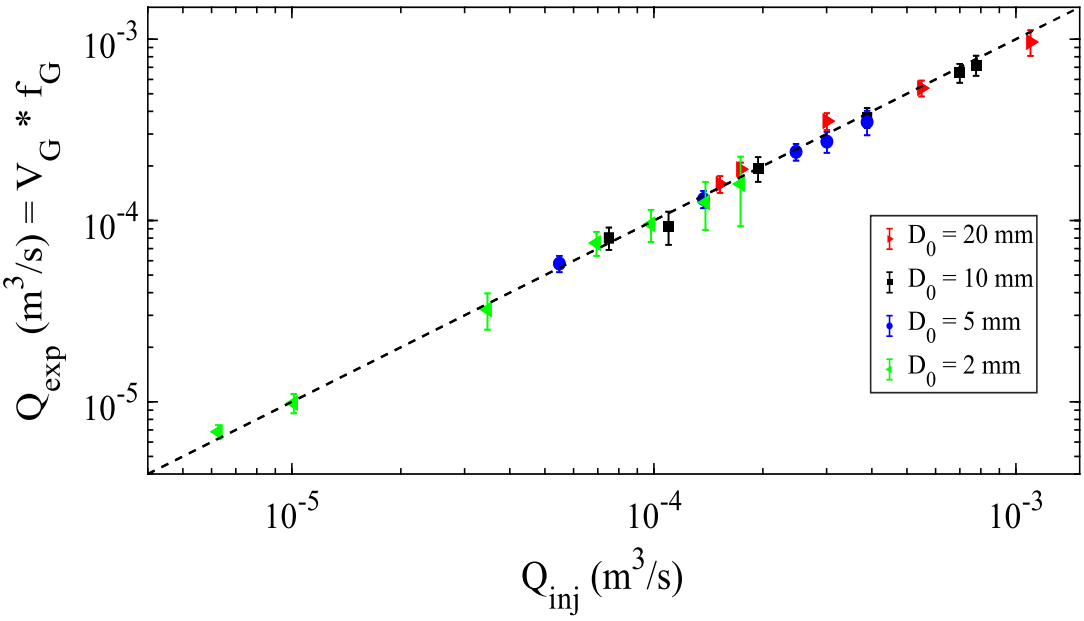

Figure III.42- Validation of experimental flowrate with the real injected flowrate, where the dashed lines (--) corresponds to identity line (y=x).

III.4.2. Impact of contamination

In order to reveal impact of contamination of carrier gas on the globule dynamics, the globules formation in injection zone were examined and compared with and without presence of contamination in injected air. Figure III.43 and Figure III.44 report no significant influence of this contamination on the globule sizes, for the different D_0 and at different Q_{inj}.

Regarding the aerosols, caesium iodide is soluble in water and the size's ratio of the aerosol's particles to average globule volumes is less than 5×10^{-3}. This ratio, depending on the aerosol

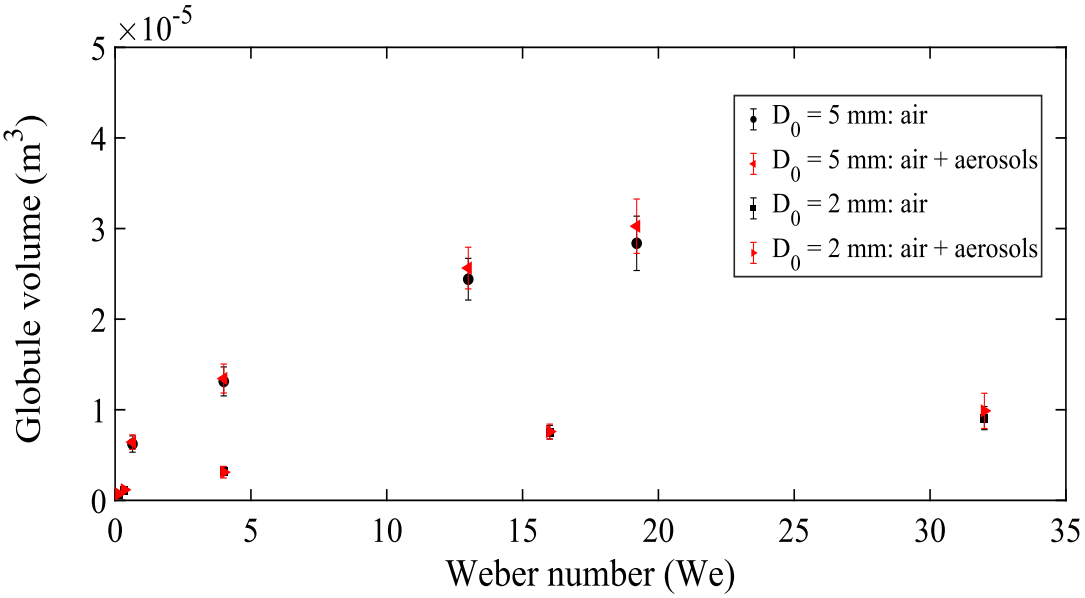

Figure III.43- Impact of the contamination of carrier gas with aerosols suspension on the volume of globules.

mass concentration knowing the inlet concentration, seems to be low and of no influence, especially for aerosols suspension [98]. Within the same analogy and for the case of contamination with gaseous CH_3I, the methyl iodide was injected in a way to respect a composition within the carrier gas around 5 ppmv.

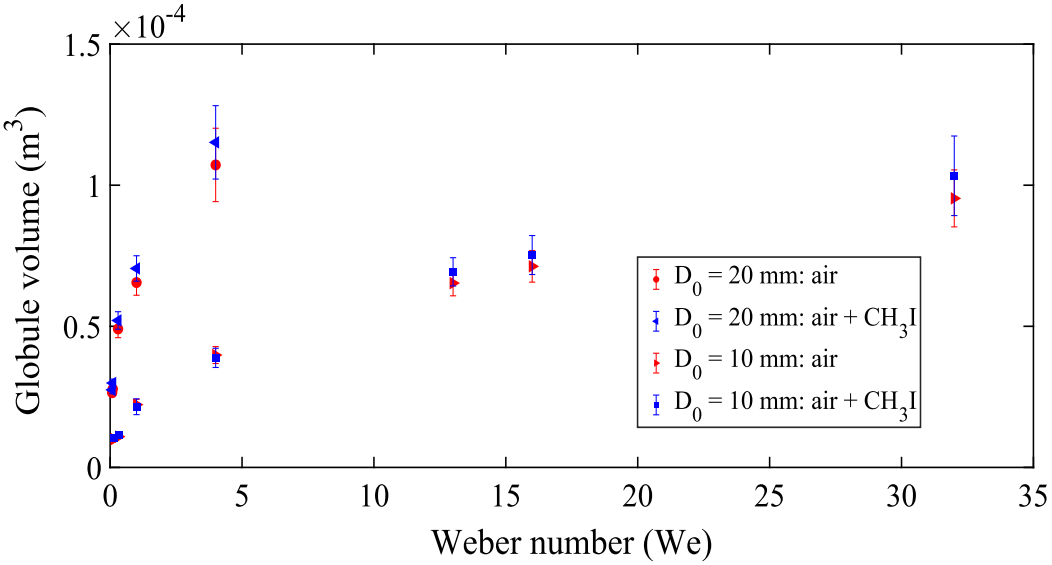

Figure III.44- Impact of carrier gas contamination with CH_3I composition on the volume of globules.

Thus, and within the range in our examined experiments, this concentration seems to be very low and might not have an impact on the carrier gas. Moreover, considering the domination of the inertial forces leading to large globule volumes, it is suggested that the carrier gas composition is not affecting its surface tension properties, thus, its volume. Very high concentrations of iodine species probably modify globule volume, but it has not been investigated regarding the context of the study.

Globule formations are affected by the wake and entrainment of the flow, depending on the injection flowrate. Thus, in order to study the possible effects of contamination on the globule formation, the characterization of the frequency of bubbling is considered. Globule formation frequencies are determined by tracking the coalescences of bubbles leading to the formation of a large bubble [82].

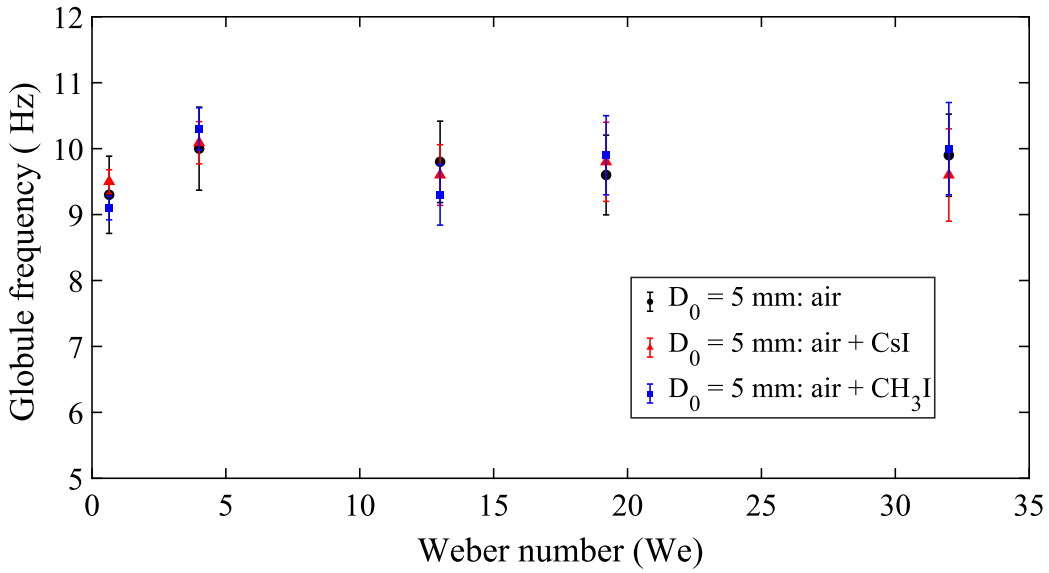

Figure III.45- Impact of gas contamination on globules frequency.

In addition to negligible effect of contamination on globule volumes, the different test configurations have shown no effect also on the globule frequency as shown in Figure III.45. In fact, the average frequency of globules at different flow rates tends to be stable at constant frequency. As no impact of contamination on globule volume and frequency is observed, it can be deduced that globule formation is also not affected. This suggest that, as injection flow rate increases inducing more inertial forces and dominance over the possible effects of contamination, the classification of flow regimes according to Weber number will not be altered or modified in our concentration ranges.

III.4.3. Impact of pool submergence

In the TYFON facility and thanks to pressure sensors that permits knowing the level of water in the column, the pool submergence was set to 5 different altitudes according to L_{inj} that refers to the length of the injection zone (i.e.: the onset of breakup zone where the globule starts fragmentation). This length was determined for different test configuration, where it is considered after the globule formation and just before its fragmentation (at the top of the globule).

According to Kumar and Kuloor [116], it is generally agreed that this variable does not influence the bubble volume at the tip of the nozzle. Davidson et al. [106] and Hughes et al. [117] reported that volume of bubbles forming at a submerged nozzle for a constant air flow rate are not affected with the variation of pool submergence. Nevertheless, it may affect the bubble volume appreciably in the upper zones. On the other hand, Hayes et al. [118] and Spells et al. [119] reported that a variation of bubble volumes occur due to the liquid circulation at submergence less than two bubble diameters.

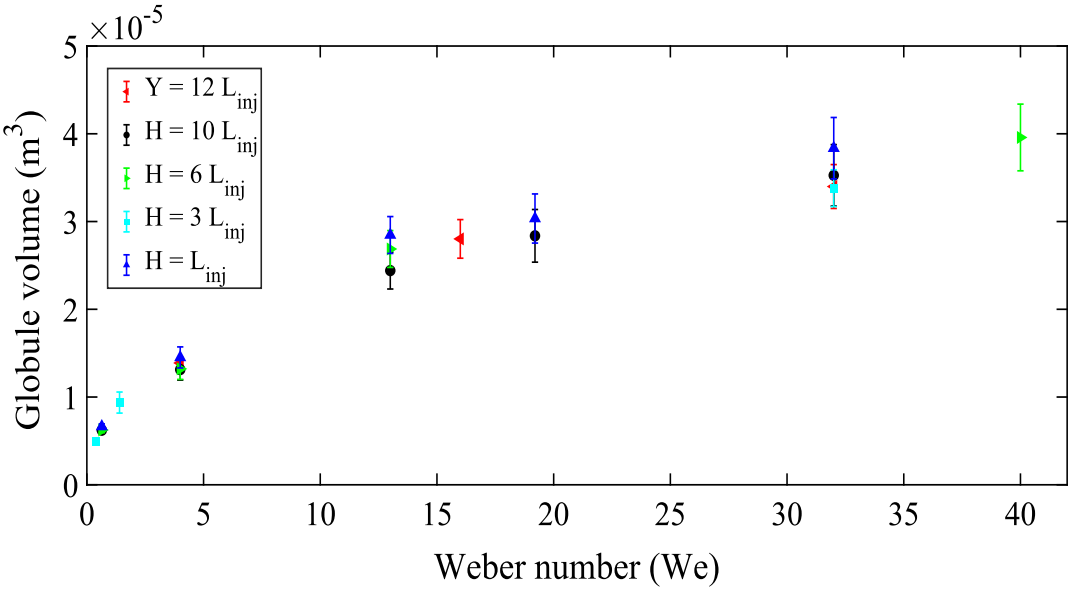

Figure III.46- Globule volume for different pool submergences (D_0 = 5 mm) at ambient temperature.

For the examined Weber numbers in the bubbly regimes, no significant variation was found on the volume of globule except for the lowest submergence where Y = L_{inj}, as shown in Figure III.46. At this altitude, it is suggested that the globule undergoes a bit larger expansion due to liquid circulation [118, 119]. However, the inertial effects over dominate the latter mechanism, leading to a comparable volume of globules at the different altitudes.

III.5. Dimensionless analysis of globules formation

In this section, a dimensionless approach for analyzing the globules dynamics is discussed.

Many models have described the bubbles formation and estimated their sizes in stagnant pool and most of them adopted a sort of force balance for predicting one or more stages in bubble growth [59, 88, 93, 94, 105-107, 120-123]. For simplification, these models assumed that the bubble would have a spherical shape throughout the growth period. There are one-stage models were bubbles are described as structures that grow smoothly until their detachments, which occurs when the rear of the bubble passes the nozzle or when buoyancy exceeds the retarding forces, as for single bubbling regime (see III.2.1.1). On the other side, in multiple stage models it is assumed that there is a basic change in the growth mechanism at one or more points in the growth process. Typically, it is assumed that the bubble resides on the nozzle during the first stage, and that the second stage begins at lift-off with the bubble subsequently fed by a tongue of gas from the nozzle.

Withing the context of pool scrubbing, some forces are highlighted, and others could be neglected, moreover, phenomena such as bubble-bubble interactions and coal scene should be considered. Different models of varying complexity have been proposed, considering the inertial forces such as Krevelen et al. [107] and Davidson et al. [105-107], whom presented models for bubble formation in dynamic regime at submerged nozzles for viscous and inviscid liquids.

Gaddis et al. [59] briefly discussed various parameters affecting the bubble formation. Since then, bubble formation has received continuous attention in literature, for example, Zhang et al. [93], Jamialahmadi et al. [94], Badam et al. [65], Dietrich et al. [88, 123]. Most of these studies can be classified on basis of the operating conditions in the gas phase, such as constant flow rate or constant pressure. However, observations of many investigators are not concordant because of variations induced by the injection gas velocity, the size of nozzles and the operating parameters (system pressure, etc.). Hence, more observations are required to clarify the bubble formation process, and dimensionless models that overcome the difference between experimental facilities are required.

The current study was encouraged after the validation of phenomenological approach developed throughout this thesis to determine the globule volumes, as seen in Figure III.24 and Figure III.42, especially after the observation of the maximum frequency phenomenon (see Figure III.41) described by Clift et al. [58] Davidson et al. [105-107], and McCann et al. [95].

As a first attempt and based on the equality of injection flow rate $Q_{exp} = Q_{inj}$ (see III.3.3.3), and assuming an equivalent diameter d_G for the sphere of volume V_G we can write:

$$V_G\, f_G = U_{inj}\, \frac{\pi}{4} {D_0}^2 \qquad (24)$$

$$d_G = \sqrt[3]{\frac{6}{\pi} V_G} \quad (25)$$

And by proposing the Strouhal number, which is relevant to frequency analysis in unsteady flow morphologies, such that

$$Str = \frac{f_G D_0}{U_{inj}} \quad (26)$$

We can describe a dimensionless globule diameter with the Strouhal number through the following correlation:

$$\frac{d_G}{D_0} = \sqrt[3]{\frac{3}{2\,Str}} \quad (27)$$

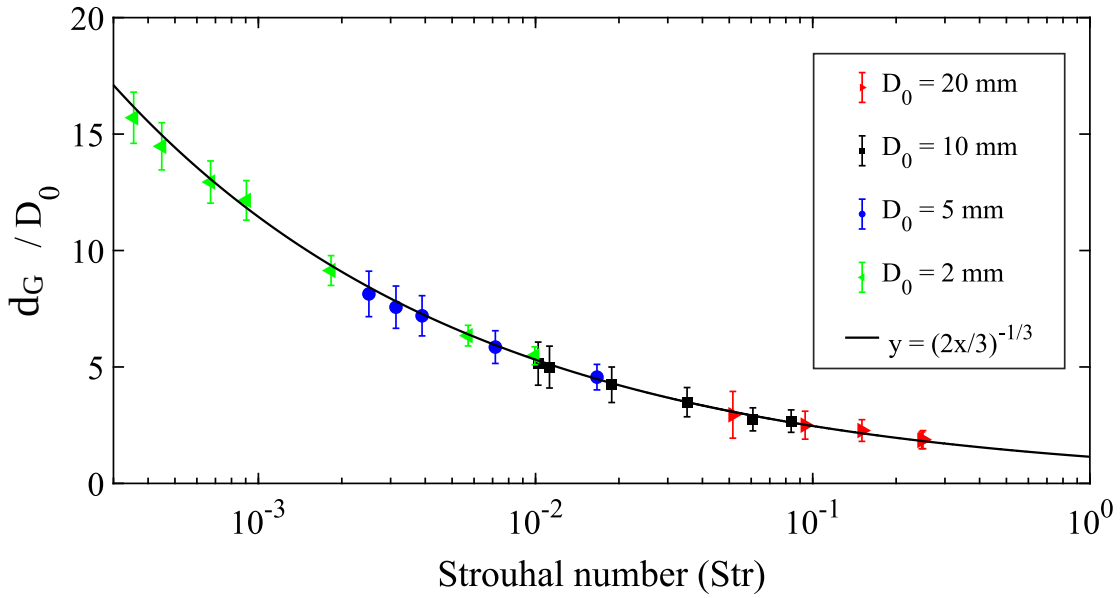

Figure III.47- Dimensionless analyses as function of Strouhal number.

Although Figure III.47 shows good estimation, however, this approach implies some weaknesses such as:

- Implication of an experimental output which is the f_G used to determine the Strouhal number.

- The frequency of globules tends to have a constant value in dynamic regimes, which is the maximum frequency, therefore it will not contribute to the globule volumes (discussed in the paragraph below).

In the next paragraph, we attempt to improve this approach by depending on some correlations and notions from the literature.

III.5.1. Maximum frequency

With increasing the injection flowrate Q_{inj}, gas momentum force F_M (see eq.(28)) become important, and both bubble volume and frequency increase with gas flow.

$$F_M = \rho_g \pi \frac{{D_0}^2}{4} {U_{inj}}^2 \quad (28)$$

However, Davidson et al. [105-107] reported that the further increase of injection flow rate in dynamic regimes will not affect the bubbles frequency, which levels out to a nearly constant value, termed the maximum frequency. Otherwise, it would only affect the bubble volume. For that, Clift et al. [58] suggested to describe the bubbles formation at quite high flowrates as "constant frequency formation". Krevelen et al. [107] correlated the maximum frequency of bubbles with the rising bubble velocities in the dynamic regime, supposing spherical bubbles, such that:

$$U = (r_b\ g\ )^{1/2} \quad (29)$$

$$U = 2\ r_b\ f_{max} \quad (30)$$

Where U is the velocity of rise bubbles in series, r_b is the bubble radius, g is the gravitational acceleration, and f_{max} is the maximum frequency. By substitution of equations (29) and (30), the maximum frequency can be written as the function of bubble diameter and gravitational acceleration. In our experiments, we considered the diameter equivalent to globule of volume V_G, therefore, the maximum frequency can be written as:

$$f_{max} = \frac{\sqrt{2}}{2} \frac{g^{1/2}}{{d_G}^{1/2}} \quad (31)$$

As we observed a sort of maximum frequency phenomenon (see Figure III.41) in our experiments, we investigated this maximum frequency and compared it with the globule frequency f_G. Figure III.48 shows the convergence of globule frequencies toward the maximum frequency with the increase of inertia. For the largest diameter D_0 = 20 mm, it is shown that with the increase of Weber number, the globule frequency was approaching f_{max}.

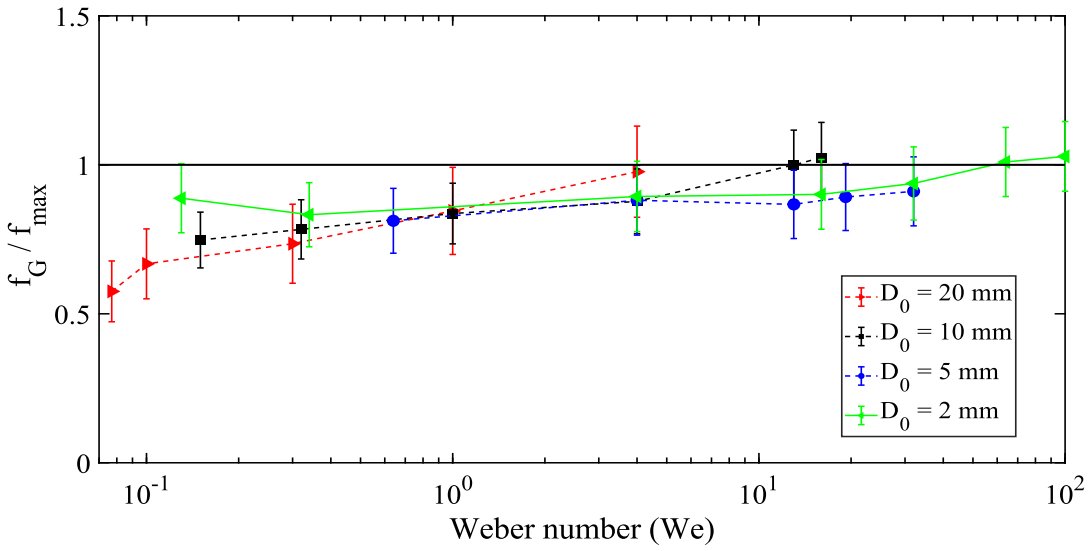

Figure III.48- Comparison between maximum frequency correlation [107] and globule frequencies.

From Figure III.48 and when We > 1, it is observed that experimental frequency of globules for different nozzle sizes D_0 are consistent with the maximum frequency correlations of Krevelen et al. [107]. These results therefore the approach of adopting maximum frequency in our experiments.

Davidson et al. [105] suggested that in dynamic regimes, nozzle dimensions are not important for constant gas flow conditions. In fact, this can be observed from the models developed by him and Krevelen et al. [107] (see Table III.4), where they excluded the nozzle size from the model and considered only the injection flow rate and gravitational acceleration.

III.5.2. Correlation

Now, and as we can consider the correlation of Krevelen et al. [107] for the maximum frequency in eq.(31), we can write:

$$V_G \, f_{max} = U_{inj} \, \frac{\pi}{4} {D_0}^2$$

After development, eq.(32) becomes:

$$\frac{d_G}{D_0} = \left(2.12 \, \frac{U_{inj}}{\sqrt{g \, D_0}} \right)^{\frac{2}{5}} \qquad (33)$$

Where $U_{inj} / (g \, D_0)^{1/2}$ is the Froude number *Fr* comparing the inertial forces to the gravitational forces. It is worth saying that these forces are the essential contributors to the globules volume. Therefore eq.(33) can be expressed as:

$$\frac{d_G}{D_0} = \sqrt[\frac{2}{5}]{2.12\ Fr}$$

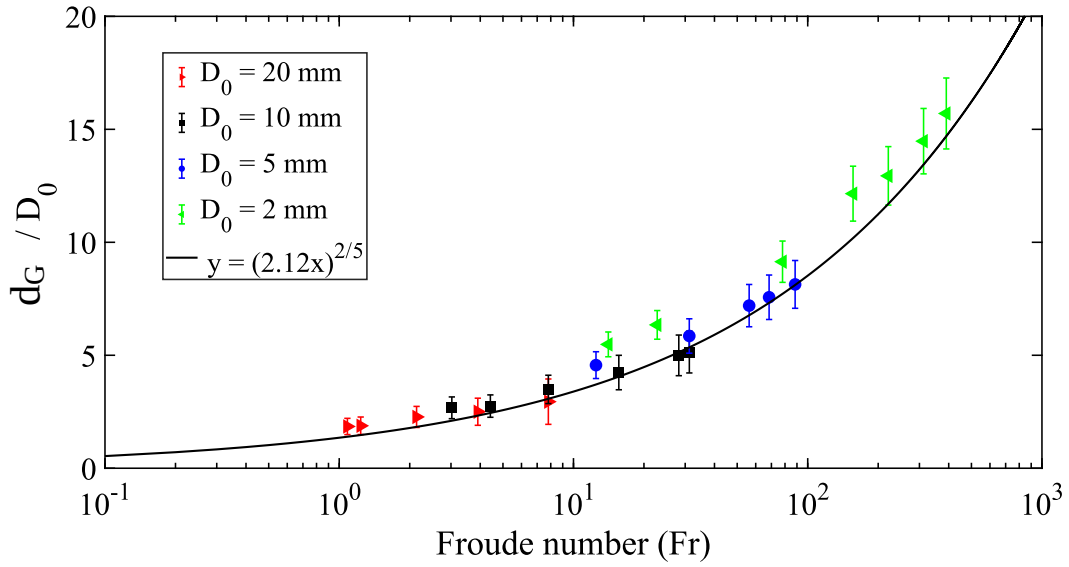

Figure III.49- Dimensionless analysis of globules equivalent diameter with Froude number in the dynamic regimes.

Figure III.49 provides a good prediction of the globules volume, The average error between experiment data and the correlation is lower than 15 %. Thus, the correlation can be used to predict the volume of a globules formed under various nozzle diameters D_0 and injection flowrates Q_{inj} in inertial dynamic regimes where We > 1.

III.6. Conclusion

Flow structure in pool scrubbing conditions, where for example air is injected at high momentum, exhibits different patterns than in conventional experiments. That recalls for approaches that better describe the bubble hydrodynamics besides the different phenomena. Within this concept and its relevance in nuclear safety, experimental work was carried out to characterize the bubble hydrodynamics in the injection zone, where flow is induced by injection of air from a submerged nozzle, and then the experimental results are provided in a systematic analysis. Through this chapter, we classified the different flow regimes, and we depicted the different morphologies of singly bubbling, pairing and doublet bubbles, coalescence above the nozzle, coalescence at the edge of the nozzle, and chaining. As can be observed from the nomination of these morphologies, the classification was based on the number and position of the bubbles' coalescences. After that, we investigated the temporal variation of bubbling in terms of XT diagrams and frequency of bubbling, described its spatial evolution in terms of bubbles size and void fraction, characterized the surface area between bubbles and the pool, and determine the rising velocity of globules in the injection zone

Through the temporal description of the bubble flow (III.3.1), we defined the frequency of departure which makes it possible to quantify a characteristic bubble volume (III.3.2). The comparisons between bubble volume and literature models have shown a good agreement. Nevertheless, the assumption of spherical bubbles being unsatisfactory regarding to images, it was important to carry out the identification and classification of the bubble morphologies in order to introduce the concept of globule formation (III.3.3). Thus, the frequency of globule formation (III.3.3.1) and the volume of these globules (III.3.3.2) have been determined and seem to be more accurate than existing models to characterize the main gas structure formed in the injection zone. The phenomenological approach implemented to determine the globule volume is validated by comparing Q_{exp} (V_G, f_G) to the real injected flowrate Q_{inj} (III.3.3.3).

The surface area of globules was determined using a method from literature (III.3.3.4), thanks to image processing which made it possible to determine parameters such as the curve length and geometric centers of the bubble's two sides. The surface area of bubbles was determined by the latter method, and by considering a spherical shape of bubbles having volumes V_G. The comparison has shown large discrepancy between the surface areas, owing to the different irregular shapes of globules that possess higher surface area. As surface area is an important parameter contributing to mass transfer, the latter results show that inaccuracies could rise from adopting spherical shapes of bubbles when modelling the mass transfer from gaseous phase to liquid phase.

Then, we characterized the gas fraction in the flow and visualize the distribution of the void fraction (III.3.3.5), also we achieved to have good agreement with data coming from correlations available in the literature. For the rising velocity (III.3.3.6), this latter was characterized thanks to image processing and tracking of bubbles center of gravity, which will be essential for determining the residence time of globules in the injection zone.

Consequently, the importance of the elaborated database that we have considered consists in the characterization of globule size, the physical phenomena and bubble-bubble interactions

and the entrainment of bubbles coalescence, which is poorly characterized in previous experimental works.

On the other hand, and regarding the investigation of pool scrubbing conditions on the globule formation process (see III.4), the presence of CsI aerosols or CH_3I composition had no influence on the globule dynamics in our concentration ranges. It is suggested that the large globule volumes can afford the deposition without interfering their surface tension. Comparable globule volumes and frequencies were reported for the small nozzles (2, 5, and 10 mm), where globule volume increases with the injection flowrate. For the large nozzle (20 mm), the increase formation time results in a larger globule volume and smaller globule frequency. Regarding the pool submergence, negligible influence on globule volume was reported where experiments were carried at constant flow and pressure conditions. The dominant inertial mechanisms in the injection zone near the nozzle attenuate the effect of hydrostatic pressure induced by the pool submergence.

Finally, a dimensionless analysis approaches were provided in an attempt to describe the globule dynamics in the injection zone (see III.5), by considering an equivalent diameter d_G to the globules of volume V_G by assuming their sphericity. The influence of inertia and existence of maximum frequency phenomenon led us to introduce the Froude's number. The latter is the ratio of inertial to gravitation forces, in which it is believed that these forces are the main contributors to the globules' sizes. A dimensionless correlation that implies only experimental parameters was provided, and it has a shown a good estimation of globule volumes when $We > 1$.

In chapter V, we are going to provide some modelling aspects of pool scrubbing by using the hydrodynamics obtained in this chapter. In fact, the hydrodynamics and experimental database established in this chapter will be useful for the modelling team in IRSN Cadarache to compare, validate, and improve existing models implemented in the ASTEC code.

Chapter IV: Decontamination factor measurements

IV.1. Preface

In this chapter we present the decontamination factor measurements realized on the TYFON facility for three iodine compounds (CsI, I_2, CH_3I). As presented in chapter II, the experimental setup of each iodine compound varies as for the generation of the compound and its injection, or for the measurement techniques (sampling, chemical analysis). Moreover, and as reported in chapter 0, these compounds can be formed during a nuclear accident for different reasons, and thus, can exhibit different behaviour while their release. The objective of this chapter is to present the different physical and chemical aspects that influence the trapping of these compounds. For that, test matrices were set, comprising different experimental conditions, in a way to study some mechanisms of trapping for each compound.

This chapter is structured to present first the trapping experiments of CsI aerosols. On the other hand, the second section discuss the retention tests of volatile iodine, thus comprising both gaseous I_2 and CH_3I. In both sections, the devoted experimental matrix and relevant experimental parameters are presented, then the results of these tests are discussed, and finally we present the conclusions relevant to the hydrodynamic and chemical aspects of trapping.

IV.2. Retention tests of caesium iodide aerosols

It is clearly observed in literature that most of the experimental programs on pool scrubbing - before and after Fukushima accident – dealt on aerosols scrubbing [15]. This relies on the fact that wet FCVS, where pool scrubbing is considered, are most efficient for aerosol scrubbing than for gaseous iodine. AREVA designed the standard FCVS on the basis to have a DF > 100 000 for large aerosols, DF > 10 000 for small aerosols, DF > 200 for molecular iodine, and DF > 5 for gaseous organic iodine [124]. However, in FCVS PLUS, where 3 stages of filtration are incorporated (2 stages other than the scrubber mainly for gaseous iodine), it is expected to show 10 < DF < 1000 for organic iodine, DF > 1000 for molecular iodine, and the same values for the aerosols species as in the standard FCVS [124].

These experiments considered different chemical species such as SiO_2, SnO_2, and CsI. However, CsI aerosols was the most common aerosol used in the experimental programs for its relevance in nuclear accidents and their post releases. In fact, based on severe accident measurements used to assess the chemical forms of iodine in containment, caesium iodide (CsI) is usually considered to be one the dominant iodine aerosol form to be released [1, 7] as experimentally shown in the CHIP/CHIP+ programs [9-12]. This statement is also supported by thermodynamic calculations [4, 125].

Based on what presented above, a major attention of our experimental work was devoted to study the scrubbing of this iodine compound.

IV.2.1. Experimental matrix

In Table IV.1, we present the test matrix on the retention of CsI aerosols. In the table, PIC stands for Pool scrubbing d'Iodure de Cesium. For each PIC test, a certain configuration of parameters is presented.

Table IV.1- Integral test matrix on the retention of caesium iodide aerosols CsI.

Test	Pool pH	Gas temp. (°C)	Pool temp. (°C)	Pool level (cm)	Mean aerosol flow rate (mg/min)	Nozzle size (mm)	Flowrate (L/min)	**Weber**
PIC 1	7	25	20	100	0.18	5	9.26	**4.99**
PIC 2	7	25	20	100	0.17	20	9.21	**0.08**
PIC 3	12	25	25	100	0.17	20	9.21	**0.08**
PIC 4	12	25	70	100	0.16	20	9.21	**0.08**
PIC 5	7	25	25	30	0.21	20	9.21	**0.08**
PIC 6	7	25	25	100	0.16	5	59.38	**205**
PIC 7	7	70	25	100	0.25	5	59.01	**196**
PIC 8	7	70	70	100	0.31	5	59.20	**196**
PIC 9	7	25	25	100	0.32	5	77.59	**350**
PIC 10	7	25	25	100	0.19	5	23.46	**32**
PIC 11	7	25	25	100	0.16	5	9.21	**4.93**
PIC 12	7	25	25	10 (L_{inj})	0.18	20	9.21	**0.08**
PIC 13	7	25	25	100	0.21	5	33.18	**64**
PIC 14	7	25	25	100	0.35	5	131.15	**1000**
PIC 15	7	25	25	100	0.31	20	73.67	**4.93**
PIC 16	7	25	25	100	0.21	20	9.21	**0.08**
PIC 17	7	25	25	100	0.35	2	131.04	**15600**
PIC 18	7	25	25	100	0.25	2	74.19	**5000**
PIC 19	7	25	25	100	0.21	2	33.18	**1000**
PIC 20	7	25	25	100	0.18	2	8.40	**64**

20 tests were performed on CsI trapping for aerosol of size ranging between 0.8 and 1 µm aerodynamic diameter (see II.3.3.3). The main investigation was to study the dependence of scrubbing on the flow regime (PIC 6, PIC 9, PIC 10, PIC 11, PIC 13, PIC 14, PIC 15, PIC 16, PIC 17, PIC 18, PIC 19, and PIC 20), represented by the Weber number, and this includes the variation of:

- Injection flowrate Q_{inj}.
- Size of the nozzle D_0.

This investigation is discussed in IV.2.2.1.
Other investigations were made on:

- Dependence on the pool submergence (PIC 5, PIC 12, PIC 16), discussed in IV.2.2.2.
- Dependence on the pH of the pool (PIC 3, PIC 16), discussed in IV.2.2.3.
- Dependence on the pool and gas temperature (PIC 3, PIC 4, PIC 6, PIC 7, PIC 8), discussed in IV.2.2.3.

In fact, and as mentioned before, drawing firm conclusion about the influence of certain test parameter requires large experimental database, that should be established from well-designed matrix of tests.

IV.2.2. Results and Discussion

As described in chapter II, CsI aerosols were trapped in the pool and the bubblers, and also deposited on the tubing connecting the sampling line, as well as depositions on the fiber filter at the end of the sampling line. Sampling from the pool and the bubblers were performed each 30 minutes, where the duration of injection of iodine compound for each test varied between 2 and 4 hours (see II.3.3). The evolution of retention in the pool and sampling line (bubblers) are shown as function of time in Figure IV.1 and Figure IV.2 respectively.

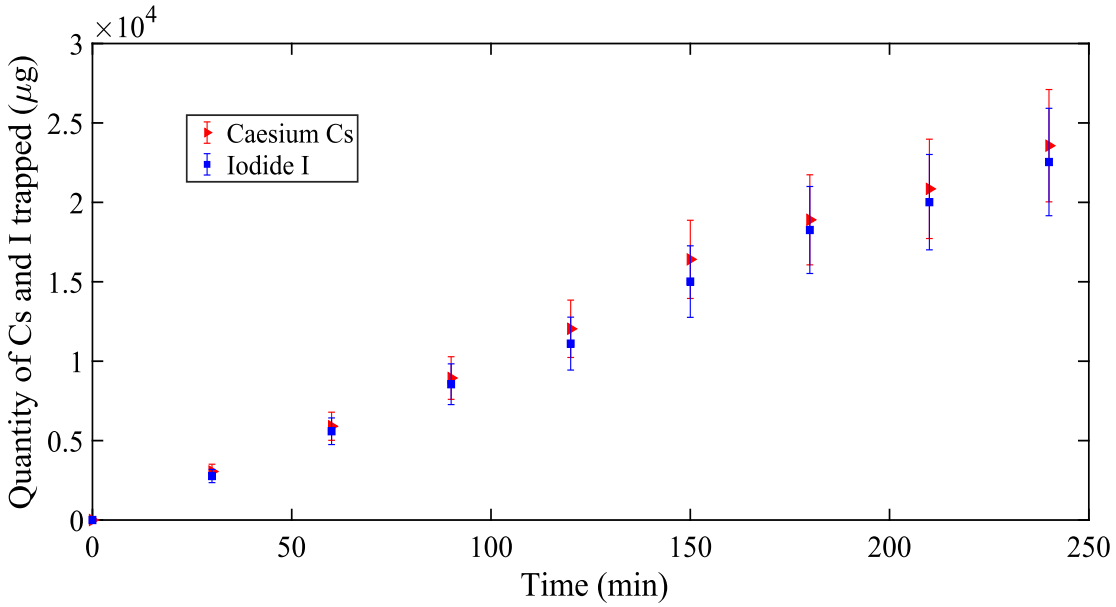

Figure IV.1- Quantity of caesium Cs and iodide I trapped in the pool (PIC 11).

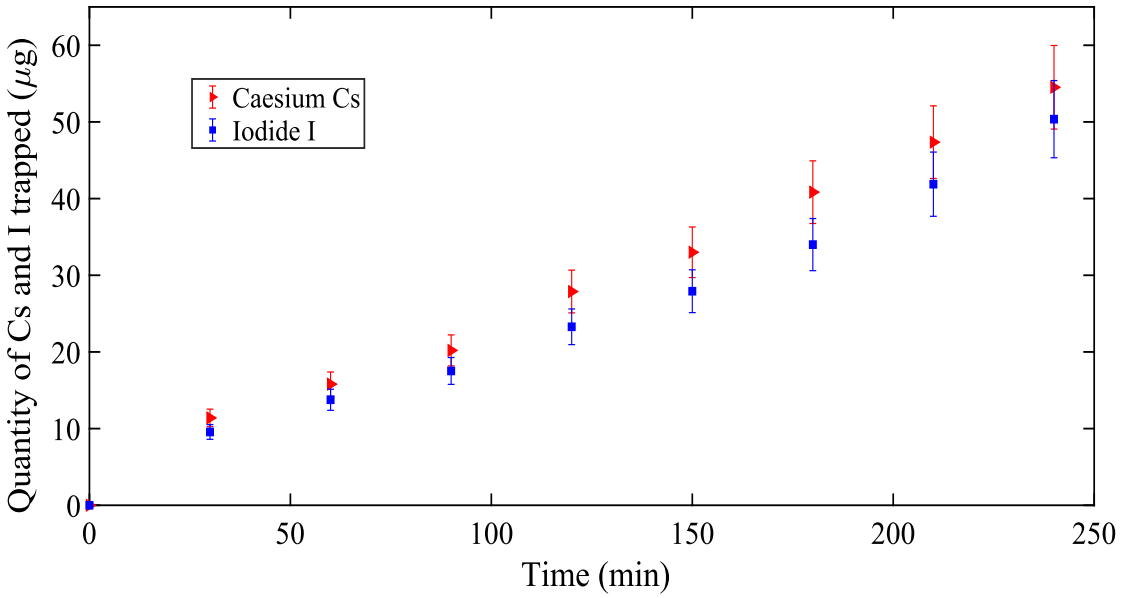

Figure IV.2- Quantity of caesium Cs and iodide I released to the sampling system and trapped in the bubblers (PIC 11).

Since the molar mass of caesium ^{133}Cs is close to that of iodide ^{127}I, it is expected that their quantities of mass trapped (CsI compound) will be relatively close. Figure IV.3 depicts the ratio of caesium to iodide trapped in the pool. This ratio shows that the trapped species remained in form of caesium iodide and didn't undergo any decomposition into other mixtures in the pool.

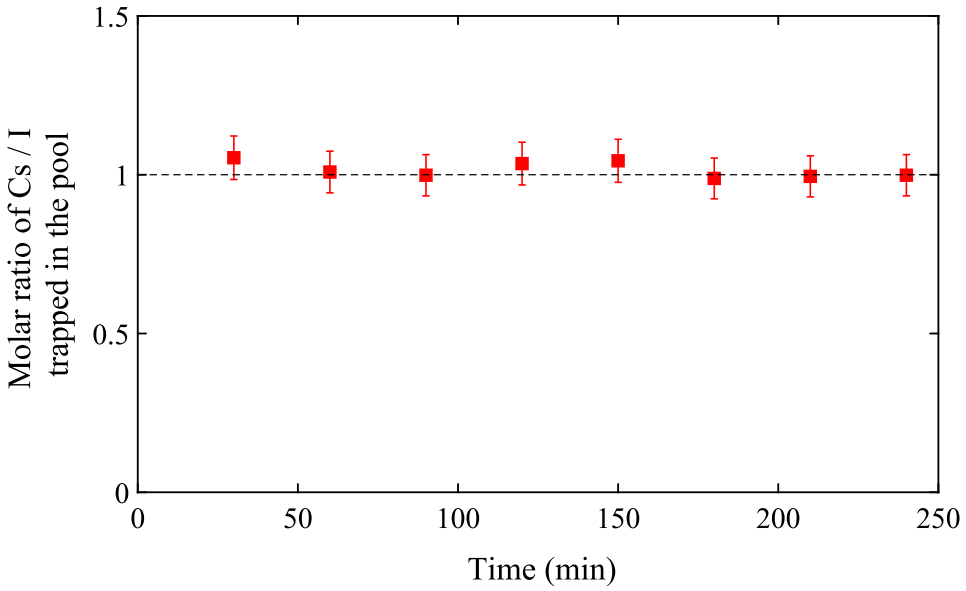

Figure IV.3- The molar ratio of species trapped in the pool.

On the other side, it is worth mentioning that the deposition of aerosols on the tubing was found to be important regardless of the test conditions. Table IV.2 presents the mass quantities of trapped CsI in the pool, bubblers, and the deposition of aerosols on the tubing for PIC 9. Therefore, the determination of the decontamination factor necessitated washing all the sampling line to collect the possible depositions and consider them.

Table IV.2- Retention and deposition in the sampling line

Test	Deposition on the tubing	Retention in bubblers	Deposition on the fiber filter
PIC 9	676 µg	2287 µg	737 µg

IV.2.2.1. Dependence on the flow regime

For this study, the submergence was set to H_{pool} = 100 cm and the temperatures of gas and pool were adjusted to 25 °C, and pH of the pool was maintained at 7. Table IV.3 shows the results of the experiments corresponding to the investigation of the dependence of decontamination on the flow regime.

The dependence of DF on gas flowrate, consequently Weber number, is still not well characterized, because it implies different removal mechanisms of counter effects [15, 36]. For that, the impact of this parameter is strongly dependent on the test conditions.

Table IV.3- Summary of experimental results regarding the flow regime

Test name	Nozzle size (mm)	Flowrate (L/min)	We	DF (± 9%)
PIC 6	5	59.38	205	5.4
PIC 9	5	77.59	350	14.3
PIC 10	5	23.46	32	6.8
PIC 11	5	9.21	4.93	30.8
PIC 13	5	33.18	64	5.8
PIC 14	5	131.15	1000	25.9
PIC 15	20	73.67	4.93	31.1
PIC 16	20	9.21	0.08	45.7
PIC 17	2	131.04	15600	285.2
PIC 18	2	74.19	5000	62.9
PIC 19	2	33.18	1000	22.2
PIC 20	2	8.40	64	8.4

It is usually believed that an increase in gas flowrate enhances the DF, as stated by Dehbi et al. [36] (notably due to the increase in interfacial area or gas/liquid exchange surface, linked to much more smaller bubbles in jet regime compared to bubbling regime). However, within the PASSAM project and the experiments conducted on the SCRUPOS facility, a higher value of DF was reported to a less gas flowrate for certain experiments at bubbling regimes [38]. This

was attributed to the higher residence time in the pool caused by a lower rising velocity, for the same water height.

The investigation carried out in this study reveals the effects of nozzle size and injection flowrate. Figure IV.4 shows the variation of decontamination factor measurements as the function of the nozzle size as well as the injection flow rate (which consequently affects the Weber number), realized throughout our experiments.

Regarding the nozzle size, the increasing of nozzle diameter D_0 from 2 mm to 5 mm hindered the scrubbing efficiency at high flowrates (Q_{inj} = 33 L/min, 75 L/min, 131 L/min), while the latter was favored for low flowrate Q_{inj} = 9 L/min. Inversely, increasing the nozzle size from 5 mm to 20 mm favored the scrubbing efficiency for the injection flowrate Q_{inj} = 75 L/min, and the same impact was reported for the low flowrate Q_{inj} = 9 L/min.

Regarding the injection flowrate, the higher was the injection flowrate the better was the scrubbing efficiency at nozzle D_0 = 2 mm. Then, at D_0 = 5 mm, the highest DF was reported for the lowest flow rate, and beyond that the scrubbing efficiency was favored for the higher flowrate. However, at D_0 = 20 mm, the scrubbing efficiency was greater for the lower flowrate.

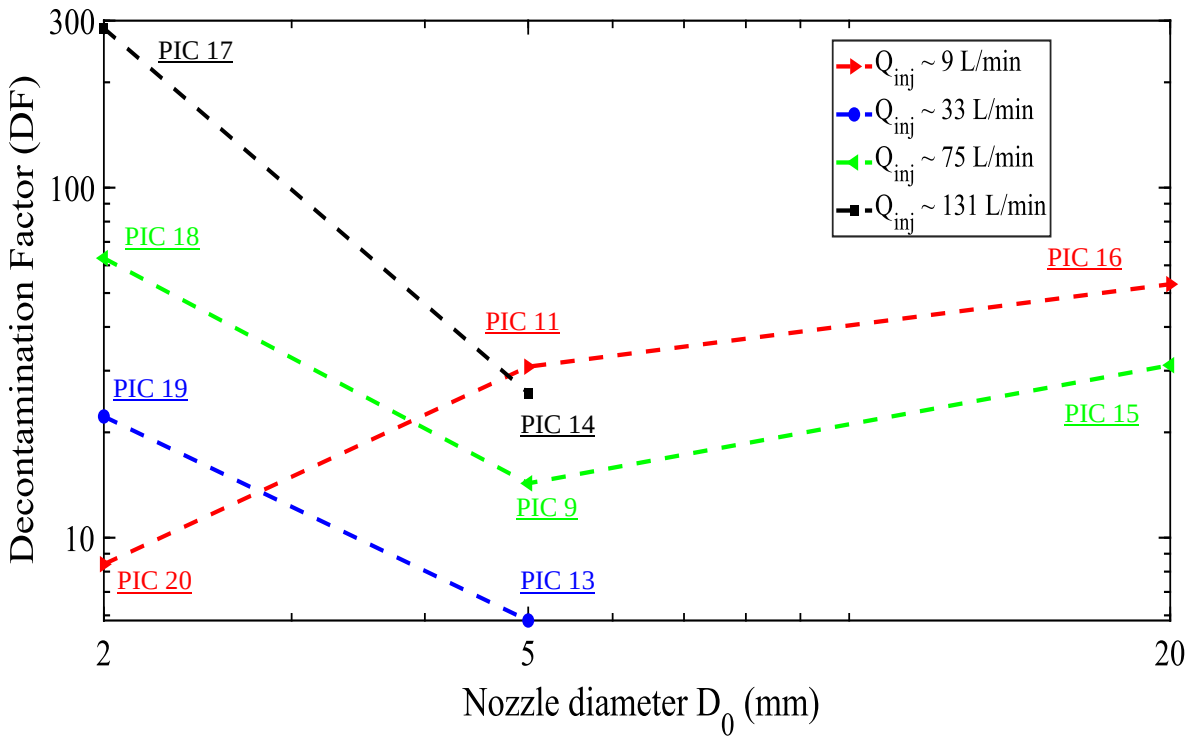

Figure IV.4- The effect of injection flowrate and nozzle size on pool scrubbing of CsI aerosols.

Therefore, an important message can be concluded from this figure, which is that there is no clear and unique sense of impact on the scrubbing efficiency from neither the nozzle size nor the injection flowrate.

These results confirm a tendency observed in the literature. Indeed, through the literature review we have showed in I.4.2, the injection flowrate has shown opposite senses between experimental work and another. Herranz et al. [40] and Yoon et al. [44] reported a favorable

impact due to the inertial impaction induced by the increase of injection flowrate. On the other side, unfavorable impact was observed by Xu et al. [54] and Beghi et al. [42], and a competitive effects was reported by Li et al. [52] and Woo et al. [47].

Taking into considerations these countereffects, an analytical approach is considered using the Weber number as it compares the inertial forces influenced by both the injection velocity and the nozzle size.

Figure IV.5 presents the decontamination factor for our work and experimental database from literature as function of Weber number. The tests conditions presented in Figure IV.5 for the different works are similar. In other words, the temperature of the pool and gas were ambient, no steam in gas mixture, single injector and no gas sparger, and submergence of nozzle ranged between 90 and 100 cm. The variable parameters are the nozzle size and injection flow rate, eventually the Weber number.

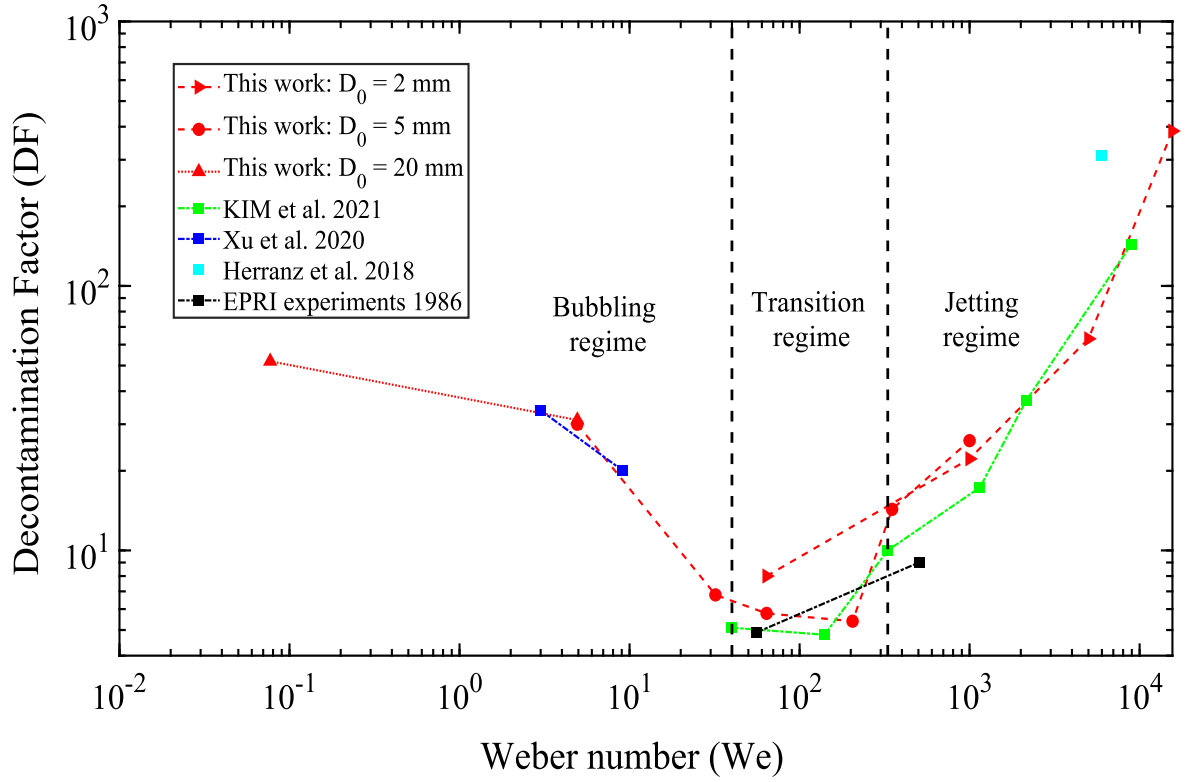

Figure IV.5- Variation of decontamination factor as function of injection flowrate and nozzle size in terms of Weber number, data from this work (see Table IV.3) compared to data from literature, Kim et al. (Same gas flowrate for different nozzle diameters; D_0 = 5 mm, 8 mm, 10 mm, 15 mm, 20 mm, 30 mm) [43], Xu et al. (D_0 = 25 mm) [54], Herranz et al. (D_0 = 6.5 mm) [40], and EPRI experiments (D_0 = 12.7 mm) [15].

Two major and important observations are shown in Figure IV.5, which can illustrate the discrepancy of the impact of injection flow rate Q_{inj} and nozzle size D_0 on the decontamination factor DF:

- Relevance of using the Weber number that comprise both D_0 and Q_{inj},
- Existence of a We corresponding to minimum scrubbing efficiency.

These two points are described below.

IV.2.2.1.1. Characterization and estimation of DF with Weber number.

The use of Weber number for pool scrubbing tests shows a good estimation of decontamination factor, despite the variation of nozzle size D_0 and injection flowrate Q_{inj}. To recall, the Weber number is a criterion for the classification of flow regimes, which means that the DFs are varying according to the flow regime exhibited in the flow. Therefore, one cannot analyze the effect of Q_{inj} without taking consideration of D_0 and vice versa, because one parameter of these parameters is sufficient to shift from a flow regime to another. This justifies why no clear impact could be concluded from neither D_0 nor Q_{inj} in Figure IV.4.

IV.2.2.1.2. Existence of minimum scrubbing efficiency.

The notion of minimum scrubbing efficiency stems from the countereffects of aerosol removal mechanisms for the different experimental configurations. Berzal et al. [15] reported that an increase in gas flowrate favors the inertial and centrifugal impaction, but it hinders the residence time and gravitational settling (as mentioned in IV.2.2.1). Through the analysis of Figure IV.5 given below, we will make this clearer according to the different flow regimes. These regimes are the bubbling regime, churn turbulent regime, and jetting regime as shown in Figure IV.6.

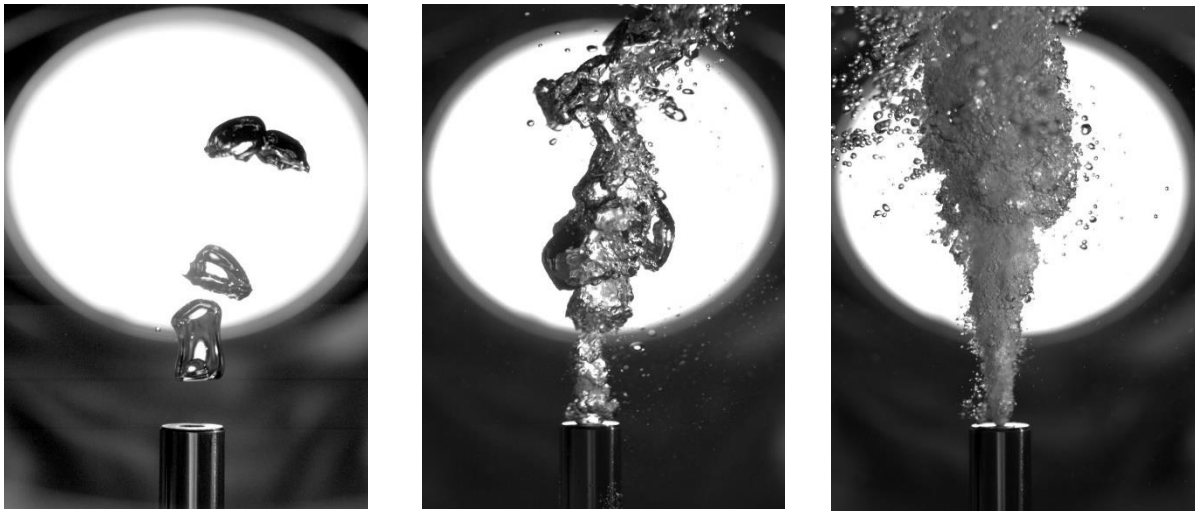

(a) (b) (c)

Figure IV.6- The morphology of flow for the different regimes; (a): We = 0.08 for bubbling regime, (b): We = 205 for churn turbulent regime, (c) We = 15600 for jetting regime.

At low Weber number ($0.08 < We < 10$), where flow regime is described as bubbling regimes with formation of globules and bubbles, the obtained DFs are relatively high but follow a descending trend. In this regime, two factors favor the low Weber number, the residence time, and the interfacial area of bubbles.

The residence time, which is related to injection velocity, will be greater if the injection flow rate is lower or the nozzle size is larger. Hence, as this parameter is greater, the aerosol removal mechanisms will act for longer period such as sedimentation, diffusion, and centrifugal impaction. The residence time of bubbles in the pool can be divided into the time spent in each hydrodynamic zone, therefore the velocity of bubbles in each of these zones. Generally, several forces act on the bubbles during their formation and rise in the pool, such as the buoyancy, drag,

inertia and lift. The contribution of these individual forces varies from experimental configuration to another, such as the injection flowrate Q_{inj}, which affects mainly the rising velocity of globules U_G (as discussed in III.3.3.6) in the injection zone. Moreover, there is the bubbles terminal velocity U_r which is achieved when buoyance forces are balanced with drag forces. Here it is worth mentioning that models and correlations developed to determine these velocities depend strongly on the size and the shape of the bubbles [110, 112, 113, 126].

On the other hand, the increase of Weber number in bubbling regimes due to an increase in the injection flowrate, will result in relatively larger bubbles, thus hindering the interfacial area. As the Weber number increases ($10 < We < 220$) introducing the transition phase referred as churn turbulent regime, the DF exhibits a sharp decrease. A minimum of DF for the different experimental works, including our work, is reported in this range of Weber number corresponding to this flow regime (cf. Figure IV.5). At this regime, same aerosol removal mechanisms will act as in the previous regime, however, for fewer residence time and decrease in the interfacial area.

Beyond that, and as Weber number indicates the onset of jetting regime ($We \approx 330$), the DF increases as the Weber increases ($We > 300$). Although that residence time is not important anymore, but as inertia dominates in this regime, aerosols are trapped by regime-induced removal mechanism, namely inertial impaction. This due to the fact that aerosols possess momentum that can deviate them from streamlines. This mechanism, inertial impaction, is represented by the dimensionless Stokes number, corresponding to the ratio of the stopping distance S of a particle to a characteristic dimension of the problem [98], here the nozzle diameter D_0:

$$St = \frac{S}{D_0} = \frac{\tau_p U_{inj}}{D_0} \tag{34}$$

where τ_p is the relaxation time of the particle, U_{inj} is the gas injection velocity and D_0 is the nozzle diameter. In the range of particle sizes and flowrates considered in our study, maximum values of particle Reynolds number Re_p[3] remain close to 1 (Stokes regime), thus τ_p can be expressed as [98]:

$$\tau_p = \frac{\rho_p \ {d_p}^2 C_c}{18 \, \mu_g} \tag{35}$$

where ρ_p is the aerosol density, d_p is the particle aerodynamic diameter, μ_g is the dynamic viscosity of gas and C_c the Cunningham slip correction factor. This latter being close to 1 for aerodynamic diameter greater than 0.1 µm [98], Stokes number can be written as:

$$St = \frac{\rho_p \ {d_p}^2 U_{inj}}{18 \, \mu_g \, D_0} \tag{36}$$

The decontamination factor by the inertial impaction mechanism is determined by:

[3] Particle Reynolds number: $Re_p = \frac{\rho_g d_p U_{inj}}{\mu_g}$

$$DF_{imp} = \frac{1}{1 - Eff_{imp}} \quad (37)$$

Where Eff_{imp} is the efficiency of deposition due to the jet impaction, knowing that $Eff_{imp} \propto St$. Through literature, different correlations are proposed to describe the efficiency deposition [127, 128]. Through our approach of estimating the retention of aerosols by inertial impaction, the correlation developed in literature by He al . [128] is considered.

$$Eff_{imp} = \begin{cases} 1.79182\ (3.4337 \times 10^{-11})^{(5.9244\times10^{-3})^{\sqrt{St}}} & \sqrt{St} \leq 0.65868 \\ 1.13893\ (1.4173 \times 10^{-6})^{(4.25973\times10^{-3})^{\sqrt{St}}} & \sqrt{St} > 0.65868 \end{cases} \quad (38)$$

Through the determination of decontamination factor due to inertial impaction in eq.(37) it is revealed that a major trapping occurs due to the mechanism of inertial impaction, as shown in Figure IV.7. Through eq.(38) the efficiency (Eff_{imp}) tends to asymptotic behavior, the effect of inertial impaction is limited such that $DF_{imp} < 129$.

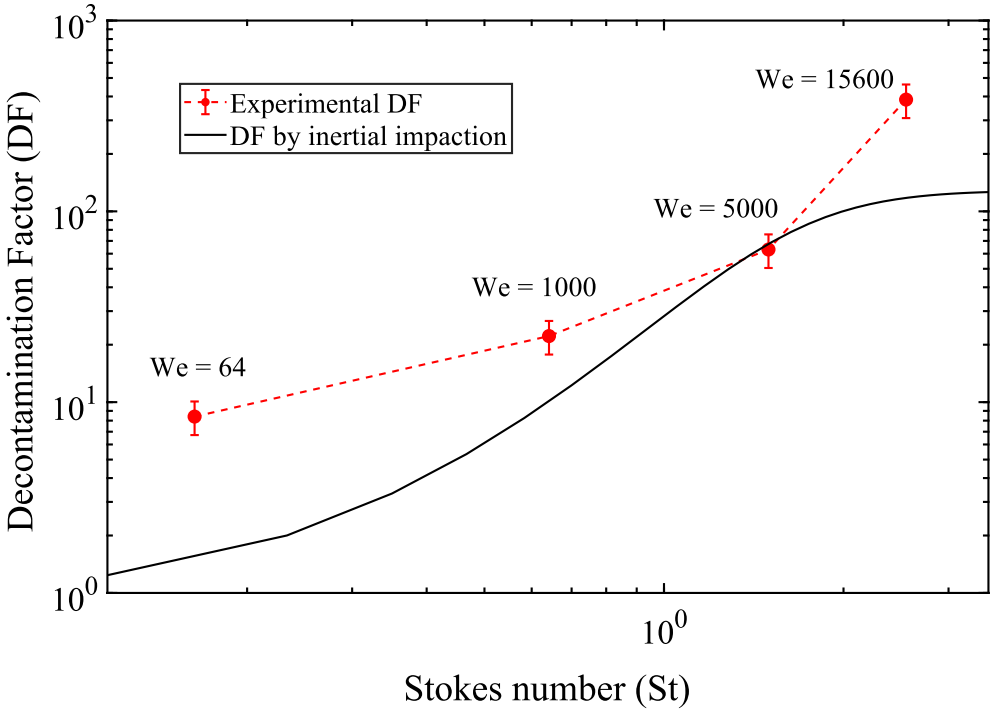

Figure IV.7- Comparison between experimental global DF and the modelling of DF determined only by inertial impaction [128]

for PIC 17 (We = 15600), PIC 18 (We = 5000), PIC 19 (We = 1000), and PIC 20 (We = 64).

Moreover, as inertia increases in jetting regimes, a higher interfacial area between the dispersed and continuous phase occurs. The latter is provoked by the breakup of the flow into tiny bubbles due to high inertial and turbulent flow [44]. In other words, the higher the Weber, the higher is the inertia of flow; therefore, the more the breakup is rapid leading to tiny bubbles distribution in the pool [129]. Figure IV.8 show the major mechanisms presented in the jetting regime. In

the following paragraph (study of Kim et al. [43]), we discuss an experimental work, from the literature, so we can conclude on this point.

In literature, a study by Kim et al. [43] was conducted to analyze the effect of the nozzle size. For same gas injection flowrate (28 kg/h) , experiments were carried out using five sizes of nozzles, where they reported an increase of scrubbing efficiency when the nozzle diameter decreases. They justified that due to the increase of inertial impaction, influence by injection velocity $U_{inj} = Q_{inj} / D_0$, when the nozzle size decrease. They also added that at smaller nozzle sizes, smaller sizes of bubbles are generated, thus introducing higher interfacial area between the pool and the gas. These statements are true since the work of Kim et al. [43] is beyond the bubbling regime, and can be described as jetting as shown in Figure IV.5. As long as the regime is jetting, the further decrease in the nozzle size for the same flowrate will increase the Stokes number, thus increasing the inertial impaction as well as the interfacial area between he bubbles and the pool.

The different trends of the decontamination factor, observed in Figure IV.5, consolidate and clarify the finding of Herranz et al. [40], Yoon et al. [44], Xu et al. [54], Beghi et al. [42], Li et al. [52], Woo et al. [47], and Kim et al. [43]. These experimental works reported different impacts of injection flowrate or nozzle size, because the examination was performed in different flow regimes, and here the importance of characterization of the flow by the Weber number is revealed.

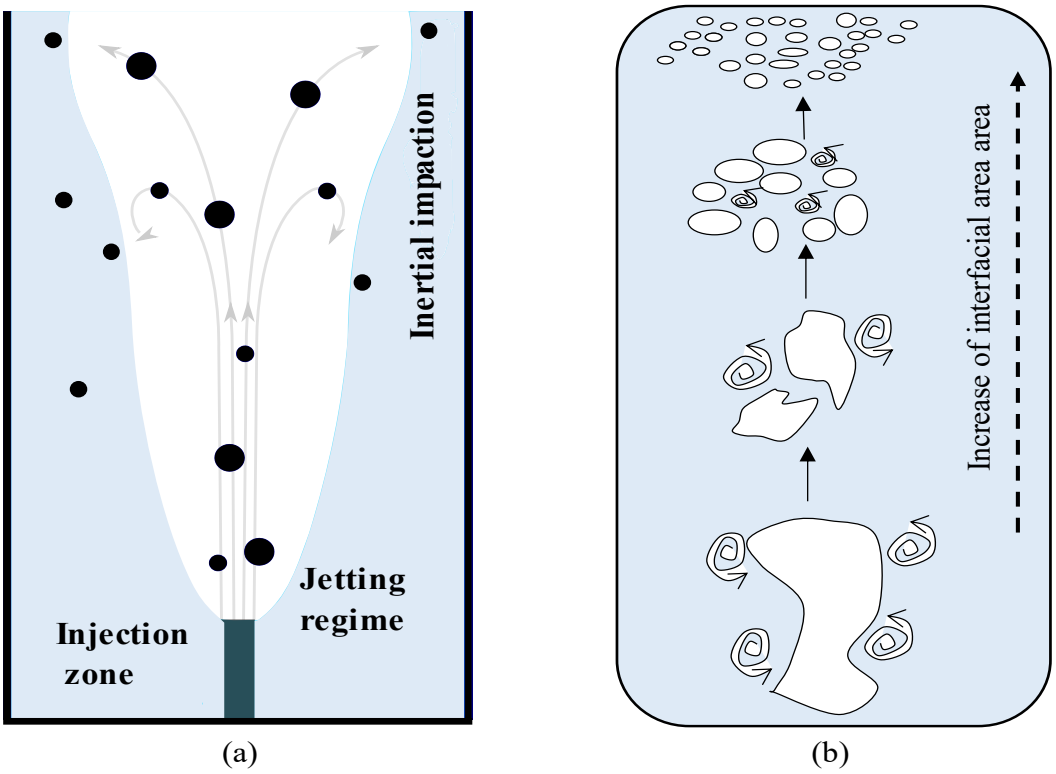

Figure IV.8- The major mechanisms of aerosol scrubbing in jetting regime; (a): Inertial impaction due to the jet at the injection zone, (b): The breakup into tiny bubbles due to inertial turbulent flow and enhancing the interfacial area at the bubble rise zone.

According to the difference behavior of aerosol removal mechanisms in bubbling and jetting regimes, we considered to compare the impact of other test parameters (pool submergence, pool, and gas temperature) on each of these regimes.

IV.2.2.2. Dependence on the pool submergence

Pool submergence is an important test parameter favoring the retention of aerosols. There are no opposite results to the latter statement. However, it may be less important in case where aerosols particles are massive, since the majority of aerosols could be trapped at once at a small distance from the injector, notably because of inertial impaction in case of jetting regime. Figure IV.9 and Figure IV.10 present decontamination factors at different submergences for bubbling and jetting regimes respectively.

IV.2.2.2.1. Submergence in case of bubbling regime

In case of bubbling regime (see Figure IV.9), the nozzle size D_0 = 2 cm was used, gas and pool temperature were adjusted at 25 °C, injection flowrate was regulated at 9.21 L/min and pool pH was set to 7. The other test conditions are shown in Table IV.4. The average residence time of bubbles in the pool is estimated such that:

$$\tau_{average} = \frac{V_{pool}}{Q_{inj}} \quad (39)$$

Various factors favoring the retention of CsI aerosols as the submergence increase: the increase of average residence time τ, hygroscopic growth of soluble CsI aerosols size and development/exhibition of a steady state of bubbles swarm at a sufficient submergence.

Table IV.4- Summary of tests examining the impact of pool submergence

Test	Weber	Pool level (cm)	Volume of pool (m^3)	Residence time τ (s)	DF (± 9%)
PIC 16	0.08	100	0.1964	1279	45.7
PIC 5	0.08	30	0.0589	384	18.0
PIC 12	0.08	10 (L_{inj})	0.0196	128	6.1

Regarding the hygroscopic growth, the size of aerosols particles increases as the relative humidity of carrier gas increases when it rises in the pool, as reported by Li et al. [52]. The evolution of aerosol size makes larger particles easier to retain than small ones, due to the mechanism of deposition and sedimentation [15, 36, 52]. It is suggested that this effect occurred in our experiments, when the pool submergence increased from L_{inj} to 100 cm.

Despite the attenuation of retention due to decrease in the submergence, experiment PIC 12 that represents approximately the altitude of injection zone, shows that the contribution of this zone in aerosol retention is also important (DF = 6.1). This agrees with the analysis performed by Lee et al. [103] to reveal the contribution of each of the hydrodynamic zones to the scrubbing of aerosols.

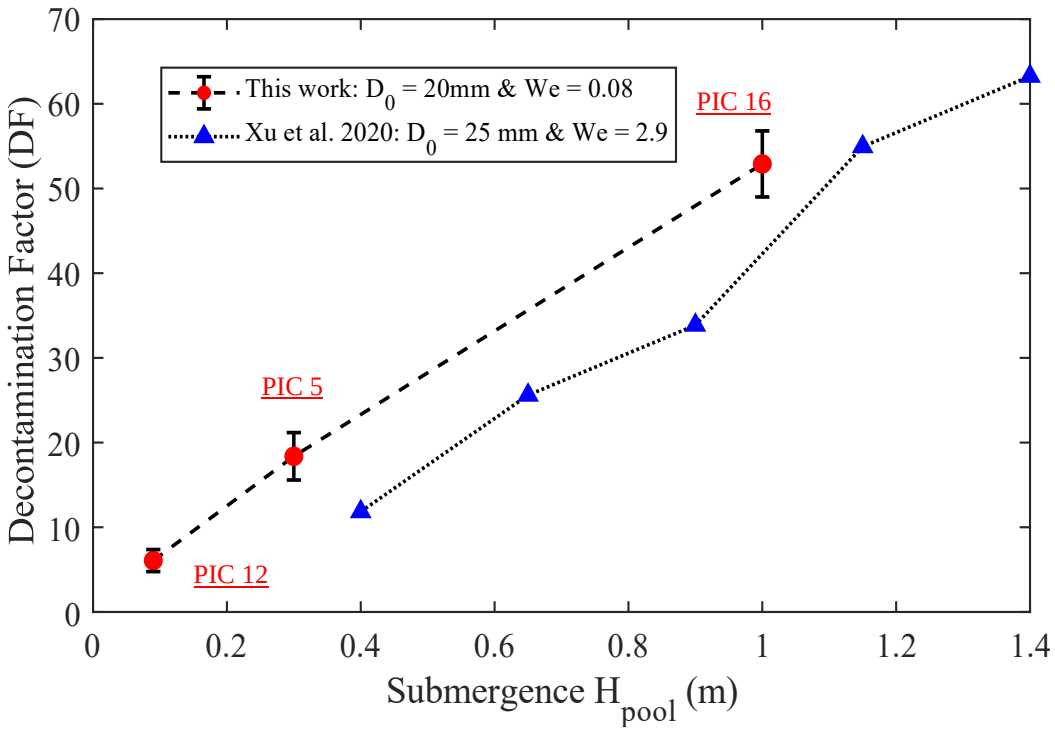

Figure IV.9- The impact of submergence on DF in bubbling regimes at We = 0.08 with comparison at We = 2.9 from Xu et al. [54].

IV.2.2.2.2. Submergence in case of jetting regime

In case of jetting regime (see Figure IV.10), we compared our obtained decontamination factor measurements at H_{pool} = 100 cm, with the experiments realized by Yoon et al. [44] with relatively same Weber number but at H_{pool} = 50 cm.

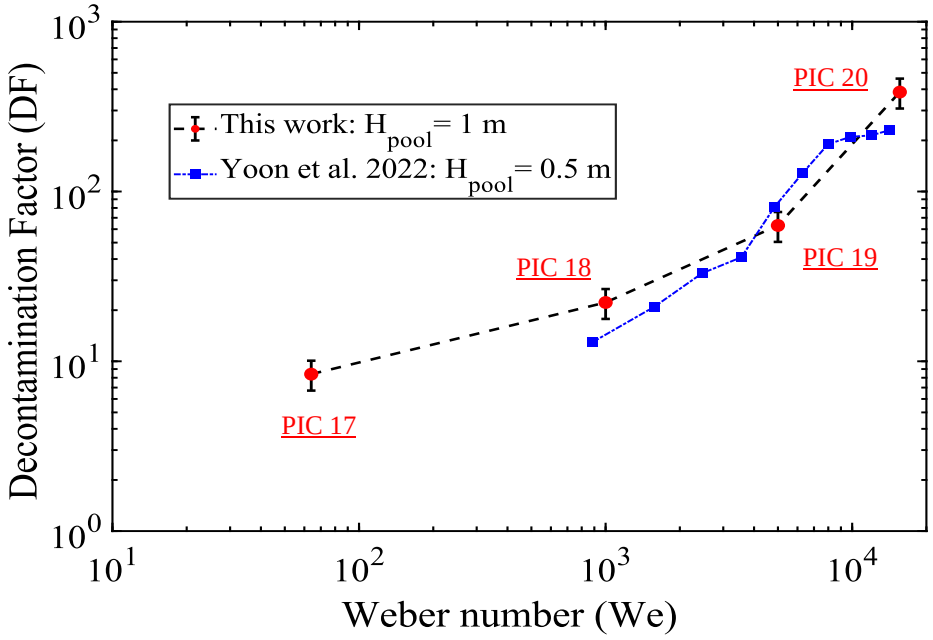

Figure IV.10- The influence of submergence in case of jetting regime; and Yoon et al. [44].

The scrubbing efficiency shows no difference between the two configurations. It should be said that other experimental conditions, such as the injected species and its properties (SiO_2 of size 0.7 µm), might influence the variation of decontamination factor, and contributing to the similar DFs obtained as our experiments.

However, it is worth saying that for low pool submergence such, that H_{pool} < 100 cm, such altitude could not be sufficient for the exhibition and formation of plume with tiny bubbles rising with a plume terminal velocity, which is described by the bubble rise zone. In this case, the main major mechanism responsible for the aerosols' removal will be the inertial impaction that occurs near the nozzle. Herranz et al. [129] consolidated the latter statement, as they considered that inertial impaction is the dominant removal mechanism in jetting regimes for pool submergences Hpool ≤ 1.25 m.

In chapter V of this report, we performed modelling of aerosol removal mechanism where the influence of this removal mechanism will be revealed and discussed according to pool submergence.

IV.2.2.3. Dependence on the pool and gas temperature

Liquid pools at ambient temperature are expected to be present in all non-severe accidents and in those severe scenarios in which pool cooling is functional. Throughout the campaigns of pool scrubbing experiments, it is clearly observed that aerosols' retention is strongly dependent on the thermal-hydraulic conditions [15, 36]. Moreover, this parameter has been investigated in different experimental campaigns, where the gas used is air/steam mixture. The main drawn conclusion is that DF decreases as the temperature in the pool increases [130]. In fact, condensation at the water/gas interface caused by the gradients in steam concentration and temperature, favors the aerosol transport from hot to cold region (thermophoresis). Consequently, as the pool temperature increases, its capability to condense steam diminishes thus hindering thermophoresis.

IV.2.2.3.1. Impact of temperature and pH in bubbling regime

The tests realized to investigate the impact of gas and pool temperature in bubbling regimes are show in Table IV.5. These experiments were performed without steam. However, thermophoresis seems to have a little but apparently existing influence at ambient temperatures, by comparing PIC 2 to PIC 16.

Table IV.5- Summary of tests examining the impact of temperature in bubbling regime

Test	Weber	pH	Gas temperature (°C)	Pool temperature (°C)	Δtemp. (°C)	DF (± 9%)
PIC 2	0.08	7	25	20	5	53.2
PIC 16	0.08	7	25	25	0	45.7
PIC 3	0.08	12	25	25	0	43.0
PIC 4	0.08	12	25	70	- 45	20.0

On the other side, the effect of water pH on removal efficiency of aerosols seems not to be the main phenomenon influencing retention, by comparing PIC 16 to PIC 3. Although that DF was higher with demineralized water than alkaline water, but the difference needs to be studied carefully before drawing any firm conclusion. In fact, pH's impact on DF has not been studied intensively by previous experimental campaigns, although that this parameter is considered to be important when chemical reactions are involved in the trapping mechanisms.

However, the significant decrease of DF in PIC 4 can be justified by the absence of thermophoresis [130]. Temperature of pool was 70 °C and gas temperature was 25 °C, so the gradient temperature in this experiment was opposing thermophoresis and was much more important (45°C between gas and pool in PIC 4 comparing to 5°C in PIC 2). Given the absence of steam in our case, another explanation could also be linked to a change in hydrodynamics, as the viscosity strongly depends on temperature.

In order to enhance the interpretation of DF, bubble dynamics were characterized in the injection zone where the formation of large globules takes place. The globule volume, frequency, surface area, as well as the interfacial area were determined as shown in Table IV.6.

Table IV.6- Hydrodynamic measurements of PIC 2, PIC 3, and PIC 4.

Test	Weber	V_G (cm^3)	S_G (cm^2)	S_G / V_G (cm^{-1})	f_G (Hz)	DF (± 9%)
PIC 2 - 16	0.08	26.48	50.70	1.91	6.8	45.7
PIC 3	0.08	24.22	44.35	1.83	7.1	43.0
PIC 4	0.08	38.11	59.64	1.56	5.4	20.0

In terms of interfacial area, the globule dynamics in PIC 4 are considerably different than in PIC 2 and PIC 3. As the pool temperature, globule volume increased significantly, which is reported also by Colombo et al. [131] and Kim et al. [132]. This will be discussed in chapter V as we model the influence of interfacial area in the injection zone on the decontamination factor.

IV.2.2.3.2. Impact of temperature in transition regime

Based on the dependence of aerosol removal mechanisms on the flow regime, the dependence of DF in the transition regimes on the pool and gas temperatures is investigated separately from bubbling regimes, as shown in Table IV.7.

Table IV.7- Summary of tests examining the impact of temperature in transition regime

Test	Weber	pH	Gas temperature (°C)	Pool temperature (°C)	Δtemp. (°C)	DF (± 9%)
PIC 6	205	7	25	25	0	5.4
PIC 7	196	7	70	25	45	6.2
PIC 8	196	7	70	70	0	7.8

The first three tests exhibit similar DF despite the variation of temperature. This tends to show that the impact of thermophoresis, especially with the absence of steam composition in the gas, is attenuated and over dominated by other mechanisms. Herranz et al. [40] reported the same justification as they observe no impact of gas-pool temperature difference on scrubbing efficiency in case of jetting regime, and they considered that there is a dominance of mechanical processes contributing to the DF.

Nevertheless, the condensation in PIC 7 presents strongly comparing to PIC 6, due to the gradient of temperature (thermophoresis) between the carrier gas and the pool. Regarding PIC 8, the increase in DF maybe attributed to the higher interfacial area when comparing with PIC 6 and PIC 7. In fact, as pool temperature increases, the surface tension of water decreases which implies a faster breakup of the jet into smaller bubbles. The breakup is considered a removal mechanism by some pool scrubbing codes such as SPARC and BUSCA, otherwise is attributed to inertial impaction.

One can note that these tests have been performed before the study of the DF minimum presented in Figure IV.5, and appear to be close to the We corresponding to the minimum DF for aerosols (~200). Actually, this would have been interesting to test this influence at higher We: it may be more difficult to highlight a potential influence of temperature gradient on DF in this zone.

IV.3. Retention tests of volatile iodine

As mentioned in Chapter 0, the main physical and chemical forms of iodine that can be found in the containment after a severe accident are iodine in aerosol form (CsI), gaseous molecular iodine (I_2), and gaseous organic iodine (CH_3I). As we discussed previously the release and trapping of CsI aerosols, we discuss in this section the decontamination factor measurements examined on I_2 and CH_3I.

The release of molecular iodine (I_2) as fission product and organic iodides (subsequently due to its reaction with paints and cables etc.) are the considerable volatile and radioactive species. Among the organic iodides, methyl iodide (CH_3I) is the major and most volatile component in the containment vent exhaust. Removal and retention of these volatile radioactive iodine species is dependent upon competing time scales defined by the gas hold up time, mass transfer rate and the decomposition reaction in the aqueous phase [3, 26]
Therefore, the trapping of volatile iodine species (molecular I_2, methyl iodide CH_3I) can be significantly influenced by the prevailing thermal-hydraulics and chemical conditions.

Molecular iodine I_2 is formed by the radiolytic oxidation of iodide ions with the overall reaction:

$$2\,I^- + h\vartheta_f \rightleftharpoons I_2$$

The forward rate is linked to the oxidation of iodide by the hydroxyl radical whereas the backward reaction is mainly due to the reduction of I_2 by the hydrogen peroxide formed [20].

On the other side, organic compounds of iodine such as methyl iodide, can be produced over time as a result of the molecular iodine reactions with organic materials [20]. Organic iodide formation as a result of reactor accidents has been surveyed in WASH-1233 report [133].
It has to be noted that other organic iodides are typically less volatile than methyl iodide CH_3I, therefore they are considered to pose less challenges in terms of environmental releases [134].

The experimental tools at our laboratory L2EC in IRSN Cadarache that are dedicated for the DF measurements of these species (I_2, CH_3I) have been presented in II.3.3.2 and II.3.3.4.

IV.3.1. Experimental matrix

Although that an extensive experimental work on iodine chemistry was conducted in the lasts decades and provided wide knowledge of significant reactions occurring in the reactor containment in severe accidents [135], however limited work was conducted on the specific topic of gaseous iodine in pool scrubbing.

After Fukushima accident, European countries commonly required DFs capabilities for molecular iodine ranging from 10 to 1000 depending on the regulation [136]. Beghi et al. [ref] conducted some experiments on I_2 retention where the effects of flow regime, iodine concentration, and residence time were investigated. The trapping mechanism of this species showed a countereffect of the test parameters within the different flow regimes, as discussed in IV.2. Moreover, hydrolysis and kinetics of chemical reactions showed a significant contribution to the improving of scrubbing efficiency of I_2 [134].

Therefore, and within our matrix of I_2, two main parameters were investigated:

- Impact of flow regime
- Impact of the pool's pH

We performed seven tests on I_2 trapping, and the experimental configuration and results of these tests are shown in Table IV.8, where PI stands for Pool scrubbing de dIode. These tests aimed at simulating possible scenarios of Steam Generator Tube Rupture SGTR where this particular element is expected to be released into the secondary circuit, thus presenting a potential risk [23]. Although that the conditions presented in Table IV.8 are not well representative (radioactive composition, pressure gradient, temperature gradient) for the SGTR scenarios [23], however, we aimed in a first approach to characterize the trapping of this iodine compound in order to provide an insight for prospective experimental work.

Table IV.8- Results of the integral test matrix on the retention of molecular iodine I_2.

Test	Pool pH	Gas temp. (°C)	Pool temp. (°C)	Pool level (cm)	Nozzle size (mm)	Weber	DF
PI 1	7	25	25	100	20	5	6.4
PI 2	12	25	25	100	20	5	14.1
PI 3	12	25	25	100	20	0.08	118.4
PI 4	7	25	25	100	20	0.08	25.9
PI 5	9.5	25	25	100	5	330	8.9
PI 6	7	25	25	100	5	500	11.2
PI 7	7	25	25	100	5	330	7.1

On the other hand, DF measurements by pool scrubbing of organic iodine were not performed in previous experimental works from literature as much as aerosols pool scrubbing. This is due to the low efficiency of this mechanism, thus relatively lower interest of organic iodine pool scrubbing. In fact, pool scrubbing in FCVS is compensated by incorporation of FCVS scrubbers with zeolite based molecular sieve filters impregnated with silver [2, 26]. This incorporation is presented in third and final stage of the modern FCVS, which is described as the section of organic iodine sorbent. The second section is the metal fiber filter section (dry section) and the first is the venturi scrubber (pool scrubbing).

Accordingly, the trapping efficiency for this species was consider varying with the pool chemistry (pH and additives) and the temperature of the pool and carrier gas [134, 135, 137].

In Table IV.9, the experimental configuration and results of these tests are shown, where PIM stands for Pool scrubbing d'Iodure de Méthyle.

Table IV.9- Results of the integral test matrix on the retention of methyl iodide CH_3I.

Test	Pool pH	Gas temp. (°C)	Pool temp. (°C)	Pool level (cm)	Nozzle size (mm)	Weber	DF
PIM 1	12	25	25	100	20	0.08	1.3
PIM 2	12	70	70	100	20	0.08	2.4
PIM 3	12	25	25	100	5	64	1.1
PIM 4	12	70	25	100	5	350	1.2
PIM 5	12	70	70	100	5	350	1.6
PIM 6	12	70	25	100	5	1000	1.2
PIM 7	12	25	25	100	5	1000	1.2
PIM 8	12	25	25	100	5	3000	1.1
PIM 9	13	70	70	100	20	0.08	5.6

IV.3.2. Results and discussion

According to the planned test matrix, DF measurements were carried out on TYFON facility. The methodology of I_2 trapping was similar to that of CsI aerosols, whereas it was less constraining for the experiments on CH_3I. This was due to the high volatility and behavior of CH_3I, in which its deposition on the sampling system was negligible. The dependence of DF on the flow regime, pH of the pool, and temperature will be discussed for each species.

IV.3.2.1. Dependence on flow regime

The temperature of injected gas and pool were set to 25 °C. The variation of Weber number comprised the change of injection flowrate and nozzle size, in order to consider the different hydrodynamics presented in each flow regime. Figure IV.11 presents the decontamination factor measurements at different Weber number, for pool pH adjusted at 7 and 12 for I_2 and CH_3I respectively.

IV.3.2.1.1. Molecular iodine I2

The trapping efficiency of I_2 is found to be dependent on the Weber number, moreover the phenomenon of minimum scrubbing seems to exist. Similar to CsI aerosol scrubbing, the DF was relatively high at bubbling regime where residence time is high, then it decreases as Weber increases in the intermediate regime. Beghi et al. [42] reported this significant reduction of DF at the transition from bubbling to churn-turbulent flow, and they justified that due to two factors: the less residence time as well as the smaller interfacial area (with the increase of bubbles size) as for aerosol trapping.

Beyond jetting regime, DF shows an increasing trend. We must note that in scrubbing of gaseous I_2, the inertial impaction does not exist as it is totally diluted in the gas flow. Despite that, with the increase of Weber, turbulent mixing is induced so an increase in interfacial area by the breakup of jet into tiny bubbles is supposed to be responsible for the increase of DF.

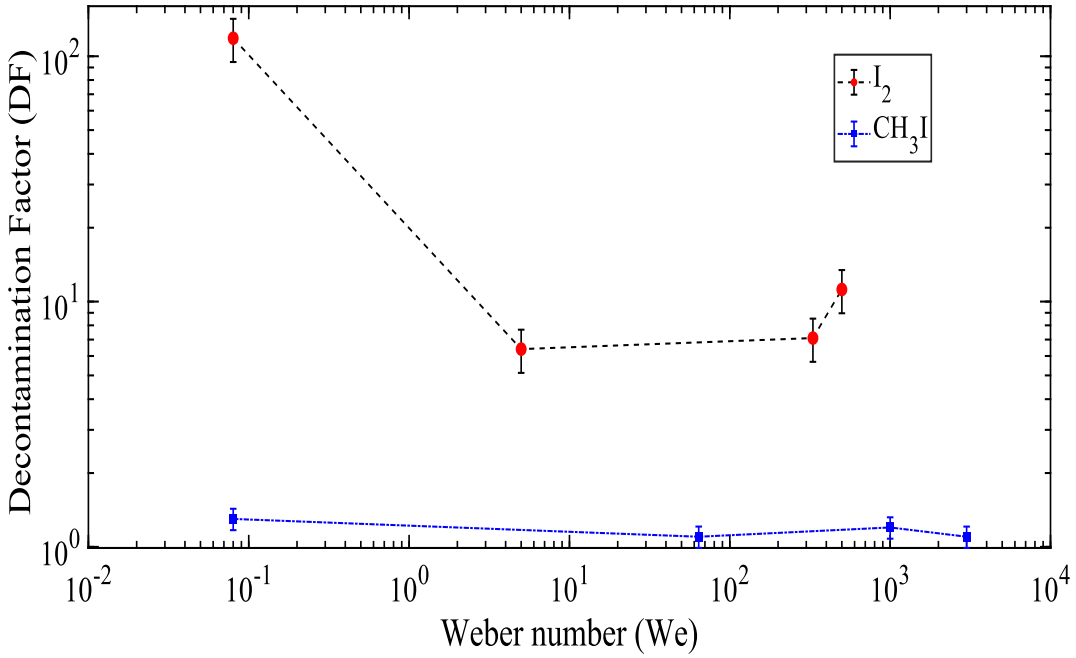

Figure IV.11- Dependence of iodine species (I_2, CH_3I) on flow regimes; Tgas = Tpool = 25 °C.

IV.3.2.1.2. Methyl iodide CH_3I

As shown in Figure IV.11, a low DF of CH_3I is found along all the experiments, such that for tests where DF < 1.5 we can consider that there is almost no trapping of CH_3I. The DF of CH_3I being close to unity despite the increase of Weber number, reveals negligible effects of inertial mechanisms on trapping. Moreover, it shows that varying interfacial area isn't sufficient to enhance the possible increase in mass transfer.

The low scrubbing efficiency of CH_3I by pool scrubbing is expected and common issue through literature, however, it is reported that the trapping of gaseous methyl iodide is dependent of water chemistry [134, 135, 137] and not on the hydrodynamic aspects of the flow.

IV.3.2.2. Dependence on pH and temperature of the pool

Mass transfer at the interface of gas/liquid phases are effected by intervening terms of chemical kinetics, which alter and control the reaction. The key factors influencing the transfer are pH, temperature, and concentration of species. The main chemical reaction is hydrolysis (considered as a fast reaction). It is common that organic iodine (CH_3I) is decomposed by reactions with air radiolysis products [3, 26]. Experimental campaigns from literature showed that the decomposition rate of organic iodine is proportional to the pool chemistry, moreover temperature has also shown an effect on the rate of the "destruction" reaction [2, 3, 13, 26].

Therefore, with the variation of pool temperature and pH, we expect that effects on hydrolysis and decomposition rate would enhance the decontamination factor.

IV.3.2.2.1. Molecular iodine I_2

Figure IV.12 presents the DF for different configurations of I_2 that intend to examine the effect of pH. For molecular iodine, the course of hydrolysis depends on the pH value, following the equation: $I_2 + H_2O \rightleftharpoons I^- + HIO + H^+$.

In fact, the pH has an impact on the concentration of I_2 in the liquid phase. For basic matrix (pH > 7), hydrolysis is more rapid and I_2 is not stable to pass through.

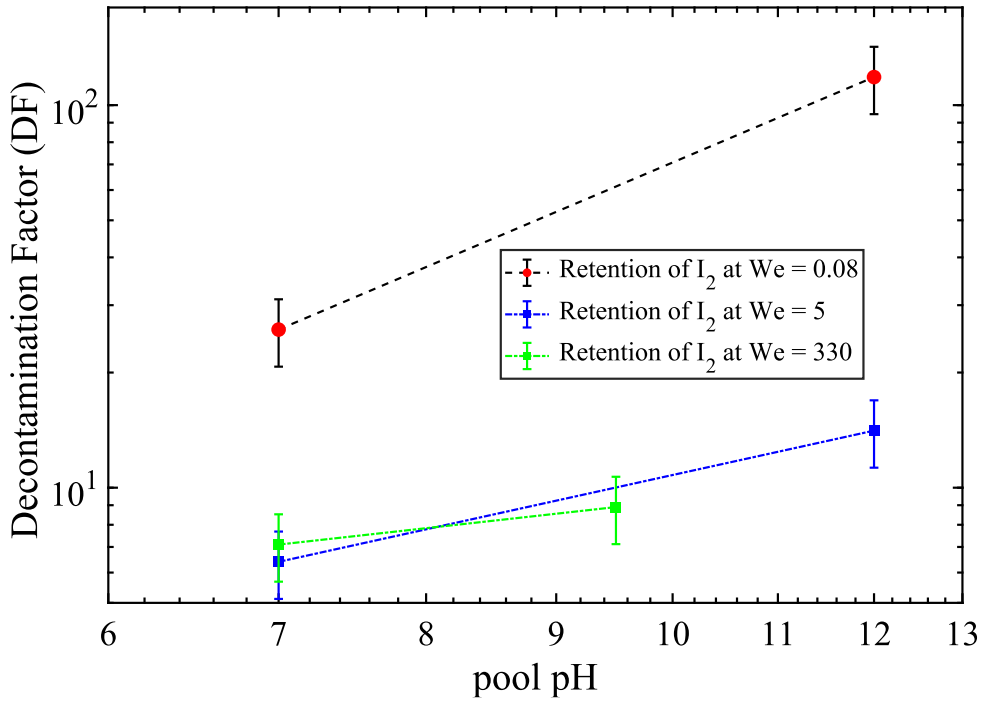

Figure IV.12- Effect of pH on the hydrolysis of I_2 resulting in increasing the DF.

However, in our experiments, we examined the increase of pH from 7 to 12. Indeed, the pH influenced kinetics of mass transfer as shown in Figure IV.12. In addition to hydrolysis, there is the residence time of gas which aid the mass transfer, and this can be shown in Figure IV.12 where the effect of pH is more effective as the Weber number is less. The effect of pool temperature was not examined in I_2, but this investigation was studied with CH_3I experiments.

IV.3.2.2.2. Methyl iodide CH_3I

Generally, kinetics of organic methyl iodide depends strongly on thermal hydraulic conditions [138], of which pool temperature and submergence are considered.
As we consider PIM 1 as the reference test, we showed before that the modification of flow regime has no effect, and that we can assume that no retention of CH_3I occurred. In addition to that, the increase of gas temperature (PIM 4) only has not shown an influence on the DF.

Table IV.10 shows a relative increase of DF > 1.5 as the pool pH and temperature are varied.

According to Wren et al. [139], the rate constant of the reaction can be calculated such that:

$$k_1(T) \approx k_0(T_0).e^{-\frac{E_a}{R}\frac{1}{T}}$$

Where E_a is the activation energy of the element. Therefore, this rate increases significantly with temperature. Then, as pH varies from 12 to 13, the hydrolysis rate increases by a factor of 10 between PIM2 and PIM9. It can be seen that trapping in the liquid phase, which depends on the transfer of matter to the liquid phase and the chemical reaction at the interface, is mainly driven by the transfer of matter, which in turn depends strongly on the partition coefficient.

Regarding the pH, a significant increase is observed between PIM 1, PIM 2, and PIM 9. The hydrolysis of methyl iodide follows the irreversible reaction: $CH_3I + H_2O \rightleftharpoons I^- + CH_3OH + H^+$.

Table IV.10- Investigation of the impact of pool temperature and pH on retention of CH_3I.

Test	Pool pH	Gas temp. (°C)	Pool temp. (°C)	Pool level (cm)	Nozzle size (mm)	Weber	DF
PIM 1	12	25	25	100	20	0.08	1.3
PIM 2	12	70	70	100	20	0.08	2.4
PIM 4	12	70	25	100	5	350	1.2
PIM 5	12	70	70	100	5	350	1.6
PIM 9	13	70	70	100	20	0.08	5.6

Regarding the pool temperature, there are 2 opposite effects, the rate constant of CH_3I decomposition reaction into I^- and CH_3OH that strongly increases with temperature. On the other hand, the partition coefficient of CH_3I decreases with temperature because CH_3I is higher volatile and tends to remain in gas phase at the interface liquid/gas [104]. In our experiments, the pool temperature is shown to promote kinetics, and thus enhance the DF rather than hindering it. In addition to that, imposed temperature gradient as shown in PIC 4 hasn't induce any retention mechanism and transfer of methyl iodide from gaseous to liquid phase, knowing that this effect (thermophoresis) has a significant impact in case of aerosols trapping.

IV.4. Conclusion

Pool scrubbing is a mean of filtration that aims at reducing the release of fission products following a nuclear accident. In FCVS, the discharged gas into liquid pools has the potential to trap released fission products in a pool of water. Complementary techniques are implemented in order to enhance the trapping of organic iodide, which are not sufficiently trapped by pool scrubbing. Based on the iodine species, the trapping efficiency defined by the decontamination factor DF depends on a set of physical and chemical aspects.

In this chapter, we examined the hydrodynamic aspects on the trapping of different iodine species. Experimental work was carried out in the TYFON facility in IRSN Cadarache, which permits to performed decontamination factor measurements. The examined iodine species were CsI in aerosol form, molecular I_2 in gaseous form, and organic CH_3I in gaseous form.

According to the realized experimental work, the following conclusion can be drawn:

- For CsI aerosols, the pool scrubbing efficiency is significant due to the dependence of aerosol removal mechanisms on the hydrodynamic aspects. The countereffects of gas flowrate and nozzle size is characterized by a Weber number, which seems to be efficient in dimensionless analysis of the decontamination factor. Moreover, a minimum of decontamination factor occurs in the transition zone between bubbling and jetting regime, due to the weak sensitivity of aerosol removal mechanisms in this zone. Throughout our examination, we shown the important influence of residence time in bubbling regime, that led to high scrubbing efficiency. On the other hand, the inertial impaction at the jetting regime and increase of interfacial area led to high scrubbing efficiency beyond the transition zone which has shown lower DF.

- In our experiments, where $H_{pool} \leq 1.25$ m, the influence of submergence has been more important in bubbling regime than in case of jetting regime. This due to the fact, that in jetting regime and within this altitude, inertial impaction is the dominant mechanism as the height of pool does not permit the generation and expansion of bubbles swarm with high interfacial area (plume) with tiny bubbles having reached their terminal velocity.

- Regarding the impact of temperature, the same impact of submergence was reported for the dependence of jetting regime experiments on the gradient of temperature (dominance of inertial impaction). Whereas for bubbling regime, and as expected, increase in pool temperature showed a negative effect of decontamination factor, as thermophoresis was hindered for gas flow at ambient temperature.

- For molecular iodine I_2, the countereffect of flow regime on DF was seen to be the same as in CsI aerosols trapping, except that inertial impaction does not exist. Contrary to CsI trapping, the pH has shown an important effect in enhancing the retention due to hydrolysis.

- A weak trapping is shown for CH_3I by pool scrubbing. Moreover, the retention mechanisms of CH_3I by pool scrubbing are not affected by the different flow morphology and regimes. The trapping efficiency increased when the pools' temperature and pH increased, as hydrolysis and decomposition rate of CH_3I seemed to

favor the DF. This suggests that chemical aspects like water chemistry and additives favors the retention of CH_3I, rather than the hydrodynamic aspects.

Chapter V: Modeling Aspects

V.1. Preface

Modelling the pool scrubbing phenomenon and hydrodynamic behavior of gas in pools has been approximated differently in the codes already developed for pool scrubbing simulation. Within this context, an extensive review has been done by Catherine Marchetto [78] to provide and propose models to be validated within the ASTEC code (see I.7.3). This code aims at predicting the Decontamination Factor DF of a water pool for pool scrubbing situations [79], by considering and implementing bubble hydrodynamics models that are needed as parameters for the determination of different trapping and retention mechanisms.

Taking in consideration that this modelling work is under development at IRSN, the experimental work presented in this manuscript will be used for the validation and improving the existing modelling within the aforementioned code. The basis of the bubble hydrodynamic modelling considers dividing the pool in several zones allowing to distinguish the main parameters linked to the bubble behavior. These parameters are notably the volume and surface area of the bubbles (see III.3.3.2 and III.3.3.4), the void fraction of the water pool (see III.3.3.5), and the rising velocity, residence time (see III.3.3.6).

In this chapter, a first attempt of modelling the trapping of aerosols by pool scrubbing is presented. The experimental database established in chapters III and IV will be implemented for determining the decontamination factor, and then an analysis will be provided to compare and draw some conclusions. Table V.1 presents the experimental decontamination factor measurements that we intend to use in order to compare the experimental DF with numerical DF determined by the modelling. In the following paragraph, the overview of the modelling and work, assumptions, and needed parameters will be illustrated.

Table V.1- Experimental tests devoted to compare with modelling work

Test name	Nozzle size (mm)	Flowrate (L/min)	We	Experimental DF (± 9%)
PIC 9	5	77.59	350	14.3
PIC 11	5	9.21	4.93	30.8
PIC 13	5	33.18	64	5.8
PIC 14	5	131.15	1000	25.9
PIC 15	20	73.67	4.93	31.1
PIC 16	20	9.21	0.08	45.7
PIC 17	2	131.04	15600	285.2
PIC 18	2	74.19	5000	62.9
PIC 19	2	33.18	1000	22.2
PIC 20	2	8.40	64	8.4

V.2. Decontamination factor expressions

V.2.1. Overview and assumptions

As we consider in this chapter the modelling of decontamination factor measurements carried out in our experiments, some assumptions are taken for the aerosol removal mechanisms and the hydrodynamic zones.

V.2.1.1. Aerosol removal mechanisms

IRSN has taken the decision to entirely review the pool scrubbing modelling and to develop a new pool scrubbing modelling in the ASTEC code [76, 78, 79]. Currently, the SPARC code [73] (see I.7.1) is integrated in the ASTEC code for determining the DF in the SOPHAEROS module [140]. The latter aims at evaluating the transport and the chemistry of fission products in light water reactor in case of severe accident. The following representation of the aerosol removal mechanisms are developed by Owczarski et al. [73] within the modelling work in the SPARC code .

As presented in the nomenclature, the index b in the following expressions refers to the bubble whether it was in the injection zone or in the bubble rise zone. If the zone is intended to be specified, the indices G and r are used to represent the injection and bubble rise zone respectively as shown in Figure I.4.

According to the different aerosol removal mechanisms presented in I.6.1, we can neglect the effect of steam condensation in the tests presented in Table V.1 with considering the gravitational settling, inertial impaction, diffusion, and centrifugal impaction. Hence, the global decontamination factor can be written as the following:

$$DF_{tot} = \prod_i DF_i = DF_{imp} \times DF_{gs} \times DF_{di} \times DF_{ci} \qquad (40)$$

For decontamination factor by inertial impaction, we have presented and discussed its expression in IV.2.2.1.2 (see eq.(36), eq.(37), and eq.(38)). It is usual in pool scrubbing modelling to assume that the aerosol deposition mechanisms do not evolve significantly with the time and can be described separately by a deposition velocity [73]. In SPARC, the velocity is integrated over the whole bubble surface area and over the residence time in the hydrodynamic zone Δt_{inj} or Δt_{rise}, such that:

$$DF_i = \exp\left[\int_0^{\Delta t_b} \int \frac{U_N}{V_b}\, dS_b\, dt\right] \qquad (41)$$

Where U_N is the net deposition velocity for the different aerosol removal mechanism. This net deposition velocity (U_N) from all forces is the vector sum of the gravitational settling velocity (U_{gs}), Brownian diffusion velocity (U_{di}), and centrifugal deposition velocity (U_{ci}) [73].

For sedimentation or gravitational settling, SPARC code [73] considers this model during injection and during bubble rise, the sedimentation velocity of particles falling freely as a result

of gravitation (assuming spherical particles) force of the aerosol particles. The expression used for the gravitational settling component is the following:

$$DF_{gs} = exp^{\left[\frac{3}{2}(U_a)\times\frac{\Delta t_{res}}{d_b}\right]} \quad (42)$$

Here U_a is the terminal settling velocity of aerosols inside the bubble in the bubble rise zone, resulting from the equilibrium of the gravitational force and the drag force, therefore:

$$U_a = \frac{{d_p}^2 \rho_p \; g \; C_c}{18 \; \mu_g} \quad (43)$$

C_c represents the Cunningham slip correction factor, which is considered close to 1 as aerodynamic diameter of the aerosols is greater than 0.1 µm [98]. As this velocity is directly proportional to squared value of particle diameter, thus, the gravitational sedimentation mechanism is relevant for particles around and larger than 1 μm [73].

The expression used for the Brownian diffusion component in the SPARC code [73] is the following:

$$DF_{di} = exp^{\left[\frac{6\,S_b}{\pi {d_{eq}}^3}\; k_m \; \Delta t_{res}\right]} \quad (44)$$

Here k_m is the mass transfer coefficient from Higbie's penetration theory [141, 142],

$$k_m = 2\sqrt{\frac{U_b \; D_p}{\pi \;\; d_b}} \quad (45)$$

Where D_p is the diffusion coefficient, such that:

$$D_p = \frac{k \; T_{gas}}{3 \; \pi \; d_p \; \mu_g} \quad (46)$$

Where k is the Boltzmann constant and T_{gas} is the bubble temperature, which is at ambient temperature since the experiments presented in Table V.1 are carried out for T_{gas}= 25 °C and T_{pool}= 25 °C.

Here it should be noted that S_b and d_b are respectively the surface area and spherical equivalent diameter of the bubbles. Depending on the hydrodynamic zone these parameters can be either S_G and d_G if the bubbles are in the injection zone or S_r and d_r if the bubbles are in the bubble rise zone. The same for U_b which can be either U_r the terminal velocity in the bubble rise zone, or U_G the globule rising velocity in the injection zone.

The expression used for the centrifugal impaction in the SPARC code [73] component is the following:

$$DF_{ci} = exp^{\left[\frac{6\,S_b}{\pi {d_{eq}}^3} U_d\, t_{res}\right]} \quad (47)$$

Here U_d is the drift velocity caused by the centrifugal force such that:

$$U_d = \frac{(\pi\, U_{rel})^2 U_b}{2\, g\, d_b} \quad (48)$$

Here U_{rel} is the relative velocity between the bubble U_b and the liquid. Besides it is supposed in a first approach that the pool is stagnant and there is no liquid entrainment, thus the relative velocity could be represented by the velocity of the gaseous phase such that $U_{rel} = U_b$.

It is recalled that a part of the bubble parameters such as d_G, S_G, U_G, were determined in this work (see III.3.3), and the rest of the bubble parameters will be determined thanks to adopted models that will be described in V.2.1.2.2.

V.2.1.2. The hydrodynamic zones

Generally, and according to Ramsdale et al. [27, 70] the pool is divided into three hydrodynamic zones such that sum of these zones represent the level of liquid in the pool:

$$H_{pool} = L_{inj} + L_{trans} + L_{rise} \quad (49)$$

In the paragraphs below, the characterization of these zones is reported.

V.2.1.2.1. Expressions and assumptions

It is common through literature that the total decontamination factor can be expressed as the product of decontamination factor of each zone [15, 73]. The transition zone, between the injection zone and the bubble rise zone, is characterized by the globule's disintegration. Whereas, in case of jetting regime the hydrodynamic zones are only the injection and bubble rise zone as the jet breaks up: tiny bubbles are formed directly presenting the bubble swarm. As there is a lack of models in the literature on the transition zone and taking into consideration the lower sensitivity of the transition zone in bubbly regimes, moreover its absence in case of jetting regime, it is not considered as a zone in this study. However, the transition zone is included in the bubble rise zone in case of bubbly regime. Thus, the second expression of global decontamination factor can be written as in eq.(50), and the hydrodynamic zones considered are shown in Figure V.1.

$$DF_{tot} = \prod_i DF_i = DF_{inj} \times DF_{rise} \quad (50)$$

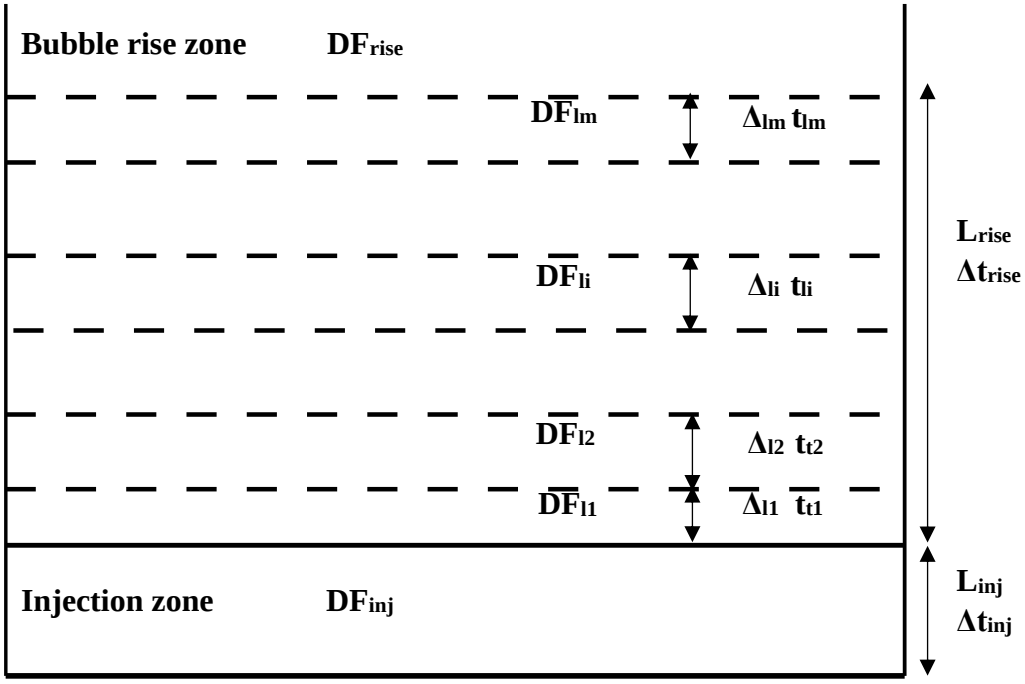

Figure V.1- Hydrodynamic zones considered in the current modelling [78].

It is worth mentioning that each aerosol removal mechanism presented above can be presented as the product of this mechanism in each of the two zones, except for inertial impaction as it only specified near the nozzle. Therefore, these aerosol removal mechanisms can be written as the following:

For gravitational settling (applicable when terminal velocity of aerosol achieved):

$$DF_{gs} = DF_{gs,rise} \tag{51}$$

For Brownian diffusion,

$$DF_{di} = DF_{di,inj} \times DF_{di,rise} \tag{52}$$

For centrifugal impaction

$$DF_{ci} = DF_{ci,inj} \times DF_{ci,rise} \tag{53}$$

In a different way of expression, the decontamination factor in the injection zone and bubble rise zone can be determined as in eq.(54) and eq.(55):

$$DF_{inj} = DF_{di,inj} \times DF_{ci,inj} \tag{54}$$

$$DF_{rise} = DF_{gs,rise} \times DF_{di,rise} \times DF_{ci,rise} \quad (55)$$

V.2.1.2.2. Length of hydrodynamic zones

In the current modelling, two hydrodynamic zones are considered. First, thanks to image processing and tracking the globule formations, the length of the injection zone L_{inj} was determined experimentally as reported in III.4.3. On the other hand, empirical correlations were developed by Tacke al. [143], Iguchi et al. [144], and Castello et al. [145] for the onset of the bubble rise zone. Kubasch et al. [110] investigated these correlations and proposed some correction factors after comparing it the with the experimental measurements such that:

$$\frac{Y_{rise}}{D_0} = 13.2\ Fr_m^{\ 0.23} \quad (56)$$

Where Y_{rise} is the onset of the bubble rise zone (altitude at which this zone starts above injection) and D_0 is the nozzle size, and Fr_m is the modified Froude number such that:

$$Fr_m = \frac{\rho_g\ U_{inj}^{\ 2}}{(\rho_l - \rho_g)\ g\ D_0} \quad (57)$$

The difference between L_{inj} and Y_{rise} is therefore the length of the transition zone, since Kubasch et al. [110] considered the three zones so that Y_{rise} is the transition altitude from transition zone to bubble rise zone. In this modelling, and as we did not characterize the transition zone, but we included it in the bubble rise zone, Y_{rise} is then equivalent to L_{inj}. Kubasch et al. [110] reported that this correlation is valid for $1 < Fr_m < 10^5$, although that the experimental measurements they provided fitted until $Fr_m = 10^{-2}$.

Therefore, the length of the bubble rise zone can be determined such that

$$L_{rise} = H_{pool} - Y_{rise} \quad (58)$$

Where H_{pool} is the submergence of the nozzle in the column, in other words, it is the level of water in the pool. Figure V.2 shows the variation of the bubble rise zone onset Y_{rise} , determined using the correlation of Kubasch et al. [110], as function of injection flowrate Q_{inj}.

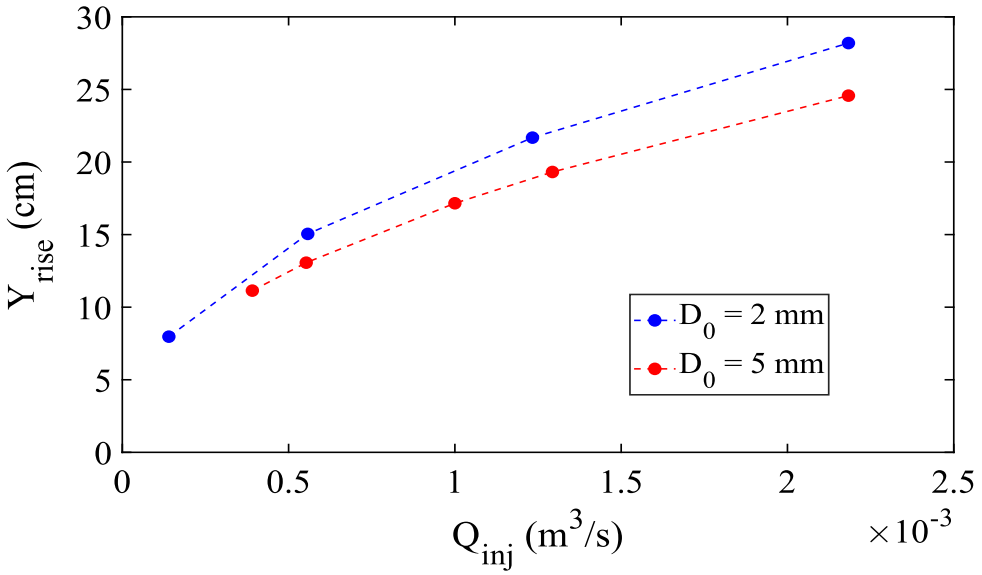

Figure V.2- The onset of the bubble rise zone for different Q_{inj} using the correlation of Kubasch et al. [110], where $Y_{rise} = 13.2\ Fr^{0.23}\ D_0$ as in eq.(56).

V.2.2. Parameters needed

The hydrodynamic measurements carried out throughout this thesis provided the bubble dynamics and parameters needed for the calculation of decontamination factor in the injection zone only as shown in eq.(54).

For the bubble rise zone, models are specified in order to determine the needed parameters for the calculation of the decontamination factor in the bubble rise zone as shown in eq.(55).

In the following paragraphs, the parameters needed for the determination of the global decontamination factor, as depicted in eq.(50), are highlighted.

V.2.2.1. Injection zone

In this zone, as it has been explained before, two types of regimes can take place in the injection zone: the bubbly regime and the jet regime. For bubbly regime, it is required to determine the residence time Δt_{inj}, the final size of the globule (equivalent diameter d_G assuming a spherical shape of bubble volume V_G determined in III.3.3.2, and surface area S_G determined in III.3.3.4) at the detachment stage.

For the jetting regime, instead of that, we will consider only DF by inertial impaction as it dominates over the other mechanisms (Brownian diffusion and centrifugal impaction) in this zone (see Figure IV.7).

V.2.2.1.1. Residence time

The residence time is determined as follows in eq.(59):

$$\Delta t_{inj} = \frac{L_{inj}}{U_G} \quad (59)$$

It is worth mentioning that the length of the injection zone L_{inj}, and the rising velocity U_G in the injection zone (see III.3.3.6) are determined experimentally. Therefore, within this consideration, no models were adopted.

In case of jetting regime, and for deducing the axial coordinate corresponding to the beginning of the bubble rise zone, it is crucial to determine the L_{inj} for the pulsating jet. Berna et al. [67] proposed a model for the jet penetration length L_{jet}, which is equivalent to the distance from the nozzle exit to the point at which the gas jet extinguishes and the bubble rise zone begins. The equation eq.(60) is defined as:

$$\frac{L_{jet}}{D_0} = 10.7\, Fr^{0.46} \left(\frac{\rho_g}{\rho_l}\right)^{0.35} \quad (60)$$

Where D_0 is the nozzle diameter and Fr is the Froude number.

V.2.2.2. Bubble rise zone

V.2.2.2.1. Residence time

Generally, for each mesh of this zone (see Figure V.1), the residence time Δt_i, the bubble terminal velocity, the void fraction, and the bubble surface and volume have to be evaluated.

Δt_{rise} can be determined as function of the length of the rising zone and the terminal velocity of the bubble in the bubble rise zone U_r, such that

$$\Delta t_{rise} = \frac{L_{rise}}{U_r} \quad (61)$$

Knowing that the length of this zone is characterized as mentioned in V.2.1.2.2.

V.2.2.2.2. Bubble diameter

In some experiments dedicated to the pool scrubbing [146], the bubble size distribution in the bubble rise zone is given by a log-normal distribution with the following probability density function in each mesh of this zone, as follows:

$$f(d_r) = \frac{1}{d_r} \frac{1}{\sqrt{2\pi}\ln(\sigma_g)} \exp\left(-\frac{ln^2\left(\frac{d_r}{d_{gm}}\right)}{2\, ln^2(\sigma_g)}\right) \quad (62)$$

Where d_r is the bubble diameter in the bubble rise zone and σ_g and d_{gm} are respectively the standard deviation and the geometrical bubble diameter, which are the parameters of the log-normal probability density function. A correlation is provided by Seinfeld et al. [147] to correlate the mean diameter d_m to the geometrical bubble diameter, as follows:

$$d_{gm} = d_m \exp\left(-\frac{\ln(\sigma_g)^2}{2}\right) \quad (63)$$

V.2.2.2.3. Surface area and void fraction

In order to evaluate the surface of the bubbles in the bubble rise zone, the shape of the bubbles has to be determined. In this study, we considered that the shape of bubbles is spherical, so the surface area can be defined such that:

$$S_r = \pi {d_r}^2 \quad (64)$$

The number of the bubbles in the bubble rise zone can be determined by considering the pool void fraction and the volume of one bubble. For the void fraction, two correlations are implemented and considered, first is the radial void fraction profile developed by Castillejos et al. [111] in eq.(20). The second deals with the centerline void fraction profile along the axial distance Y, developed by Kubasch et al. [110] such that:

$$\varepsilon_g(Y) = 4.9\, {Fr_m}^{0.26} \left(\frac{Y}{D_0}\right) \quad (65)$$

Knowing that the volume of the bubble rise zone, as we know L_{rise} and the diameter of the Column (500 mm), then the gaseous volume in the bubble rise zone is given by:

$$V_{g,rise\ zone} = \left(\frac{\varepsilon_g}{1-\varepsilon_g}\right) V_{bubble\ rise\ zone} \quad (66)$$

Then the number of bubbles in the bubble rise zone N_{rise} can be expressed as:

$$N_{rise} = \frac{V_{g,rise\ zone}}{V_r} = \frac{6\, V_{g,rise\ zone}}{\pi\, {d_r}^3} \quad (67)$$

Where V_r and d_r are respectively the bubble volume and diameter in the bubble rise zone (I.5.1).

By substitution eq.(64) and eq.(67), we can get

$$S_{g,rise\ zone} = N_{rise}\, S_r = \frac{6\, V_{g,rise\ zone}}{d_r} \quad (68)$$

V.2.2.2.4. Interfacial area

The average interfacial area in the bubble rise zone can be estimated as indicated in eq.(2) such that:

$$a_{average\ (bubble\ rise\ zone)} = \frac{S_r\, \varepsilon_g}{V_r} = \frac{6\, \varepsilon_g}{d_r} \quad (69)$$

V.2.2.2.5. Bubble terminal velocity

Rodrigue et al. [148, 149] have carried out an extensive review on the bubble motion and, consequently have developed a correlation to determine the bubble velocities as a function of their diameters. The following expressions were derived for expressing the terminal velocity U_r:

$$U_r = V\left(\frac{{\rho_{liq}}^2 {d_b}^2}{\sigma\mu_{liq}}\right)^{-1/3} \quad (70)$$

Where

$$V = \frac{F}{12}\frac{(1 + 1.31 \times 10^{-5} \times {M_o}^{11/20} \times F^{73/33})^{21/176}}{(1 + 0.02F^{10/11})^{10/11}} \quad (71)$$

and

$$F = g\left(\frac{{\rho_{liq}}^2 {d_b}^8}{\sigma {\mu_{liq}}^4}\right)^{1/3} \quad (72)$$

F and V are respectively the flow number and the velocity numbers, introduced by Rodrigue et al. [148, 149] such that $F = E_o\,(\frac{Re}{Ca})^{2/3}$, Mo Morton number such that Mo = $\frac{g\,\mu_l}{\rho_l\,\sigma^3}$, and $V=(Re^2\,Ca)^{1/3}$ where Ca is the capillary number $Ca = \frac{\mu U_b}{\sigma}$.

V.3. Analysis and comparison with experimental database

In the section V.2.2, the parameters needed for the determination of aerosol removal mechanisms in the two hydrodynamic zones, as specified in eq.(54) and eq.(55), are presented. The inertial impaction is only considered in the jetting regime and not in the bubbly regime.

For each configuration, the decontamination factor in the injection and bubble rise zone is determined. Then the total modelled DF_m is calculated upon the product of the two aforementioned DF. Table V.2 presents the values of determined decontamination factors, and Figure V.3 shows the influence of both Q_{inj} and D_0 on the decontamination factor.

Table V.2- Comparison between global experimental DF, modelled DF_{inj}, modelled DF_{rise}, and global modelled DF for different experimental configurations.

Test name	Nozzle size (mm)	Flowrate (L/min)	We	Experimental DF (± 9%)	DF_{inj}	DF_{rise}	Model DF_m
PIC 9	5	77.59	350	14.3	5.8	20.7	120
PIC 11	5	9.21	4.93	30.8	3.9	15.6	61
PIC 13	5	33.18	64	5.8	4.3	16.2	70
PIC 14	5	131.15	1000	25.9	7.7	19.4	150
PIC 15	20	73.67	4.93	31.1	5.9	26.1	155
PIC 16	20	9.21	0.08	45.7	4.1	25.3	103
PIC 17	2	131.04	15600	285.2	216.8	2.2	477
PIC 18	2	74.19	5000	62.9	95.4	2.3	213
PIC 19	2	33.18	1000	22.2	15.4	4.1	63
PIC 20	2	8.40	64	8.4	3.3	7.7	25

Different observations can be seen in Table V.2 and Figure V.3:

- The divergence between calculated and experimental decontamination factors for all the configurations: modelled DF is systematically greater than the experimental DF.

- A different trend is shown in calculated DF with the variation of flow regimes, shown in IV.2.2.1.2. The calculated decontamination factor increased with the increasing of injection flowrate. This owes for the implication of higher deposition velocity, which increases with the increase of the injection flowrate.

- For bubbly regimes and owing to the difference between the length of the bubble rise zone and that of the injection zone ($L_{rise} >> L_{inj}$), the discrepancy of the contribution to

the decontamination factor of the zones is obvious. The majority of the scrubbing occurred in the bubble rise zone, where the residence time is much greater.

- For jetting regime, it is shown the that major scrubbing and trapping of aerosols occurred in the injection zone. This finding consolidates the experimental results presented in IV.2.2.1.2, especially in Figure IV.7.

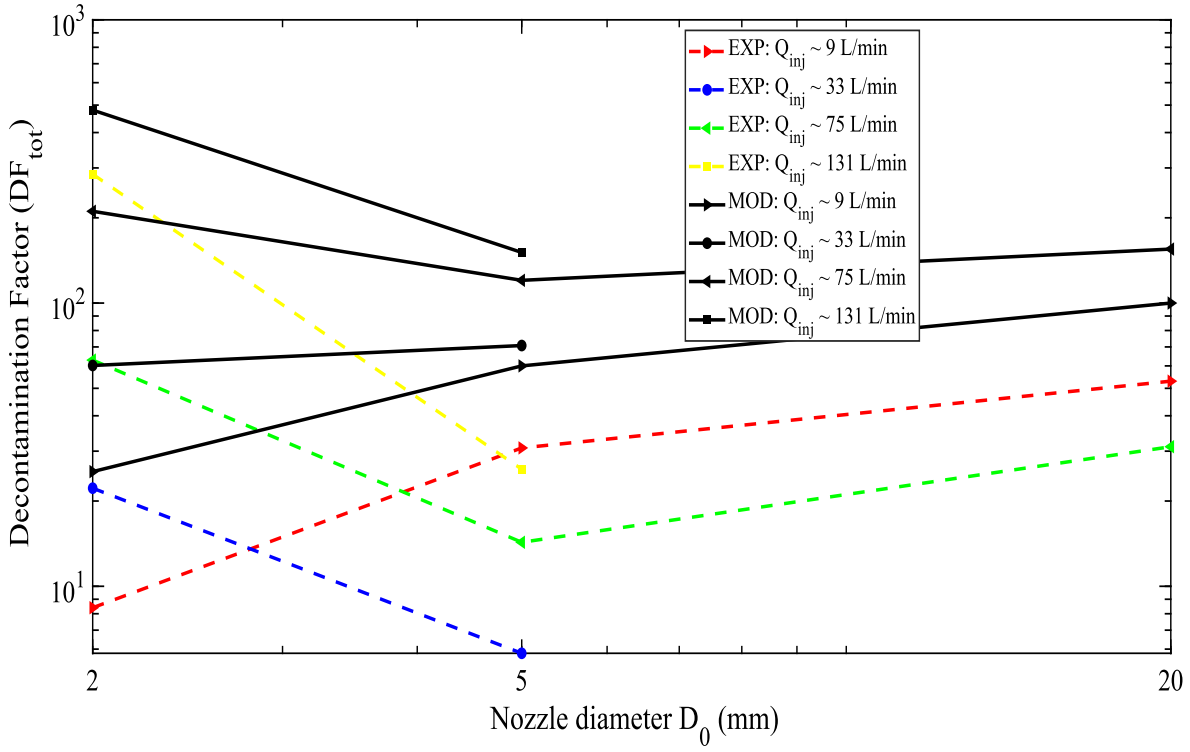

Figure V.3- The impact of injection flowrate and nozzle size on the modelled decontamination factor DF_m.

V.4. Conclusion

The results obtained with the application models overestimate the experimental decontamination factor measurements realized on the TYFON facility. The numerical quantification of aerosol removal mechanisms provided larger values of the DF, and this might stem from different reasons.

We considered that there is weak contribution of the transition zone to the scrubbing efficiency. Some analysis work performed by Lee et al. [103] reported that decontamination factors in the transition zone are not negligible. However, they also reported a higher contribution of the bubble rise zone than that of the transition zone. In our study, the transition zone is considered implied within the bubble rise zone, and we applied the mechanisms corresponding to the latter zone with neglecting the length of transition zone. Moreover, the correlation of Kubasch et al. [110] seemed not so consistent with our experimental observations of the length of the injection zone. Table V.3 shows the overlapping between the injection zone determined experimentally and the bubble rise zone determined numerically $L_{inj} > Y_{rise}$, where L_{inj} is the length of the injection zone from the tip of nozzle and Y_{rise} is the altitude where the bubble rise zone begins. This overlap leads to higher contribution of bubble rise zone, more residence time, and therefore higher scrubbing efficiency.

Table V.3- Comparison between the experimental length of the injection zone and the onset of bubble rise zone determined numerically, for experiments with submergence H_{pool} = 1m.

Test name	D_0 (mm)	Q_{inj} (L/min)	We	Experimental DF (± 9%)	Experimental L_{inj} (cm)	Model Y_{rise} (cm) [110]	Model DF
PIC 11	5	9.21	4.93	30.8	10	7	61
PIC 15	20	73.67	4.93	31.1	20	15	155
PIC 16	20	9.21	0.08	45.7	9	6	103
PIC 20	2	8.40	64	8.4	17	8	25

On the other side, it is worth mentioning that most of hydrodynamic formulations are correlations and, hence, their validity extends only over the range of conditions encompassed by the data they were based on. Through the majority of experimental studies, the developed correlations were obtained out of the nuclear safety field, therefore their applicability is sometimes questionable for our device. On the other side, some hydrodynamic phenomena potentially relevant for pool scrubbing are poorly characterized, since there are very rare experimental data corresponding for them, such as the chaotic behavior of bubbles, which occurs at high gas flowrates, non-spherical shape of bubbles, and multiple coalescence that could occur in the bubble rise zone. This encourages the development of coupled hydrodynamics and chemical models, relevant to pool scrubbing, that contribute to accurate determination of decontamination factor DF.

General conclusion

The featuring of nuclear power plants with accident management systems aims mainly at mitigation and reducing the release of fission products into the environment. Mitigation, hence, refers for all processes that may lead to the trapping and retention of containment atmosphere, thus, reducing the potential risks of radioactive material release into the environment. Efficient engineering systems for fission products retention are containment sprays, suppression pools in boiling water reactors, and filtered containment venting systems FCVS in pressurized water reactor. The efficiency of these systems is expressed in terms of Decontamination Factor DF, which is defined as the ratio of the quantity of fission products at the inlet to the outlet of the filtration system. Therefore, the retention process of radioactive substance is a serious concern in the evaluations of the source term and the post-management of the accident. This concerns notably pool scrubbing, occurring in wet filtered containment venting systems, and also encountered following the steam generator tube rupture, where fission products could be directly released outside.

Pool scrubbing refers to the mechanisms which lead to the retention of radioactive fission products, in the aerosol form and in the gaseous form, from being carried into the containment atmosphere or to the environment. The injection of the carrier gas through the pool leads to the formation of bubbles and, during their rise along the pool, fission products can reach the bubble surface due to aerosol deposition mechanisms and mass transfers for gaseous species and then, are trapped in water. Aerosol deposition will occur due to different mechanisms such as Brownian diffusion, thermophoresis, diffusiophoresis, inertial and centrifugal impaction, condensation, electrophoresis, and sedimentation (gravitational settling). Among these mechanisms, each one has its own significant impact considering the hydrodynamics' aspects of the accident. In fact, the retention of aerosols is mainly based on the physical behavior of the gas flow in the liquid, considering the present interactions and phenomena. As a consequence, the hydrodynamics aspects are highly regarded in contributing to the efficiency of decontamination factor in pool scrubbing.

Throughout this thesis, two experimental campaigns were carried out, one at IUSTI-Marseille mainly for developing the hydrodynamic methods, and other at IRSN-Cadarache. The facility at Cadarache, named TYFON, was built during the thesis and it is dedicated to the examination of the pool scrubbing phenomenon. TYFON is designed to afford coupling of hydrodynamic and Decontamination Factor measurements, therefore, permitting the investigation of hydrodynamic aspects on the trapping and retention of different forms of iodine compounds (gaseous methyl iodide CH_3I, gaseous molecular iodine I_2, and caesium iodide aerosols CsI).

Concerning the hydrodynamics, flow structure in pool scrubbing conditions, where for example air is injected at high momentum, exhibits different patterns than in conventional experiments. That recalls for approaches that better describe the bubble hydrodynamics besides the different phenomena. Based on the different bubble's morphologies that have been observed, we first investigated the bubble-bubble interactions and then classified different bubbling regimes depending on the position of coalescence. The biggest bubble formed above the nozzle, after

the coalescence of bubbles, is referred by a globule. On the basis of the morphological description of bubbles throughout our experiments, two approaches in characterizing the bubbles sizes are investigated. The first conventional approach is based on the same assumptions than most of literature models, where the single bubbling regime and spherical shape of bubbles are assumed. The comparison of characteristic bubble size, which is computed after determining the bubble departure frequency, shows a good agreement with literature models. However, this approach is not consistent with flow morphology experimentally observed. Therefore, and through a proposed phenomenological approach, we aimed to characterize experimentally the globules size. First, the globule frequency by tracking the globules formation through image processing is quantified. Then its volume is computed by reconstructing the shape of bubbles based on axisymmetric assumption. The globule sizes are found to be generally larger than sizes determined by the classical approach, showing a weak applicability of literature models to predict bubbles size at high Weber number in the injection zone of such flows. This phenomenological approach is validated by comparing experimental flowrate to the real injected flowrate, which are consistent. This disparity between phenomenological investigation and conventional approach is relevant for industrial applications, where air is often injected at high flowrates. In this paper, awareness is raised in modelling of such applications regarding the precision of dynamics quantification, notably mass transfer mechanisms.

Different investigations were carried out to study the impact of pool scrubbing conditions such as the nozzle size, contamination of carrier gas, pool submergence on the bubble dynamics. Comparable globule volumes and frequencies were reported for the small nozzle, where globule volume increases with the injection flowrate. For the large nozzle size, the increase formation time results in a larger globule volume and smaller globule frequency. Regardless of the Weber number, the presence of CH_3I or CsI aerosols in the composition of the carrier gas has no influence on the globule dynamics, neither globules volume nor their frequency. It is suggested that the carrier gas composition is not affecting its surface tension properties, due to the low concentration of compounds in the gas flow. Regarding the pool submergence, negligible influence on globule volume was reported where experiments were carried at constant flow and pressure conditions. The dominant mechanisms, such as inertial forces due to gas momentum, in the injection zone near the nozzle attenuate the effect of hydrostatic pressure and surface tension forces induced by the pool submergence.

Dimensionless analysis approaches were provided in an attempt to describe the globule dynamics in the injection zone by introducing the Froude number, which has a shown a good estimation of globule volumes.

On the other hand, decontamination factor measurements were performed on TYFON facility to investigate the hydrodynamic aspects on the trapping of different iodine species. The examined iodine species were CsI in form of aerosols, molecular I_2 in gaseous form, and organic CH_3I in gaseous form. The influence of pH, pool temperature, submergence, and temperature of inlet gas, gas flowrate, nozzle size on DF of the latter iodine compounds was investigated.

For caesium iodide aerosols, the pool scrubbing efficiency reported to be significant due to the dependence of aerosol removal mechanisms on the hydrodynamic aspects. The countereffects of gas flowrate and nozzle size were characterized by a Weber number, which is used to classify the flow regimes. This approach seems to be efficient and consistent in dimensionless analysis of the decontamination factor, when compared to different experimental works. The impact of

injection flow rate Q_{inj} and nozzle size D_0 can induce countereffects, favoring and hindering the retention of aerosols by pool scrubbing. However, the sense of their impact depends on the examined flow regime. As the change of these two parameters tends the flow toward the transition regime, then, this would lead to unfavorable impact and vice versa. A minimum of decontamination factor is observed in the transition zone between bubbly and jetting regime, due to the weak sensitivity of aerosol removal mechanisms in this zone, mainly explained by low residence time and absence of inertial impaction. Throughout our examination, we have shown the important influence of residence time in bubbly regime, that led to high scrubbing efficiency. On the other hand, the inertial impaction at the jetting regime and increase of interfacial area led to high and increasing scrubbing efficiency beyond the transition zone. The pool submergence has been more important in bubbly regime than in case of jetting regime. This due to the fact, larger submergence induces higher residence, whereas in jetting regime, inertial impaction is the dominant mechanism as the height of pool does not permit the generation and expansion of bubbles swarm with tiny bubbles.

For molecular iodine I_2, the countereffect of flow regime on DF was seen to be the same as in CsI aerosols trapping, except that inertial impaction does not exist. Contrary to CsI trapping, the pH has shown an important effect in enhancing the retention due to hydrolysis. On the other hand, a weak trapping is shown for CH_3I by pool scrubbing. Moreover, the retention mechanisms of CH_3I by pool scrubbing was shown to be not affected by the different flow morphology and regimes. Instead, the trapping efficiency was found to be dependent of pool temperature and pH due to the impact of hydrolysis and decomposition of CH_3I.

Regarding the modelling of pool scrubbing, it is worth mentioning that the reliance on correlations, which were developed in the scope of different aspects than pool scrubbing, is questionable. Therefore, it is suggested that there should be development of coupled hydrodynamics and chemical models, relevant to pool scrubbing and based on such experiments, in order to contribute to accurate and better determination of decontamination factor DF and the estimation of pool scrubbing efficiency for different experimental configuration. As this thesis aimed at establishing experimental databases in order to compare with the output of models implemented in the ASTEC code such as the bubble final size, velocity, length of injection zone. In future, and upon the comparison and validation of implemented models, improvements for the modelling of bubble hydrodynamics and thermal hydraulics are expected.

On the other side, further experimental work is going to focus on more complex chemical composition of the liquid pool, which can be a saline aqueous solution in several scenarios of interest for nuclear safety: sea water, pool water contaminated…. Besides, among all the Small Modular Reactors (SMR) projects considered, SMR using light water as coolant will inevitably induce in the next years many reflexions with accidental scenario involving pool scrubbing phenomena.

References

1. Sehgal, B.R., *Nuclear safety in light water reactors: severe accident phenomenology*2011: Academic Press.

2. Jacquemain, D., et al., *OECD/NEA/CSNI status report on filtered containment venting*, 2014, Organisation for Economic Co-Operation and Development.

3. Jacquemain, D., et al., *Nuclear power reactor core melt accidents. Current State of Knowledge.* 2015.

4. Commission, N.R., *Technical bases for estimating fission product behavior during LWR accidents. Technical report*, 1981, Nuclear Regulatory Commission.

5. Commission, C.N.S., *International Nuclear and Radiological Event Scale.* 2014.

6. Steinhauser, G., A. Brandl, and T.E. Johnson, *Comparison of the Chernobyl and Fukushima nuclear accidents: a review of the environmental impacts.* Science of the total environment, 2014. **470**: p. 800-817.

7. Beahm, E., et al., *Iodine chemical forms in LWR severe accidents. Final report*, 1992, Nuclear Regulatory Commission, Washington, DC (United States). Div. of ….

8. Ducros, G., Y. Pontillon, and P. Malgouyres, *Synthesis of the VERCORS experimental programme: separate-effect experiments on fission product release, in support of the PHEBUS-FP programme.* Annals of Nuclear Energy, 2013. **61**: p. 75-87.

9. Ohnet, M., et al., *CHIP programme strategy Technical Report*, 2004, Cadarache.

10. Cantrel, L., et al., *Research Works on Iodine and Ruthenium Behavior in Severe Accident Conditions.* Journal of Nuclear Engineering and Radiation Science, 2018. **4**(2).

11. Grégoire, A.-C. and T. Haste, *Material release from the bundle in Phébus FP.* Annals of Nuclear Energy, 2013. **61**: p. 63-74.

12. Grégoire, A.-C. *Main Outcomes of the IRSN experimental ISTP-CHIP and CHIP+ Programs*. in *27th Int. Conf. Nucl. Energy New Eur. Sept. 10-13*. 2018.

13. Jacquemain, D., et al. *Conclusion of the International OECD/NEA-NUGENIA Iodine Workshop*. in *11th International Topical Meeting on Nuclear Reactor Thermal Hydraulics, Operation and Safety, NUTHOS-11*. 2016.

14. Allelein, H.-J., et al., *State of the art report on nuclear aerosols.* Organ. Econ. Coop. Dev. Nucl. Energy Agency, 2009.

15. Swiderska-kowalczyk, M., et al., *State-of-the-art review on fission product aerosol pool scrubbing under severe accident conditions*, 1996, Institute of Nuclear Chemistry and Technology: Poland. p. 48.

16. Albiol, T., et al., *Main results of the European PASSAM project on severe accident source term mitigation.* Annals of Nuclear Energy, 2018. **116**: p. 42-56.

17. Dong, S. and J. Yang, *Overview of the experimental studies and numerical simulations on the filtered containment venting systems with wet scrubbers.* Annals of Nuclear Energy, 2019. **132**: p. 461-485.

18. Van Dorsselaere, J.-P., et al., *Safety assessments and severe accidents, impact of external events on nuclear power plants and on mitigation strategies.* EPJ Nuclear Sciences & Technologies, 2020. **6**: p. 39.

19. Leroy, O. and C. Monsanglant-Louvet, *Trapping measurements of volatile iodine by sand bed and metallic filters.* Journal of Radioanalytical and Nuclear Chemistry, 2019. **322**(2): p. 913-922.

20. Cantrel, L., *Radiochimie Des Produits de Fission Dans Un Réacteur Nucléaire À Eau Pressurisée en Cas D'accident Grave*, 2012.

21. MacDonald, P., et al., *Steam generator tube failures*, 1996, Nuclear Regulatory Commission.

22. Auvinen, A., et al., *Steam generator tube rupture (SGTR) scenarios.* Nuclear engineering and design, 2005. **235**(2-4): p. 457-472.

23. Cartonnet, A., *Contribution à l'étude du rejet à l'environnement de l'iode radioactif lors d'une séquence accidentelle de type RTGV*, 2013, Thesis, Cadarache (Bouches-du-Rhône).

24. López Del Prá, C., *A Theoretical Investigation of Aerosol Retention within the Secondary Side of a Steam Generator under a SGTR Severe Accident Sequence in a PWR Nuclear Power Plant*, 2012, Universitat Politècnica de València.

25. Betschart, T.T., *Two-phase flow investigations in large diameter channels and tube bundles*, 2015, ETH Zurich.

26. Jacquemain, D., et al., *Summary of OECD/NEA status report on filtered containment venting*, 2015, Atomic Energy of Canada Limited.

27. Ramsdale, S., et al., *Status of research and modelling of water-pool scrubbing.* 1992.

28. Cunnane, J., M. Kuhlman, and R. Oehlberg, *Scrubbing of fission product aerosols in LWR water pools under severe accident conditions-experimental results*, 1985.

29. McCormack, J., D. Dickinson, and R. Allemann, *Experimental results of ACE vent filtration.* Pool Scrubber Tests AA1-AA4 and DOP1-DOP5 (No. ACETR-A1), 1989.

30. Marcos, M., et al., *Lace-Espana experimental programme on the retention of aerosols in water pools.* 1994.

31. Hashimoto, K., K. Soda, and S. Uno. *High Pressure Pool Scrubbing for a PWR SEvere Accident*. in *ANS Thermal Reactor Safety Meeting, Portland, USA*. 1991.

32. Hashimoto, K., et al., *Effect of pool scrubbing of insoluble aerosol in two phase flow in a pipe*, in *Severe accidents in nuclear power plants*1988.

33. HILLARY, J., et al., *Iodine removal by a scale model of the SGHW reactor vented steam suppression system.* No. TRG Report, 1966. **1256**.

34. Güntay, S., *Experiment poseidon: Elemental iodine retention in water pools.* Transactions of the American Nuclear Society;(USA), 1990. **62**(CONF-901101-).

35. Council, N.R., *Lessons learned from the Fukushima nuclear accident for improving safety of US nuclear plants*2014.

36. Dehbi, A., D. Suckow, and S. Guentay, *Aerosol retention in low-subcooling pools under realistic accident conditions.* Nuclear Engineering and Design, 2001. **203**(2-3): p. 229-241.

37. Gupta, S., L. Herranz, and J. Van Dorsselaere. *Integration of pool scrubbing research to enhance source-term calculations (IPRESCA).* in *8th european review meeting on severe accident research*. 2017.

38. TURNI, M., *Experimental study and modeling of a pool scrubbing system for aerosol removal.* 2016.

39. Lopez, C. and L.E. Herranz, *ARI3SG: Aerosol retention in the secondary side of a steam generator. Part II: Model validation and uncertainty analysis.* Nuclear engineering and design, 2012. **248**: p. 282-292.

40. Herranz, L.E., C. Lopez, and J. Penalva, *Investigation on jet scrubbing in nuclear reactor accidents: From experimental data to an empirical correlation.* Progress in Nuclear Energy, 2018. **107**: p. 72-82.

41. Betschart, T., T. Lind, and H.-M. Prasser, *Investigation of two-phase flow hydrodynamics under SGTR severe accident conditions.* Nuclear engineering and design, 2020. **366**: p. 110768.

42. Beghi, I., T. Lind, and H.-M. Prasser, *Experimental studies on retention of iodine in a wet scrubber.* Nuclear engineering and design, 2018. **326**: p. 234-243.

43. Kim, Y.H., J. Yoon, and Y.H. Jeong, *Experimental study of the nozzle size effect on aerosol removal by pool scrubbing.* Nuclear engineering and design, 2021. **385**: p. 111544.

44. Yoon, J., Y.H. Kim, and Y.H. Jeong, *Observation of the jet transition at a single vertical nozzle under pool scrubbing conditions.* Annals of Nuclear Energy, 2022. **171**: p. 109041.

45. Choi, Y.J., et al., *Experimental investigation on bubble behaviors in a water pool using the venturi scrubbing nozzle.* Nuclear Engineering and Technology, 2021. **53**(6): p. 1756-1768.

46. Kim, S.I., et al., *Introduction of filtered containment venting system experimental facility in KAERI and results of aerosol test.* Nuclear engineering and design, 2018. **326**: p. 344-353.

47. Jung, W.Y., et al., *Experimental study of pool scrubbing under horizontal gas injection.* Annals of Nuclear Energy, 2022. **171**: p. 109014.

48. Vennemann, R., M. Klauck, and H.-J. Allelein, *Experimental Investigation on the Retention of Soluble Particles by Pool Scrubbing.* Journal of Nuclear Engineering and Radiation Science, 2022. **8**(4).

49. Li, Y., L. Tong, and X. Cao, *Experimental Study on Influencing Factors of Aerosol Retention by Pool Scrubbing.* Frontiers in Energy Research, 2021. **9**.

50. Gupta, S., et al., *Experimental investigations on fission-product retention and hydrogen mitigation for design-basis and severe accidents in the containment - THAI-VI Final report*, 2019: Germany.

51. Abe, Y., et al., *Bubble dynamics with aerosol during pool scrubbing.* Nuclear engineering and design, 2018. **337**: p. 96-107.

52. Li, Y., et al., *Deposition characteristic of micro-nano soluble aerosol under bubble scrubbing condition.* Annals of Nuclear Energy, 2019. **133**: p. 881-888.

53. Zablackaite, G., H. Nagasaka, and H. Kikura, *Experimental study on bubble parameters for pool scrubbing models under wetwell venting conditions.* Journal of Nuclear Science and Technology, 2020. **57**(7): p. 766-781.

54. Xu, Y., et al., *Experimental study on aerosol behavior in water pool scrubbing under severe accident conditions.* International Journal of Advanced Nuclear Reactor Design and Technology, 2020. **2**: p. 111-116.

55. Lee, J., et al., *Experimental study on aerosol scrubbing efficiency of self-priming venturi scrubber submerged in water pool.* Annals of Nuclear Energy, 2018. **114**: p. 571-585.

56. Sun, H., et al., *Experimental Investigation of Decontamination Factor Dependence on Aerosol Concentration in Pool Scrubbing.* Science and Technology of Nuclear Installations, 2019. **2019**: p. 1743982.

57. Diao, H., et al., *Experimental study on the scrubbing efficiency of aerosols contained in horizontal and vertically downward submerged gas jet.* Progress in Nuclear Energy, 2020. **126**: p. 103406.

58. Clift, R., J.R. Grace, and M.E. Weber, *Bubbles, Drops, and Particles*2005: Dover Publications.

59. Gaddis, E. and A. Vogelpohl, *Bubble formation in quiescent liquids under constant flow conditions.* Chemical Engineering Science, 1986. **41**(1): p. 97-105.

60. Zhao, Y.-F. and G.A. Irons, *The breakup of bubbles into jets during submerged gas injection.* Metallurgical Transactions B, 1990. **21**(6): p. 997-1003.

61. Leibson, I., et al., *Rate of flow and mechanics of bubble formation from single submerged orifices. I. Rate of flow studies.* AIChE Journal, 1956. **2**(3): p. 296-300.

62. Hoefele, E. and J. Brimacombe, *Flow regimes in submerged gas injection.* Metallurgical Transactions B, 1979. **10**(4): p. 631-648.

63. Kyriakides, N.K., et al., *Bubbling from nozzles submerged in water: Transitions between bubbling regimes.* The Canadian Journal of Chemical Engineering, 1997. **75**(4): p. 684-691.

64. Cai, Q., et al., *A simple method for identifying bubbling/jetting regimes transition from large submerged orifices using electrical capacitance tomography (ECT).* The Canadian Journal of Chemical Engineering, 2010. **88**(3): p. 340-349.

65. Badam, V.K., V. Buwa, and F. Durst, *Experimental Investigations of Regimes of Bubble Formation on Submerged Orifices Under Constant Flow Condition.* The Canadian Journal of Chemical Engineering, 2007. **85**(3): p. 257-267.

66. Hur, Y.G., et al., *Origin of regime transition to turbulent flow in bubble column: Orifice- and column-induced transitions.* International journal of multiphase flow, 2013. **50**: p. 89-97.

67. Berna, C., et al., *Enhancement of the SPARC90 code to pool scrubbing events under jet injection regime.* Nuclear engineering and design, 2016. **300**: p. 563-577.

68. Rýdl, A., L. Fernandez-Moguel, and T. Lind, *Modeling of Aerosol Fission Product Scrubbing in Experiments and in Integral Severe Accident Scenarios.* Nuclear Technology, 2019. **205**(5): p. 655-670.

69. Wassel, A.T., M. S. Hoseyni, J. L. Farr Jr, D. C. Bugby, and A. F. Mills, *SUPRA: Suppression Pool Retention Analysis Computer Code*, in *Report EPRI NP-7518-CCML*1991.

70. "Ramsdale, S.A., S. "Guentay, and H.G. "Friederichs, *BUSCA-JUN91. Reference manual for the calculation of radionuclide scrubbing in water pools*, 1995, ; Gesellschaft fuer Anlagen- und Reaktorsicherheit (GRS) mbH, Koeln (Gemany): Germany. p. Medium: P; Size: 64 p.

71. Calvo, M., S. Guntay, and S.A. Ramsdale, *Development and validation of BUSCA code: a modelto assess the aerosol and fission product retention in a water pool.* Journal of Aerosol Science, 1991. **22**: p. S765-S768.

72. "Polo, J., et al., *Removal of volatile iodine from gas bubbles rising in water pools: review and assessment of pool scrubbing codes*, 1996, ; Paul Scherrer Inst. (PSI), Villigen (Switzerland): Switzerland. p. Medium: ED; Size: pp. 665-681.

73. Owczarski, P.C. and K.W. Burk, *SPARC-90: A code for calculating fission product capture in suppression pools*, 1991: United States. p. Medium: ED; Size: Pages: (81 p).

74. Gauntt, R., et al., *MELCOR computer code manuals.* Sandia National Laboratories, NUREG/CR, 2000. **6119**.

75. van Dorsselaere, J.P., et al., *The ASTEC Integral Code for Severe Accident Simulation.* Nuclear Technology, 2009. **165**(3): p. 293-307.

76. Chatelard, P., et al., *Main modelling features of the ASTEC V2.1 major version.* Annals of Nuclear Energy, 2016. **93**: p. 83-93.

77. Gouëllo, M., et al., *Interaction between caesium iodide particles and gaseous boric acid in a flowing system through a thermal gradient tube (1030 K–450 K) and analysis with ASTEC/SOPHAEROS.* Progress in Nuclear Energy, 2021. **138**: p. 103818.

78. C.Marchetto, *Pool scrubbing modelling in ASTEC V2.1 Part I : bubble hydrodynamics*, in *Rapport no PSN-RES/SAG/2017-00318 indice 1*2017.

79. C.Marchetto, *Pool scrubbing modelling in ASTEC Part II : Heat exchanges and phase change processes between the bubbles and the water pool*, in *Rapport no PSN-RES/SAG/2018-00191 indice 1*2018.

80. FARHAT, M., *Bibliographical study on pool scrubbing.*, in *Rapport IRSN/2020-00557,*2020.

81. FARHAT, M., *Etude expérimentale de l'hydrodynamique du barbotage pour différents régimes: application au piégeage des iodes. Rapport d'avancement de première année de thèse*, in *Rapport IRSN/2020-00691,*2020.

82. Farhat, M., et al., *Characterization of bubbles dynamics in aperiodic formation.* International Journal of Heat and Mass Transfer, 2021. **180**: p. 121646.

83. FARHAT, M., *Pool scrubbing of iodine compounds - Tests on caesiuml iodide aerosols retnetion*, in *Rapport n°IRSN/2021-00823*, 2021.

84. Abdulkadir, M., et al., *Experimental investigation of the characteristics of the transition from spherical cap bubble to slug flow in a vertical pipe.* Experimental Thermal and Fluid Science, 2021. **124**: p. 110349.

85. Gréhan, G., et al., *Measurement of bubbles by Phase Doppler technique and trajectory ambiguity*, in *Developments in laser techniques and applications to fluid mechanics*1996, Springer. p. 290-302.

86. Mikaelian, D., A. Larcy, and S. Dehaeck, *A new experimental method to analyze the dynamics and the morphology of bubbles in liquids: Application to single ellipsoidal bubbles.* Chemical engineering science, 2013. **100**: p. 529-538.

87. Laupsien, D., A. Cockx, and A. Line, *Bubble plume oscillations in viscous fluids.* Chemical Engineering & Technology, 2017. **40**(8): p. 1484-1493.

88. Dietrich, N., et al., *Bubble formation at an orifice: A multiscale investigation.* Chemical engineering science, 2013. **92**: p. 118-125.

89. Cieslinski, J. and R. Mosdorf, *Gas bubble dynamics—experiment and fractal analysis.* International journal of heat and mass transfer, 2005. **48**(9): p. 1808-1818.

90. Huisman, S.G., P. Ern, and V. Roig, *Interaction and coalescence of large bubbles rising in a thin gap.* Physical Review E, 2012. **85**(2): p. 027302.

91. Aboulhasanzadeh, B. and G. Tryggvason, *Effect of bubble interactions on mass transfer in bubbly flow.* International journal of heat and mass transfer, 2014. **79**: p. 390-396.

92. Mosdorf, R. and T. Wyszkowski, *Experimental investigations of deterministic chaos appearance in bubbling flow.* International journal of heat and mass transfer, 2011. **54**(23-24): p. 5060-5069.

93. Zhang, L. and M. Shoji, *Aperiodic bubble formation from a submerged orifice.* Chemical engineering science, 2001. **56**(18): p. 5371-5381.

94. Jamialahmadi, M., et al., *Study of bubble formation under constant flow conditions.* Chemical Engineering Research and Design, 2001. **79**(5): p. 523-532.

95. McCann, D. and R. Prince, *Regimes of bubbling at a submerged orifice.* Chemical engineering science, 1971. **26**(10): p. 1505-1512.

96. Martinet, L., *Rapport de qualification "Génération d'aérosols tracés à l'iode 131 déposés sur coupon",* in *Rapport IRSN/2014-00205,* 2014.

97. Martinet, L., *Etude de la distribution granulométrique des aérosols de CsI générés par l'AGK2000.*, in *Rapport IRSN/2017-00460,*2017.

98. Hinds, W.C., *Aerosol technology: properties, behavior, and measurement of airborne particles*1999: John Wiley & Sons.

99. Bosland, L., et al., *Study of the stability of CsI and iodine oxides (IOx) aerosols and trapping efficiency of small aerosols on sand bed and metallic filters under irradiation.* Progress in Nuclear Energy, 2021. **142**: p. 104013.

100. Tornabene, C., *Procédure d'utilisation du Générateur d'Iode (GI) du programme CHIP – LP*, in *Document qualité IRSN/DPAM/SEREA/LEA/PRO/15*, 2008.

101. Tornabene, C., *Dosage multi-élémentaire par ICP/MS,* in *Document qualité PSN/SEREX-L2EC-MOP-004*, 2014.

102. Alvarez, C., *Procédure d'utilisation de la chromatographie en phase gazeuse Agilent 7820A,* in *Document qualité PSN/SEREX/L2EC-PRO-32,* 2019.

103. Lee, Y., Y.J. Cho, and I. Ryu, *Preliminary analyses on decontamination factors during pool scrubbing with bubble size distributions obtained from EPRI experiments.* Nuclear Engineering and Technology, 2021. **53**(2): p. 509-521.

104. Wassel, A., et al., *Analysis of radionuclide retention in water pools.* Nuclear Engineering and Design, 1985. **90**(1): p. 87-104.

105. Davidson, J., *Bubble formation at an orifice in an inviscid liquid.* Transactions of the Institution of Chemical Engineers, 1960. **38**: p. 335-342.

106. Davidson, L. and E.H. Amick Jr, *Formation of gas bubbles at horizontal orifices.* AIChE Journal, 1956. **2**(3): p. 337-342.

107. Krevelen, D.v. and P. Hoftijzer, *Studies of gas-bubble formation.* Chemical Engineering Progress, 1950. **46**(1): p. 29-35.

108. Legendre, D., R. Zenit, and J.R. Velez-Cordero, *On the deformation of gas bubbles in liquids.* Physics of Fluids, 2012. **24**(4): p. 043303.

109. Shen, X., et al., *Flow characteristics and void fraction prediction in large diameter pipes*, in *Frontiers and Progress in Multiphase Flow I*2014, Springer. p. 55-103.

110. Kubasch, J.H., *Bubble hydrodynamics in large pools*, 2001, ETH Zurich.

111. Castillejos, A. and J. Brimacombe, *Measurement of physical characteristics of bubbles in gas-liquid plumes: Part II. Local properties of turbulent air-water plumes in vertically injected jets.* Metallurgical Transactions B, 1987. **18**(4): p. 659-671.

112. Clift, R., J.R. Grace, and M.E. Weber, *Bubbles, drops, and particles.* 2005.

113. Wallis, G.B., *The terminal speed of single drops or bubbles in an infinite medium.* International Journal of Multiphase Flow, 1974. **1**(4): p. 491-511.

114. Colombet, D., et al., *Dynamics and mass transfer of rising bubbles in a homogenous swarm at large gas volume fraction.* Journal of Fluid Mechanics, 2015. **763**: p. 254-285.

115. Sekoguchi, K., T. Sato, and T. Honda, *Two-phase bubbly flow (first report).* Transactions of JSME, 1974. **40**: p. 1395-1403.

116. Kumar, R. and N. Kuloor, *The formation of bubbles and drops*, in *Advances in chemical engineering*1970, Elsevier. p. 255-368.

117. Hughes, R. *Formation of bubbles at simple orifices*. 1955. Library of Congress.

118. Hayes III, W.B., B.W. Hardy, and C.D. Holland, *Formation of gas bubbles at submerged orifices.* AIChE Journal, 1959. **5**(3): p. 319-324.

119. Spells, K. and S. Bakowski, *A study of bubble formation at single slots submerged in water.* Transactions of the Institution of Chemical Engineers, 1950. **28**: p. 38.

120. Kuipers, J., W. Prins, and W.P.M. Van Swaaij, *Theoretical and experimental bubble formation at a single orifice in a two-dimensional gas-fluidized bed.* Chemical engineering science, 1991. **46**(11): p. 2881-2894.

121. Corchero, G., J. Montañés, and J.C. Téllez, *Effect of flow rate conditions on bubble formation.* International journal of heat and mass transfer, 2012. **55**(19-20): p. 5044-5052.

122. Simmons, J.A., J.E. Sprittles, and Y.D. Shikhmurzaev, *The formation of a bubble from a submerged orifice.* European Journal of Mechanics-B/Fluids, 2015. **53**: p. 24-36.

123. Dietrich, N., et al., *Experimental investigation of bubble and drop formation at submerged orifices.* Chemical Papers, 2013. **67**(3): p. 313-325.

124. Welker, M., *AREVA's containment venting technologies and experience worldwide.* Sociedad Nuclear Espanola, A Coruna, 2015: p. 23-25.

125. Cantrel, L., F. Louis, and F. Cousin, *Advances in mechanistic understanding of iodine behaviour in PHEBUS-FP tests with the help of ab initio calculations.* Annals of Nuclear Energy, 2013. **61**: p. 170-178.

126. Jamialahmadi, M., C. Branch, and H. Müller-Steinhagen, *Terminal bubble rise velocity in liquids.* Chemical engineering research & design, 1994. **72**(1): p. 119-122.

127. Herranz, L., A. Cabrer, and V. Peyres, *Modelling inertial impaction within pool scrubbing codes.* Journal of Aerosol Science, 2000. **31**: p. S43-S44.

128. He, L., et al., *Investigation on aerosol pool scrubbing model during severe accidents.* Frontiers in Energy Research, 2021: p. 503.

129. Herranz, L.E., et al., *Experimental and analytical study on pool scrubbing under jet injection regime.* Nuclear Technology, 1997. **120**(2): p. 95-109.

130. Uchida, S., et al., *Temperature dependent fission product removal efficiency due to pool scrubbing.* Nuclear engineering and design, 2016. **298**: p. 201-207.

131. Colombo, M. and M. Fairweather, *Prediction of bubble departure in forced convection boiling: A mechanistic model.* International journal of heat and mass transfer, 2015. **85**: p. 135-146.

132. Kim, J., B. Do Oh, and M.H. Kim, *Experimental study of pool temperature effects on nucleate pool boiling.* International Journal of Multiphase Flow, 2006. **32**(2): p. 208-231.

133. Postma, A.K. and R. Zavadoski, *Review of organic iodide formation under accident conditions in water-cooled reactors*. Vol. 1233. 1972: Battelle Pacific Northwest Laboratories.

134. Lind, T., B. Jaeckel, and S. Güntay. *A summary of the PSI Investigations on Iodine Chemistry in the Presence of Impurities and Additives*. in *Proceedings of the International OECD-NEA/NUGENIA-SARNET Workshop on the Progress in Iodine Behaviour for NPP Accident Analysis and Management*. 2015.

135. Clément, B., et al., *State of the art report on iodine chemistry*, 2007, Organisation for Economic Co-Operation and Development.

136. Hillrichs, C., D. Vignon, and P. Felten, *Review of European filtered containment venting systems.* European Nuclear Society (ENS), 2012: p. 9-12.

137. Chebbi, M., et al., *Effects of water vapour and temperature on the retention of radiotoxic CH3I by silver faujasite zeolites.* Journal of Hazardous Materials, 2021. **409**: p. 124947.

138. Cantrel, L. and P. March, *Mass transfer modeling with and without evaporation for iodine chemistry in the case of a severe accident.* Nuclear Technology, 2006. **154**(2): p. 170-185.

139. Wren, J. and J. Ball, *LIRIC 3.2 an updated model for iodine behaviour in the presence of organic impurities.* Radiation Physics and Chemistry, 2001. **60**(6): p. 577-596.

140. F. Cousin, L.B., *Astec v2.1.1 sophaeros module - theoritical manual. Technical report,*, in *PSN-RES/SAG/2017-00215*.2017.

141. Prasher, B.D. and G.B. Wills, *Mass transfer in an agitated vessel.* Industrial & Engineering Chemistry Process Design and Development, 1973. **12**(3): p. 351-354.

142. Dietrich, N. and G. Hebrard, *Visualisation of gas-liquid mass transfer around a rising bubble in a quiescent liquid using an oxygen sensitive dye.* Heat and Mass Transfer, 2018. **54**(7): p. 2163-2171.

143. Tacke, K., et al., *Characteristics of round vertical gas bubble jets.* Metallurgical Transactions B, 1985. **16**(2): p. 263-275.

144. Iguchi, M., K. Nozawa, and Z.-i. Morita, *Bubble characteristics in the momentum region of air-water vertical bubbling jet.* ISIJ International, 1991. **31**(9): p. 952-959.

145. Castello-Branco, M.A. and K. Schwerdtfeger, *Large-scale measurements of the physical characteristics of round vertical bubble plumes in liquids.* Metallurgical and materials transactions B, 1994. **25**(3): p. 359-371.

146. López-Jiménez, J., et al., *Pool scrubbing*, 1996, Centro de Investigaciones Energeticas.

147. Seinfeld, J.H. and S.N. Pandis, *From air pollution to climate change.* Atmospheric chemistry and physics, 1998. **1326**.

148. Rodrigue, D., *Generalized correlation for bubble motion.* AIChE Journal, 2001. **47**(1): p. 39-44.

149. Rodrigue, D., *A general correlation for the rise velocity of single gas bubbles.* The Canadian Journal of Chemical Engineering, 2004. **82**(2): p. 382-386.

Appendix 1. Generation of caesium iodide aerosols

A- Principle

A generator will form and propel aerosols in a conduit and these, driven by a gas flow, will be injected through the connecting tubes. This generation is carried out from a solution of soluble iodinated compounds called solution of generation, which is prepared prior to the tests.

B- Description

The generator used is a commercial generator of reference AGK2000 produced by PALAS company. The assembly used for the generation includes besides the basic generator :

- A drying tube modified by adding a screw thread at its end.
- A stainless-steel curved collection tube fitted with two nuts.
- A marking box, its cover closed by 4 screws and the adapted coupon support, or the marking box closed by a nut
- A 50 ml reservoir bottle.
- A plastic nut allowing the reservoir bottle to be joined to the generator four bubbler bottles containing sodium hydroxide 0.1 mol. l^{-1} connected in two lines of two bubblers.

C- Operating

The general principle of operation is as follows:

- The generating solution containing the soluble iodine compound is introduced into a reservoir bottle
- The pressurized air is driven to the binary nozzle.
- The peristaltic pump brings the generating solution to the binary nozzle.
- The aerosol cloud generated in the nozzle flows towards the cyclone.
- The droplets are then separated by centrifugal force and fall back into the reservoir bottle containing the generating solution.

Appendix 2. Analysis of caesium iodide CsI and molecular iodine I_2 by the Inductively Coupled Plasma – Mass Spectrometry

Inductively Coupled Plasma (ICP), coupled with a mass spectrometer (MS), is an analytical technique based on the separation, identification, and quantification of the constituent elements of a sample according to their mass. It is based on the coupling of an ion generating plasma torch and a mass spectrometer (quadrupole) allowing the separation of ions according to their mass-to-charge ratios. The ICP-MS technique allows multi-element trace determinations (1µg/g) in solution.

The ICP-MS analysis of the samples can be divided into four stages: introduction-atomizing, ionization, separation in mass, detection as shown in Figure A.1:

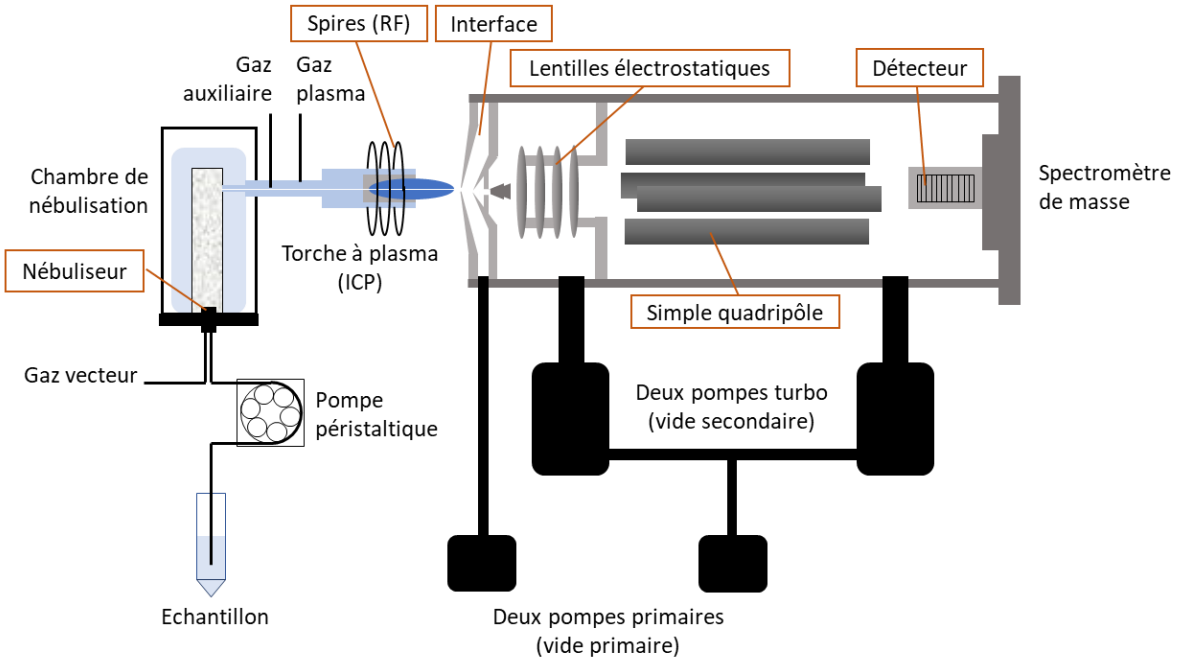

Figure A.1- ICP- MSscheme

- The liquid sample is injected into the system through a capillary tube and driven by a peristaltic pump to the nebulizer. It is then nebulized in the nebulizer chamber and pumped into the plasma torch as an aerosol. Thus, the aerosol formed is sent in an argon plasma torch at very high temperature (from 5000 to 10000K), which is sufficient to allow the liquid aerosol to vaporize, dissociate, atomize, and ionize completely the majority of the elements.

- The generated ions are then extracted through the interface region and into a set of electrostatic lenses called the ion optics. The ion optics focuses and guides the ion beam into the quadrupole mass analyzer.

- A quadrupole (mass analyzer) is based on the separation of the ions according to their mass to charge ratio and the ions having the desired ratio m/z (mass/charge) will be transmitted to the detector.

- The ion detector can thus generate a measurable signal pulse (counts) from the impact of a single ion, which is proportional to the concentration.

The sample in solution is injected into the nebulizer through a capillary tube and driven by a peristaltic pump. The sample nebulized in the nebulizer chamber is then introduced into the flare as aerosols by pumping. The ions formed in the torch are led through the interface and the quadrupole to the detector by an electrostatic field. Finally, the mass spectrum of the sample with the concentration of the analyte is obtained by external calibration. An internal standard is also added to prevent deviations of the apparatus.
The method chosen for the analysis of iodine 127 in soda matrix is as follows :

- Plasma argon flow rate: 18 L/min.
- Auxiliary argon flow rate: 1.8 L/min.
- Nebulizer argon flow rate: 1.1 L/min.
- Sheath flow rate: 0.15 L/min.
- Radio frequency (RF) power: 1.40 kW.
- Stabilization time: 95 s.
- Spray chamber temperature: 3°C.
- Scan mode: peak jump.
- Dwell time: 800 ms.
- Replica per scan : 10.
- Replica per sample: 10.

The analysis of each sample placed in the autosampler takes about 3 minutes. The limits of detection (LOD) and quantification (LOQ) of the instrument for Iodine-127 are 4x10-9 mol/L and 13x10-9 mol/L respectively. For a 95% confidence level, the expanded uncertainty on the concentration determination is ±9%.

Appendix 3. Gas chromatography

Gas chromatography (GC) is a widely used analytical technique. It is a separation technique applicable to gaseous compounds or compounds that can be volatilized by raising temperature without decomposition (with a molecular weight of less than 300 atomic mass units). The mobile phase is a gas (helium), so it allows the advancement of analytes in the column which are in the gaseous state. The mobile phase behaves like an inert carrier gas, it does not cause any interaction with the analytes to be separated.

1- **Injection:** The CPG present at the L2EC [8] allows the use of two different injection modes: manual injection and injection through the thermo-desorber.

- Manual injector: The sample to be analyzed is introduced into the chromatograph using a gas sampling syringe (10 or 25 mL) or Tedlar® bag (500mL or 1L). Manual injection includes an injection loop. The choice of the loop volume is based on the size of the column and the assumed concentration of the products to be analyzed. The injection loop system avoids dead volume and ensures a constant injection volume, which is important for quantitative analysis.
- Injection through the thermo-desorber: The sample to be analyzed is not introduced directly into the chromatograph. This technique is used when the analyte is not concentrated enough to be detected or quantified. A pre-concentration step is required. This technique uses the possibility for the analyte to adsorb on a solid phase (cold-trap), and conversely to desorb in the injector under the effect of heat. Several modes of injection in the cold-trap are possible: Tedlar® gas bag or sample tube.

The GC has a split/split-less injector that allows the fraction of the sample sent to the column to be adjusted in relation to the total quantity introduced into the chromatograph. In split mode, a stream of carrier gas arrives in the injection chamber where it mixes with the injected sample. A leakage valve divides into two fractions, the smaller of which is the only one to enter the column. The fraction of the sample entering the column is equal to the split ratio, which can vary between 1 and 165.

In split-less mode, the entire sample is injected and then entrained into the first turns of the capillary column. The injector is then swept by the carrier gas which removes the excess solvent. This procedure is reserved for highly diluted samples. When injecting via the thermo-desorber, the injection method on the GC must be in split-less mode (because the TD has its own split).

2- **Column**: The gas chromatographic column may be considered the heart of the GC system, where the separation of sample components takes place. Columns are classified as either packed or capillary columns.

   Packed columns are stainless steel or glass tube filled with particulate packing material (an adsorbent material, or a support material coated or impregnated with a solid phase). Packed columns produce broad band shapes and have low separation performance but can also handle large sample volumes and are not susceptible to contamination.

   The capillary columns usually consist of a fused silica (quartz, SiO2) capillary that is coated with a polyimide layer. The polyimide layer provides the capillary with flexibility and stability, as well as its characteristic brownish color. Capillary columns

produce sharp band shapes, achieve excellent separation performance, and are suited to high-sensitivity analysis. The 260-column used in our experiments is a GASPRO capillary (open tube) column. The internal diameter of the column is 0.32 mm and is 30 m long (twice 15 m). The maximum operating temperature of this column is 350°C.

3- **Detector:** The detector senses a physicochemical property of the analyte and provides a response which is amplified and converted into an electronic signal to produce a chromatogram. In L2EC laboratory the GC has two detectors: Thermal Conductivity Detector (TCD) and Electron Capture Detector (ECD).

The TCD is a universal response detector but is relatively insensitive (of the order of ppb). This detector is based on a continuous comparison between the heat flux carried by the pure carrier gas and the heat flux carried by the carrier gas loaded with the molecules to be analyzed. These heat fluxes are produced by thermistors, through which a direct current of fixed voltage flows, in a thermostatically controlled enclosure. The thermistors are mounted in a Wheastone bridge, which allows the evolution of the current to be monitored as a function of the variation in resistance due to temperature variations around the filaments.

The ECD is a more selective detector and sensitive to halocarbon compounds such as iodomethane. It is a very sensitive detector that can analyze samples with concentrations of the order of ppt. ECD has a low-energy radioactive source that allows free electrons to be sent into the detector. When substances with an affinity for free electrons pass through the detector, ions are produced which are collected in the existing electrostatic field by an anode and form an ionization current.

Appendix 4. Estimation of the measurements uncertainties of the obtained results in chapter 4.

For all the results presented in chapter 4, the relative uncertainty Ur at 95% confidence (enlargement coefficient ke=2), expressed as a percentage, can be evaluated using the method of propagation of uncertainties, considering the different uncertainties perfectly independent of each othes. This gives:

$$U_r = k_e\sqrt{u_r^2(dilution) + u_r^2(sample\ measurment) + n.u_r^2(weighed)}$$

With:

- $u_r(dilution)$ the standard relative uncertainty related to the dilution operation of the sample taken in a bubbler
- $u_r(sample\ measurment)$ the standard relative uncertainty related to the measurement of absorbance using ICP-MS of GC,
- n the number of weighing carried out to determine the final mass of iodine compounds. This number depends on the sample considered (more weighing to be carried out for a sample at the end of the test,
- $u_r(weighed)$ the standard uncertainty associated with determining the mass of a sample (which makes it possible to deduce its volume, and then to determine the mass of iodine compounds by multiplying by the concentration measured by ICP-MS or GC).

These quantities are estimated as follows:

- $u_r(dilution) = \frac{EMT(dilution)}{3}$ with $EMT_{(dilution)}$ l'Erreur Maximale Tolérée[4] on the dilution operation. Given the use of precise pipettes to take the desired volumes of solutions, $EMT_{(dilution)}$ is conservatively estimated at ±5%,
- $u_r(sample\ measurment) = \frac{U_{r\ (spectrometer\ used)}}{k_e}$ with $U_{r\ (spectrometer\ used)}$ the expanded relative uncertainty of the spectrometer used for the analyses.

[4] The EMT is used when the uncertainty is not readily available (no data or calibrations linked to a measuring device). The experimenter evaluates the error of measurement or graphical reading that he is likely to commit. The EMT is given here as a percentage. It is the ratio between the MPE in the unit considered according to the measured quantity and the measured value. For example, concerning the dilution operation, for a volume V, $EMT_{\%} = EMT_V/V_{measured}$.